Water vapor and gas barrier properties of cellulose-based materials

by

Alemayehu H. Bedane

M.Sc in Quality, Safety and Environment, Otto-von-Guericke University of Magdeburg, 2008 and M.Sc in Forest Engineering, University of New Brunswick, 2010

A Dissertation Submitted in Partial Fulfillment of the Requirements for the Degree of

Doctor of Philosophy

in the Graduate Academic Unit of Chemical Engineering

Supervisor: Mladen Eić, PhD, Chemical Engineering.

Examining Board: Huining Xiao, PhD, Chemical Engineering.
Yonghao Ni, PhD, Chemical Engineering.
Meng Gong, PhD, Forestry and Environmental Management.
John Kershaw, PhD, School of Graduate Studies (Chair)

External Examiner: Phillip Choi, PhD, Department of Chemical and Materials Engineering, University of Alberta, Edmonton.

This dissertation is accepted by the Dean of Graduate Studies

THE UNIVERSITY OF NEW BRUNSWICK
June, 2015

ABSTRACT

Mass transport properties in polymeric materials are of fundamental importance for different applications, such as food and pharmaceutical packaging, membrane-based gas and liquid separations, etc. In this thesis, adsorption equilibria, structure and mass transport properties (water vapor, CO_2 and oxygen) of modified papers, nanofibrillated cellulose (NFC) and regenerated cellulose films, derived from different sources, were investigated to evaluate their potential as food and pharmaceutical packaging materials. The gravimetric-IGA system was used for measuring water vapor mass transfer rates (WVPR's), structure and permeabilities (WVP's) of the samples. Water vapor adsorption equilibria (isotherms) were also measured using the Belsorp instrument, while the vapor diffusivities for cellulose-based films were determined from the uptake rate measurements, at a wide range of relative humidities, using appropriate diffusion models. The diffusivities were found to depend on the moisture content of the samples. The effective diffusion coefficients of modified paper samples (e.g., PLA, PHBV coated papers), NFC and regenerated cellulose films are 1-2 orders of magnitude lower in comparison to the unmodified paper sample (made from bleached Kraft pulp), depending on the moisture content.

Water vapor transmission rates (WVTRs) of regenerated cellulose and NFC films were found to be close to each other, but lower compared to unmodified paper for all relative humidity gradients. WVPs of the NFC and regenerated cellulose films were found to be moisture concentration dependent. Their values are relatively low up to RH=25%, but then show a rapid increase above 25 %. This behavior is attributed to an increase in the

solubility and surface diffusivities of water vapor in the film at the higher moisture contents according to the solution-diffusion theory. Among the investigated paper samples, PHBV and PLA/polyhedral oligomeric silsesquioxane (POSS)-bentonite modified papers showed higher mass transfer resistance to water vapor and the gases (CO_2 and O_2) investigated in this study. The barrier properties are enhanced by the addition of fillers and surface coating onto cellulose based paper; however, surface coating is more effective in increasing the barrier properties of the modified papers.

In the further study, the mechanisms of water vapor transport through the cellulose films were also determined from the uptake rate measurements. The results showed that the external surface resistance (surface barrier) and/or polymer chain relaxation rate were a more dominant mechanism for mass transfer in the NFC and regenerated cellulose films compared to unmodified paper. Mass transfer for the unmodified paper was found to be consistent with internal diffusion control, except at the high moisture contents. However, at high moisture content of the films, both external surface resistance and diffusion process equally control the mass transport mechanism for all investigated samples. Finally, theoretical modeling of parallel pore-surface diffusion of water vapor transmission rates through the paper sample and regenerated cellulose film are developed from experimentally determined mass transfer parameters. The results showed that the moisture transport dynamics can be well analyzed using parallel pore-surface diffusion for the cellulose-based materials.

ACKNOWLEDGEMENTS

I would like to thank my supervisor Prof. Mladen Eić for giving me this opportunity to work with his research group and for his enthusiastic supervision and for always being encouraging and providing useful critiques during the course of this work. I am particularly indebted to him for his support and fruitful discussions at every stage of the present work. Thanks also go to Dr. Xiao and his research group for their collaboration in this project and for providing samples for my study. Dr. Xiao is also thankfully acknowledged for the wonderful collaborative efforts as a co-author in our publications. I would also like to thank former undergraduate students, Ms. Maja Mitrovic and Mr. Nikola Mijatovic, for assisting in experimental work during their summer works in our research group.

I would like to acknowledge the financial support provided by Natural Sciences and Engineering Research Councils of Canada (NSERC) Strategic Network Innovative-Wood Fibre Products and also like to thank the Green Fibre Network organizers for creating a supportive and stimulating environment for discussion and presentation of our projects on semi-annual Network meetings.

Many thanks are due to my friends, Mr. Madjid Farmahini-Farahani, Ms. Zhaoping (Sandy) Song, Mr. Babak Shirani, Mr. Srikanth Narayanan and Ms. Hua Ye (Flower) for many invaluable discussions and their support. I would like to thank Mr. Carl Murdock, Mr. Keith Rollins and Mr. Adon Briggs for technical support and helping in setting-up experimental instruments. Most of all I would like to thank the faculty and staff in the Department of Chemical Engineering.

I would like to thank my mother, Mrs. Bekelech B. Gebremariam and father Mr. Hailu Bedane for their encouragements and continued support over the years and their enthusiasm as I neared my goal. Finally, but most importantly, I wish to thank my wife, Ms. Haregewoyin Tsega and my daughter, Ruth A. Hailu for their patience, assistance, support and faith in me. I would like to thank my family members who have given me the strength to finish what I have started.

Table of Contents

List of Tables

List of Figures

List of Symbols, Nomenclature and Abbreviations

a_w	*water vapor activity* (p/p_o)
A	*area* (m^2)
A_c	*specific surface area* (m^2/g)
BET	*Brunauer, Emmett and Teller*
C_i	*vapor concentration in the gas* $(mol/m^3$ *or* $g/m^3)$
C	*Guggenheim parameter*
CO_2TR	*carbondioxide transfer rate*
D_q	*surface diffusivity* (m^2/s)
D_{eff}	*effective diffusivity* (m^2/s)
D_p	*pore diffusivity* (m^2/s)
DSC	*Differential Scanning Calorimetry*
E_{eff}	*activation energy of permeability (kJ/mol)*
E_d	*activation energy for diffusion (kJ/mol)*
GAB	*Guggenheim Anderson de Boer*
GTR	*gas transmission rate* $(g/m^2.day$ *or* $cm^3/m^2.day)$
K_o	*overall mass transfer coefficient (m/s)*
J	*mass flux* $(g/m^2.s)$
k_c	*convective mass transfer coefficient (m/s)*
k'	*mass transfer rate (1/s)*
H-H	*Hailwood-Horrobin*
H_d	*heat of desorption (kJ/g)*

H_{evap}	*heat of evaporation (kJ/g)*
H_L	*heat of condensation of water vapor (kJ/g)*
H_N	*heat due to multilayer water vapor adsorption(kJ/g)*
M	*moisture content (% wt.)*
M_h	*monolayer moisture content (% wt.)*
M_s	*polylayer moisture contents (% wt.)*
MFC	*microfibrillated cellulose*
N	*molar flux* ($mol/m^2/sec.$)
NFC	*nanofibrillateted cellulose*
O_2TR	*oxygen transfer rate*
O_2P	*oxygen permeability*
P	*total pressure (Pa)*
p	*partial pressure (Pa)*
P^{sat}	*saturation pressure(Pa)*
q	*moisture content in the solid (g water/g dry solid)*
q_{st}	*net isosteric heat of sorption (kJ/g)*
Q_{st}	*isosteric heat of sorption (kJ/g)*
R	*universal gas constant, (J/mol. K)*
RH or h	*relative humidity (%)*
L	*half film thickness (m)*
t	*time (s)*
T	*Temperature* (^oC)

TGA	*Thermogravimetry Analysis*
S	*solubility (g/m^3.pa)*
x	*length (m)*
WVTR	*water vapor transmission rate (g/m^2.day)*
WVP	*water vapor permeability (g/s.m.Pa)*
Z	*film thickness (m)*
ΔH	*heat of adsorption (kJ/kg)*
ΔRH	*relative humidity driving force (%)*
Δp	*partial pressure difference (Pa)*
e_p	*sample porosity*
e_b	*bed porosity*
u_z	*interstitial velocity (m/s)*

Chapter 1: Introduction

1.1. Background

Synthetic-plastic materials are mainly consumed in packaging and other industries, such as food, pharmaceutical, cosmotics, electronics. The demand for global consumer packaging is increasing rapidly and the demand is valued at approximately US $400-$500 billion (Nail-Boss and Brooks, 2013; Nair et al., 2014). However, using plastic as packaging material raises some concerns from both economical and environmental perspectives. Continued use of finite petroleum resources, as a consequence, could lead to acute prospect of a decreasing trend in availability of petroleum products, thus increasing the cost of raw materials, e.g., oil and natural gas. Because of the lack of biodegradability, petroleum-based products can pose significant waste disposal problems. This provoked a strong interest in the field of green materials, e.g., cellulose-based materials to replace plastic packaging. According to a new market report by Pira (2013), the global market for sustainable packaging is forecast to reach $244 billion by 2018 (see also Allen, 2014). Cellulose fiber-based materials are low cost and also considered to be more environmentally friendly because of their renewable, recyclable and biodegradable properties (Khare et al., 2007; Nair et al., 2014). Wood and cotton are the raw materials for commercial production of cellulose (Varshney and Naithani, 2011). Cellulose has several applications e.g., in paper making and paperboard, nanofibrillated cellulose (NFC) and cellophane (thin transparent film), fire retardant (insulation) materials and membranes (filtration). Cellulose fibers are mainly used for paperboard and papermaking. Paper is a network of natural polymer composite cellulose fibers. The ability of the fibers to bond together and form a random layered structure is the main property of paper (Tanner and Amos, 2006). Paper can be used for packaging applications, and this is one of the largest markets next to metal, glass, and plastic (Allen, 2014). Despite these advantages, more wide-spread applications of cellulose-based materials are limited. Cellulose based-films are very sensitive to moisture and water vapor, and gas barrier properties are much lower compared to many other plastic polymers used in packing applications. “Water vapor or gas barrier property” is the term used for sealing the contents from humidity, oxygen, carbon dioxide and other gases, to prevent degradation in quality. Paper-based packaging materials can readily adsorb and desorb moisture when exposed to different environments, depending on the initial moisture content of the material and the relative humidity of the atmosphere. High moisture content in paper-based packaging materials adversely affects physical, mechanical properties and long-term stability (Twede and Selke, 2005).

The absorbed moisture reduces the barrier property since water enters the polymer and interacts with the bonds that hold the chains together, and as a result the polymer swells and the chain becomes loose/soft thus allowing permeation to continue at a faster pace. Several physical and chemical modification techniques, such as coating, adding fillers, and grafting have been used with the aim of improving the barrier properties of cellulose fiber-based materials (Andersson, 2008; Larotonda et al., 2005; Narayan, Bloembergen, & Lathia, 1999; Kuusipalo, 2000; Jansson and Jarnstrom, 2005; Kugge and Johnson, 2008). The packaging material must have sufficient barrier properties to protect goods from microbial, chemical and physical contamination, thus minimizing product quality loss. Polymer structure, moisture interaction, additives and thickness or multiple layers can have influence on the packaging performance. Based on this requirement, this study further investigates water vapor and gas transport properties, water vapor adsorption capacities, and interaction of water vapor and substrate of the cellulose fiber-based materials.

Permeation and diffusion properties are important in a variety of industrial and biomedical applications of polymers, e.g., in the separation of gas and liquids, food packaging, protective coatings (e.g., paints and varnishes) (Balser et al., 1986; Barndt, 1986; Varshney and Naithani,, 2011; Davidson, 1980; Whistler and BeMiller, 1973; Nicholson and Meritt, 1985), controlled drug release (Grabovac et al., 2005; Movassaghian et al., 2011), and biomedical devices (Stern, S.A. and Fried, J.A., 2007). Water transport in paper is also of prominence in operations such as coating, surface sizing, packaging and printing (Hashemi et al, 1997). The potential of biodegradable polymers has been recognized by implementing them for different applications since they could provide an efficient way to overcome the limitation of the petrochemical resources in the future. Most paper-based packaging materials are being coated with sustainable biodegradable polymers to improve their barrier properties with regard to water vapor and gases, e.g., oxygen, CO_2 (Andersson, 2008; Kuusipalo, 2000; Jansson and Jarnstrom, 2005; Kugge and Johnson, 2008). Understanding the diffusion and permeation processes is critical in developing reliable polymer composites and coatings for use in demanding environments. Therefore, in this study different modified/coated paper samples, commercial papers and transparent cellulose films (e.g., nanofibrillated cellulose and regenerated cellulose films) are evaluated with regard to their barrier properties, which include water vapor adsorption equilibria, kinetics and water vapor and gas (O_2 and CO_2) transport properties.

1.2. Thesis objectives

The primary objective of this study was to determine the transport parameters, namely water vapor diffusion coefficient, gases (CO_2 and O_2), water vapor transmission rates and permeability of cellulose-based materials (e.g., unmodified paper, coated papers, regenerated cellulose and nanofibrillated cellulose (NFC) films) from experimental measurements. This involves the characterization of the mechanism of water vapor transport properties in functional-modified wood fibre network and coated paper.

The second objective is to determine the water vapor adsorption capacities of modified cellulose fiber materials and formation of water molecules on the surface from adsorption isotherm equilibria. This can be used to evaluate the hygroscopic properties of the materials and also to identify which methods of modification (e.g., coating, fillers) provide the best barrier properties against water vapor and gas.

The final objective is to extract mass transfer parameters from the experimental measurements and to develop theoretical water vapor transmission rates and compare them to the experimentally obtained water vapor transmission rates. The specific objectives of this study are:

1. to develop experimental methodologies for characterizing the structural, equilibrium and transport characteristics of water vapor, oxygen and CO_2 in functional-modified wood fibre network and coated paper;
2. to use obtained experimental information to study interactions between sorbate molecules and fibre substrates and mechanisms of water vapor, oxygen and CO_2 transport through modified fibre-based pacakging materials;
3. to model experimental results using parallel pore-surface diffusion model, and to establish the structure-property relations in terms of the barrier properties and the structures of the functional-modified fibre-based materials.

Therefore, the ultimate objective is to relate the barrier properties to different cellulose-based films and also to different methods of paper modification, e.g., coating and filler adding.

1.3. The significance of the study

Fundamental understanding of the structural and transport properties of the cellulose films and the mechanism of water transport through these materials are required for different applications, such as food packaging, drying of paper during the papermaking process and vapor/gas separation in membrane applications. This study will also provide information regarding the interaction between the sorbate molecules and fiber substrate necessary for further modifications and development of the cellulose fiber–based materials and coated papers. It can also provide information for pulp and paper industries for improving a variety of barrier properties to the conventional paper products, thus leading to various new products and/or improved products. Moreover, the results obtained on surface characterization of cellulose fiber material can also be applied to water and waste water treatments (e.g., green industrial membranes).

1.4. Thesis layout

This thesis was written in the form of articles and it consists of eight chapters. Each chapter has its own references and is a stand-alone document. Chapter 1 provides the background of the project and the objectives of this study. A literature review is presented in Chapter 2 to summarize the theoretical approach and methods for determining permeation through polymer sheets and within polymeric materials. The barrier properties of cellulose fiber-based materials, other polymers and factors affecting permeation, modeling approaches and also techniques for characterizing samples, and an overview of various experimental approaches have been reviewed.

Chapter 3 reports the experimental studies on the mass transport properties of gases (CO_2 and O_2) and water vapor in different coated paper samples. The effects of sample film thickness, temperature, and relative humidity driving force on water vapor transmission rates (WVTRs) were also examined. Water vapor adsorption equilibria in unmodified and modified papers were investigated in order to determine their hygroscopic properties in Chapter 4. Monolayer and multilayer moisture contents of the samples were determined from their adsorption isotherms using the BET, H-H, and GAB models. The relation between the hygroscopic properties of the sample and its mass transport properties were also analyzed. Then, the structural and thermodynamics characterization of modified cellulose fiber materials, as well as the interactions between water vapor and the fiber surfaces are reported in Chapter 5. Mass transport properties, as well as mechanisms of water vapor transport in regenerated cellulose and nanofibrillated cellulose (NFC) films were studied and compared to unmodified and coated paper samples in Chapter 6.

In Chapter 7, theoretical water vapor transport using parallel pore-surface diffusion model in paper sheet was developed and the theoretical WVTRs were compared with the experimentally obtained WVTRs. Pore diffusion values were estimated using dynamic breakthrough modeling of stacked paper films similar to packed bed configuration. Other mass transfer parameters were extracted from the experimental results obtained from adsorption and kinetics measurements that have been presented in Chapters 3 to 6. Conclusions drawn from this study and recommendations for future studies are given in Chapter 8.

Limitations

This thesis is concerned with hygroscopic, i.e., water vapor and gases (e.g., O_2 and CO_2) mass transport in cellulose fiber-based materials (paper, coated paper, NFC and regenerated cellulose films) and does not include liquid transport.

References

Allen, B. and Pira, S. (2014). Sustainability Packaging Market to Reach $244 Billion by 2018. http://news.thomasnet.com/imt/2014/05/01/sustainable-packaging-market-to-reach-244-billion-by-2018.

Anderson, C. (2008). New ways to enhance the functionality of paperboard by surface treatment-a Review. Packag. Technol. Sci. 21(6), 339-373.

Barndt, L (1986). Cellulose ethers. In: Gerhartz, W., Stephen, Y.Y., Thomas, C.F., Pfefferkorn, R., James, F., (Eds), Ullmann's encyclopedia of industrial chemistry. Wiley, New York.

Balser, K., Hoppe, L., Eicher, T., Wandel, M., Astheimer, H.J., Steinmeier, H., Allen, J.M. (1986). Cellulose esters. In: Gerhartz W, Stephen YY, Thomas CF, Pfefferkorn R, James F (eds) Ullmann's encyclopedia of industrial chemistry. Wiley, New York.

Davidson, R.L. (1980). Handbook of water soluble gums and resins. McGraw-Hill, New York.

Grabovac, V., Guggi, D., Bernkop-schnurch, A. (2005). Comparison of the mucoadhesive properties of various polymers. Advanced Drug Delivery Reviews, 57(11), 1713-1723. DOI: 10.1016/j.addr.2005.07.006.

Hashemi, S.J., Gomes, V.G., Crotogino, R.H., Douglas, W.J.M. (1997). In-Plane Diffusivity of Moisture in paper. Dry. Technol., 15(2), 265-294.

Jansson, A. and Jarnstrom, L. (2005). Barrier and mechanical properties of modified starches. Cellulose, 12, 423-433.

Khare, V.P., Greenberg, A.R., Kelley, S.S., Pilath, H., Roh, II J., Tyber, J. (2007). Synthesis and characterization of dense and porous cellulose films. J. Appl. Polym. Sci., 105, 1228-1236.

Kugge, C. and Johnson, B. (2008). Improved barrier properties of double dispersion coated liner. Progress in Organic Coatings, 62, 430-435.

Kuusipalo, J. (2000). PHB/V in Extrusion Coating of Paper and Paperboard-Study of Functionla Properties. Part II. J. Polym. & Environ. 8(2), 49-57.

Larotonda, F.D.S., Matsui, K.N., Sobral, P.J.A., Laurindo, J.B. (2005). Hygroscopicty and water vapor permeability of Kraft paper impregnated with starch acetate. J. Food Eng., 71, 394-402.

Movassaghian, S., Barzegar-jalali, M., Alaeddini, M., Hamedyazdan, S. Afzalifar, R., Zakeri-milani, P., Mohammadi, G., Adibkia, K. (2011). Development of amitriptyline buccoadhesive tablets in management of pain in dental procedures. Drug Dev Ind Pharm., 37(7), 849-854.

Neil-Boss, N., Brooks, K. (2013). Unwrapping the Packing Industry. Seven factors for success.http://www.ey.com/Publication/vwLUAssets/Unwrapping_the_packaging_industry_%E2%80%93_seven_factors_for_success/$FILE/EY_Unwrapping_the_packaging_industry_-_seven_success_factors.pdf

Nair, S.S., Zhu, J.Y., Deng, Y., Ragauskas, A.J. (2014). High performance green barrier based on nanocellulose. Sustainable Chem. Process, 2:23.

Narayan, R., Bloembergen, S., and Lathia, A. (1999). US patent, 5,869,647. Method of preparing biodegradable modified-starch moldable products and films.

Nicholson, M.D. and Meritt, F.M. (1985). Cellulose ethers. In: Nevell, T.P., Zeronian, S.H. (Eds). Cellulose chemistry and its applications. Ellis Horwood, Chichester.

Pira, S. (2013). The Future of sustainability in packaging to 2018. https://www.smitherspira.com/products/market-reports/packaging/innovations-and-technologies/the-future-of-sustainability-in-packaging-to-2018.

Stern, S.A. and Fried, J.R. (2007). Permeability of polymers to gases and vapors. In Chapter 61, Physical properties of polymers handbook (James E. Mark). @2007 Springer Science-Business Media, LLC.

Sun, C.C. (2008). Mechanism of moisture induced variation in true density and compaction properties of microcrystalline cellulose. International J of Pharm.346, 93-101.

Tanner, D. and Amos, N. (2006). Paper and card packaging of frozen foods. Handbook of frozen food processing and packaging, Taylor & Francis Group, LLC. Page, 653-665.

Twede, D. and Selke, S.E.M. (2005). Cartons, Crates and Corrugated Board, Handbook of paper and wood packaging, DEStech Publicationa, Inc., Lancaster, Penyslvania, U.S.A.

Varshney, V.K. and Naithani, S. (2011). Chemical functionalization of fellulose derived from nonconventional sources. Cellulose fibers: Bio- and Nano-Polymer Composites, Chapter 2. Springer-Verlag Berlin Heidelberg. DOI 10.1007/978-3-642-17370-7_2.

Whistler, R.L. and BeMiller, N.J. (1973). Industrial gum, polysaccharides and their derivatives. Academic, New York.

Chapter 2: Literature Review

2.1. Introduction

Polymers are natural or synthetic materials composed of very large organic molecules. Cellulose is one of the most abundant organic materials on earth. Cellulose is a complex carbohydrate $(C_6H_{10}O_5)_n$, consisting of a linear chain of many glucose units. It is a major constituent of the cell wall for most plants and woods (shown in Fig. 2.1). The anhydroglucose units are linked together as beta-cellobiose; therefore, anhydro-beta-cellobiose is the repeating unit of the polymer chain. The number of repeat units linked together to form the cellulose polymer is referred to as the “degree of polymerization”.

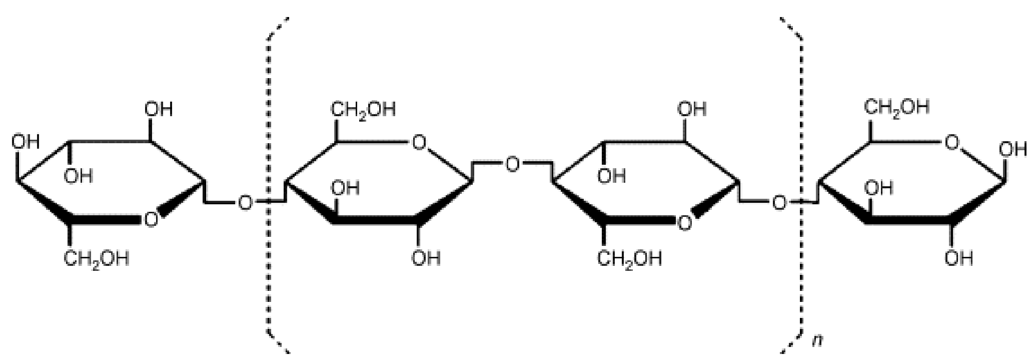

Figure 2.1. Cellulose chemical structure

Cellulose fibers constitute amorphous and crystalline regions and have crystallinity typically in the range of 40-60%. Cellulose is very stiff and strong and has a typical average density of 1.5 g/cm^3. However, the density of the crystalline region is greater than that of the amorphous region (Haslach, 2000). These microfibrils have disordered (amorphous) regions and highly ordered (crystalline) regions. In the crystalline regions, cellulose chains are closely packed together by a strong and highly intricate intra- and intermolecular hydrogen-bond network (shown in Figure 2.2), while the amorphous domains are regularly distributed along the microfibrils (Zhou and Wu, 2012).

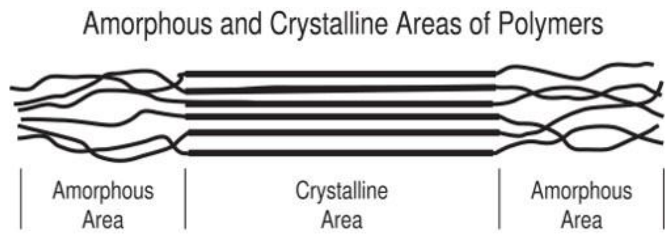

Figure 2.2. Cellulose microfibril structure

Polymers that have polar groups (e.g., cellulose, ethylene vinyl alcohol) have higher permeability for water vapor than for oxygen gas. Polyethylene, on the other hand, has much higher permeability for oxygen than for water vapor. Polymers used for food and other applications need to have the appropriate barrier properties. For example, polymer films are typically used as packaging to store food. If the air and water diffuse through the film, the food may spoil. Cellulose has been used for paper based industrial packaging for products of great volume, due to low cost and high mechanical resistance to tearing and to tension forces (Larotonda et al., 2005; Khare, 2007). However, due to their hygroscopic and porous properties, the water vapor barrier property of the papers is not suitable for foodstuff storage in environments with high relative humidity. Paper can adsorb water vapor from the environment or from food, which can cause the loss of its original mechanical properties. Modification of cellulose-based materials using hydrophobic or less hydrophilic materials is more preferable to provide a barrier against moisture migration.

Paper is made from the network of polymer composite cellulose fibers such as wood, linen or cotton. A paper sheet of ordinary basis weight can have from 10-20 layers of bonded fibers (Akker, 1970; Haslach, 2000). The basis weight or grammage is the weight per unit surface area of a sheet. Biodegradable polymers for different application have been a growing field in the paper and polymer industries. A great number of biodegradable polymers (e.g., cellulose, chitin, starch, polyhydroxyalkanoates, polylactide, polycaprolactone, collagen and other polypeptides, etc) have been produced. These polymers can be found in agro-resources (e.g., starch or cellulose), microbial production such as the polyhyrdoxyalkanoates (PHAs), and chemically synthesized from monomers obtained from agro-resources, e.g., the polylactic acid (PLA) (Averous and Pollet, 2012). Several techniques have been used to reduce the hygroscopicity and improve the water vapor and gas barrier properties of paper-based packaging. This led to development of nanocomposites, surface physical, and surface chemical modification of biodegradable polymers, e.g., coating, grafting, impregnation, with non-hygroscopic and biodegradable materials, like starch, PLA and PHBV (Johansson et al. 2012; Larotonda et al. 2005; Morillon et al. 2002). Bio-based polymers applied as dispersion coatings on paper and paperboard for packaging applications and bioplastics provide sufficient barrier properties with respect to fats, but are usually only moderate water vapor barriers. Protein poses films that have potential for use in food packaging applications. These are used as barrier layers on paper and paperboard and have been made from whey protein/sodium caseinate as well as wheat gluten, soy proteins, and zein. Protein-based films often have very low oxygen transfer rates (OTR's) but high WVTR's due to their intrinsically hydrophilic nature (Johansson et al., 2012). Cellulose is the basic component of paper and can also be used as a coating to enhance the barrier properties. Nanoscaled cellulose fibers are promising as candidates for the preparation of bio-nanocomposites, owing to their high abundance, strength and stiffness, low weight, and biodegradability. There is a broad range of nanocellulose applications, the packaging sector being one area in which nanocellulose-reinforced polymeric films are of interest. Films can be produced with high transparency and with improved mechanical and barrier properties when compared with unfilled polymeric films (Spence et al., 2011; Ramires and Dufresne, 2011; Johansson et al., 2012). Microcrystalline cellulose, now more commonly referred to as nanofibrillated cellulose or NFC, has also seen a renaissance over the past two decades. Turbak et al. (1983) were the first to produce the microfibrillated cellulose (MFC) from wood. Nanofibrillated cellulose (NFC) has been used in different studies related to paper coating (Aulin et al., 2011; Hult et al., 2010; Syverud and Stenius, 2009). In general, modification of cellulose-fiber based material has influence on their water vapor or gas adsorption and transport. There are different techniques for characterizing cellulose and cellulose fiber-based materials in order to understand their properties when considering them for different applications.

2.2. Characterization Methods

2.2.1. Sorption Isotherms

Water vapor and gas sorption properties are important for the characterization of polymer membranes and films because they are relevant to the wide applications of these materials in the food, pharmaceutical, sensors, electronics, and biomedical fields (Metz, S.J., 2002; Gu and Alexandridis, 2004; Hancock et al., 1998; Han et al., 1998; Cornejo-

Bravo et al., 1996; Tsiapouris and Linke, 2000). Sorption isotherms are obtained from experimental measurements and represent the relationship between the sorbate (e.g., water vapor, O_2, CO_2, etc) content of an unloaded material (adsorbent sample) and the sorbate in the surrounding ambient, e.g., gas at constant temperature. Adsorption is the process in which the sorbate molecules attach to sites in solids, while desorption is the process of detachment of the sorbate molecules from the solid surface. The term sorption includes both processes. In some cases the sorption isotherm obtained when a material is losing sorbate, e.g., moisture, (desorption branch of isotherm) does not coincide with the isotherm when a material is gaining the sorbate, e.g. moisture, (adsorption branch of isotherm). This phenomenon is called hysteresis. The isotherm shape can provide qualitative means for the analysis of the adsorption processes. These results can also reveal isosteric heats of adsorption. The sorption of water vapor on materials is also useful to determine the hygroscopicity of a material under normal atmospheric conditions. The amount of water vapor that can be adsorbed by an adsorbent material depends on its chemical composition, physical-chemical state, and physical structure. There are two types of adsorption: physical and chemical adsorption. Generally, a molecule is physisorbed if the bond energy is less than 10 kcal/mole and chemisorbed if bond energy is more than 10 kcal /mole. In chemisorption there is a direct chemical bond involved while physical forces, e.g., van der Waals and electrostatic forces are responsible for physical sorption.

According to the International Union of Pure and Applied Chemistry (IUPAC) standard (Sing, *et al.*, 1985), porous materials can be classified into 3 categories: pores < 2 nm in diameter are micropores, pores in the range of 2-50 nm are mesopores, and pores > 50 nm are macropores. Generally, there are many different shapes of isotherms depending on the type of adsorbent/absorbate and intermolecular interactions between the gas and the surface. These have been formally classified by Brunauer et al. (1940). The Brunauer, Deming, Deming and Teller (BDDT) (1940) classification has also become the basis of the modern IUPAC classification of adsorption isotherms, as shown in Figure 2.2 (see also Brunauer, 1945; Hines and Maddox, 1985; Ruthven, 1985; Sing, 1985). Six broad categories of adsorption isotherms are shown in Figure 2.1 (Sing, 1985). Type I is classified as Langmuir type and commonly showed by microporous adsorbent that only form monolayer of sorbate molecules on the adsorption sites with relatively small external surfaces. A Type II isotherm is characteristic of the unrestricted monolayer-multilayer formation on the solid surface, which describes adsorption on non-porous or macroporous adsorbent with strong adsorbate-adsorbent interactions. This type of adsorption isotherm is known as the BET after Brunauer, Emmett, and Teller (1938). The Type III isotherm designates adsorption on non-porous or macroporous adsorbent with weak adsorbate-adsorbent interactions, e.g., unfavorable isotherm. The Type IV represents adsorption isotherm with hysteresis and is commonly associated with capillary condensation in mesopores. The type V adsorption is related to the Type III and represents adsorption isotherm with hysteresis and the pores present in the mesopore range. The Type VI adsorption isotherm forms stepwise multilayer adsorption on a uniform non-porous surface which is theoretically important, but rarely encountered (Sing, 1982). Types II, III, IV and V can be described by the BET isotherm model.

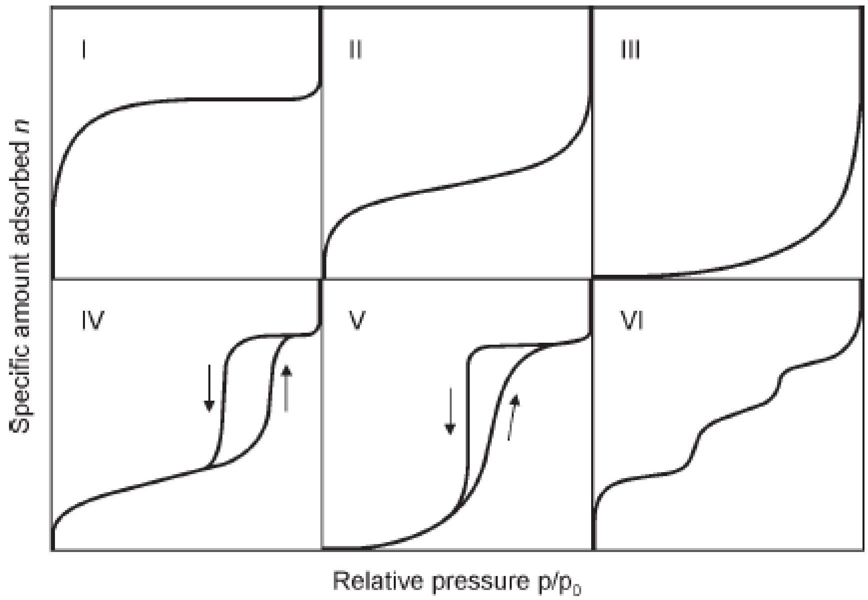

Figure 2.3. Classification of adsorption isotherms (Sing, 1985)

Gas adsorption measurements are widely used for determining the surface area and pore size distribution of different solid materials. The measurement of adsorption is an essential part to investigate the nature and behavior of solid surfaces. A number of models have been developed to fit adsorption isotherms and to analyze surface area, pore size distribution, and to estimate the formation of sorbate in the solid surface.

2.2.1.1. Adsorption Isotherm Models

A number of mathematical models have been developed to describe the adsorption process and some of them are Langmuir isotherm, Freundlich isotherm, BET (Brunauer, Emmett and Teller) isotherm, Guggenheim Anderson de Boer (GAB) isotherm. Brunauer, Emmett and Teller reported the multilayer adsorption theory (BET theory) and they extended the Langmuir's monolayer theory to multilayer adsorption (Brunauer et al., 1938). The BET equation has been utilized to determine the monolayer volume of adsorbed gas, from which the surface area of adsorbent can be calculated (Brunauer et al., 1938). In this study, the BET equation was also used for the calculation of water vapor adsorbed as a monolayer on the surface of solid material:

$$\frac{x}{M\,(1-x)} = \frac{1}{M_h C} + \frac{(C-1)x}{M_h C} \qquad 2.1$$

M_h is the moisture content in % corresponding to a monolayer, x is the partial vapor pressure of water, and M is the moisture content at x. C is a constant, which is approximately equal to $\exp\{(\mathrm{E}_1 - \mathrm{E}_\mathrm{L})/\mathrm{RT}\}$, where E_1 is the heat of adsorption on the first and E_L that on the succeeding layers.

The BET equation is also considered to be a general method for practical surface area determination by using nitrogen adsorption at 77K. The monolayer moisture content M_h can be related to the specific surface area A_c (m^2/g) of the materials by

$$A_c = M_h \frac{N_A}{M_W} a_w \qquad 2.2$$

where N_A is the Avogadro's number, M_W is the molecular weight of water, and a_w is the area of water molecule projected to material surface, e.g. for cellulose surface it is estimated at about $14.8 \times 10^{-20} m^2$ /molecule (Li, 1991; Daniel and Olle, 2001).

Guggenheim Anderson de Boer (GAB) Model is an extension of the BET method, which includes the concept of an intermediate state of vapor between the first layer and condensed upper layers. The concept enabled Guggenheim, Anderson and de Boer to independently derive a formula (the GAB model) that produces better fits at high pressures (Anderson, 1946; Guggenheim, 1966; de Boer, 1968). The GAB model is commonly applied to fit the water vapor adsorption of food and cellulose-based materials.

Sorption isotherms of active polar vapors (e.g., water) by cellulosic materials of sigmoidal shape, similar to multilayer adsorption isotherms are reported in most literatures (Chirkovo at el., 2007; Ioelovich et al., 2011). Different techniques of paper preparation, such as beating and bleaching, may also affect the adsorption isotherm shape. Beating is a physical treatment carried out on pulp (mixture of pulp and water) in order to improve the strength of the finished paper sheet (Parker et al., 2006). It serves the purpose of increasing the contact area between the fibers, thus improving hydrogen bonding potential by increasing the surface concentration of free hydroxyl groups. As a result, beaten Kraft paper and pulp have higher equilibrium moisture contents than unbeaten pulps. Further, there is an increase in the volume of fine structure capillaries that allow condensation to occur more easily (Seborg et al., 1931). Bleaching of pulp in the paper making is a chemical process that is used to increase the whiteness of the paper. Seborg et al. (1936) reported that the bleaching produced a marked decrease in the hygroscopicity of the spruce and silver fir sulfite pulps, i.e., a decrease in the equilibrium moisture content compared to unbleached pulp.

Water vapor adsorption isotherm on hydophobic polyethylene, Teflon, and polytetrafluoroethylene powder are reversible and of type-III in shape. Polyethylene polymer has a limited heterogeneity in the surface, with heat of about 2 kcal/mol above the heat of condensation at low coverage based on calorimetrically measured differential adsorption heats (Cadenhead et al., 1974).

2.2.2. Gas and water vapor transmission rates and permeability

Permeability of package material is one of the main factors in determining application fields and content material quality. Since vapor and gases, such as oxygen and carbon dioxide, permeating through the package will exert obvious influences on product quality; material with proper permeability should be selected to design package for specific products. There are different method/techniques in measuring gas permeability in a film, e.g, the differential pressure method and the equal pressure method (Labthink, 2012).

Permeation processes through polymer materials include collision with the polymer surface, sorption on the high permeant concentration side, diffusion through the material, and finally desorption of the permeant on the low concentration side. The permeation process can be described mathematically by Fick's first law. The flux (*J or N*) of molecules through the material, which is proportional to the concentration gradient normal to the section, can be expressed in one direction as follows:

$$J = -D_{eff} \frac{\partial C}{\partial Z} \qquad 2.3$$

where *J (or N)* is the flux which is the net amount of solute that diffuses through unit area per unit time ($g/m^2.s$ or $ml/m^2.s$); D_{eff} is the effective diffusivity (m^2/s); *dC* is the differential of concentration of the diffusing substance in the film (g/m^3 or ml/m^3), and *dZ* is the differential thickness of the film (m) (Crank, 1975). If the diffusion is at steady state and the diffusion coefficient and diffusion area are constant, then the flux (*J*) can be obtained by a direct integration of Eq. 2.3 and given by:

$$J = -D_{eff}\frac{C_2 - C_1}{Z} = \frac{Q}{A \times t} \qquad 2.4$$

where Q is the amount of gas diffusing through the film (g or ml), C_2 and C_1 are concentrations in the film (g/m^3 or ml/m^3), Z is a thickness of the film, A is the area of the solid (film) (m^2), and t is the time (*s*). The application of Henry's law, e.g., low concentration region, allows expression of the driving force in terms of the partial pressure differential of gas. Re-arrangement of the terms yields the following equation in terms of permeability.

$$\frac{Q}{A \times t} = D \times S\,\frac{p2 - p1}{Z} = P\,\frac{\Delta p}{Z} \qquad 2.5$$

where S is Henry's law constant (solubility) given in *mol/m*^{3}*.atm or g/m*^{3}*.pa*, Δp is the partial pressure difference of the gas across the film (*Pa*), and P is permeability ((*ml or g*). *m/ m*^{2}*.s. Pa*). According to the "solution-diffusion" model developed by Londsdale (Lonsdale et al., 1965), a permeant (a diffusing gas or vapor) dissolves in the membrane material and passes through by diffusion in response to a concentration gradient. Solubility is the process of adsorption of sorbate in the polymer and depends on the affinity (interaction energy) of the polymer for the adsorbing molecule, the volume available for adsorption in the polymer, and the external sorbate concentration. Diffusion is the concentration gradient driven process whereby the adsorbed molecules are transported within the polymer and diffusion properties are characterized via diffusion coefficients. The model defines three terms: flux, described by the permeability coefficients P; equilibrium water concentration, described by the solubility coefficients

(S); and diffusivity, described by the diffusion coefficient (D). Therefore, the permeability of gases and water vapor can be calculated from the following equation:

$$P = S \times D \qquad 2.6$$

The permeability coefficient can also be calculated using the measured flux, J, according to Eq. 2.6. The flux of water vapor/gas can be obtained from the slope of the mass of the water/gas permeating through the film versus time:

$$P = \frac{J \times Z}{(A \times \Delta p)} \qquad 2.7$$

where J is the mass of water/gas permeating, Z is the thickness of the film, and Δp is the difference between the water vapor pressure across the film.

The diffusion coefficients can be related to temperature (T) by the Arrhenius expression given in Eq. 2.8:

$$D = -D_0 exp\left(\frac{-E}{R \times T}\right) \qquad 2.8$$

Similarly, permeability can also be related to temperature (T) by an Arrhenius expression:

$$P = -P_0 exp\left(\frac{-E_p}{R \times T}\right) \qquad 2.9$$

In the equations above (Eq. 2.8-Eq. 2.9), D_o and P_o are a pre-exponential factors, R is universal gas constant, and E and E_p are the activation energy and activation energy associated with the permeation, respectively.

The diffusion coefficient depends not only on temperature but also on the concentration of diffusing species and the composition of the matrix. Under the unsteady state circumstance at which the penetrant accumulates in the certain element of the system, Fick's second law describes the diffusion process in one dimension by Eq. 2.10 (Comyn, 1985; Crank and Park, 1968) as follows:

$$\frac{\partial C}{\partial t} = \frac{\partial}{\partial x}\left[D\,\frac{\partial c}{\partial x}\right] \tag{2.10}$$

Sorption kinetics can be conveniently analyzed from experimental measurements and is commonly used to study the diffusion of small molecules in polymers. Diffusion coefficient can be calculated from the uptake measurement data recorded at fixed temperature. In this technique, a polymer film of thickness 2*L* is immersed into the infinit bath of penetrant, then concentrations, *c(t)* , at any point within the film at time *t*, according to the solution of the Fick's second law (Eq. (2.10)) for slab geometry, is given by Eq. 2.11 (Comyn, 1985).

$$\frac{c(t)}{c(\infty)} = 1 - \frac{4}{\pi^2}\sum_{n=0}^{\infty}\frac{(-1)^n}{(2n+1)^2}\; exp\left(-\frac{\pi^2(2n+1)^2 D_{eff}}{4L^2}t\right) \times cos\left(\frac{(2n+1)\pi x}{2L}\right) \tag{2.11}$$

where c(∞) is the amount of accumulated penetrant at equilibrium, i.e., the saturation equilibrium concentration within the system, 2L is the thickness of the film x is a coordinate in that direction. Integrating Eq. 2.11 for the whole slab thickness 2L and fixed time t, yields Eq. 2.12 giving the adsorbed mass M(t) as a function of time t relative to the mass at equilibrium, M (∞), i.e., fractional uptake.

$$\frac{M(t)}{M(\infty)} = 1 - \frac{8}{\pi^2} \sum_{n=0}^{\infty} \frac{1}{(2n+1)^2} \; exp\left(-\frac{\pi^2 (2n+1)^2 D_{eff}}{4L^2} t\right) \qquad 2.12$$

The short time solution of Eq. 2.12, e.g., M (t)/M (∞) ≤0.5 can be represented as follows (Gu and Alexandridis, 2004; Balik, 1996):

$$\frac{M(t)}{M(\infty)} = \frac{4}{L}\left(-\frac{D_{eff}}{\pi} t\right)^{1/2} \qquad 2.13$$

For the long time, e.g., M (t)/M (∞) ≥0.), only the first term of Eq. 2.12 is considered, and the solution is given as:

$$\frac{M(t)}{M(\infty)} = 1 - \frac{8}{\pi^2} \exp\left[-\frac{D_{eff} \pi^2}{4L^2} t\right] \qquad 2.14$$

The thickness of the film is an important parameter that affects the kinetics of diffusion besides the diffusion coefficient, as can be seen from Eqs. 2.12-2.14.

There are various mechanisms of diffusion processes in solids that depend on the structure of the solid and the nature of the process. Diffusion through porous materials could be molecular or bulk, Knudsen, and surface diffusion. Bulk diffusion occurs when the pore diameter of the material is large in comparison to the mean free path of the gas molecules. Knudsen diffusion is the transport mechanism through pores that are small in comparison to the mean free path of the gas, e.g., mesopores. The third type of mechanism for molecule transport in porous materials is surface diffusion, and in this case, the adsorbed molecules on the surface of the solid transport from one site to another in the direction of decreasing concentration. Due to strong sorbate-adsorbent interactions this process is an activated process, unlike other two mechanisms. However, in most cases surface diffusion has been assumed to contribute little to the overall transport in nonhyrophilic porous materials (Hines and Maddox, 1985).

In addition to the dependency of the permeability of polymer films on temperature and relative humidities, the intrinsic polymer structure affects the permeability of the polymer films. The permeability of polymer materials depends on the internal structure of the polymer such as a degree of crystallinity, crystalline to amorphous ratio, nature of polymer, chemical properties (e.g., polarity), degree of cross-linking, and glass transition temperature (Mrkić et al., 2006; Galić et al., 2000). The higher crystallinity fraction of a semicrystalline polymer, the lower the water solubility in the polymer (Van Krevelen, 1990). In addition, the degree of crystallinity greatly reduces the permeability of gas and water vapor molecules because of the closer structural packing in crystalline parts, which renders diffusion path of a sorbate molecule more obstracted (Vieth, 1991; Kuusipalo, 2000). The apparent activation energy of water diffusivity in low density polyethylene (LDPE) and isotactic polypropylene (iPP) polymers are 59.4 and 67.8 kJ/mol, respectively (Hedenqvist and Gedde, 1996). Low density polyethylene (LDPE) and high density polyethylene (HDPE) polymers have water vapor permeability of $1.0\text{-}1.5\times10^{-13}$ and $3\text{-}4\times10^{-14}$ g/m.s.Pa , respectively, at RH=90% and T=38 ^{o}C (Ashely, 1985).

2.2.3. Sorbate-substrate interaction studies

Water molecules are highly dipolar, and this character is due to the high electronegativity of oxygen compared to hydrogen. Partial electrostatic charges due to this difference in electronegativity result in strong interactions of water and other charged or polar groups. In the surface of polymers, it is common for sorbed water molecules to exist at least in three different states or forms (van der Wel and Adan, 2000; Nakamura et al., 1983; Hodge et al., 1996). The first form is a single water molecule, which neither shows significant interaction with other molecules nor with its environment. The second form is a formation of water molecules in agglomerates or clusters, due to interactions with other molecules. The third form is the molecules that interact with polymer groups. Fourier transform infrared spectrometry (FT-IR), nuclear magnetic resonance (NMR), thermogravimetric analysis (TGA) and differential scanning calorimetric (DSC) techniques are commonly used to investigate the state of water present in the materials and also to determine the interaction between the sorbate-solid surfaces (Froix and Nelson, 1975; Nakamura et al., 1981; Ping et al., 2001; Topgaard and Soderman, 2002; Weise et al., 1996). These techniques categorized the sorbed water in fiber into three different forms, e.g., unbound water, freezing bound, and non-freezing bound water, based on the water associated with cellulose fibers. Infrared spectroscopy provides quantitative and qualitative chemical analysis information. Water content of polymers and adhesives can be quantified using infrared spectroscopy (Roberts et al., 1994). Near infrared regions contain bands suitable for determining water in many solids, liquids and gases. The 4000-1600 cm^{-1} is the fundamental region that has been used to study water in most materials. The region in the frequency range of 4000-3000 cm^{-1} (i.e., the O-H stretching band) is commonly used to determine the strength between the water molecule-surface interactions of materials. Simultaneous DSC-TGA analysis can also be used to assess the binding energy between water and the surface directly (Ruckold et al., 2003). In this study, simultaneous TGA-DSC techniques and FT-IR were used to investigate the state of water vapor on the fiber materials and also the strength of interaction between the water vapor and surface. In addition, TGA-DSC was used in determining the glass transition temperature (Tg), the melting point (Tm), and the percentage of crystallization of polymers. Glass transition temperature (Tg) is the point at which the polymer hardens into an amorphous solid. Polymers such as most of the polyamide (nylon), polypropylene, polyethylene, and the thermoplastic polysters (PET) are semi-crystalline materials. The percentage of crystallinity of polyethylene and polypropylene are ranges between 45-80%. In addition, the glass transition temperature of synthetic materials (e.g., polyethylene, polypropylene, Teflon) are between -20 ^{o}C to -125 ^{o}C (Fakirov and Krasteva, 2000; Rae and Dattelbaum, 2004).

2.3. Factors Affecting Mass Transport in Polymeric Materials

Polymers cover a wide range of materials where the principal component consists of long chain of organic polymer molecules. These materials can exhibit a wide range of mass transport properties (Duncan et al., 2005). The mass transport of small molecules into polymers is a function of both the polymer and the diffusing molecule. Factors which influence permeability include the following:

2.3.1. Polymer Chemistry

The chemical composition of the polymer matrix can influence the mass transport properties, e.g., solubility and diffusion of small molecules through the polymer. Polymers with polar chemical groups, such as cellulose or nylon, have a strong affinity for polar molecules including water vapor molecules. However, non-polar polymers (e.g., polyethylene or polypropylene) have much lower affinity toward polar molecules. In polar matrices, the diffusion coefficients and solubility of polar molecules can increase due to strong interactions between the molecules and polymer chains that induce structural transformations such as swelling and dissolution of the polymer matrix (Crank and Park, 1968). Coating the polar polymer surface with less polar or non-polar polymer has been used to reduce the water vapor adsorption and increase barrier properties of a film (Andersson, 2008; Rhim et al., 2007; Schuman et al., 2004; Kuusipalo, 2000). Bio-polymers such as polylactic acid (PLA), poly(ε-caprolactone) (PCL), poly (hydroxybutyrate-co-valerate) (PHB/V), starch film, hydroxypropyl (HPC), poly(vinyl alcohol) (PVOH), and PCL-chitosan films are recommended as a first choice in the development of new functionalities of paper-based materials due to their biodegradable properties (Andersson, 2008).

2.3.2. Crystallinity

Crystallites are generally considered impermeable for all non-reactive molecules, even though the smallest gases may penetrate the crystalline matrix (Vieth, 1991; Hedenqvist and Gedde, 1996). Crystallinity regions in polymers are more ordered than amorphous regions and free volume will be lower in these regions. The crystal structure lacks both the sorption sites as well as the mobility of the chains to allow high mass transfer of gas molecules. Semicrystalline polymers generally exhibit better barrier properties than amorphous polymers. In most cases, penetrants do not dissolve in the crystalline region of semi-crystalline polymers (Hedenqvist and Gedde, 1996). Shogren (1997) reported that high crystalline biodegradable materials reduced water vapor transmission properties.

2.3.3. Porosity and Voids

Pores and voids provide space and sites into which molecules can be adsorbed and thus provides less transport barrier properties compared to a solid polymer. Pores may also provide sites into which liquids and vapors can condense and thereby dramatically increase the uptakes. A high level of porosity will increase permeability by increasing both the solubility and the effective diffusion coefficient. If pores are linked (open pores), then diffusion rates through these channels will lead to much higher permeation than if the pores are isolated (closed pores). Coating and filler adding on a porous solid surface can also reduce surface porosity, and air and vapor permeability (Kugge and Johnson, 2008; Syverud and Stenius, 2009; Spence et al., 2011).

2.3.4. Pigments and Filler Particles

Filler particles are usually employed to fill the voids or pores in the polymers, thus modifying their physical and processing properties and barrier performance. Most fillers are cheap natural minerals and can also be used to reduce the cost of polymer coating polymer (Andersson, 2008). Pigments and filler particles (e.g., clay, talc, quartz, chalk, calcium carbonate, iron oxide, titanium dioxide or aluminium flakes) can influence the gas and vapor adsorption behavior depending on the solubility and diffusion coefficient of penetrant molecules in the filler relative to the polymer matrix (Andersson, 2008; Duncan et al., 2005). Filler particles increase path lengths (tortuosity) of the diffusing molecules, through the film, which leads to reduced mass transport rates, e.g., reduced effective diffusivity. Nano-sized fillers can be expected to provide improved barrier properties of polymers due to increased lengths of diffusion paths (Andersson, 2008; Plackett et al., 2006; Spence et al., 2011). Pigmentation can significantly lower moisture transport through coatings. However, factors like incomplete dispersion, flocculation, and poor binding between pigment and polymer may lessen this effect substantially and may even lead to an overall rise in moisture transport compared to non-pigmented films (van der Wel, and Adan, 2000).

2.3.5. Temperature

Temperature significantly affects thermodynamics and kinetics properties, thus affecting the permeability and diffusion of molecules in polymers (Auras et al., 2004; Morillon et al., 2002). As the temperature increases, the mobility of the molecular chains increases and thermal expansion leads to a reduced density. Therefore, the free volume in the system will increase, leading to an increased solubility. Adsorption and diffusion phenomena normally follow Arrhenius temperature behavior.

2.3.6. Concentration

Henry's law for ideal gas absorption states that solubility is directly proportional to the external gas pressure. Some systems seem to exhibit two stage absorption processes; a Henry's law type process at low concentrations and a second process occurring once a critical concentration is reached (Crank and Park, 1968). Diffusion coefficients can be highly dependent on concentration if there is a significant interaction between the diffusing species and the polymer (Duncan et al., 2005). The concentration of diffusing molecules within the polymer may influence their diffusion properties. Diffusion is driven by concentration gradient, and initially high external concentrations imply high concentration at the surface causing large concentration gradient and, hence, rapid diffusion. The permeability of hydrophilic films depends both on the relative humidity difference (ΔRH) or mass transfer driving force across the film, and on the absolute humidity value. For the same RH gradient, the permeability increases with the vapor pressure; however, the effect of RH gradient is less important for hydrophobic films (Morillon et al., 2002).

2.3.7. Molecular Size

The size and shape of the diffusing molecules influence the diffusivity. Small gas molecules can diffuse faster than larger ones, because diffusion of larger molecules is generally more hamperd by the size of pores, e.g., proximity of sorbate molecules and active sites, thus requiring higher activation energies for diffusion. Water is a polar compound having small size that tends to favour both sorption and diffusion in dense materials, which are then more permeable to moisture than to non-condensable gases (Morillon et al., 2002).

References

Andersson, C. (2008). New ways to enhance the functionality of paperboard by surface treatment – a review**.** Packag. Technol. Sci., 21(6), 339-373.

Anderson, R. (1946). Modifications of the BET equation, J. Am. Chem. Soc., 68, 686–691.

Ashely, R.J. (1985). Permeability and plastic packaging, in: polymer Permeability, Comyn J (Ed.). Elsevier Applied Science: London, UK, pp. 269-308.

Auras, R., Harte, B. and Selke, S. (2004). Effect of water on the oxygen properties of polyethylene tetraphalate and poly (lactide) films, J. Appl. Polym. Sci., 92(3), pp 1790-1803.

Aulin, C., and Lindstrom, T. (2011). Biopolymer coatings for paper and paperboard. In Plackett, D. (ed.) Biopolymers-new materials for sustainability films and coatings, John Wiley and Sons Ltd, Chichester, West Sussex, UK, Chapter 12.

Averous, L. and Pollet, E. (2012). Biodegradable Polymers. Environmental Silicate Nano-Biocomposites, Green Energy and Technology, DOI: 10.1007/978-1-4471-4108-2_2,_ Springer-Verlag London 2012.

Balik, C.M. (1996). On the extraction of diffusion coefficients from gravimetrical data for sorption of small molecules by polymer thin films. Macromolecules, 29, 3025-3029.

Brunauer, S. (1945). The adsorption of Gases and Vapors. Princeton University Press, Princeton, N.J.

Brunauer, S., Deming, L, Deming, W., Teller, E. (1940). J. Am. Chem. Soc., 62, 1723.

Brunauer, S., Emmett, P.H., and Teller, E. (1938). Adsorption of Gases in Multimolecular Layers. J. Am. Chem. Soc., 60 (2), 309-319.

Cadenhead, D.A., Danielli, J.F., and Rosenberg, M.D. (1974). Progress in surface and membrane science, Voulme 8, Academic press, Inc., New York, USA, pp. 285-299.

Chirkova, J., Andrsons, B., and Andersone, I. (2007). Study of the structure of wood-related biopolymers by sorption methods. BioResour., 4(3), 1044-1057.

Cornejo-Bravo, J.M.; Siegel, R. Water vapour sorption behavior of copolymers of N, N-diethylaminiethyl methacrylate and methyl methacrylate. Biomater. 1996, 17, 1187 – 1193.

Crank, J. and Park, G.S. (1968). Diffusion in Polymers, Academic Press, London.

Comyn, J. (1985). Introduction to Polymer Permeability and the Mathematics of Diffusion, In: Polymer Permeability, J. Comyn, 1-10, Elsevier Appl. Sci., ISBN 0-85334-322-5, Northern Ireland.

de Boer, J.H. (1968). The Dynamic Character of Adsorption (Oxford: Clarendon).

Duncan, B., Urquhart, J. and Roberts, S. (2005). Review of Measurement and Modelling of Permeation and Diffusion in Polymers. National Physical Laboratory (NPL) Report DEPC MPR 012.

Fakirov S. and Krasteva, B. (2000). On the Glass transition temperature of polyethylene as revealed by microhardness measurements. J. Macromol. Sci.—Phys., B39 (2), 297–301.

Froix, M.F. and Nelson, R. (1975). The interaction of water with cellulose from nuclear magnetic resonance relaxation times. Macromol. 8(6), 726-730.

Galić, J., Galić, K., Kurtanjek, M. and Ciković, N. (2000): "Gas permeability and DSC characteristics of polymers used in food packaging," Polym. Test., 20(1), 49–57.

Gu, Z and Alexandridis, P. (2004). Sorption and Transport of Water Vapor in Amphiphilic Block Copolymer Films. J. of Dispers. Sci. & Technol., 25(5), 619-629.

Guggenheim, E.A. (1966). Applications of Statistical Mechanics. Oxford: Clarendon Press.

Haase, R. and Siry, M. (1968). Z. Phys. Chem. Frankfurt, 57, 56-73.

Hodge, R.M., Bastow, T.J., Edward, G.H., Simon, G.P., Hill, A.J.(1996). Free volume and the mechanism of plasticization in water-swollen poly(vinyl alcohol), Macromol., 29, 8137-8143.

Hancock, B.C.; Shamblin, S.L.(1998): Water vapour sorption by pharmaceutical sugars. Pharm. Sci. Technol., 1, 345 –351.

Han, H.; Seo, J.; Pyo, S.M.; Gryte, C.C. (1998). Water sorption and diffusion behaviours in thin films of photosensitive polyimides. Polym., 39, 2963 – 2972.

Haslach Jr., H. W., (2000): The moisture and rate-dependent mechanical properties of paper: A review. Mechanics of Time Dependent Materials 4: 169-210. @2000 Kluwer Academic Publishers. Printed in the Netherlands.

Hedenqvist, M. and Gedde, U.W. (1996). Diffusion of small-molecule penetrants in semicrystalline polymers. Prog. Polym. Sci., 21, 299-333.

Hines, A.L. and Maddox, R.N. (1985). Mass transfer fundamentals and application. Prentices-Hall, Inc., Englewood Cliffs, New Jersey 07632.

Hult, E.L., Iotti, M., and Lenes, M. (2010). Efficient approach to high barrier packaging using microfibrillated cellulose and shellac. Cellulose, 17(3), 575-586.

Ioelovich, M. and Leykin, A. (2011). Study of Sorption Properties of Cellulose and Its Derivatives. BioResour. 6(1), 178-195.

Johansson, C., Bras, J., Mondragon, I., Nechita, P., Plackett, D., Simon, P. et al. (2012). Renewable Fibers and Bio-based materials for packaging applications-A review of recent development. BioResour. 7(2), 2506-2552.

Khare, V.P., Greenberg, A.R., Kelley, S.S., Pilath, H., Roh, II J., Tyber, J. (2007). Synthesis and characterization of dense and porous cellulose films. J. Appl. Polym. Sci., 105, 1228-1236.

Kishimoto, A., Fujita, H., Odani, H., Kurata, M. and Tamura, M. (1960). Successive Different Absorption of Vapors by Glassy Polymers. J. Phys. Chem. 64, 594-598.

Kugge, C. and Johnson, B. (2008). Improved barrier properties of double dispersion coated liner. Prog. in Org. Coat., 62, 430-435.

Kuusipalo, J. (2000). PHB/V in Extrusion Coating of Paper and Paperboard-Study of Functional Properties-Part II. J. Polym. and the environ. 8(2), 49-57.

Labthink (2012): http://www.labthinkinternational.com.cn/literatures/testing-methods-and-instruments-of-gas-permeability.html. Testing Methods and Instruments of Gas Permeability.

Larotonda, F.D.S, Matsui, K.N., Sobral, P.J.A., Laurindo, J.B. (2005). Hygroscopicity and water vapor permeability of Kraft paper impregnated with starch acetate. J. Food Eng. 71, 394-402.

Lonsdale, H.K., Merten, U., Riley, R.L. (1965). J. Appl. Polym. Sci. 9, 1341.

Morillon, V., Debeaufort, F., Blond, G., Capelle, M. and Voilley, A. (2002): Factors Affecting the Moisture Permeability of Lipid-Based Edible Films: A Review. Critical Reviews in Food Sci. and Nutr., 42(1), 67-89.

Mrkić, S. Galić, K., Ivanković, M., Hamin, S. and Ciković, N. (2006): "Gas transport and thermal characterization of mono- and Di-polyethylene films used for food packaging," Journal of Appl. Polym. Sci., 99(4), 1590–1599.

Nakamura, K., Hatakeyama, T., and Hatakeyama, H. (1983). Relationship between hydrogen bonding and bound water in polyhydroxystyrene derivatives, Polymer, 24,871-876.

Nakamura, K., Hatakeyama, T., and Hatakeyama, H. (1981). Studies on bound water of cellulose by differential scanning calorimetry. Text. Res. J. 51(9), 607-613.

Parker M.E., Bronlund, J.E. and Mawson, A.J. (2006). Moisture Sorption Isotherms for Paper and Paperboard in Food Chain Conditions, Packag. Technol. Sci., 19, 193-209.

Ping, Z.H., Nguyen, Q.T., Chen, S.M., Zhou, J.Q., and Ding, Y.D. (2001). State of water in different hydrophilic polymers-DSC and FTIR studies. Polym. 42(20), 8461-8467.

Plackett, D.V., Holm, V.K., Johansen, P. et al. (2006). Chracaterization of L-polylactide and L-polylactide-polcaprolactone co-polymer films for use in cheese-packaging applications. Packag. Technol. Sci., 19, 1-24.

Rae, P.J., and Dattelbaum, D.M. (2004). The properties of poly(tetrafluoroethylene) (PTFE) in compression. Polym. 45, 7615-7625.

Ramires, E.C., and Dufresne, A. (2011). “A review of cellulose nanocrystals and nanocomposites,” TAPPI J., 9-15.

Rhim, J.W., Lee, H.H., Hong, S.I. (2007). Increase in water resistance of paperboard by coating with poly (lactide). Packag. Technol. Sci. 20(6), 393-402.

Ruckold, S., Isengard, H.D., Hanss, J., Grobecker, K.H. (2003). The energy of interaction between water and surfaces of biological reference materials. Food Chem. 82, 51-59.

Ruthven, D.M. (1984). Principles of adsorption and adsorption processes. A Wiley-Interscience publication, pp. 124-126.

Roberts, S. S.J., Dawson, J., Yates, T. (1994): Sensing Techniques for Detection of Water in Adhesives, AEA Technology Report AEA/TPD 91.

Rogers, C.E. (1965). Solubility and Diffusivity in physics and Chemistry of the organic solid state. Ed. Fox D. et al. Interscience Publ. New York.

Schuman, T., Wikstrom, M., Rigdahl, M. (2004). Dispersion coating with carboxylated and cross-linked styrene-butadiene lattices. 1. Effect of some polymer characteristics on film properties. Prog. Org. Coat. 51, 220-227.

Seborg C.O., Stamm AJ. (1931). Sorption of water vapor by papermaking materials: Effect of beating, Industrial and Engineering Chemistry, 23, 1271-1275.

Seborg C.O., Stamm AJ. (1936). Sorption of water vapor by papermaking materials: Effect of physical and chemical processing, Industrial and Engineering Chemistry, 28 (11), 1245-1250.

Sing, K.S. W. (1982). Reporting physisorption data for gas/solid systems. Pure and Appl. Chem., 54 (11), 2201-2218. Pergamon Press Ltd.

Sing, K. S. W., Everett, D.H., Haul, R.A., Moscou, L., Pierotti, R.A., Rouquerol, J. and Siemieniewska, T. (1985): "Reporting Physisorption Data for Gas/Solid Systems with Special Reference to the Determination of Surface Area and Porosity (Recommendations 1984)," Pure and Appl. Chem. 57, 603-619.

Spence, K.L, Venditti, R.A., Rojas, O.J., Pawlak, J.J., Hubbe, M.A. (2011): Water vapor barrier properties of coated and filled microfibrillated cellulose composites. BioResour. 6(4), 4370-4388.

Syverud, K. and Stenius, P. (2009). Strength and Barrier properties of NFC films. Cellulose 16, 75-85.

Tanner, D. and Amos, N. (2006). Paper and Card Packaging of Frozen Foods. Handbook of Frozen Food Processing and Packaging, Taylor & Francis Group, LLC. pp. 653-665.

Topgaard, D. and Soderman, O. (2002). Changes of cellulose fiber wall structure during drying investigated using NMR self-diffusion and relaxation experiments. Cellulose 9(2), 139-147.

Tsiapouris, A.; Linke, L. (2000): Water vapor sorption determination of starch based porous packaging materials. Starch-Sta¨rke, 52, 53 –57.

Turbak, A.F., Snyder, F. W.; Sandberg, K. R., (1983). Microfibrilated cellulose, a new cellulose product: properties, uses, and commercial potential. J. Appl. Polym. Sci.: Appl. Polym. Symp., 37: 815-827.

van den Akker, J.A.(1970): 'Structure and tensile characteristics of paper', Tappi 53(3), 388-400.

van der Wel, G.K. and Adan, O.C.G. (2000). Moisture transport and equilibrium in organic coatings. HERON, 45(2), 125-152. ISSN 0046-7316.

Van Krevelen, D.W. (1990). Properties of Polymers. Elsiever Science, Amesterdam.

Vieth, W.R. (1991). Diffusion In and Through Polymers. Carl Hanser Verlag, Munich.

Vyas, S., Pradhan, S.D., Pavaskar, N.R., Lachke, A. (2004). Differential Thermal and Thermogravimetric Analyses of Bound Water Content in Cellulosic Substrates and Its Significant During Cellulose Hydrolysis by Alkaline Active Fungal Cellulases. App. Biochem. and Biotechnol. 118, 177-188.

Shogren, R. (1997). Water Vapor permeability of biodegradability polymers. J. Of Environ. Polym. Degrad. 5(2), 91-95.

Wadso, L., (1992). A Critical review on Anomalous or Non-Fickian vapor Sorption. Published as internal report 7017. Division of Building Materials. Lund University.

Weise, U., Maloney, T. and Paulapuro, H. (1996). Quantification of water in different states of interaction with wood pulp fibers. Cellulose 3(4), 189-202.

Zhou, C. and Wu, Q. (2012): Recent Development in Applications of Cellulose Nanocrystals for Advanced Polymer-Based Nanocomposites by Novel Fabrication Strategies. In Nanotechnology and Nanomaterials » "Nanocrystals - Synthesis, Characterization and Applications".

Chapter 3: Mass transfer of water vapor, carbon dioxide and oxygen on modified cellulose fiber-based materials

Alemayehu H. Bedane[a], Qinglin Huang[b], Huining Xiao[c] and Mladen Eić[c]

University of New Brunswick

Nordic Pulp and Paper Res. J. 27(2); 409-417, 2012

[a]Graduate Student, Department of Chemical Engineering, UNB

[b]Research Associate, Department of Chemical Engineering, UNB

[c]Professor, Department of Chemical Engineering, UNB

Abstract

Mass transfer properties of fibre network and coated paper are essential for understanding the barrier properties of the products and further advance in their application. In this study, different unmodified and coated papers, e.g., (Poly lactic acid (PLA), zein grafted paper) were prepared and characterized with regard to mass transfer properties. Water vapor, carbon dioxide (CO_2) and oxygen (O_2) transmission rates through the cellulose paper films were measured and the results discussed. The effects of sample film thickness and temperature on water vapor transmission rates (WVTR's) were also examined. The WVTR's of the investigated samples were found to be strongly dependent on the temperature and the relative humidity difference (mass transfer driving force). On the other hand, water vapor permeabilities (WVP's) were found independent of relative humidity.

Water vapor diffusivities of the samples were also measured from the uptake rate measurements using Fickian diffusion slab model for a wide range of relative humidities. WVTR's and vapor diffusivity of the modified samples were found to be generally low compared to unmodified (reference) paper sample. Among the investigated samples, PLA/polyhedral oligomeric silsesquioxane (POSS)-bentonite modified paper sample showed higher mass transfer resistance to water vapour and the gases investigated in this study (CO_2 and O_2). It showed lower water transmission rate (104 g/m^2.day) compared to PLA-coated paper (130 g/m^2.day), zein coated paper (179 g/m^2.day) and control sample (659 g/m^2.day) at the relative humidity gradient ΔRH=74% and temperature of 25^{o}C. The oxygen transmission rate for PLA/(POSS-bentonite) coated paper was found to be lower than for the other modified papers. Zein grafted paper showed better barrier property for

water vapor than oxygen. Water vapor permeation through paper films shows an Arrhenius type of dependency with temperature, indicating activated process. The activation energies reveal diffusion dominated process for all paper samples investigated in this study, according to the solution-diffusion mechanism used to describe the permeation processes.

Keywords: modified paper, water vapor transmission rate, gas transmission rate, relative humidity, effective diffusivity.

3.1. Introduction

Chemically-modified wood fibres and fibre networks along with surface treatment of paper play a central role in rendering fibres hydrophobic and oleophobic, which improve barrier properties of the conventional paper products. Cellulose fiber-based materials have been utilized as common packaging materials, substituting plastic materials, because they are considered more environmentally friendly. Biodegradable materials such as starch, poly lactic acid (PLA), corn- zein and cellulose derivatives have been used as common coating materials in order to improve the barrier properties (Jansson et al., 2005; Kugge et al., 2008; Andersson, 2008). PLA polymers have acquired increasing attention in the last few years as food packaging materials, because they can be obtained from renewable resources, in addition to being recyclable and compostable. The chemistry of PLA involves the processing and polymerization of lactic acid monomer. This monomer can easily be produced by fermentation of carbohydrate feedstock. The carbohydrate feedstock may be agricultural products such as maize, wheat or alternatively may consist of waste products from agricultural or the food industry (Gupta et al., 2007). Zein is a protein that is derived from corn grains and can also be used as a potential material for the preparation of edible and biodegradable film, because of its hydrophobicity and impermeability to gases (Lawton, 2002; Padua and Wang, 2002). In packaging industry, the polymer materials are generally required to have low permeability to gases and vapors in particular water vapor. The barrier properties are also crucial for cellulose based packaging materials.

Improved surface barrier properties by functional coating require a surface-located layer with minimized penetration of the chemicals into the substrate (Andersson, 2008). An improved (increased) barrier property of the packaging material can help to increase the shelf time of foodstuff (Koide et al., 2007; Del Nobile et al., 2006). Besides the high water vapor barrier properties (low permeability), food packaging materials should also have low oxygen permeability (Paine et al., 1992). If the oxygen permeability of the packaging material is too high, this can lead to the development of oxidative reactions that degrades proteins and lipids resulting in spoilage of the food (Robertson, 1993). In addition, microorganisms present in the food can start to grow at certain oxygen contents.

Mass transfers through food packaging films can occur for any type of material used, if there is a partial pressure difference across the film, even in the case of surface treated multilayer packaging (Lange et al., 2003). Understanding the equilibrium and transport characteristics of water vapor, CO_2 and O_2 in modified fiber-based materials and coated paper products, is necessary to improve properties of the fiber-based packaging materials. A number of different experimental methods are available for the measurement of permeability of gases and water vapor through polymer films (Nilsson et al., 1993; Auras et al., 2003; Park et al., 1995; Curtzwiler et al., 2008; Thomas et al., 1998). In this study gravimetric IGA- system is used for accurate and fast measurement of water vapor, CO_2 and O_2 transmission rates.

Gas and vapor transmission rates through a polymer film depend strongly on the temperature and the relative humidity difference (driving force) of the barrier film, and also on the type of coating applied, and thickness of the film. The mass transfer mechanism through a packaging film depends on the porosity of the film. Transport mechanism of water vapor can occur through the void space (pore) or along the fiber cell wall (Bandyopadhyay et al., 2002). Permeation follows solution-diffusion mechanism: the gas first dissolves (adsorbs) at the surface of the material on the high-pressure side, then diffuses through the polymer phase, and finally desorbs or evaporates at the low-pressure side. Water vapor transport in the cellulose fiber materials is very important in the application of coating, surface sizing, printing and packaging. There are a few studies available on the measurement of diffusivity on paper surface by using various experimental techniques; however some of the results obtained from different studies vary significantly. For example, Hashemi et al. (1997) reviewed diffusivity results from different literature sources pointing out to the contradictory results; in particular the study was focused on the dependency of diffusivity on moisture content.

It is therefore important to understand how textural properties of various cellulose fiber materials, e.g., physically and chemically treated paper can affect gas and water vapor properties, such as diffusion, transmission rate and permeability. The main objectives of this study are to:

1) Measure WVTR's on the selected wood-fibre samples by using different driving force (ΔRH) in investigations and to analyze the results with regard to potential application for the packaging purposes.
2) Measure the diffusivity of water vapor from uptake rate measurements and analyze the mechanisms of mass transfer of the investigated samples.
3) Measure CO_2 and O_2 transmission rates through the selected paper samples.

3.2. Materials and Experimental

3.2.1. Materials

Several types of paper samples that were prepared for this study are listed in *Table 3.1*. Unmodified paper samples were made from pure cellulose with different thickness or densities. Modified paper samples such as PLA-coated paper, PLA/polyhedral oligomeric silsesquioxane (POSS)-bentonite modified paper with coating weight of 25-30 g/m^2 and base paper (85±4 g/m^2), as well as zein grafted paper (8 wt.% corn zein) were prepared according to procedures further explained in this section. The PLA coating solution was prepared by dissolving 0.25 g of PLA in 6 ml of chloroform by stirring with a magnetic stirrer (Rhim et al. 2007). The PLA/bentonite solution was prepared by blending 90 wt.% PLA with 10 wt.% modified bentonite clay. The bentonite clay was modified by POSS in the presence of *sophorone diisocyanate* (IPDI) as cross linker in *tetrahydrofuran* (THF) at 50^{o}C for 6 h. Before processing, PLA was dried overnight at 60^{o}C under vacuum and then stored in the presence of a P_2O_4 desiccant. The clay was dried at 40^{o}C under vacuum for 4 h. For the preparation of PLA nanocomposite films, 0.025 g of bentonite was dispersed in the 2 ml of chloroform by vigorous stirring for 1 h using a magnetic stirrer. This was followed by sonication for 1 h at room temperature using a High Intensity Ultrasonic Processor (Bransonic, USA). The bentonite solutions were mixed with the previously prepared PLA solution (0.225 g in 4 ml of chloroform), and sonicated for 1 h. Completely dissolved coating solutions were cast onto printing paper (8.8 cm diameter), in three casting steps, by using a glass spoon-shape bar, to reduce the penetration of the solution into the paper substrate. The paper was mounted on a flat glass petri dish. In the first two steps, 1 ml of solution was used, and in the last step the rest of solution was cast into the paper substrate. The obtained coated paper samples were dried under ambient condition (23 ± 2^{o}C) for 24 h.

Table 3.1. Paper samples and their physical properties

Physical Properties	Paper types							
	Unmodified paper			Zein grafted/ coated paper	PLA coated paper	PLA/(POSS-bentonite) coated paper	Commercial Papers	
							Copy paper	Calendered coated paper
Grammage (g/m^2)	60	120	180	88	115	118	82	150
Density (kg/m^3)	343	368	391	628	907	910	820	1083
Thickness (mm)	0.200	0.330	0.480	0.140	0.127	0.130	0.099	0.140

Zein, a class of prolamine protein-based natural products with highly hydrophobic and barrier properties, was grafted onto the paper consisting of sulphite fibre using IPDI as a coupling agent. The zein solution was prepared by dissolving a certain weight of zein powder in the mixture of 70% acetone and 30% water (v/v) (Yamada et al. 1996). Then the additive-free hand sheets were reacted with the diluted zein solution and the IPDI at the temperature of 50-60oC, followed by a magnetic stirring for a few hours. The samples were finally washed several times and dried overnight at 100oC.

3.2.2. Water vapor and gas transmission rates

Water vapor and gas transmission rates measurement on paper samples were performed using a state-of-the-art sorption apparatus, consisting of high sensitivity microbalance

(0.1 μg) and turbomolecular high vacuum pumping system (IGA-003; Hiden-Isochema, Warrington, UK).

3.2.2.1. Water vapor transmission rates

The IGA instrument can be easily adapted to measure water vapor transfer rate, in accordance to the method described by ASTM E 96/E96M-05 standard (2005). The experimental set-up is shown in Fig 3.1. The measurements were carried out at the relative humidity differences ranging from 26 to 74% (ΔRH %) and temperature range of 15–35oC. In these experiments, sample (paper film) was first saturated at 76% RH using a saturated salt solution (NaCl), followed by desorption in a flow of purge gas (nitrogen) partially saturated with water vapor, e.g., relative humidity of 2, 20 and 50%, controlled by an automatic humidity generator (HumidSys, InstruQuest Inc., USA), to study the effects of driving force (□RH) on the rates. Two to three replicates were made per each RH depending on the variation of the results and the average values were taken for analysis. Reproducibility of the results was within 5-10% range.

At constant temperature and ΔRH (%), a steady state will be reached where WVTR can be calculated from the change in weight of the container, at a specified time interval, and the area of exposed film, as described by *Eq 3.1*:

$$WVTR = \frac{Weight\ Change}{Area \times time} \qquad 3.1$$

WVTR refers to a specific sample configuration, e.g., thickness of the sample film. Water vapor permeability (WVP) can be calculated from WVTR as follows:

$$WVP = \frac{WVTR \times Z \times 100}{P^{sat} \times \Delta RH(\%)} \qquad 3.2$$

where Z is film thickness, P^{sat} is water vapor saturation pressure at the experimental temperature, and ΔRH (%) is percentage relative humidity gradient.

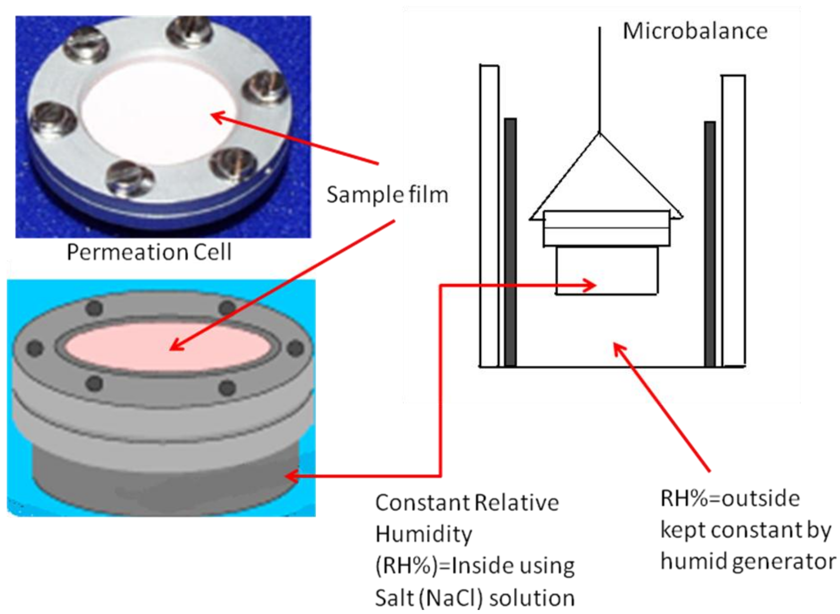

Figure 3.1. Experimental set-up for WVTR measurement.

3.2.2.2. Gas transmission rates

For gas transmission rate (GTR) measurement the method similar to the WVTR method was employed. However, in this case an adsorbent material, such as zeolite13X, was kept inside impermeable container as a “sink” and the paper sample was used to seal the container.This method is used only for a pure dry gas meausrement since the adsorbent can take or adsorb other gases or moisture if other gases or vapors are fed to the system. During measurement the sample film container was placed in the gravimetric IGA chamber, and the system was evacuated using high vacuum, until the constant weight was obtained. Then oxygen or carbon dioxide gas was introduced into the IGA system and kept at the pressure of 20 kPa. It was assumed that the constant O_2/CO_2 concentration gradient was maintained across the sample film. The microbalance measures the periodic weight change or the uptake of the adsorbent. In order to accurately determine gas transmission rate through the paper film, the contribution of mass transfer in the adsorbent should be corrected from the blank measurement using the method described by Nilsson et al. (1993). Gas mass transmission rates ($\dot{m}_T$, $\dot{m}_b$) can be determined from uptake measurements on adsorbent with and without paper film (blank experiment), respectively, where their values are taken from the slopes of the weight change in time (the initial linear section of uptake curves). $\dot{m}_T$ and $\dot{m}_b$ are represented by the following equations (Nilsson et al., 1993),

$$\dot{m}_T = \frac{M(c_1 - c_2)}{\frac{1}{k_{film}A} + \frac{1}{k_b A}} \qquad 3.3$$

$$\dot{m}_b = \frac{M(c_1 - c_2)}{\frac{1}{k_b A}} \qquad 3.4$$

where $\dot{m}_T$ is gas mass transmission rate determined from uptake measurement with paper film; $\dot{m}_b$ is gas mass transmission rate determined from uptake measurement without paper film (blank experiment); A is area of the adsorbent container or paper film; c_1 and c_2 are gas concentrations outside and inside of sample container, respectively. k_b is mass transfer coefficient of gas in the adsorbent; k_{film} is mass transfer coefficient of gas in the paper film; M is gas molecular weight. Therefore, corrected gas mass transmission rate ($\dot{m}_c$) after blank correction can be obtained from Eqs 3.3 and 3.4:

$$\dot{m}_c = \frac{M(c_1 - c_2)}{\frac{1}{k_{film}A}} = \frac{1}{\frac{1}{\dot{m}_T} - \frac{1}{\dot{m}_b}} \qquad 3.5$$

The gas transmission rates, CO_2 TR or O_2 TR (ml/m^2.day), are then calculated by the following equation:

$$CO_2\ or\ O_2TR = \frac{\dot{m}_c}{\rho A} \qquad 3.6a$$

where ρ is gas density at experimental temperature (T=25^{o}C) and pressure (20 kPa). Two to three GTR replicates were done per film depending on the results variability.

3.2.2.2.1. Isostatic, steady state oxygen transfer rates

Isostatic, steady state oxygen transmission rates through paper films were measured in accordance to ASTM D3985. This method provides oxygen transmission rate measurements through a film at dry and wet gas conditions. Steady state O_2TR method involves a permeation cell in which the sample material separate two chambers, as shown in Fig. 3.6b. Gases (N_2 and O_2) at similar absolute pressures (100 kPa) and flow rates (30 ml/min.) pass on either side of the sample film at specific relative humidities.The temperature of the sample were kept at a temperature of 25±2.0 ^{o}C inside the oven. The humidity at one side of the stream was controlled by an automatic humidity generator (HumidSys, InstruQuest Inc., USA), and the humidty on other side of the gas stream was controlled by using gas bubbler filled with water. Both sides of the gas streams were kept at the same humidity to keep the moisture content of the sample in equilibrium at a given relative humidty. Oxygen transfers from high concentration side through the film into the nitrogen gas stream. After leaving the sample chamber, the carrier gas passes through oxygen meter (Oxygen Analyzer Model 600, Engineered Systems & Designs, Inc., USA) to measure the oxygen concentration in the carrier gas stream (N_2 gas). When the oxygen concentration reading in the oxygen meter was constant, oxygen transmission was considered to have reached steady state. O_2TR is estimated using the carrier gas flow rate, the concentration of oxygen in the carrier gas and the sample area at different relative humidities (RH=0, 30, 50, 70, 85 and 95%), using Eq. 3.6b. Each test was repeated three times, and an avarge was calculated.

$$O_2TR = \frac{C_{oxy} \times F}{A} \qquad 3.6b$$

where C_{oxy} is the volumetric concentration of O_2, determined from the analyzer at the steady state (% vol.), F is the carrier gas (N_2) flow rate (ml/min.) and A is the film area (m^2).

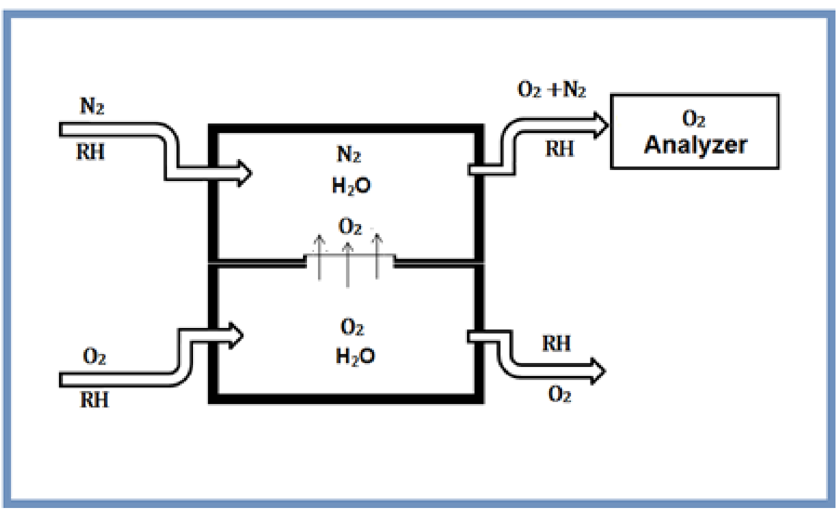

Figure 3.1b. Experimental set-up for oxygen transmission rate measurement.

Oxygen permeability (O_2P) can also be calculated from a specific sample configuration, e.g., thickness of the sample film, similar to water vapor permeability measurement. The oxygen permeability (O_2P) can be calculated from O_2TR as follows:

$$O_2P = \frac{C_{oxy} \times F \times Z}{A \times \Delta pO_2} \qquad 3.6c$$

where C_{oxy} is the volumetric concentration of O_2 in the steady state (% vol.), F is the carrier gas flow rate (ml/min.), Z is the thickness in m, A is the film area (m^2), ΔPO_2 is the difference in the partial pressure of O_2 across the film (Pa).

3.2.3. Water vapor kinetics

Water vapor uptake measurements on paper samples were performed at different relative humidities using IGA system. Before starting the experiment, paper sample film was placed in the measurement chamber and dried with pure nitrogen, until constant weight was obtained. After that, the chamber was evacuated to a high vacuum, using turbo-pumping system. Uptake rates were measured under controlled sample temperature of $T=25^{o}C$ and total pressure of 100 kPa using a thermo regulated water bath (PolyScience, USA). The relative humidity surrounding the sample was increased in appropriate steps up to the saturation vapor pressure (RH=100%) using nitrogen as a carrier gas. In each step, the mass gain was measured as a function of time until an equilibrium state was reached as shown in the Fig 3.2. Reproducibility of the experimental results was ± 5%.

Transient moisture adsorption studies were conducted to determine the rate of moisture uptake and diffusivity through the paper sample film. Mass uptake initially increases rapidly followed by more gradual increase, until equilibrium state is reached. The Fickian diffusion model was used to determine moisture diffusion coefficient for different paper sample films (Crank, 1975). The mathematical model for the fractional uptake, M(t)/M(∞), following transient Fickian diffusion for slab geometry is given by Eq 3.7:

$$\frac{M(t)}{M(\infty)} = 1 - \frac{8}{\pi^2}\sum_{n=0}^{\infty}\frac{1}{(2n+1)^2}\ exp\left(-\frac{\pi^2(2n+1)^2D}{4L^2}t\right) \tag{3.7}$$

where, M (∞) is the asymptotic (equilibrium) uptake, D is effective diffusivity, L is a half thickness of the film and t is an uptake time corresponding to M (t).

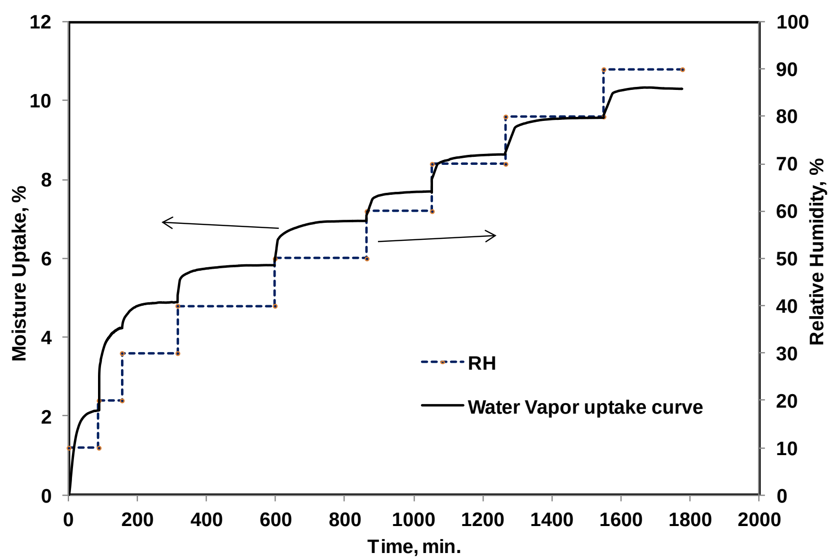

Figure 3.2. Example of plot showing curve from a typical water vapor uptake measurement on unmodified paper at T=25 °C and 100 kPa.

3.3. Results and Discussion

3.3.1. Oxygen/Carbon dioxide transmission rates

GTRs were obtained at the conditions of T=25^{o}C, P=20 kPa and 0% relative humidity, using gravimetric technique, and are presented in *Table 3.2*. The O_2/CO_2 transfer rates of some samples (e.g., unmodified paper, commercial copy and calendered coated papers) could not be analyzed since the values were too high (beyond the measurement range). The lower gas transmission rate was obtained for PLA/(POSS-bentonite) coated paper compared to other modified papers. The CO_2 transmission rates are higher than O_2 and the rate ratio of CO_2/O_2 is generally greater than 3. Higher transmission rate of CO_2 was also obtained for PLA film at T=23^{o}C and RH=0% as reported by Curtzwiler et al. (2008). In the same study the rate ratio of CO_2/O_2 was found to be 5.5, which is very close to our result. The gas transmission rates obtained in this study are generally higher than those reported in literatures (Auras et al., 2003; Hult et al., 2010). However, results from the literature were obtained at 50% relative humidity clearly indicating the effect of relative humidity on the gas barrier properties, e.g., increase of the barrier properties for gases in the presence of water vapor (relative humidity effect). Other studies also reported that the permeability of gases was reduced in the presence of humid environment, i.e. the presence of water vapor might lower the free volume thereby increasing the resistance for permeation (Chern et al., 1983; Pye et al., 1976). Zein grafted paper exhibited poor CO_2 and O_2 barrier properties. Thomas et al. (1998) performed O_2TR measurement on corn zein coated paper and also found poor oxygen barrier properties (high O_2TR).

Table 3.2. Gas transmission rates of paper samples at T=25 °C, P=20kPa and RH=0%.

Paper Type	Sample Thickness (mm)	$O_2TR \times 10^{-3}$ (cm^3/m^2.day)	$CO_2TR \times 10^{-3}$ (cm^3/m^2.day)	CO_2TR/O_2TR
PLA Film	0.060	12	42	3.5
PLA/(POSS-Bentonite) coated paper	0.150	1,226	4,079	3.3
PLA coated paper	0.130	1,468	7,888	5.4
Zein grafted paper	0.260	1,901	-----	-----

3.3.1.2. Oxygen transmission rates

Oxygen transmission rates were measured for PLA and PHBV coated paper samples at dry and humid conditions. The measured O_2TR results for different relative humidities are presented in Table 3.2b. Figure 3.3a shows the oxygen permeabilities measured at various relative humidities. The PHBV coated paper sample showed lower O_2TR than PLA coated paper. The O_2 permeability through the films is constant up to relative humidity of 50%, but then shows an increasing trend with increased relative humidity. The reason for the increase in O_2 permeability can be attributed to the swelling effect of moist fibers, thus results to create spacing between adjacent fibers for gas to diffuse more readily. The O_2 permeability of PLA coated paper starts to decreases at very high relative humidities, i.e., greater than RH=70%. This could be due to the surface pores being partly or totally filled with water to block the O_2 passage through pores. Yang et al. (2011) reported the dependency of oxygen permeability on moisture content of cellulose film and found that the oxygen permeability of transparent cellulose films increases linearly with increased relative humidty. The obtained oxygen permeability at dry condition in isostatic method is lower than the gravimetric technnique due to similar absolute pressures on both side of the film; however, there is a total pressure difference on both side of the film in case of gravimetric technique and this enhances higher oxygen permeability in the film.

Table 3.2b. Oxygen transmission rates (O_2TRs) and permeabilities (O_2Ps) of coated paper samples at different RHs and T=25 ^oC.

Paper Type	RH=0 %		RH=50 %		RH=70 %		RH=95 %	
	O_2TR* $\times 10^{-3}$	O_2P* $\times 10^{8}$	O_2TR* $\times 10^{-3}$	O_2P* $\times 10^{8}$	O_2TR *$\times 10^{-3}$	O_2P* $\times 10^{8}$	O_2TR* $\times 10^{-3}$	O_2P* $\times 10^{8}$
PLA coated	506	1.5	506	1.5	3066	3.54	506	1.25
PHBV coated	506	0.70	506	0.70	1018	1.82	1530	2.56

***unit for O_2TR is in cm^3/m^2.day and O_2P is in cm^3/m.s.Pa**

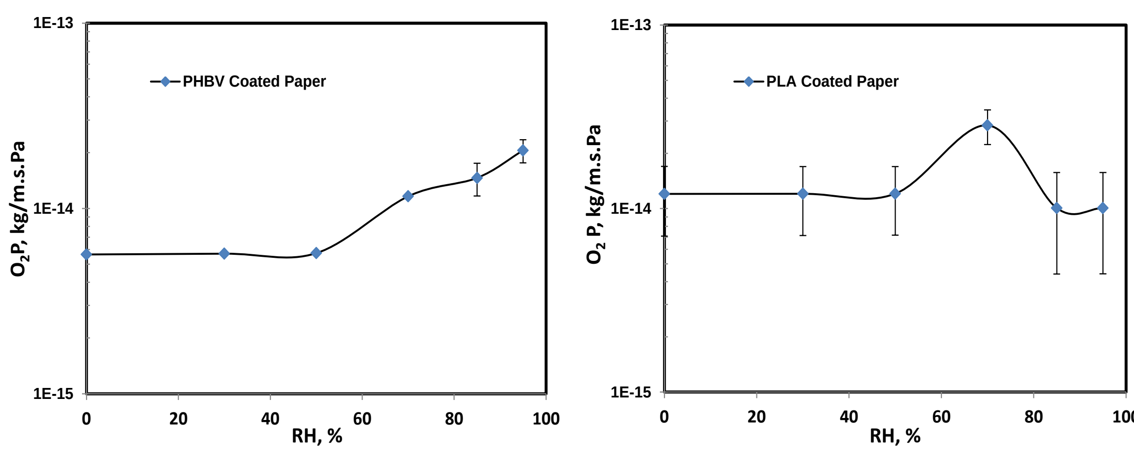

Figure 3.3a. Effect of relative humidity on oxygen permeability of coated papers.

3.3.2. Water vapor transmission rates

WVTR's of several paper samples were measured at different relative humidity gradients (ΔRH= 56 and 74%) and temperature of 25^{o}C. They were calculated from the slope of the weight change against time using the exposed surface area of the film (120 mm^2) as shown in Fig 3.3. The calculated WVTR and WVP results for relative humidity gradient of 56 and 74% are summarized in Table 3.3. All modified paper samples showed lower or much lower WVTR's compared to unmodified (control sample) and commercial samples, as expected. For example the PLA/(POSS-bentonite) modified paper sample showed the lower transmission rate compared to the unmodified sample at normalized film thickness of 100 µm. On the other hand, PLA coated paper has higher WVTR than PLA film, which is probably due to the deficiency of continuous film formation during coating process on the paper. However, the addition of bentonite in the film produced higher water vapor barrier properties. Zein grafted paper has a WVTR of 179 g/m^2.day as it reduces water vapor transfer rate much more than commercial calendered coated paper.

Rhim et al. (2007) also found lower WVTR for PLA coated paper board (9.7 g/m^2.day) for paper basis weight of 180 g/m^2 and coating weight about 50 g/m^2 (Anderson, 2008). The thickness of the paper and coating weight have an influence on WVTR, i.e., the higher the paper density and coating weight of similar samples the more WVTR of the film is reduced. The WVP of PLA/ (POSS-bentonite) coated film is lower than that of cellophane (0.84×10^{-10} g/m.s.Pa), a cellulose-derived film commonly used for food packaging (Taylor, 1986).

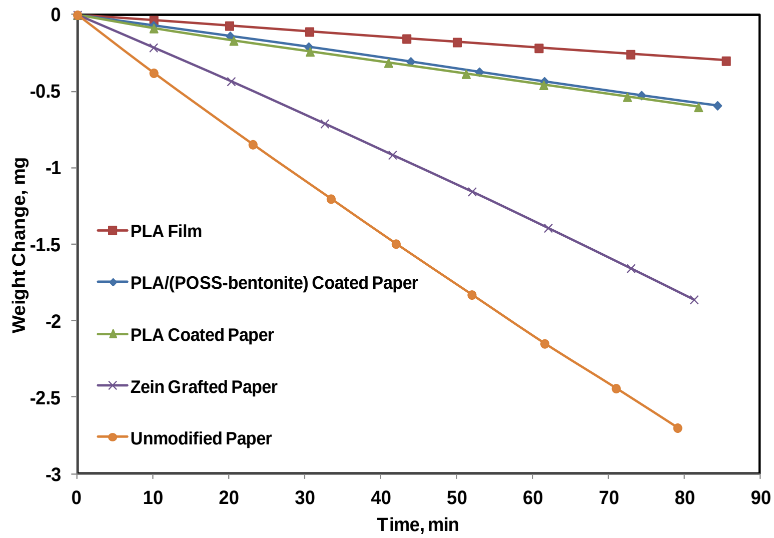

Figure 3.3. Results of the WVTR study for different samples at ΔRH=74%, T=25°C and P=100 kPa using the permeation container.

Zein grafted film exhibited the comparable WVP value to those reported in the literature (Lai and Padua 1998; Thomas et al., 1998). It was also observed that WVTR values were lower with the decrease of relative humidity gradient, which is expected due to the lower driving force for mass transfer. The effect of relative humidity gradient on WVP results was different than WVTR. As expected, relative humidity gradient showed no significant effect on the permeabilities of all the samples investigated in this study. In general, the results showed expected trend of decreasing WVTR's and WVP's with the increased hydrophobicity of the modified samples as shown in Table 3.3.

Table 3.3. WVTR, normalized to Z=100 μm, and permeabilities (WVP) of different paper sample films at T=25 ^oC and P=100 kPa.

Paper samples	WVTR (g/m^2.day)	WVP (10^{-10} g/m.s.Pa)	WVTR (g/m^2.day)	WVP (10^{-10} g/m.s.Pa)
	ΔRH=74%		ΔRH=56%	
Unmodified Paper (60 g/m^2)	659	3.20	516	3.40
Calendered Coated Paper (commercial)	263	1.31	209	1.38
Zein Grafted Paper	179	0.89	160	1.05
PLA Coated Paper	130	0.65	---	----
PLA/(POSS-bentonite) Coated Paper	104	0.51	78	0.51
PLA Film	38	0.19	----	----

3.3.3. Effects of sample film thickness and temperature on WVTR and WVP

The effects of sample thickness on the barrier property of water vapor were studied for three different unmodified paper samples at different relative humidity gradient of 74, 56 and 26%. As the film thickness (sample density) increases, the water vapor transmission rate decreases as shown in Fig 3.4. Similar result was reported by Martin-Polo et al. (1992). Nilsson et al. (1993) reported that the effective water vapor diffusivity of various paper films decreased with an increase of the density, which implied that, WVTR decreased with increasing film thickness. However, contrary to these results, other studies showed that the water vapor permeability increased as film thickness of starch, amylase and cellulose derivative films increased, due to strong hydrophilic film properties (Bertuzzi et al., 2007; Rankin et al., 1958; Park, Chinnan, 1995; Park et al., 1993).

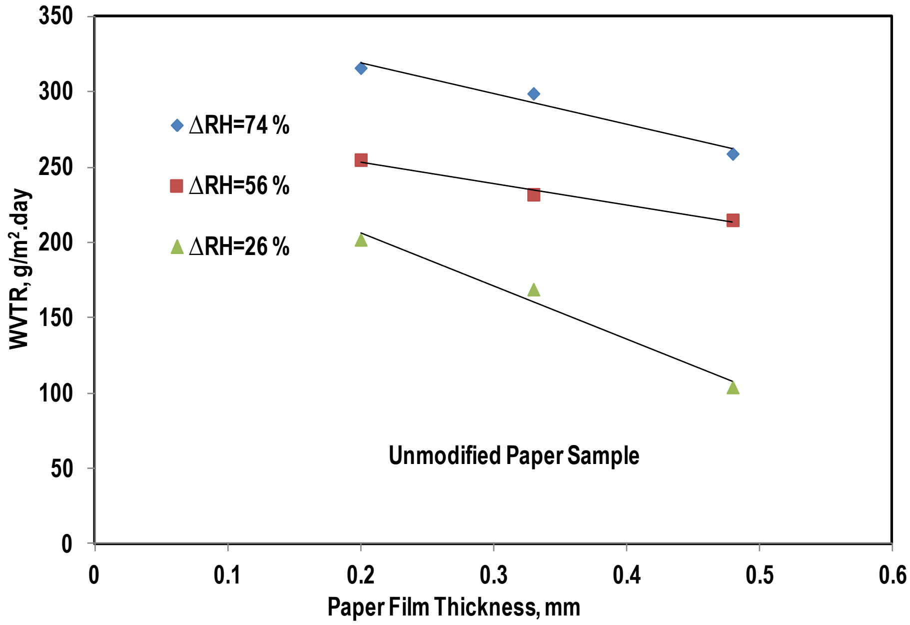

Figure 3.4. Effect of film thickness on WVTR of unmodified paper at different relative humidity gradients.

Film WVP's values were calculated for three different temperatures (15, 25 and 35^{o}C). Temperature has shown strong effect on WVP, as shown in Fig 3.5. Activation energies were determined from the Arrhenius type of relationship, e.g., slope of ln (WVP) versus 1/T. The obtained effective activation energies (E_{eff}) for three different paper sample films are presented in Table 3.4. The activation energy of water vapor permeation in high amylose starch film was reported to be 5.611 kJ/mol (Bertuzzi et al., 2007) and in cellophane was 1.67 kJ/mol (Rogers et al., 1982). A negative activation energy (-9 to -10 kJ/mol) of PLA film was also reported (Auras et al., 2003). A peculiar behavior of PLA coated film with regard to the negative activation energy, as reported by Auras et al. (2003), indicates a complex nature of mass transfer in coated papers. According to solution/diffusion theory permeability (π_A) is defined as:

$$\pi_A = K \times D_{eff} \qquad 3.8$$

where K is equilibrium constant, e.g., Henry's constant and D_{eff} is effective diffusivity. According to Eq 3.8 both equilibrium and kinetics (diffusion) can play a role in the permeation of sorbate, e.g., water vapor, through paper or coated paper. The temperature dependence of the permeability will therefore be given by:

$$\pi_A = K' exp\left(\frac{-E_{eff}}{RT}\right) \qquad 3.9$$

where E_{eff}, effective activation energy of permeation is defined by:

$$-E_{eff} = (-\Delta H) - E_a \qquad 3.10$$

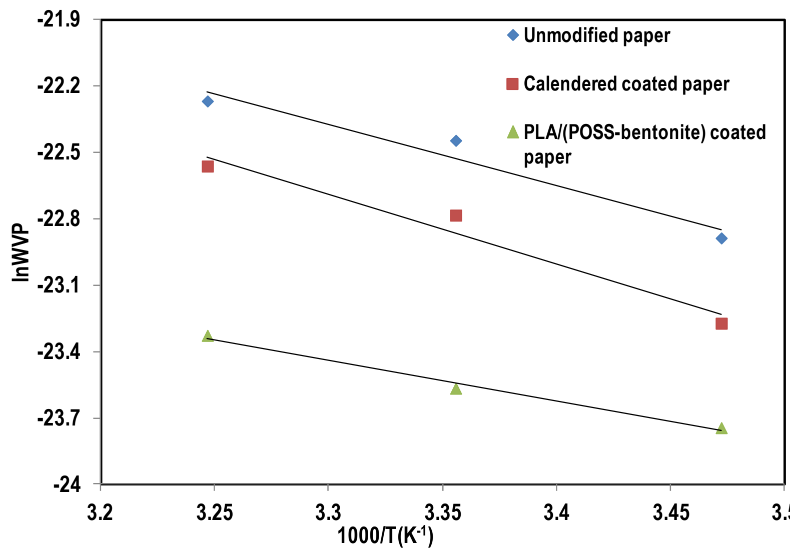

Figure 3.5. Effect of temperature on WVP of unmodified and modified papers at ΔRH=74%.

In Eqs 3.9 and 3.10 K' is a constant, ΔH is the enthalpy (heat) of adsorption and E_a is the activation energy of diffusion. The dissolution of a gas (vapor) in a paper film (membrane) is generally an exothermic process, so (-ΔH) is normally a positive quantity. Depending on the magnitude of the energy of adsorption relative to the diffusional activation energy one can therefore expect the permeability to either increase or decrease with temperature. In other words, the effective activation energy of gas (vapor) permeation can be positive or negative, which can explain negative value of activation energy reported by Auras et al. (2003). In this case, it is a larger magnitude of the adsorption energy relative to the diffusion activation energy, which gives negative value to the overall (effective) activation energy according to Eq 3.10. The results of our study (Fig 3.5 and Table 3.4) show an increase in permeability with the increase of temperature, according to the Arrhenius type of dependency, for all three samples, indicating positive effective activation energies. This is consistent with the diffusion dominated processes for water permeation through the samples, in particular for unmodified and calendered coated paper samples (the highest effective activation energies). A significant decrease of activation energy for PLA/POSS-bentonite coated paper sample is indicative of relatively larger heat of adsorption contribution to the effective activation energy, due to the higher solubility of water vapor in this material, i.e., equilibrium plays a more significant role in the permeation, thus reflecting significant changes in the textural properties and homogeneity of this material compared to unmodified paper samples. Future equilibrium and extended diffusion studies should shed more light on the effects of heat of adsorption and diffusion activation energy on the overall kinetics behavior of the samples investigated in this study.

Table 3.4. Effective activation energies for permeation of water vapor through paper films at ΔRH=74%.

Paper samples	Effective activation energy (kJ/mol)
Unmodified Paper (60 g/m^2)	23.0
Calendered Coated Paper	26.3
PLA/(POSS-bentonite) coated paper	15.4

3.3.4. Water vapor diffusivities

The effective diffusion coefficients were determined from uptake rate measurements on the plane sheet of paper samples by fitting the data with the Fickian model (Eq 3.7, truncated at n=6) at different moisture contents (relative humidities). Fig 3.6 shows a typical uptake curve for zein grafted paper measured for incremental humidity changes, e.g., RH=40-50% and 60-70% at 25^{o}C. It should be noted that the diffusivities presented and discussed in this section are transport (Fickian) diffusivities related to concentration gradients applied in the measurements. No attempts were made to compare these results with self diffusivities obtained by microscopic methods, e.g., NMR, because the values for these two types of measurements are generally very different, except at very low concentration levels, e.g., infinite dilution (Karger and Ruthven, 1991). Summary of diffusion results with regard to the relative humidities is shown in Table 3.5 and illustrated in Fig 3.7. The diffusivities of modified and unmodified paper samples are very sensitive to the moisture content, e.g. higher diffusivity is observed at higher water vapor concentration until it reaches the maximum, and then it starts to decline with a further increase of concentration.

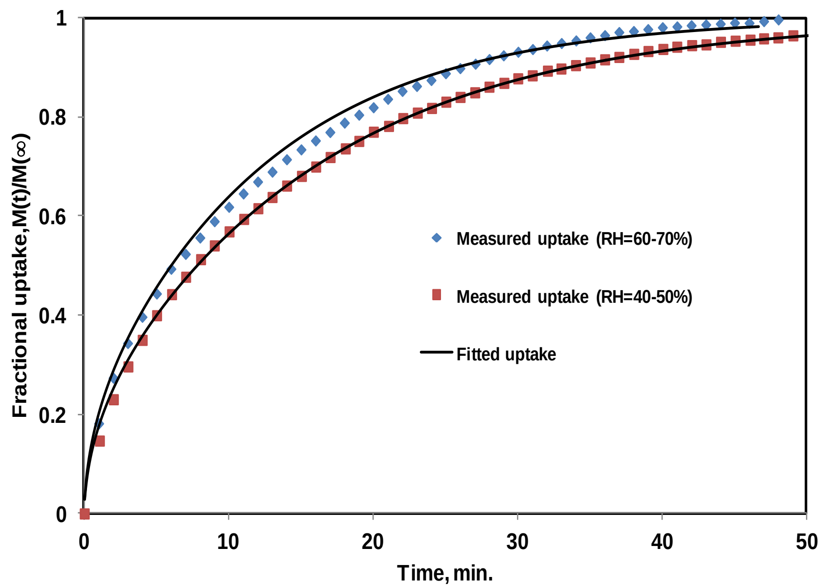

Figure 3.6. Typical water vapor uptake curves for Zein grafted paper at 25 ^{o}C and 100 kPa total pressure.

The effective vapor diffusivity at 25^{o}C of unmodified paper sheet varied from 2.9×10^{-13} to 2.9×10^{-12} m^2/s with the maximum diffusivity exhibited at relative humidity of about 60 %. The maximum diffusivity for unmodified paper is 6.8×10^{-12} m^2/s. The modified paper samples showed the maximum diffusivities in the relative humidity range of 70-80%. The effective diffusivity of modified papers was lower than unmodified paper samples as expected, e.g., the lowest was found for PLA coated papers. Sharper increase in diffusivity is noticeable for both unmodified and modified paper samples above the relative humidity of 30% and 40%, respectively. Increase in diffusivity, starting from relative humidity of 30% for unmodified paper was also reported by Ahlen (1970). Other studies (Dury-Brun et al., 2006; Bessadok et al., 2008; Hashemi et al., 1997) showed similar trends related to variation of vapor diffusivity values with moisture content for cellulose fibers and papers. Effective water vapor diffusivity of calendered latex coated paper at 25^{o}C was found to vary from 2.97×10^{-13} to 1.44×10^{-12} m^2/s for RH ranging from 0% to 97% (Dury-Brun et al., 2006). These results are in close agreements with the diffusivity values obtained for calendered coated paper. In general, from low to intermediate relative humidity, the transport behaviour of water vapor is controlled by molecule and or Knudsen diffusion in pores of the cellulose network, where diffusivity is nearly independent of relative humidity. This is in line with water vapor equilibrium characteristics at low concentration levels, where water molecules are strongly adsorbed by binding to the cellulose hydroxyl groups at surface, which are the most active sites and also responsible for monolayer formation (primary water). With a further increase of relative humidity, surface diffusion in the pore wall (solid diffusion), which is considered to run in parallel with the molecule/Knudsen diffusion in the pore, starts to play more important role in the transport process (Gupta and Chatterjee 2003; Dury-Brun et al. 2006). Since surface diffusion strongly depends on gas phase concentration in non-linear region of adsorption isotherms (Ruthven, 1984), a sharp increase of effective diffusivity with the relative humidity, at higher humidity levels, is expected due to dominant contribution from the surface diffusion. This behaviour is consistent with thermodynamics consideration at higher concentration levels. With the further increase of concentration, additional water molecules continue to be adsorbed as secondary water by interacting with the molecules already bound at the surface, thus forming multilayer configuration characterized by the weaker adsorption interactions. Due to the weaker interactions, the molecules that are involved in the multi-layer formation are more mobile, which is revealed by an increase in surface (solid phase) diffusivity.

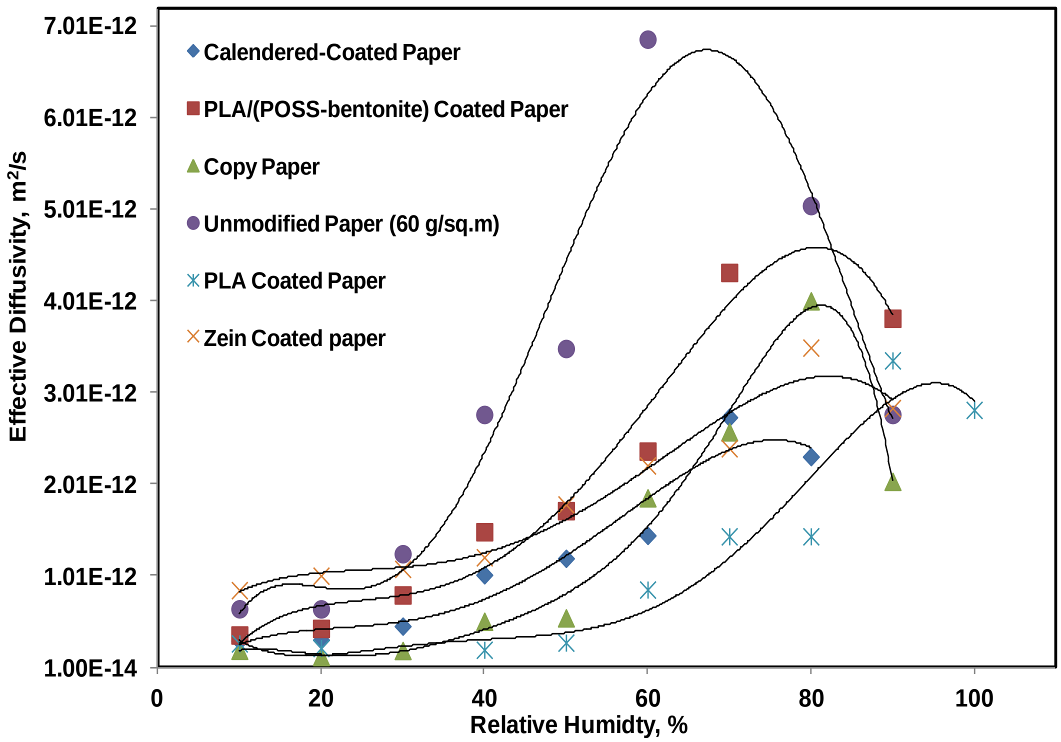

Figure 3.7. Dependency of diffusivity of paper samples on relative humidity at T=25 °C.

However, at the very high relative humidities, e.g., beyond the maxima on Fig 3.7, the diffusivities show opposite (decreasing) trend with a further increase in RH's. This behaviour complies with the model proposed by Park (Park, 1986; Bessadock et al., 2009). According to Park's model, at very high concentration levels the water molecules start to form aggregates (clusters), thus causing low mobility and consequently leading to the decrease in the effective diffusivities as shown in Fig 3.7 and Table 3.5. It should also be noted that in some other studies (Gupta and Chatterjee, 2003) using bleached craft paperboard samples) a continuous increase of diffusivities with RH's, even at the very high humidities, was reported These differences in reported diffusivity trends relative to

RH reveal a complexity of water transport in wood fibres, in particular involving chemically treated fibers. Further studies to investigate the interaction between water and fiber substrates using spectroscopic techniques, e.g. FT-IR, will be conducted to shed more light regarding this issue.

Table 3.5. Effective diffusivities for paper samples at different relative humidity and T=25°C.

Paper Types	$D \times 10^{12}$ (m^2/s) RH=20%	$D \times 10^{12}$ (m^2/s) RH=50%	$D \times 10^{12}$ (m^2/s) RH=60%	$D \times 10^{12}$ (m^2/s) RH=70%	$D \times 10^{12}$ (m^2/s) RH=80%	$D \times 10^{12}$ (m^2/s) RH=90%
Unmodified paper (60 g/m^2)	0.65	3.49	6.87	-	5.10	2.80
PLA/(POSS-bentonite) coated Paper	0.44	1.72	2.37	4.32	-	3.82
PLA coated paper	0.22	0.28	0.86	1.40	1.44	3.36
Zein grafted paper	1.01	1.79	2.21	2.52	3.50	2.84
Copy paper	0.13	0.55	1.86	2.53	4.01	2.04
Calendered coated paper	0.31	1.20	1.45	2.74	2.31	-

3.4. Conclusions

Water vapor transmission rates (WVTR) and O_2 and CO_2 gas transfer rates involving different modified paper samples and unmodified paper (control sample) were determined for different measurement conditions. Modified paper samples showed lower water vapor and gas transfer rates as well as lower effective water vapor diffusivities. Among the modified papers, PLA/(POSS-bentonite) paper has the lowest water vapor and O_2/CO_2 transmission rates, which renders it the best candidate for food packaging use. Zein grafted paper showed reduced water vapor and O_2 transmission rates compared to unmodified (control sample). Furthermore, zein grafted paper showed better barrier property for water vapor than O_2. This is possibly due to less hydrophilic character of zein grafted on the paper which affects the water vapor transport more than O_2. The diffusivity of water vapor from uptake rate was determined from differential uptake measurements on the paper samples. At low moisture contents, the obtained effective water vapor diffusivities were basically independent of relative humidity. However, at higher humidity levels, the diffusivities strongly depend on the moisture content (relative humidity). This varied behavior could be explained by the different transport mechanisms at different relative humidity levels. Relative humidity gradient showed no significant effect on the WVP of all the samples investigated in this study. Increased film thickness reduced the WVTR. Effective activation energy of water vapor permeation follows a complex sequence involving both adsorption equilibrium and diffusion effects according to the solution-diffusion permeation mechanism. In general, WVTR can be measured accurately and rapidly using gravimetric-IGA system.

References

Ahlen, A.T. (1970): Diffusion of Sorbed Water Vapor through Paper and Cellulose Film, Tappi J. 53(7), 1320-1326.

Andersson, C. (2008): New ways to enhance the functionality of Paperboard by Surface Treatment-a Review, Packag. Technol. Sci. DOI:10.1002/pts.823.

Auras, R.A, Harte, B., Selke S. and Hernandez, R. (2003): Mechanical, Physical, and Barrier Properties of Poly (lactide) Films, Journal of Plastic Film and Sheeting, 19,123-135.

ASTM Standard E96/E96 M-05 (2005): Standard test methods for water vapor transmission of materials: ASTM International, West Conshohocken, PA, USA. DOI: 10.1520/ E0096_E0096M-05.

Bandyopadhyay, A., Ramarao, B.V. and Ramaswamy, S. (2002): Transient moisture diffusion through paper board materials, Colloids and Surfaces A., 206,455-467.

Bertuzzi, M.A., Castro Vidaurre, E.F., V., Armada, M. and Gottifredi, J.C. (2007): Water vapour permeability of edible starch based films, Journal of Food Engineering, 80, 972-978.

Bessadok, A., Langevin, D., Gouanve F., Chappey, C., Roudesli, S. and Marais, S. (2008): Study of water vapor sorption on modified agave fibres, Carbohydrate Polymers, article in press.

Chern, R. T., Koros, W.J., Sanders, E. S. and Yui, R.E. (1983): Effects in Sorption and Permeation of gases in glassy polymers, Journal of Membrane Science, 15 (2), 157-169.

Crank, J. (1975): The Mathematics of Diffusion, Clarendon Press, Oxford, United Kingdom.

Curtzwiler, C., Vorst, K., Palmer, S. and Brown, J.W. (2008): Characterization of current environmentally-Friendly Films, Journal of Plastic Film and Sheeting, 24, 213-226.

Del Nobile, M.A., Baiano, A. Benedetto, A. and Massignan, L. (2006): Respiration Rate of Minimally Processed Lettuce as Affected by Packaging, Journal of Food Engineering, 74(1), 60–69.

Dury-Brun, C., Jury V., Guillard, V., Desorbry, S., Voilley, A. and Chalier, P. (2006): Water barrier properties of treated –papers and application to sponge cake storage, Food Research International, 39, 1002-1011.

Gupta, B., Revagade, N. and Hilborn, J. (2007): Poly (lactic acid) fiber: An overview. Progress in Polymer Science, 32(4), 455-482.

Gupta, H. and Chatterjee, S.G. (2003): Parallel Diffusion of Moisture in Paper Part 1: Steady-State Conditions. Ind. Eng. Chem. Res., 42, 6582-6592.

Hashemi, S.J. Gomes, V.G. Crotogino, R.H. and Douglas, W.J.M. (1997): IN-Plane Diffusivity of Moisture in Paper, Drying Technology, 15(2), 265-294.

Hult, E.L., Iotti, M. and Lenes, M. (2010): Efficient Approach to high barrier packaging using microfibrillar cellulose and shellac, Cellulose, 17, 575-586.

Jansson, A. and Jarnstrom L. (2005): Barrier and mechanical properties of modified starches, Cellulose 12, 423-433.

Karger, J. and Ruthven, D.M. (1991): Diffusion in Zeolites and Other Microporous Solids, Wiley-Interscience Publisher, John Wiley and Sons, New York..

Koide, S. and Shi, J. (2007): Microbial and Quality Evaluation of Green Peppers Stored in Biodegradable Film Packaging, Food Control, 18(9), 1121–1125.

Kugge, C. and Johnson, B. (2008): Improved barrier properties of double dispersion coated liner, Progress in Organic Coating, 62, 430-435.

Lawton, J.W. (2002): Zein: A History of Processing and Use, Cereal Chem., 79(1), 1–18.

Lai, H.M. and Padua, G.W. (1998): Water Vapor Barrier Properties of Zein Films Plasticized with Oleic Acid, Cereal Chem., 75(2), 194–199.

Lange, J. and Wyser, Y. (2003): Recent Innovations in barrier technologies for plastic packaging-a review, Packaging technology and Science, 16, 149-158.

Martin-Polo, M., Mauguin, C. and Voilley, A. (1992): Hydrophobic Films and Their Efficiency against Moisture Transfer 1: Influence of Film preparation Technique, J. Agric. Food Chem., 40, 407-412.

Nilsson, L., Wilhelmsson, B. and Stenstrom, S. (1993): The diffusion of water vapor through pulp and paper, Drying Technology, 11(6), 1205-1225.

Padua, G. W., and Wang, Q. (2002): Formation and Properties of Corn Zein Films and Coatings: In Protein based coatings and films, Gennadios, A., Ed., CRC Press, Boca Raton, Chapter 2, pp 43-69.

Paine, F. A. and Paine, H.Y. (1992): A Handbook of Food Packaging, Blackie Academic & Professional, Glasgow, UK.

Paragkumar, N.T., Edith, D. and Jean-Luc, S. (2006): Surface Characterization of PLA and PLGA films, Applied Surface Science, 253, 2758-2764.

Park, H.J., Weller, C.L., Vergano, P.J. and Testin, R. F. (1993): Permeability and mechanical properties of cellulose-based edible materials, Journal of Food Science, 58(6), 1361-1364.

Park, H. J. and Chinnan, M.S. (1995): Gas and water vapor barrier properties of edible films from protein and cellulosic materials, Journal of Food Engineering, 61, 459-466.

Park, G.S. (1986): Transport principle: Solutions, diffusion and permeations in polymer membranes, In P. M. Bungay et al. (Eds.). Synthetic membranes: science, engineering and applications, 57, Holland: Reidel Pub..

Pye, D. G., Hoehn, H. H. and Panar, M. (1976): Measurement of gas permeability of polymers. II. Apparatus for determination of permeabilities of mixed gases and vapors, Journal of Applied Polymer Science, 20, 287-301.

Rankin, J.C., Wolff, A., Davis, H.A. and Rist, C. E. (1958): Permeability of amylase film to moisture vapor, selected organic vapours and the common gases, Industrial and Engineering Chemistry, 3, 120-123.

Rhim, J-W, Lee, J-H. and Hong, S-I. (2007): Increase in water resistance of paper board by coating with poly (lactide), Packag. Technol. Sci., 20(6), 393-402.

Robertson, G.L. (1993): Food Packaging Principles and Practice, Marcel DekkerInc, New York, USA.

Rogers, C.E., Fels, M. and Li, N.N. (1982): Separation by permeation through polymeric membranes. In. N.N. Li (Ed.), Recent developments in separation science, Florida: CRC Press, pp.107-152.

Ruthven, D.M. (1984): Principles of Adsorption and Adsorption Processes. A Wiley-Interscience publication, John Wiley and Sons, New York.

Taylor, C.C. (1986): Cellophane in: Wiley Encyclopedia of Packaging Technology, M. Bakkar, ed. John Wiley and Sons, New York, PP. 159-163

Thomas, T.A., Wiles, L. J. and Vergano, J. P. (1998): Water vapor and oxygen barrier properties of corn zein coated paper, Tappi Journal, 81(8), 171-176.

Yamada, K., Noguchi, A. and Takahashi, H. (1996): Effects of the solvents on properties of zein, Nippon Shokuhin Kagaku Kaishi, 43 (3), 306–312.

Chapter 4: Water vapor adsorption equilibria and mass transport in unmodified and modified cellulose fiber-based materials

Alemayehu H. Bedane[a], Huining Xiao[b] and Mladen Eić[b]

University of New Brunswick

Adsorption 20; 863-874, 2014

[a]Graduate Student, Department of Chemical Engineering, UNB

[b]Professor, Department of Chemical Engineering, UNB

Abstract

Water vapor adsorption isotherms of different unmodified and coated paper samples were studied to determine their suitability as water barrier packaging materials. The sorption behavior of these samples was compared with commercially available paper. The experimental data were analyzed using the Hailwood-Horrobin (H-H), Guggenheim-Anderson-De Boer (GAB) and BET models for extraction of isotherm parameters and determination of monolayer moisture contents. The H-H and GAB models were found to provide good fits to the experimental data. The monolayer moisture content of modified papers was less than 3.0 % (dry basis) as compared to unmodified paper samples (4.20%), at saturation. It was also observed that the sorption behavior of modified paper samples differed with substrate type.

Water vapor permeability (WVP) of unmodified and coated paper samples at the temperatures of 25 and 38 ^{o}C were also measured for a wide range of vapor partial pressure gradients. The permeabilities of the modified samples were found to be generally low compared to the unmodified (reference) paper sample. Among the investigated samples, PLA and PHBV coated paper samples showed higher mass transfer resistance to water vapor transport. Furthermore, the water vapor permeabilities of different samples were found to be relatively constant up to the modest relative humidity levels; however, at the higher humidity levels they showed increasing trend with the further increase in relative humidity.

Results of this study confirmed that blocking of active surface sites by coating with PLA and PHBV is the most effective way to increase the water vapor barrier properties of

modified papers, thus making them the appropriate candidates for green-based food packaging materials.

Keywords: adsorption isotherms and equilibrium models, coated-paper, moisture content, cellulose fibers, water vapor permeability, solution-diffusion model.

4.1. Introduction

Cellulose fiber based materials, like papers, can be potentially used as packaging materials because they are considered environmentally friendly due to their recyclability and biodegradation properties. A variety of paper-based packaging materials have been widely used for both food and non-food products. There are many industries where moisture control is critical, especially for food and pharmaceutical packaging. The moisture content of paper-based materials at different relative humidity of the surroundings, and water vapor barrier properties of the substrate material play a key role in maintaining food product quality. Adsorbed moisture on the paper could affect the physical and mechanical properties of the paper-based packaging materials (Twede and Selke 2005). Moisture sensitive foods and pharmaceuticals can be placed in packaging with controlled water vapor and gas transmission rates to achieve the required quality, safety, and shelf life (Ashley 1985; Del Nobile et al. 2006; Koide et al. 2007).

Paper is made from chemical or mechanical pulps and has a network of natural cellulosic fiber made up of microfibrils which are composed of long chain cellulose molecules in a crystalline structure. The cellulose fiber possesses a high crystalline content, inaccessible to water molecules but also contains a para-crystalline component to which water molecules can gain access. The microfibril units have a high content of surface OH groups that is accessible to water. Paper-based packaging materials readily absorb moisture from the atmosphere due to the composition of highly porous cellulose fibers and OH sites in the basic unit of cellulose ($C_6H_{10}O_5$). The water molecules are adsorbed in the cell wall. These that are closely associated with OH groups form monolayer water, unlike those that are not intimately associated, and are forming polylayer water (Hill et al. 2009). Andersson C. (2008) reviewed new methodologies for improvement of functionality of fiber-based materials by surface treatment. Parker et al. (2006) reported sorption isotherm data for different unmodified paper samples, but no isotherm data were provided for coated paper samples. Hence, characterizing modified paper samples is essential for further improvement paper's barrier and isotherm properties, in order to increase its viability as a packaging material and quality paper.

Adsorption isotherm measurements of a material provide essential information about water vapor sorption mechanism and interaction of packaging materials with water vapor at different humid environments. Hailwood-Horrobin (H-H), GAB and BET models were primarily used in this study to determine the monolayer moisture contents of different paper samples. H-H model was also used to access the availability of the adsorbed water vapors to form polylayers on the paper surface. Monolayer moisture content has a significant effect on the physical and chemical stability of cellulose fiber materials. It is defined as the minimum moisture content, covering hydrophilic sites on the material surface, and is usually accepted as a criterion for achieving safe storage with minimum quality loss during long time exposures (Jong 2009; Moreira et al. 2008). Determination of monolayer moisture content of cellulose fiber materials is essential to estimate shelf stability and maintain high functionality of packaging materials. The H-H model is used mostly in the area of wood fiber science to analyze the adsorption isotherm, but is less often applied for the analysis of paper packaging materials (Hill et al. 2008; Spalt 1958; Simpson 1980).

The permeability coefficients can be used to predict the rate of water vapor diffusion that takes place in response to a concentration gradient. They also provide a means of predicting the equilibrium water content that is available for hydrolysis (Siparsky et al. 1997). There are a few numbers of studies on the water vapour permeability of bio-films but a limited number of studies as a coating on cellulose-fiber material (Bertuzzi 2007; Kuusipalo 2000; Siparsky 1997; Shogren 1997; Tsuji 2006). In this study, gravimetric-IGA system is used for accurate and fast measurements of water vapor transmission rates (WVTR's) and water vapor permeability (WVP) on the selected fibre samples.

The hydrophilic surface of cellulose has to be modified to be more compatible with non-polar or less polar polymer matrices. Biodegradable materials, such as polylactic acid or polylactide (PLA), poly-3-hydroxybutyrate-co-3-hydroxyvalerate (PHBV) and zein have a significant potential as packaging materials. These bio-based polymers have also been used for modification of cellulose fiber materials in order to increases water barrier properties. Zein was used to fill gaps between fibers on the treated papers, thus making them less permeable for water vapor. On the other hand, PLA and PHBV were used to block active hydroxyl groups on surface areas of modified papers in order to achieve the same effects. Related to this, it is very important to understand the characteristic of physical and chemical treatments applied to paper surface on the influence of water adsorption capacity and water vapor transport properties. The main objectives of this study were:

- To investigate water vapor sorption behavior on unmodified and coated paper samples, and compare with commercially available papers.

- To measure and analyze the water vapor permeabilities (WVP's) on the selected cellulose fiber-based samples at different humidities, e.g., ΔRH, and ultimately determine the effects of different modification methods (pore filling or active surface blocking) on hydrophobic properties of modified papers.

4.2. Materials and Experimental

4.2.1. Preparation of samples

Several types of paper samples that were prepared for this study are listed in Table 1. Unmodified paper samples were made from pure cellulose. Modified paper samples such as PLA and PHBV coated paper, with coating weight of 20-23 g/m^2 and base paper (95±4 g/m^2), as well as zein grafted paper (8 % wt. corn zein) were prepared according to the procedures further explained in this section. The PLA was purchased from NatureWorks LLC, and chloroform used as the solvent was purchased from Sigma- Aldrich (Shanghai) Trading Co. Ltd.. All compounds were used without further purifications. The PLA coating solution was prepared by dissolving 0.25 g of PLA in 6 ml of chloroform and stirring with a magnetic stirrer (Rhim et al. 2007). Before processing, PLA was dried overnight at 60 ^{o}C under reduced pressure and stored under vacuum in the presence of a P_2O_4 desiccant. Completely dissolved coating solutions were cast onto printing paper (8.8 cm diameter), in three steps. In the first two steps, 1 ml of each solution was cast into the paper, and then the rest of solution was cast onto the paper to decrease the penetration into the paper substrate, which was mounted on a flat glass petri dish. PLA coating solutions were spread over on different printing papers by using a glass spoon-shape bar, and dried under ambient condition (23 ± 2 $^{\circ}$C) for 24 h.

Poly-3-hydroxybutyrate-co-3-hydroxyvalerate, with a hydroxyvalerate content of 3 *%* wt. was purchased from *Sunrise Global, Inc. NJ. USA.* PHBV coating solution was prepared at room temperature, under magnetic stirring by dissolving powder of PHBV in 6 ml of chloroform sonicated for 1 hour. The coating solution was then spread onto paper (10×10 cm, thickness ca 90 µm) mounted on a Teflon sheet (10×10 cm) , in the three step process. In each step 2 ml of solution was added using a glass spoon-shape bar with 1 minute intervals, and dried under ambient conditions (23 ± 2 ◦C) for 24 h.

Zein, a class of prolamine protein-based natural products with highly hydrophobic and barrier properties, was grafted onto the paper consisting of sulphite fibre using Isophorone Diisocyanate (IPDI) as a coupling agent. The zein solution was prepared by dissolving a certain amount of zein powder in the mixture of 70% acetone and 30% water (v/v) (Yamada et al. 1996). Then the additive-free hand sheets were reacted with the diluted zein solution and the IPDI at the temperature of 50-60 ^{o}C, followed by a magnetic stirring for a few hours. The samples were finally washed several times and oven dried overnight at 100 ^{o}C before the characterization tests were carried out.

Table 4.1. Paper samples and their physical properties.

Physical Property	Paper types					
	Unmodified paper	Zein grafted/ coated paper	PLA coated paper	PHBV coated Paper	Commercial papers	
					Copy/printing (base-paper)	Calendered coated paper
Grammage (g/m^2)	60	88	115	110	85	150
Density (kg/m^3)	543	628	1153	967	820	1083
Thickness (mm)	0.110	0.140	0.127	0.120	0.099	0.14

4.2.2. Water vapor adsorption isotherms

Water vapor adsorption isotherms were measured using Belsorp-Max (BEL JAPAN, INC., Osaka, Japan). The Belsorp-max is an automatic gas adsorption /desorption instrument using volumetric method to measure adsorption isotherm in the relative pressure range $p/po=10^{-8}$-0.997. The adsorption isotherms of the samples used in this study were measured at 15, 25 and 35 ^oC.

4.2.3. Water vapor transport properties

Water vapor transmission rates (WVTR's) measurements on paper samples were performed using a state-of-the-art sorption apparatus, consisting of high sensitivity microbalance (0.1 µg) and turbomolecular high vacuum pumping system (IGA-003; Hiden-Isochema, Warrington, UK). The IGA instrument can be easily adapted to measure water vapor transfer rates, in accordance to the method described by ASTM E 96/E96M-05 standard (2005).The measurements were carried out at the relative humidity differences ranging from 10 to 90% (*ΔRH%*) and temperature of 25 and 38^oC. In these experiments, sample (paper film) was first saturated at different RH using a salt solution

($MgCl_2$ (33*%RH*), $Mg(NO_3)_2$ (52*%RH*), NaCl (76*%RH*), KNO_3 (92 *%RH*)) in the base of the sample holder. It was then, followed by desorption step using a flow of purge gas (nitrogen) partially saturated with water vapor, e.g., relative humidity of 2, 20 and 50%, obtained by an automatic water vapor generator (HumidSys, InstruQuest Inc., USA), in order to study the effects of driving force (ΔRH) on the water vapor permeability. Two to three replicates were made per each RH depending on the variation of the results and the average values were taken for the analysis. Reproducibility of the results was within 5-10% range.

4.3. Theory

4.3.1. Adsorption Isotherm Models

4.3.1.1. Hailwood-Horribon (H-H) Model

In order to understand the formation of water vapor in the cellulose fiber based material, water vapor adsorption isotherms were studied by Hailwood-Horribon model. The model was primarily used to evaluate the form of water existing in chemically modified and unmodified cellulose fiber materials. According to the model postulates, adsorption of water vapor by porous material is governed by two sets of equilibria: the first is the formation of a solid solution of water in the material (polylayer water), and second is the formation of hydrates between water and active surface group of the fiber material (monolayer water). Based on the model postulations the three distinct regions in the cell wall are: unhydrated polymer (a unit of the hypothetical polymer molecule of dry fiber, which can adsorb one molecule of water to form a monohydrate), hydrated polymer (the bound moisture, described as a monohydrate), and polylayer water (the water molecules loosely bound to the cell wall in layers that superimpose to the water monolayer). Furthermore, these three formations are supposed to behave as an ideal solid solution. The H-H model examines the state of equilibrium existing between a vapor phase, a liquid phase and a solid solution (Hailwood and Horrobin, 1946). The H-H theory predicts that plotting the ratio of the humidity to the uptake (h/M) against relative humidity ($\%\ h$) should give a parabolic relationship of the form shown by the following equation:

$$\frac{h}{M} = A + B(h) - C * (h)^2 \qquad 4.1$$

where h is the relative humidity ($\%$); M is the equilibrium moisture content ($\%$); and *A*, *B*, and *C* are the empirical parameters (Skaar 1988).

$$M = M_h + M_s = \frac{W}{18} \qquad 4.2$$

In terms of relative humidity, $H = 100h$, and percentage moisture content $M = 100m$:

$$M = M_h + M_s = \frac{1800}{W}\left[\frac{K_1K_2H}{100+K_1K_2H}\right] + \frac{1800}{W}\left[\frac{K_2H}{100-K_2H}\right] \qquad 4.3$$

$$A = \frac{W}{18} * \left[\frac{1}{K_2(K_1+1)}\right] \qquad 4.4$$

$$B = \frac{W}{1800} * \left[\frac{K_1-1}{K_1+1}\right] \qquad 4.5$$

$$C = \frac{W}{1800} * \left[\frac{K_1K_2}{K_1+1}\right] \qquad 4.6$$

The molecular mass of the dry cell wall material per adsorption site (W) gives a comparative indication of the susceptibility of the cellulose fiber material and can be calculated from the constants *A*, *B* and *C* in (4.1).

$$W = 1800\sqrt{B^2 + 4AC} \tag{4.7}$$

In the above equations M_h and M_s are the fractional moisture contents of the monolayer and polylayer water, respectively, and M is the total fraction of moisture content (all based on the dry weight of cell wall polymer), K_1 is the equilibrium constant related to the hydrate formation from dissolved water and dry cellulose fiber material, K_2 is the equilibrium constant between dissolved water and water vapor, *W* is the weight of dry wood per mole of sorption sites and *1/W* indicates the amount of sorption sites.

4.3.1.2. Brunauer, Emmett and Teller (BET) Model

Brunauer, Emmett and Teller (BET theory) is the extended Langmuir's monolayer theory, which also considers formation of multilayers during adsorption. The BET model is used as a standard method to determine the surface area of adsorbents (Brunauer et al. 1938). The BET equation is shown below:

$$\frac{a_w}{M\,(1-a_w)} = \frac{1}{M_h C} + \frac{(C-1)a_w}{M_h C} \tag{4.8}$$

M_h is the moisture content in % corresponding to a mono- layer, a_w is water activity defined as (p/po), where *p* is the partial pressure and *po* is the saturation pressure of water vapor at a relevant temperature, M is the total equilibrium moisture content at a_w. The equilibrium constant *C* can be approximated (Moreira et al., 2008):

$$C = C_o \, exp((H_M - H_N)/RT) \quad 4.9$$

where H_M is the heat of adsorption of the first and H_N of the consecutive layers.

4.3.1.3. Guggenheim Anderson de Boer (GAB) Model

GAB model has been used for predicting moisture sorption isotherms for cellulosic products. The GAB model is usually written in the form (Timmermann, 2003):

$$M = M_h \times \frac{C \times K \times a_W}{(1 - K \times a_W)(1 - K \times a_W + C \times K \times a_W)} \quad 4.10$$

where *M* is the moisture content of the material in (%), M_h is the content of water sorbed in the first layer (monolayer moisture content), a_W is the water activity (p/po), and K and C are the Guggenheim constants corresponding to the heat of sorption of the sorbed layer. C is a constant that relates to the strength of water molecule bindings to primary adsorption sites can be determined by Eq. 4.9, and *K* is related to the heat of multilayer sorption. The parameters M_h and K can also be calculated by Arrhenius equations as (Moreira et al. 2008):

$$M_h = M_{ho} \, exp(\Delta H/RT) \quad 4.11$$

$$K = K_o \, exp((H_L - H_N)/RT) \quad 4.12$$

where H_L is the average heat of condensation of water vapor and ΔH is the heat of adsorption. The parameters, H_M and H_N have the same physical meaning as in the BET model. The heat parameters: ΔH , H_M and H_N can be calculated from Eq. (4.9) – (4.12), after extracting M_h, K and C parameters by fitting the GAB model to the experimental isotherm data.

4.3.1.4. Water vapor transport properties

At constant temperature and relative humidity gradient (ΔRH (%)), a steady state will be attained and at that condition WVTR can be directly calculated from the change in weight of the paper sample, at a specified time interval, and the area of exposed film, as described by Eq. 4.13:

$$WVTR = \frac{Weight\ Change\ of\ sample}{Area \times time} \qquad 4.13$$

WVTR refers to a specific sample configuration, e.g., thickness of the sample film. Water vapor permeability (WVP) can be calculated from WVTR as follows:

$$WVP = \frac{WVTR \times Z \times 100}{P^{sat} \times \Delta RH(\%)} \qquad 4.14$$

where Z is film thickness, P^{sat} is water vapor saturation pressure at the experimental temperature, and ΔRH (%) is percentage relative humidity gradient.

4.4. Results and Discussion

4.4.1. Water vapor adsorption equilibria

Water vapor adsorption isotherms of unmodified paper (control sample) and PLA coated paper samples at three different temperatures (15, 25 and 35 ^{o}C) are shown in Fig. 4.1a (additional figures are available in Appendix-I). All isotherms are of type IV according to IUPAC classification. It should be noted that dry, non-treated paper belongs to category of nonporous materials with typical BET surface area about 0.5 m^2/g. However, in the presence of water vapor, paper samples create relatively high BET areas due to swelling, e.g., over 100 m^2/g, which is a characteristic of porous materials (Bismarck et al., 2002). As expected, the equilibrium moisture content increased with an increase in relative water vapor pressure (relative humidity) at constant temperature. At the lower relative humidity, the isotherms show a rapid change, due to stronger sorbate-adsorbent interactions, leading to monolayer formation. At the intermediate relative humidities, corresponding to the multilayer sorption region, a more modest adsorption uptake increase is noticeable, whereas at higher relative humidity region, corresponding to the capillary condensation region, the adsorption uptake increases rapidly for unmodified samples. All samples generally show effects related to capillary condensation, in particular the isotherms at 15 ^oC. The smallest effects are observed for PLA coated paper at 35 ^oC, but at this temperature the experimental data at the highest RH's are most constrained (no data available beyond 90*% RH*). However, even for these cases there is, at least, indication that the capillary condensation may exist (change of the slope is noticeable), except for the PLA coated sample. The absence of capillary condensation in PLA coated paper could be due to the variations in pore volume and pore size distribution of the coated paper samples (Chow et al., 1999). In addition to the pore size distribution, the shape of the vapor adsorption isotherm can also be affected by the degree of crystallinity (Parker et al., 2006; Newman, 1995). Paper with high crystalline cellulose content has the lowest adsorption capacity (Ciolacu, 2011 and Parker et al., 2006). Wadsworth and Cuculo (1978) showed, using XRD analysis, that water molecules do not penetrate the crystalline region, thus indicating that the moisture is adsorbed in the amorphous regions and on the surface of crystallites. Water vapor adsorption isotherms vary with temperature and, as expected, the moisture equilibrium content decreases with increase in temperature at the constant vapor pressure, as shown in Fig. 4.1a. Similar results were reported for cellulose fiber and cellulose fiber-based materials in other studies (Rhim et al., 2009 and Wahba et al., 1957).

The adsorption-desorption isotherms of water vapor for unmodified and PLA coated paper samples are depicted in Fig. 4.1b. From the figure, the existence of H3 hysteresis loops is noticeable with the adsorption and desorption branches nearly parallel for the entire range of relative humidities. The existence of this kind of hysteresis loop related to water vapor adsorption/desorption isotherms on cellulose-fiber and wood was reported by others (Hill et al., 2008; Morrison et al., 1959). During water vapor adsorption a significant increase of the surface area occurs, due to the swelling effect of fibers leading to strong interaction of water molecules with active surface sites. This creates conditions for the hysteresis loop during desorption, e.g., the water molecules are strongly attached to the adsorption sites rendering the vapor pressure during desorption lower for the same amount of water being adsorbed during the adsorption step of isotherm measurement (Morrison et al., 1959).

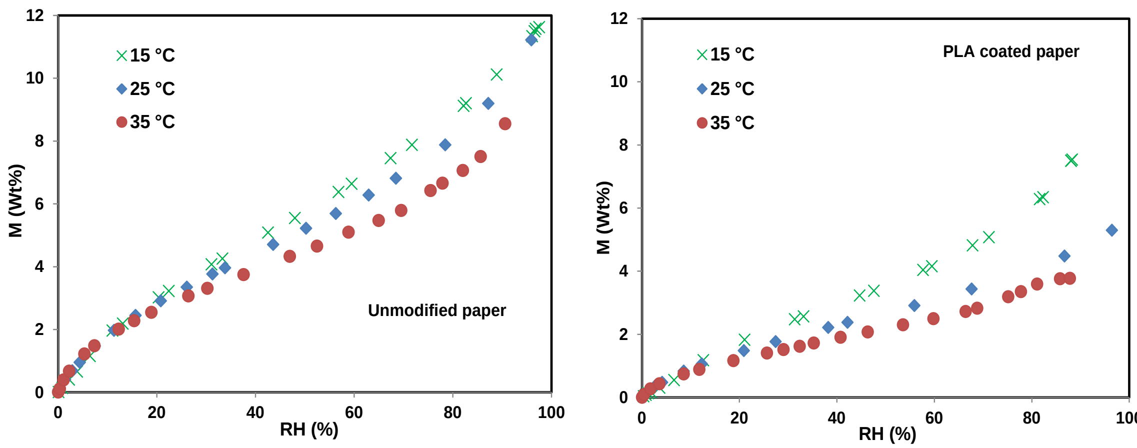

a) Adsorption isotherm of different paper samples at 15, 25 and 35 °C.

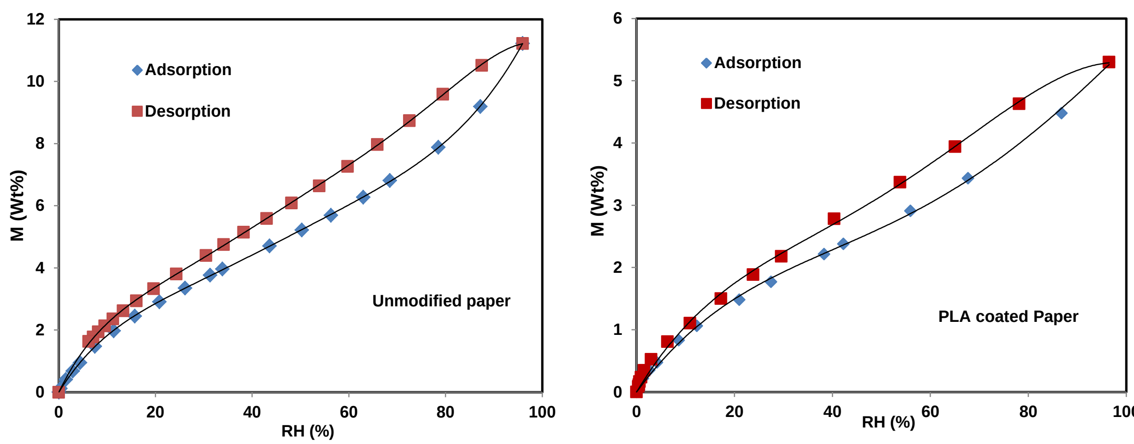

b) Adsorption/desorption isotherm of different paper samples 25 °C.

Figure 4.1. Adsorption/desorption isotherm of different paper samples.

4.4.2. Hailwood-Horrobin Data Analysis

The ratio of humidity to the equilibrium uptake versus equilibrium uptake gives parabolic curves as shown in the Fig. 4.2, in accordance to the Hailwood-Horrobin (H-H) model prediction (Hailwood and Horrobin, 1946). The fitting of H-H model to the experimental data for five samples is shown in the same figure. The monolayer and polylayer moisture contents of the paper samples were determined using the model Eqs. (4.1)-(4.5).

Summary of the H-H parameters (A, B, C, K_1, K_2 and W) of different investigated paper samples are provided in Table S1 (Appendix-I). The results from the H-H analysis (M_h and M_s) for two samples are also graphically displayed in Fig. 4.3 (additional diagrams are provided in Figure S2 in the Appendix-I).

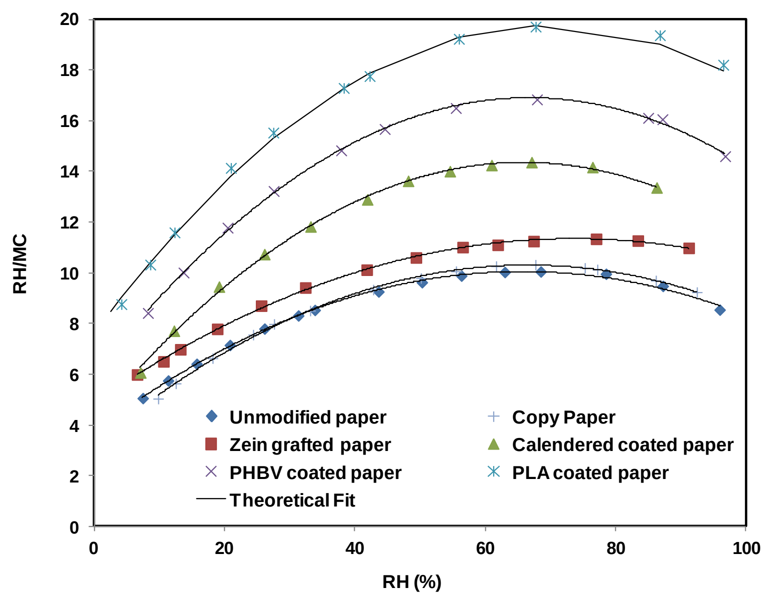

Figure 4.2. Parabola predicted by H-H theory and observed experimentally.

The total adsorbed water content is divided into monolayer and polylayer contents that are referred as hydrate and dissolved water, respectively. The results reveal that for low relative humidities (pressures), adsorption on primary sites dominates while, with increasing RH, adsorption on secondary sites (multilayer formation) gains in significance. The monolayer fraction *(M_h)* is of a particular interest, as it indicates the amount of water that is strongly adsorbed to specific sites. It is considered an optimum moisture content for food products, because it increases food stability and also at this condition, the rates of spoilage reactions are minimal (Moreira et al., 2008). Therefore, at a given temperature, the safest water activity level or relative humidity condition corresponds to monolayer moisture content or lower. Low monolayer moisture content (low hygroscopicity of the paper) is also beneficial in maintaining the high functionality of paper-based packaging materials. Although the H-H model cannot be used to determine moisture content due to the capillary condensation, nevertheless it provides useful information regarding the monolayer water content, i.e., strongly bound water molecules to the surface of the paper, as well as multilayer water vapor content below 80 % RH. At very high humidity (>80% RH) conditions, the water vapor condenses in the capillary or pores of the materials. At this region, mechanism of capillary condensation plays an important role and the pore size distribution on the paper surface determines the equilibrium moisture content (Parker et al., 2006). Equilibrium moisture contents of modified paper samples were reduced at each relative humidity level compared to the untreated paper, indicating the reduction in the hygroscopicity of paper.

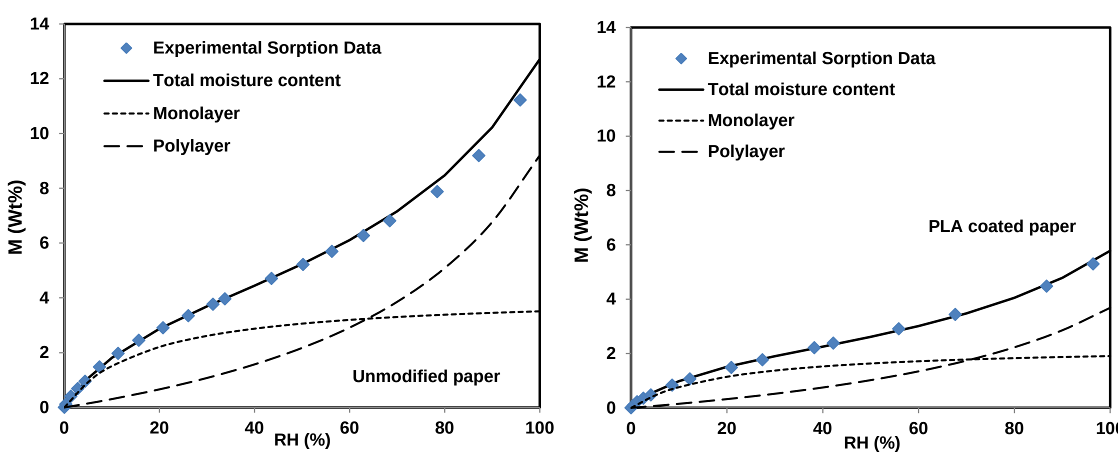

Figure 4.3. Water vapor adsorption experimental data showing agreement with H-H theory of multi-stage adsorption at T=25 °C.

Table 4.2. Values of monolayer (M_h) and polylayer (M_s) water derived from Hailwood Horrobin fits at 100 % relative humidity and T=25 °C.

Paper samples	Monomolecular M_h (%)	Polymolecular (M_s) (%)	Total (M_h+M_s) (%)	Total Sorption Percentage reduction (%)
Unmodified Paper	3.51	9.20	12.71	-
Commercial copy paper	3.42	8.39	11.81	7.10
Zein grafted paper	3.46	6.03	9.49	25.30
Calendered coated pap.	2.32	4.80	7.12	44.00
PLA Coated Paper	1.81	3.98	5.79	54.40
PHBV Coated Paper	2.07	4.87	6.94	45.40

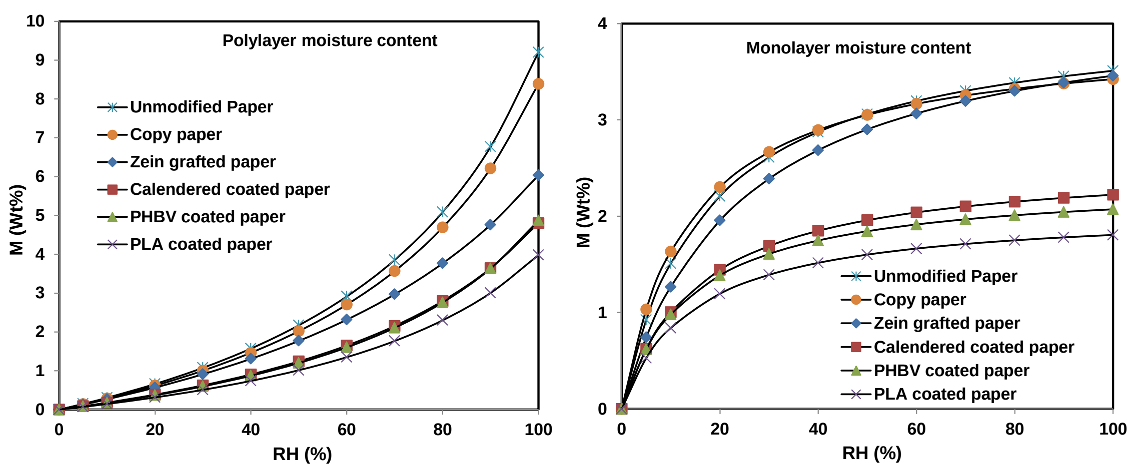

Figure 4.4. Monolayer and polylayer moisture content of different paper samples at T=25 °C.

Table 4.2 and Figure 4.4 summarize the results obtained by H-H theory at 25 °C. From Fig. 4.4, it is clear that the contribution of polylayer water is insignificant at low relative humidities, but at higher RH values (>*RH*=75%) the contribution is significant for all the samples. It can also be seen that the application of the PLA and PHBV on coated paper sample reduces the total sorption by 54.4% for PLA and 45.4% for PHBV compared to the control sample. Monolayer moisture sorption is reduced by 48.4% and 41.03% and polylayer moisture sorption by 56.74% and 47.1% for PLA and PHBV respectively compared to the control sample. These paper samples also show lower monomolecular sorption compared to the commercial calendered coated paper. From the H-H analyses, it can be asserted that grafting zein on the paper has no influence in reducing the monolayer moisture content. It is plausible that it does not block the primary surface groups, but only fills the pores of the paper, thus only reducing the equilibrium moisture content at higher relative humidity due to polylayer formation. In general, surface coating (using PLA and PHBV) reduces the active sites on the cellulose fibers, resulting in a significant change of monolayer moisture content. Effects of temperature on monolayer and polylayer moisture content of paper samples are explained in Section S1.3 (Appendix-I).

4.4.2. GAB model

Summary of the GAB model fittings of experimental isotherms is shown in Fig. 4.5. As can be clearly observed from that figure, the model provides good fits for all experimental isotherms. The largest adsorption was observed for the unmodified paper sample with moisture content of 11 wt. % at RH=96%. It was reported in earlier studies that the equilibrium moisture content of cellulose was around 15 and 17 wt. % at RH=95%, at 25 ^{o}C and 20 ^{o}C, respectively (Morrison, 1959; Wahba et al., 1957). Rhim et al. (2009) reported the equilibrium moisture content of kraft paper to be around 15 wt. % at RH=95% and 25 ^{o}C. In this study, PLA and PHBV coated papers showed the lowest water vapor adsorption, e.g., equilibrium moisture contents of less than 6 wt. % at RH=96% and 25^{o}C, as shown in Fig. 4.5. PHBV is more crystalline than PLA (Shogren, 1997), and for that reason it was expected to exhibit a lower adsorption capacity than

PLA coated paper; however, contrary to the expectation, this was not found in this study. The method of preparation and the hydrophilic properties of hydoxyvalerate content in the PHBV might have caused slightly higher water vapor adsorption than in the PLA coated paper. To the best knowledge of the authors, there is no information available in the open literature on the water vapor adsorption isotherms for polymer coated papers,. Zein grafted and commercial copy paper showed lower vapor adsorption capacities compared to unmodified papers because the zein in the grafted paper and calcium carbonate fillers in the copy papers contribute to the reduction of equilibrium moisture contents due to pore filling effects. On the other hand, PLA and PHBV coated papers showed the lowest adsorption capacities, i.e., the highest hydrophobicity, thus confirming that active site blocking is more effective in increasing hydrophobicity of papers than the pore filling. The addition of sizing agents and fillers, are also expected to change the pore size distribution (Kinoshita et al., 1998). Moreover, fillers tend to decrease the overall moisture content, because of their lower hygroscopicity (Newman, 1995).

GAB model was also used to determine monolayer moisture content (M_h). From the model analysis, PHBV and PLA coated paper showed the lowest monolayer moisture content values. Monolayer moisture content and extracted constant parameters (K and C) are provided in Table S2 (in the Appendix-I). According to the GAB model, the monolayer moisture content of zein grafted paper is higher than the unmodified (control) sample. On the other hand, according to H-H model, almost the same monolayer water content was obtained for both of the above referenced samples, as shown in Table 4.2.

The M_h values obtained using GAB model for the control samples is similar to mould fiber (untreated cellulose) at 25 °C as reported by Sorensen and Hoffmann (2003).

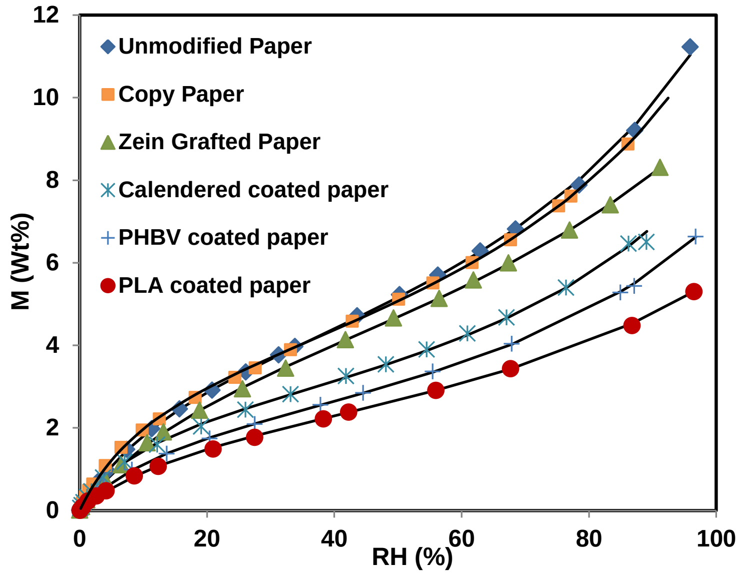

Figure 4.5. Experimental data and GAB-predicted adsorption isotherms at 25 °C.

4.4.3. Comparison of models

Table 4.3 shows comparison of H-H, GAB and BET models that were used to determine the monolayer moisture contents from the experimental isotherms. GAB model revealed comparatively higher monolayer moisture contents than others, while BET showed the lowest monolayer moisture contents for all samples. Timmermann (2003) reported that the GAB model always over predicts monolayer content compared to the BET model, and provided mathematical expression and physical reasons for the difference. The inequalities of the monolayer values are due to the effect of constant parameter (K) that measures the difference between the standard chemical potentials of the molecules in the second sorption level and in the pure liquid state (Brunauer et al., 1969; Timmermann, 2003). The GAB equation reduces to the BET equation when $K=1$, but when K is less than 1, a higher sorption is predicted than by the BET model. The other GAB constant, denoted by *C*, are energy constant but with slightly different physical meanings compared to the BET constant, *C*. The BET constant, *C*, is related to the difference between the chemical potential of the sorbate molecules in the pure liquid state and in the monolayer sorption. On the other hand, the GAB constant, *C*, is related to the difference of this magnitude in the upper layers and in the monolayer, while the constant *K* is related to this difference in the sorbate's pure liquid state and in the upper layers. The BET model generally has a difficulty to fit the isotherm data at the higher water vapor pressures (humidities) due to the formation of multi-layers. The GAB model is generally considered to provide better reproducibility of isotherm data and evaluation of the amount of water tightly bound to the primary adsorption sites (Timmermann, 1989, 2003). The obtained monolayer moisture values from H-H model were also higher than BET model but slightly lower than GAB model as shown in Table 3. In general, the GAB and H-H models can be recommended as the best models from this study for fitting experimental isotherm data in order to determine the monolayer moisture content. Based on the BET theory, a monolayer of immobilized water molecules is completed well before relative pressure of 0.5 is reached, after which an upward deviation is observed. In this study, monolayer moisture contents were done from the analysis of experimental data up to the relative pressures of 0.5. The BET monolayer water content for cellulose was also found to be 3.19 % (Morrison et al., 1959).

Table 4.3. Comparison of monolayer moisture contents derived from H-H, BET and GAB models.

Paper samples	H-H Model M_h (%)	BET-Model M_h (%)	GAB Model M_h (%)
Unmodified paper (Control)	3.51	3.27	4.12
Commercial copy paper	3.42	2.99	3.38
Zein grafted paper	3.46	2.36	4.32
Calendered coated pap. (Commercial)	2.32	2.03	2.70
PLA coated paper	1.81	1.57	2.29
PHBV coated paper	2.07	1.79	2.44

4.4.2. Water vapor transport properties

Water vapor transmission rates (WVTR's) of unmodified and coated paper samples at temperatures of 25 and 38 ^{o}C (corresponding to standard tropical condition) were calculated for different relative humidity gradients using Eq. 4.13. The summary of results is shown in Table 4.4. As expected, WVTR's are dependent on the relative humidity difference (driving force) and temperature. Zein grafted paper samples showed lower WVTR than reference sample, but higher WVTR value than coated paper samples. Zein grafting facilitates the closing of surface pores in the fiber network but does not have significant effect in reducing water solubility in the sample, as discussed in the previous section. The surface coating of papers (using PLA and PHBV) decreases WVTR's much more than using filler (zein) alone. It is plausible that coating plays a significant role in reducing both water vapor solubility and mobility (diffusion) in the modified samples. PHBV coated samples showed much lower WVTR's than other paper samples. Shogren (1997) reported that the WVTR's values of PLA and PHBV films are

172 and 21 g/m^2/day at T=25 ^{o}C and ΔRH=100%, respectively. The WVTR's values of PLA and PHBV coated paper films found in this study were higher than the values reported for the pure PLA and PHBV films. This is probably due to the deficiency of continuous film formation during coating process and possibly using thinner films for the coatings. The percentage of crystallinity in the film also affects the water vapor transmission rate. Shogren (1997) and Tsuji (2006) showed that WVTR's decreases with increased crystallinity of the film. The WVTR's decreases monotonically with increased in crystallinity from 0-20 % and levels off when crystallinity exceeds 30%. They suggested that the change was due to the higher resistance of restricted amorphous regions to water vapor permeation compared to the free amorphous regions. According to Thygesen et al. (2005), the cellulose crystallinity from wood based fibers ranged between 60-70% of cellulose content and the crystallinity of the filter paper was 57% of the sample weight.

Water vapor permabilities (WVP's) of unmodified and coated samples at 25 and 38 oC were calculated using Eq. 4.14. Fig. 4.6 shows the WVP's of the samples at different relative humidity gradients (ΔRH). As can be seen from the figure, WVP's increase slightly with the temperature. They stay relatively constant at lower relative humidity gradients, but at the higher gradients, the WVP's showed upward trends. This can be due to the dependency of diffusivity on moisture content of the sample and/or different transport mechanisms prevalent at different RH's, as reported in our previous study (Bedane et al., 2012). At the lower RH region, molecular and /or Knudsen diffusion mechanism controls the water vapor transport behavior in the pores of the cellulose network, and the diffusivity is nearly independent of the moisture content of the sample.

Table 4.4. WVTR, normalized to Z=100 μm, and permeabilities (WVP) of different paper sample films at P=100 kPa and T=25 & 38 ^{o}C.

Paper samples	WVTR (g/m^2.day) (25 ^{o}C)			WVTR (g/m^2.day) (38 ^{o}C)		
	ΔRH=33%	ΔRH=50%	ΔRH=90%	ΔRH=33%	ΔRH=50%	ΔRH=90%
Unmodified paper (60 g/m^2)	340	506	822	536	1600	2473
Calendered coated paper (commercial)	127	187	550	322	209	1275
Zein grafted Paper	---	143	335	---	---	1800
PLA coated Paper	58	95	250	99	189	647
PHBV coated paper	11	22	82	196	78	196

However, as the relative humidity increases, the surface diffusivity becomes the dominant transport mechanism, and the diffusivity increases consequently by reaching the maximum value, after which it starts to decrease due to formation of water vapor cluster at the higher humidity, as reported in our previous study (Bedane et al. 2012). According to the solution-diffusion (S-D) theory, which was proposed for the water vapor permeability through paper samples (films), permeability depends on both the solubility and diffusivity of water vapor. PHBV coated paper exhibits lower water vapor permeability than PLA coated paper, as can be seen from Fig. 4.6, even though the PHBV coated paper has higher water adsorption capacity than its PLA counterpart, i.e., higher solubility, as discussed in the section 4.1 and shown in Fig. 4.5. This result could be interpreted by applying the combined solution-diffusion effect, as per the S-D theory, for the case when diffusivities of water vapor through these films are more dominant than their solubilities (Bedane et al., 2012).

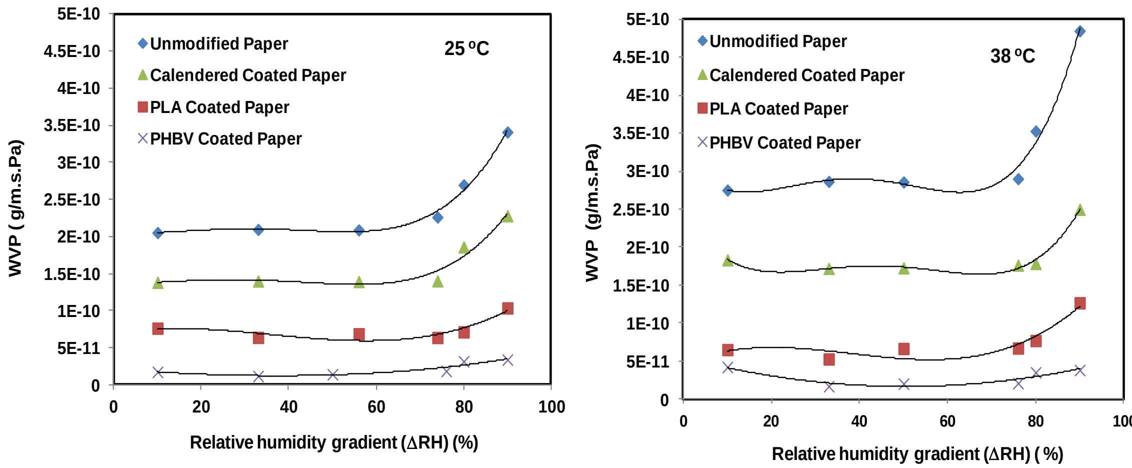

Figure 4.6. WVP of different paper samples at 25 °C and 38 °C.

Moreover, PHBV and PLA coated paper samples showed much lower water vapor permeability than unmodified and commercial calendered coated paper samples, as also shown in Fig. 4.6. Their permeability values are slightly higher than for the pure PHBV and PLA films, as reported by Tsuji et al. (2006), who found the WVP's of PLA films in the range of 1.69-2.08×10^{-11} g/m.s.Pa, and Sanchez-Garcia et al. (2008), who found the WVP's of PHBV films in the range of 0.32-1.27×10^{-11} g/m.s.Pa. This is expected due to less hydrophilic nature of PHBV and PLA films compared to the overall hydrophilicity of PHBV and PLA coated paper samples, and it also depends on the coating film thickness of the paper samples. The water vapor permeabilities of amorphous PLA and PHBV films vary from 1.8 to 2.3×10^{-11} g/m.s.Pa and 1.0 to 2.0×10^{-11} g/m.s.Pa at 25 °C, respectively, which are equivalent to PLA and PHBV coated papers (Sanchez-Garcia et al., 2008; Kalia and Avérous 2011; Tsuji et al., 2006; Siparsky, 1997). WVP's of zein coated paper was found in this study to be 1.35×10^{-10} g/m.s.Pa at T=25 °C and

ΔRH=90%, which is higher than for PLA and PHBV coated paper samples. However, WVP of zein coated paper from this study is lower than for pure starch films, which was reported in other studies to be in the range of 3-117*10^{-10} g/m.s.Pa (Bertuzzi et al., 2007; Ryu et al., 2002).This could be due to the strong hygroscopicity of starch films. The solubility of water in the starch film is also higher than in cellulose fiber, as reported by Bertuzzi et al. (2007).

4.5. Conclusions

The sorption behavior of different modified paper samples was determined from their water vapor adsorption isotherms at 15, 25 and 35 ^{o}C. The type IV isotherms measured experimentally at 25 ^{o}C were mathematically modeled using H-H, GAB and BET equations. The monolayer moisture content of each sample was determined from these models. The values of monolayer moisture content, obtained from the H-H and GAB model fittings of the experimental data, are in the close agreements for all paper samples investigated in this study and are recommended as the best models for monolayer water vapor determinations. The isotherm, according to the H-H model, can be conveniently divided into monolayer and polylayer parts for a given relative humidity. From that analysis**,** it was shown that zein grafted paper did not exhibit reduction in the monolayer moisture content, but showed decreased multilayer moisture content when compared to unmodified (reference) paper sample. The monolayer moisture contents of PLA and PHBV coated paper samples are lower compared to unmodified paper samples and commercial calendered coated samples. The application of the PLA and PHBV films on coated paper samples reduce the total sorption by 54.4% and 45.4%, respectively compared to the control sample, clearly indicating that coating has to be implemented on the substrate to obtain superior barrier properties. The amount of sorption (formation of monolayer and polylayer moisture contents) decreases as the temperature increases, in particular for the monolayer moisture contents. At low relative humidities (vapor pressures), adsorption on primary sites dominates, while with increasing RH above 75% adsorption on secondary sites (multilayer formation) gains in significance.

WVP's of unmodified and coated paper samples at the temperatures of 25 and 38 ^oC were calculated from WVTR's, which were measured at a wide range of vapor partial pressure gradients. PHBV and PLA coated paper samples showed much lower WVP's than unmodified and commercial calendered coated paper samples. The water vapor permeabilities for different samples were found to be relatively constant up to the modest relative humidity levels; however, at the higher levels they showed an increasing trend. This behavior is attributed to an increase in the surface diffusivities of water vapor at the higher moisture contents according to the solution-diffusion theory.

Based on the overall investigation performed in this study PHBV and PLA coated paper samples showed the best barrier properties to water vapor and could be considered the most appropriate candidates for packaging applications.

References

Andersson, C**.** (2008): New ways to enhance the functionality of Paperboard by Surface Treatment-a Review. Packag. Technol. Sci. (2008). doi:10.1002/pts.823

Ashely, R.J. (1985): Permeability and plastic packaging. In polymer Permeability: Comyn, J. (Ed.), J. Elsevier Applied Scie. pp. 269-308. London, UK.

ASTM Standard E96/E96 M-05 (2005): Standard test methods for water vapor transmission of materials: ASTM International, West Conshohocken, PA, USA. doi: 10.1520/E0096_E0096M-05

Bedane, A.H, Qinglin, H., Xiao H. and Eić, M. (2012): Mass transfer of water vapor, carbon dioxide and oxygen on modified cellulose fiber-based materials. J. Nord Pulp and Pap. Res. 27(2), 409-417.

Bertuzzi, M.A., Castro Vidaurre, E.F., Armada, M. and Gottifredi, J.C.: Water vapor permeability of edible starch based films. J. of Food Eng. 80, 972-978 (2007)

Bismarck A., Aranberri-Askargorta, I., Springer J. (2002): Surface characterization of Flax, Hemp and Cellulose Fibers; Surface Properties and the Water Uptake Behavior. Poly. Compos. 23 (5), 872-894.

Brunauer, S., Emmett, P., Teller, E. (1938): Adsorption of gases in multimolecular layers. J. Am. Chem.Soc. 60, 309-319.

Brunauer, S., J. Skalny, J., Bodor, E. E. (1969): Adsorption on Nonporous Solids. J. Colloid and Interface. Sci. 30, 546–552.

Hill, C.A.S., Andrew, N., Gary, N. (2009): The Water Vapor Sorption Behavior of Natural Fibers. J. Appl. Polym. Sci. 112, 1524-1537.

Ciolacu, D., Ciolacu, F., and Popa, V.I. (2011): Amorphous Cellulose –Structure and Characterization. Cellulose Che. Technol. 45, 13-21.

Chow, G-M., Ovid'ko IIya, A., Tsakalakos, T. (1999): Nanostructured Films and Coatings, Kluwer Academic Publisher, the Netherlands, 78, 55-61.

Del Nobile, M.A., Baiano, A., Benedetto, A. and Massignan, L. (2006): Respiration Rate of Minimally Processed Lettuce as Affected by Packaging, J. Food Eng.74, 60–69.

Debeaufort, F., Voilley, A., Meares, P. (1994): Water vapor permeability and diffusivity through methylcellulose edible films. J. Membr. Sci. 91, 125-133.

Hailwood, A. and Horrobin, S. (1946): Absorption of water by polymers: analysis in terms of a sample model. Trans. Far. Soc. 42B, 84-102.

Kalia, S. and Avérous, L.: Characteristics and Applications of Poly (lactide). Biopolymers (2011): Biomedical and Environmental applications, pp.183-224. Scrivener Publishing LLC, Salem, Massachusetts.

Kinoshita, N., Noda H., Toyotake, Y., Katsuzawa, H. (1998). The effects of filler contents and beating on the porous structure of high-filler-containing papers. Sen'I Gakkaishi, 54(1), 46-53.

Koide, S. and Shi, J. (2007): Microbial and Quality Evaluation of Green Peppers Stored in Biodegradable Film Packaging. Food Control 18, 1121–1125.

Kuusipalo, J.: PHB/V in Extrusion Coating of Paper and Paperboard-Study of Functional properties (Part-II). J. Polym. and the Environ. 8, 49-57 (2000)

Moreira, R., Chenlo, F., Torres, M.D. and Vallejo, N. (2008): Thermodynamic analysis of experimental sorption of loquat and quince fruit, J. Food Eng. 88, 514-521.

Morrison, J. L. and Dzieciuch, M. A. (1959): The thermodynamics properties of the system cellulose-water vapor, Canadian J. Chem. 37, 1379-1390.

Newman, R.H.: Adsorbed and absorbed moisture in bleached Kraft pulp. Industrial Research Ltd., Lower Hutt, New Zealand (1995)

Quirijns, E.J., Boxtel, A. JB., Loon, W. KP., and Straten, G. (2005): Sorption isotherms, GAB parameters and isosteric heat of sorption. J. Sci. of Food and Agric. 85, 1805-1814.

Rhim, J-W, Lee, J-H., and Hong, S-I. (2007): Increase in water resistance of paper board by coating with poly (lactide), Packag. Technol. Sci. 20, 393-402.

Rhim, J-W. and Lee, J.H. (2009): Thermodynamics Analysis of Water Vapor Sorption Isotherms and Mechanical Properties of Selected Paper-Based Food Packaging Materials. J Food Sci. 74, 502-511.

Ryu, S. Y., Rhim, J. W., Roh, H. J., & Kim, S. S. (2002): Preparation and physical properties of zein-coated high-amylose corn starch film. Food Sci. and technol., 35, 680–686.

Parker, M.E., Bronlund, J.E. and Mawson, A.J. (2006): Moisture Sorption Isotherms for Paper and Paperboard in Food Chain Conditions. Packag. Technol. Sci. 19, 193-209.

Sanchez-Garcia, M.D., Gimenez, E. and Lagaron, J.M. (2008): Morphology and barrier properties of solvent cast composites of thermoplastic biopolymers and purified cellulose fibers. Carbohydrate Polym. 71, 235-244.

Seborg, C.O., and Stamm, A.J. (1931): Sorption of water vapor by papermaking materials: Effect of Beating. Industrial and Eng. Chem. 23, 1271-1275.

Seborg, C.O. and Stamm, A.J. (1936): Sorption of water vapor by papermaking materials: Effect of physical and chemical processing. Industrial and Eng. Chem. 28, 1245-1250.

Shogren, R.(1997): Water Vapor Permeability of Biodegradable Polymers. J. of Environ. Polym. Degrad. 5, 91-95.

Simpson, W. (1980): Sorption theories applied to wood, Wood Fiber 12, 183-195.

Siparsky, G.L., Voorhees, K.J., Dorgan, J.R., and Schilling, K. (1997): Water Transport in Polylactic Acid (PLA), PLA/Polycaprolactone Copolymers, and PLA/Polyethylene Glycol Blends. J. Environ. Polym. Degrad. 5, 125-136.

Skaar, C. (1988): Wood-Water Relation. Springer-Verlag, Berlin.

Sorensen, G. and Hoffmann, J. (2003): Moisture Sorption in Moulded Fibre Trays and Effect on static Compression Strength. Packag. Technol. and Sci.16, 159-169.

Spalt, H.A. (1958): The fundamentals of water vapor sorption by wood. For. Prod. J. 8, 288-295.

Timmermann, E.O. (1989): A B.E.T.-like Three Sorption Stage Isotherm? J. Chem.Soc., Faraday Trans. 85, 1631-1645.

Timmermann, E.O.: Multilayer sorption parameters: BET or GAB values? Colloids and Surfaces, A: Physicochem. Eng. Asp, 220, 235–260 (2003)

Timmermann, E.O., Chirife, J. and Iglesias, H.A. (2001): Water sorption isotherms of foods and food stuffs: BET or GAB Parameters? J. Food Eng. 48, 19-31.

Thygesen, A., Oddershede, J., Lilholt, H., Thomsen, A.B. and Stahl, K. (2005): On the determination of crystallinity and cellulose content in plant fibres. Cellulose 12, 563–576.

Tsuji, H., Okino, R., Daimon, H., and Fujie, K. (2006): Water vapor permeability of Poly (lactide)s: Effect of molecular characteristic and crystallinity. J. Appl. Polym. Sci. 99, 2245-2252.

Twede, D. and Selke, S.E.M.(2005): Cartons, Crates and Corrugated Board. Handbook of Paper and Wood packaging Technology. DEStech Publications, Inc., Lancaster, Penyslvania, U.S.A.

Wang, N. and Brennan, J.G.(1991): Moisture Sorption isotherm characteristics of potatoes at four temperatures. J. Food Eng.14, 269-282.

Wahba, M. and Nashed, S. (1957). Moisture relations of cellulose. III. Sorption hysteresis and the effect of temperature. J. Text. Inst. Trans. 48, T1-T20 .

Yamada, K., Noguchi, A. and Takahashi, H.(1996): Effects of the solvents on properties of zein, Nippon Shokuhin Kagaku Kaishi 43, 306–312.

Chapter 5: Structural and thermodynamics characterization of modified cellulose fiber-based materials and related interactions with water vapor

Alemayehu H. Bedane[a], Huining Xiao[b], Mladen Eić[b] and Madjid Farmahini-Farahani[a]

University of New Brunswick

Applied Surface Science 351; 725-737, 2015

---

[a]Graduate Student, Department of Chemical Engineering, UNB

[b]Professor, Department of Chemical Engineering, UNB

Abstract

In this study, the surface characteristics, water vapor interactions, and state of water adsorbed on unmodified and coated paper samples were investigated in an attempt to obtain a better understanding of the fundamental principles related to thermodynamics of this process, as well as to provide essential insight that could be used for further improvement of the papers' barrier properties. Based on the BET measurement, the coated paper samples showed higher specific surface areas than unmodified paper; however, their mean pore diameters are smaller. The BJH method was used for pore size distribution analysis. The highest peak corresponding to the modified samples with smaller pore sizes was found to be in the range of 1-30 nm, while it was in the 30-100 nm pore size range for unmodified paper. The net isosteric heats of sorption for different unmodified and modified paper samples were determined from water vapor adsorption isotherms measured at 15, 25, and 35 ^{o}C. The net isosteric heats of sorption decreased with an increase of moisture content after reaching the maximum values at 12.53, 15.25, 14.71, 23.2, and 22.77 kJ/mol for unmodified, zein grafted, calendered coated, PLA, and PHBV coated papers, respectively. The state of adsorbed water and water-vapor interaction on paper surface were also studied by TGA-DSC and FT-IR spectroscopic techniques. The FT-IR results revealed the formation of water vapor clusters due to poly-layer formation at the higher relative humidity. This has a profound effect on the equilibrium properties, e.g., the intensity of interactions between water molecules and the paper surface decreases as the relative humidity (moisture content) increases. Percentage of bound and unbound water formation and also the dehydration energy at various

relative humidities were determined for the paper samples using the TGA-DSC technique.

Keywords: coated-paper, cellulose fiber, moisture content, isosteric heats of sorption, simultaneous thermal analysis(TGA-DSC), Fourier transform infrared spectroscopy (FT-IR).

5.1. Introduction

The non-biodegradable properties of synthetic polymers make them unsuitable for food or pharmaceutical packaging applications from an environmental point of view. A suitable way to overcome this problem is to replace them with biodegradable polymers, which can easily decompose when disposed as waste. Recently, cellulose fiber materials, like paper, have gained more attention for the application as packaging materials, since they are more environmentally friendly. However, cellulose fiber based materials are hygroscopic, easily adsorbing moisture when the relative humidity (RH) is high and losing it when the surrounding air is dry. Adsorbed water in the cellulose-based material affects the textural, technological qualities and long-term stability (Twede and Selke, 2005). It also affects the water vapor transition rates (WVTR's) and permeabilities (WVP's) (Bedane et. al. 2012, 2014). Moisture sensitive foods and pharmaceuticals should be placed in packaging with controlled water vapor and gas transmission rates to achieve the required quality, safety, and shelf life (Ashley, R.J. 1985; Koide et al., 2007; Del Nobile et al., 2006).

Hardwoods and softwoods are reduced to cellulose fibers forming wood pulps for making paper products. The cellulose fiber possesses a high crystalline content, inaccessible to water molecules but also contains amorphous component to which water molecules can gain access. The main adsorption sites in cellulose fiber-based material are the hydroxyl groups, and also the carbonyl groups (Olsson et al., 2004). Adsorbed water molecule has a strong affinity for hydrogen bond formation with other polar polymers, like, cellulose fiber-based materials. Those that are closely associated with OH groups form monolayer water, but those not intimately associated with OH groups form polylayer water (Hill et al., 2009). The monolayer water molecules are non-freezing bound water because the motion of the water structures is strictly limited by the association with the surface (Nakamura et al., 1981; Hatakeyama et al., 2000).

Paper is a porous medium and has a macro-pore size in the range of 0.1-10μm (Davis et al., 1989; Li et al., 1999). As the result of these, water vapor and gas penetrate easily through the paper. Porosity and pore size distribution in the paper affect its surface uniformity, moisture adsorption, homogenous ink uptake (printing ink) and so on (Dodson et al., 1996; Li et al., 1999). Coating and filler materials reduce the pore size and pore volume to some extent as a result of blocking the pores between the fibers on the paper surface. There are a variety of physical techniques to measure geometry of pores on the material surface that include: gas adsorption isotherms, mercury intrusion porosimetry, solute exclusion, thermoporosimetry, nuclear magnetic resonance and microscopic techniques (Papadopoulos et al., 2003; Li et al., 1999). In this study, nitrogen and water vapor adsorption isotherms were used for the analysis of the specific surface area, pore sizes and pore size distribution for both unmodified and modified paper samples. Characterizing modified paper samples provides essential insight for a further improvement of the paper's barrier properties, in order to enhance its viability as a packaging material and quality paper.

The thermodynamics functions (total heat of sorption (Q_{st}), net isosteric heat of sorption (q_{st}), differential enthalpy (ΔH_d) and entropy (ΔS_d)), which can be obtained from sorption isotherms, provide useful information related to the binding strength between sorbed water vapor and adsorbent's surface, and energy requirements associated with sorption process (Moreira R. et al., 2008; Rhim and Lee, 2009; Al-Muhtaseb et al., 2004; Wang and Brennan, 1991). Isosteric heat of water adsorption is a measure of energy that binds water molecules with substrate surface and, it is also identified with the energy required to remove moisture from material. Calorimetric techniques, e.g. differential scanning calorimetry (DSC) and thermogravimetry (TG) or combined simultaneous thermal analysis (STA), can also be applied to determine isosteric heat of water vapor on the materials (Mulet et al., 1999; Reidel et al., 1977; Sanchez et al., 1997).

Biopolymer films and/or coatings on cellulose fiber materials have the potential to increase the water vapor barrier properties. Biodegradable materials, such as polylactic acid or polylactide (PLA), poly-3-hydroxybutyrate-co-3-hydroxyvalerate (PHBV), and zein have shown a significant potential as packaging materials. These bio-based polymers have also been used for modification of cellulose fiber materials in order to enhance water barrier (mass transfer) properties and reduce hygroscopicity. It is therefore important to understand the physical and chemical treatments applied to paper surface and how they affect the surface characteristic, e.g., interaction between water and modified cellulose. In our earlier study we have reported transport (barrier) properties of the paper samples that were also used in this study (Bedane et al., 2012, 2014). This study focuses on structural and thermodynamics properties of the samples to better understand the physical and chemical treatments applied to paper surface and how they affect the surface characteristics, through measuring pore sizes, adsorption isotherms and analyzing interaction between water molecules and modified cellulose surface. The main objectives of this study can be summarized as follows:

- To examine the specific surface area, pore size and pore volume of modified paper samples and compare to unmodified paper sample (reference sample).
- To determine the net isosteric heats of sorption (q_{st}) from water vapor adsorption isotherms and the formation of adsorbed water and its energy of interaction on the modified paper surface at different relative humidity levels using FT-IR and TGA-DSC spectroscopic techniques.
- To use the results obtained above in order to get better understanding of water vapor transfer properties in different papers.

5.2. Materials and Experimental

5.2.1. Preparation of Samples

Several types of paper samples that were prepared for this study are listed in Table 1. Unmodified paper sample was made from pure cellulose pulp. Modified paper samples, such as PLA and PHBV coated paper, with coating weight of 25-30 g/m^2 on the base paper (85±4 g/m^2), as well as zein grafted paper (~28 g/m^2 zein coating weight) were prepared according to procedures further explained in this section. The PLA was purchased from NatureWorks, LLC; PHBV, with a hydroxyvalerate content of 3 % wt. was purchased from Sunrise Global, Inc. NJ. USA and chloroform used as the solvent was purchased from Sigma- Aldrich (Shanghai) Trading Co. Ltd.. All compounds were used without further purification. PHBV and PLA coated paper were prepared through solution bar coater machine by dissolving 0.306 g powder of each sample in 6 ml of chloroform at 50 ^{o}C afterward sonicated for 1 hour (Rhim et al., 2007). Each coating solution was then spread onto printing paper surface (10*10 cm, thickness 90 µm) mounted on a teflon sheet using a glass bar coater machine at room temperature and dried under ambient conditions (23 ± 2 ^{o}C) for 24 h.

Table 5.1. Paper samples and their physical properties

Physical Property	Paper types					
	Unmodified Paper	Zein grafted/ coated paper	PLA coated paper	PHBV coated Paper	Commercial papers	
					Copy/printing (base-paper)	Calendered coated paper
Grammage (g/m^2)	60	88	115	110	85	150
Density (kg/m^3)	546	628	1153	967	850	1083
Thickness (mm)	0.11	0.14	0.13	0.12	0.10	0.14

Zein, a class of prolamine protein-based natural products with highly hydrophobic and barrier properties, was grafted onto the paper sheet (60 g/m^2) consisting of sulphite fibre using Isophorone Diisocyanate (IPDI) as a coupling agent. The zein solution was prepared by dissolving a certain amount of zein powder in the mixture of 70% acetone and 30% water (v/v) (Yamada et al., 1996). Then the additive-free hand sheets were reacted with the diluted zein solution and the IPDI at the temperature of 50-60 ^{o}C, followed by a magnetic stirring for a few hours. The samples were finally washed several times and oven dried overnight at 100 ^{o}C before the characterization tests were carried out.

5.2.2. Water vapor and N_2 adsorption isotherms

Water vapor and N_2 adsorption isotherms of the samples were measured using Belsorp-Max (BEL JAPAN, INC., Osaka, Japan). The Belsorp-max is an automatic gas adsorption /desorption volumetric measuring unit that measures adsorption isotherm in the relative pressure range p/po=10^{-8}-0.997. The water vapor adsorption isotherms of the samples used in this study were measured at 15, 25 and 35 ^{o}C. The samples were dried for 12-24 h at 60^{o}C before the isotherm measurement.

5.2.3. TGA-DSC and FT-IR analyses

Different cellulose-based samples were analyzed by combined thermo gravimetric and differential scanning calorimeter instrument (TGA-DSC) to determine the amount and the form of water availability at different water activities, e.g., relative humidities. The samples for these measurements were prepared by drying in an oven for two days at 60^{o}C before the scan was taken. They were equilibrated at different relative humidities (RH= 10, 30, 50, 70, 90 %,) in the instrument chamber using a humidity generator (HumidSys, InstruQuest Inc., USA), and N_2 as a carrier gas, until the constant mass of the sample was established and recorded. Then the samples were heated at a heating rate of 10 ^{o}C/min. Weight loss and heat flow of the samples were recorded for the temperature range 20-300^{o}C.

FT-IR spectra were recorded using a Spectrum 100 Series (PerkinElmer Ltd, Beaconsfield, BUCKS, United Kingdom). The samples were equilibrated at various relative humidities (RH=10-100%), in the infrared chamber, using the same humidity generator (HumidSys, InstruQuest Inc., USA) as for the TGA/DSC measurements. Spectra were analyzed using the spectrum software (version 3.02.01). The spectroscopic analyses for the samples were performed within the spectral region of 650-4000 cm^{-1} with 15 scans recorded at a 4 cm^{-1} resolution. Measurements were carried out more than three times for each sample, and the average spectrum was then taken for the analysis.

5.3. Theory

5.3.1. Guggenheim Anderson de Boer (GAB) Model

GAB model has been used for predicting moisture sorption isotherms for cellulosic products. The GAB model is usually written in the form:

$$M = M_h \times \frac{C \times K \times a_W}{(1 - K \times a_W)(1 - K \times a_W + C \times K \times a_W)} \qquad 5.1$$

Where M is the moisture content of the material in (%), M_h is the content of water sorbed in the first layer (monolayer moisture content), a_W is the water activity (p/po), and K and C are the Guggenheim constants corresponding to the heat of sorption of the sorbed layer. C is a constant that relates to the strength of water molecule bindings to primary adsorption sites, and K is related to the heat of multilayer sorption. The parameters, K and C can be calculated from Arrhenius equations:

$$K = K_o \exp((H_L - H_N)/RT) \qquad 5.2$$

$$C = C_o \exp((H_M - H_N)/RT) \quad 5.3$$

where H_L is the average heat of condensation of water vapor and ΔH is the heat of adsorption. The parameters, H_M and H_N have the same physical meaning as in the BET expression. The heat values ΔH , H_M and H_N can be calculated from equations 5.2-5.3, after extracting M_h, K and C parameters by fitting the GAB model to the experimental isotherm data.

The monolayer moisture content M_h can be related to the specific surface area A_c of the materials by:

$$A_c = M_h \frac{N_A}{M_W} a_w \quad 5.4$$

Where N_A is the Avogadro's number and M_W is the molecular weight of water, and a_w is the area of water molecule projected to material surface, e.g. for cellulose surface it is estimated at about $14.8 \times 10^{-20} m^2$ /molecule (Li, 1991; Daniel and Olle, 2001).

5.3.2. Thermodynamics Analysis

Isosteric (cumulative) heat (Q_{st}) of sorption is an indicator of the state of water vapor adsorbed by the solid material. It consists of the net differential heat of sorption (q_{st}) plus the latent heat of vaporization of water (ΔH_{vap}) at the system temperature (Tolaba et al., 2003; Moreira et al., 2008).

$$Q_{st} = q_{st} + \Delta H_{vap} \quad 5.5$$

The net isosteric heat of sorption (q_{st}) for specific equilibrium moisture content (m) can be calculated from the experimental data using the Clausius–Clapeyron equation:

$$q_{st=} - R\left[\frac{\partial(\ln(p/po))}{\partial\left(\frac{1}{T}\right)}\right]_m \qquad 5.6$$

Isosteric heat of adsorption (Q_{st}) was determined from the combined thermo gravimetric-differential scanning calorimetric technique (TGA-DSC). This technique can simultaneously determine the enthalpy needed to remove adsorbed water and the weight loss during the heating process of samples with different moisture contents. The enthalpy is obtained by integrating the endothermic peak of the heat flow curve. The desorption and vaporization (cumulative) energy per mass of water evaporated can be obtained by dividing the average calculated enthalpy by the average weight loss (Eq. 5.7):

$$H_d = \frac{\int_0^m Q_{st}(m)\, dm}{\int_0^m dm} \qquad 5.7$$

where m is the moisture content of the sample and H_d is the heat of desorption and vaporization (kJ/kg), which is also called a cumulative average vaporization enthalpy (Mulet et al.,1999; Sanchez et al.,1997; Park et al., 2007).

In order to integrate Eq. 5.7 the net isosteric heat (q_{st}) has to be expressed by an exponential form based on the empirical expression proposed by Riedel (1977) using Eq. 5.8.

$$q_{st} = ce^{-bm} \qquad 5.8$$

By substituting the net isosteric heat from Eq. 5.8 into Eq. 5.5, the following expression for isosteric (cumulative) heat of adsorption/desorption can be obtained:

$$Q_{st} = ce^{-bm} + \Delta H_{vap} \qquad 5.9$$

By further substitution of Eq. 5.9 into Eq. 5.7 and integrating, the final expression (Eq. 5.9) is obtained:

$$H_d = \frac{c}{b}\left(\frac{1-e^{-bm}}{m}\right) + H_{vap} \qquad 5.10$$

The heat of desorption (H_d) and moisture content of sample (m) can be determined from the TGA-DSC experiments. The variable parameters (c and b) are determined from curve fitting of the experimentally determined heat of desorption (H_d) for the different moisture contents.

5.4. Results and Discussion

5.4.1. Surface Characterization

The BET specific surface areas of different paper samples were determined from nitrogen adsorption isotherm data at 77 K, and summarized in Table 5.2. The adsorption-desorption isotherms of nitrogen for unmodified and PHBV coated samples are shown in Fig. 5.1. The isotherms are of Type IV with H3 hysteresis loops according to IUPAC classification (IUPAC, 1985). It should also be noted that due to the strongly unfavorable character of the isotherm for unmodified paper sample, this isotherm has characteristics of Type III as well. From the figure it is noticeable that the H3 hysteresis loops are very long and the adsorption and desorption branches are nearly parallel for the whole range of p/po. This hysteresis usually observed in materials with slit-shaped pores and parallel walls, and is attributed to the existence of aggregates of plate- like particles or lamellae in the fiber (an assemblage of particles or fibrillars that are loosely coherent). Other studies have reported that the pores between the lamellae in cotton fibers resemble openings between parallel plates (Krassig, 1992). Type H3 hysteresis is also found on materials with a very wide distribution of pore sizes. It is apparent that the surfaces of fiber based materials have non-uniform pore size distribution that is caused by non-uniform fiber arrangement. The coated or modified paper samples showed higher N_2 adsorption capacities compared to unmodified samples, except the PLA coated paper (as shown in Figure S1 in Appendix-II). As a consequence, modified paper samples showed higher specific surface areas and smaller mean pore sizes than unmodified paper samples, except for the PLA coated paper, which showed a lower specific surface area. The mean pore diameters of the samples were determined from their total pore volume and BET specific surface area using Belsorp analysis program. Zein coated, copy paper and calendered coated samples showed comparatively small mean pore sizes (Table 4.2). This could be due to the blocking of the surface pores of the material by the addition of the fillers. However, no significant pore size reduction was observed in the PLA and PHBV coated papers, which is possibly due to pinhole formation on the surface, i.e. lack of perfect coating. The calendared coated paper showed the smallest mean pore diameter, because of calendaring or compressing process of the fiber network during production, which helps to reduce the void structure by increasing the degree of bonding between the fiber elements in the fiber network matrix. Resch et al. (2010) studied the effect of calendaring on the pore structure and found that the pore size of coated papers was permanently reduced by compression during calendaring. On the other hand, commercial calendered coated paper showed the highest specific surface area, that could be due to the effect of the coating material used (pigment-latex) that might create large surface area, as well as a result of low granulometry (small pore size distribution or a smaller aperture size) (Banquet and Isoard, 1997).

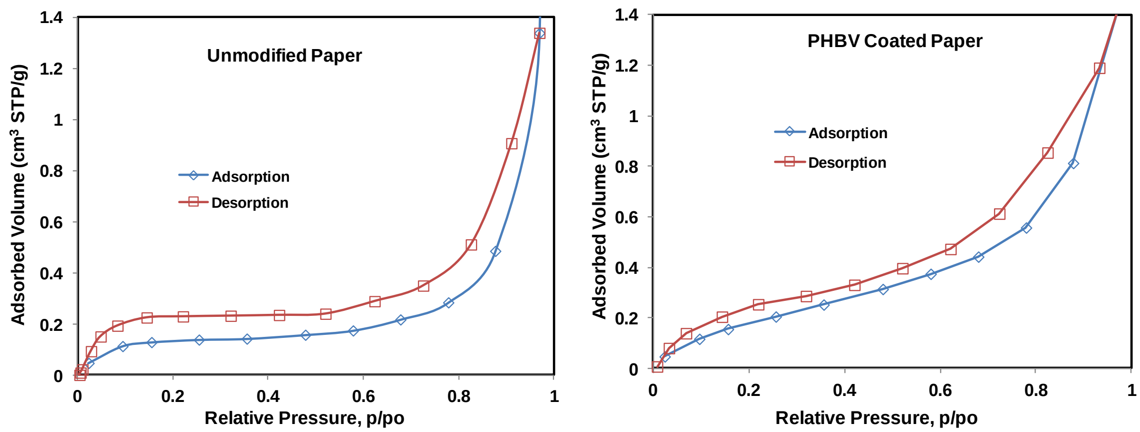

a) N_2 Adsorption/Desorption BET isotherms for unmodified paper and PHBV coated paper samples.

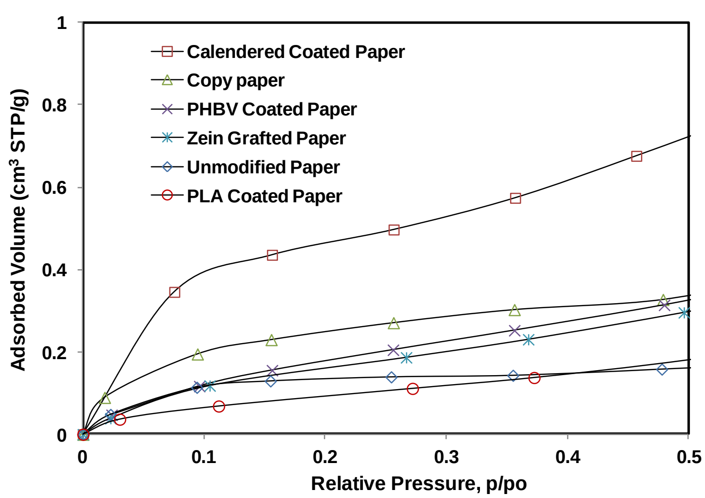

b) BET N_2 adsorption isotherms for different coated and unmodified paper samples.

Figure 5.1. BET N_2 adsorption isotherms for different coated and unmodified paper samples.

The specific surface areas measured from water vapor adsorption isotherms at 25 ^{o}C show much higher values compared to the nitrogen gas adsorption results for all the investigated samples, as shown in Table 5.2. This is due to the high dipole moment of water molecules and the formation of hydrogen bonds with the polar group of the fiber material, thus causing swelling of fiber during the adsorption. Roben et al. (2004) reported that the water vapor adsorption is not suitable as a standard for the investigation of materials' surface structures, because of the swelling effects during adsorption. However, this effect can provide a useful insight related to the extent of hydrophilicity of the modified papers. Based on water vapor adsorption results, PLA and PHBV coated paper samples showed lower BET specific surface areas than other investigated samples, thus indicating lesser hydrophilic properties. The differences in the measured BET surface areas coming from the two methods can be explained in a number of ways: first, moisture can play an important role in creating larger surface area by the effect of swollen fibers. This can cause sufficient separation of close-fitting crystallites (interlayers), thus rendering their surfaces to become more available for adsorption. Another reason is due to the smaller size and the polarity of water molecules, which enables them to penetrate into micropores or capillaries that are usually not accessible to the larger nitrogen molecules. Similar studies by Papadopoulos et al. (2003) and Bismarck et al. (2002) showed that the dried natural fibers exhibit very small specific surface area of approximately 0.5 m^2/g and also very small pore volumes. The fibers dried by water evaporation consist of only single lamellae, which cause internal fiber structure to collapse resulting in the lower surface areas. However, the swollen fibers dried by solvent exchange consist of several hundreds of lamellae, thus creating smaller pores and higher specific surface areas that range up to 200 m^2/g (Bismarck et al., 2002). The pore size of a paper depends on flocculation of papermaking fibers and grammage. Fiber flocculation helps in formation of aggregates or flocs from the raw materials presented in a papermaking furnish. Dodson et al. (1996) found that the pore radius increases with flocculation and decreases with increasing grammage.

Table 5.2. Specific surface area, mean pore diameter and WVTRs of paper samples measured at ΔRH=50% and T=25 °C from N_2 at 77 °K and water vapor at 298 °K isotherms.

Paper sample	Specific surface area (m^2/g)		Mean pore diameter (nm)*	WVTR (g/m^2.day) (normalized to 100 µm thickness) [2]
	Nitrogen	Water vapor		
Unmodified paper	0.43	162	100.50	514
Commercial copy paper	0.90	149	44.80	462
Zein grafted	0.69	117	50.42	224
Commercial calendered coated paper	1.63	101	38.51	187
PLA coated paper	0.41	78	80.06	95
PHBV coated paper	0.78	89	50.79	22

*determined from N_2 adsorption isotherm measurements

Figure 5.2 displays the pore size distribution from Barrett-Joyner-Halenda (BJH) analysis for unmodified, zein grafted and PLA coated papers using 77 K N_2 adsorption isotherms. The unmodified paper samples showed non-uniform pore size distribution because of the non-uniform fiber matrix structure. The largest pore distribution peak area of PLA coated paper shifted to smaller pore sizes, e.g., radii in the range between 10 -30 nm compared to 30-100 nm for unmodified paper. Even though no uniform pore size distribution was observed in the zein grafted paper, the largest pore distribution areas were obtained at small pore size ranges. This attributed to the filling of larger pores and coating that can facilitate the size reduction from the meso (macro)-pores to micro-pores in the paper medium (Kinoshita et al., 1998; Newman, 1995). The non-uniformity of pore distribution in the zein grafted paper sample is due to difficulty in coating/grafting uniformly on the entire paper sample. Water vapor transmission rates (WVTRs) of the samples (shown in Table 5.2) were reported in our previous study (Bedane et al., 2012). As indicated in this table, the modified paper samples showed low WVTRs (measured at ΔRH=50% (aver. RH=50±2.5%) and T=25 ^{o}C) compared to the unmodified paper. The WVTR of zein grafted paper was reduced by 56% compared to the unmodified paper. PLA and PHBV coated paper showed WVTR reduction by 79% and 95%, respectively, compared to the copy paper. Pore size reductions of the modified paper samples, as well as decrease of their hydrophilic properties (as observed from their specific surface areas measured from water vapor adsorption) are the main reasons for the reduction of WVTR's. The surface coating (using PLA and PHBV) plays a significant effect in reducing the water permeability, as it reduces both the water vapor solubility and mobility (diffusion) in the paper samples. According to the BJH analysis for pore size distribution, the highest peak (in the small pore size distribution region) for the zein grafted paper, was found at about 1.66nm in radius, as shown in Fig. 5.2. This pore size is comparatively lower than the pore radius of PLA coated paper (~12 nm) and unmodified paper sample (~ 40nm). Micropore size distribution analyses of the paper samples were performed using HK (Horvath and Kawazoe) method (supplementary Figure S1 shows HK-micropore size distribution of paper samples in Appendix-II). Average pore diameters of the paper samples corresponding to microspore sizes (using HK method) and mesopore sizes (using BJH method) of the paper samples are provided in Table 5.3. The micropores diameters of all samples are similar, as shown in Table 5.3, and these pores reflect the porosity of intra-fibers that are exposed in the fiber walls. The small and large mesopores in the papers reveal the presence of the pores between interfibers in the fiber matrix, as well as pores between fiber and filler particles, and/or pores on the coating materials. Multimodal pore size distributions are observed in the paper samples and this could be associated with coating layer and non-uniformity of paper matrix structure (Borch et. al, 2002; Robert, 1991; Chinga, 2002). Most of the modified paper samples showed the smallest mesopore sizes in the range of 2-8 nm. The PLA coated showed narrow pore size distribution (Fig. 5.2 and Table 5.3), e.g., no peaks in the very large pore (macropore) size range. This is due to more uniform coating of PLA on the paper thus producing more uniform pore size distribution.

Based on the above discussion, a fraction of water vapor can be transported through paper as a result of flow through the relatively large pore network, and the remainder part of water vapor is transferred by diffusion at the surface caused by interaction between the water vapor and the paper media.

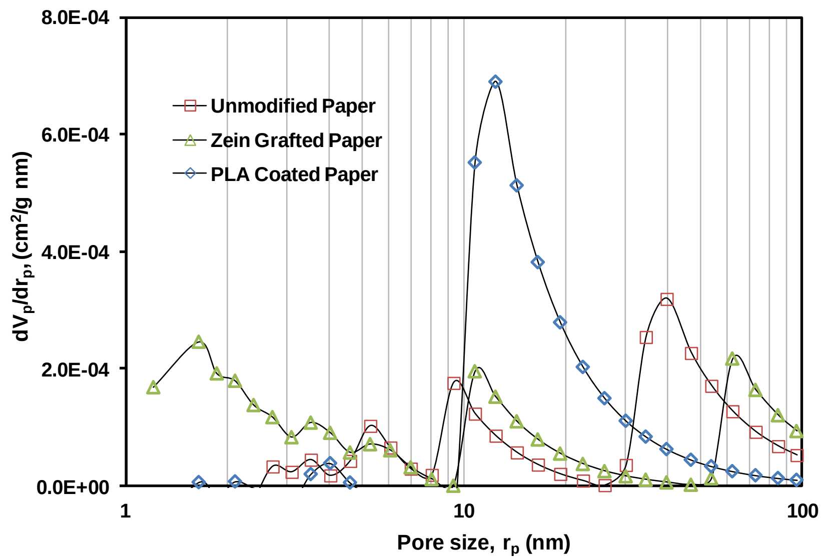

Figure 5.2. Pore size distribution from BJH method for unmodified and modified paper samples.

Table 5.3. The maximum distribution peak of micropore and mesopore sizes of the paper sample using HK (micropore size distribution analysis) and BJH (mesopore pore sizes analysis) methods.

Paper samples	Avg. micropore diameter size (nm) (HK-method)	Avg. mesopore and macropore diameter size(nm) (BJH method)		
		Small mesopore diameter	Large mesopore diameter	Macropore diameter
Unmodified paper	0.6-1.0	8-14	16-40	60-150
Commercial copy paper	0.5-1.0	4-8	16-40	60-120
Zein grafted	0.7-0.9	2-6	20-30	120-150
Commercial calendered coated paper	0.8-1.2	2-8	14-20	50-100
PLA coated paper	0.7-1.1	-	20-30	-
PHBV coated paper	0.7-1.1	2-6	16-30	70-140

Scanning electron microscope (SEM) image of different paper samples are illustrated in Fig. 5.3. (Surface and cross section image of all coated papers sample are provided in the Appendix-II). The micrograph of the unmodified paper clearly shows the fiber structure without any coating and fillers. It can also be seen from the same figure that the fibers are fully covered on the PHBV and PLA coated papers showing the smooth surfaces, except for a few random spots on the surface, especially in PHBV coated paper .This might be because of highly crystalline and more hydrophobic structure of PHBV which cause coated layer more brittle with lower adhesion to paper surface. The surface images show different colored areas and the differences in surface area appearances in dark (closed holes) and light (open holes). The dark areas appear smoother having smaller holes than the more open, lighter areas (Chinga, 2002).

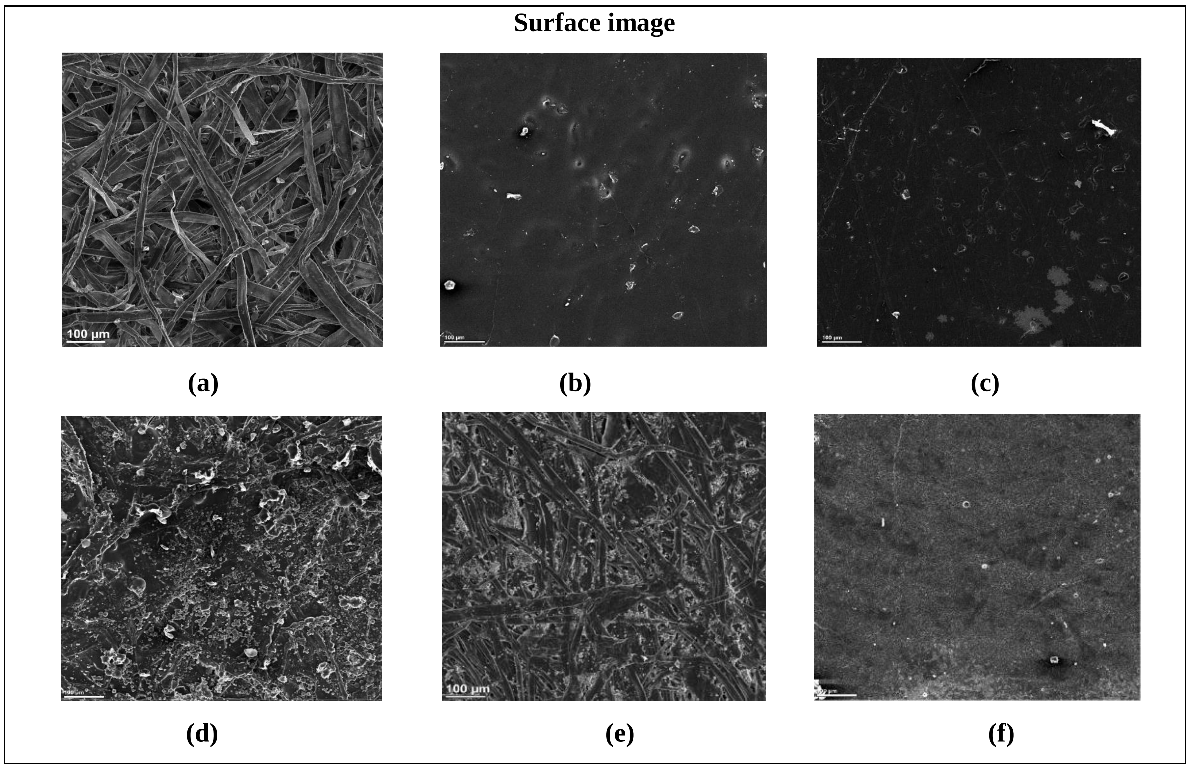

Figure 5.3. SEM surface image of (a) unmodified paper (reference sample), (b) PLA coated paper (c) PHBV coated paper, (d) zein grafted paper, (e) copy paper, and (f) commercial coated paper.

5.4.2. Water vapor adsorption equilibria and isosteric heats

Water vapor adsorption isotherms at T=25 ^{o}C for different paper samples are shown in Fig. 5.4. The isotherms formally belong to Type IV (Bedane et al., 2014), although due to their strong unfavorable character, they also have some characteristics of Type III. The Type III isotherms are usually associated with swelling of adsorbent network as sorbate, e.g., water vapor, is adsorbed by exposing more binding sites, thus increasing surface area and subsequently adsorption capacity, as shown in Table 5.2. In these kinds of adsorbents the concentration (number) of available adsorption sites is not fixed, but changes with the degree of adsorption.

The experimental adsorption data were fitted with GAB model (Eq. 5.1), as shown in the figure. The model predicts the isotherm data very successfully. The highest adsorption was observed for the unmodified paper sample with moisture content of 11 wt. % at RH=96%. Rhim et al. (2009) reported the equilibrium moisture content of kraft paper of around 15 wt. % at RH=95% and 25 ^{o}C. In this study, PLA and PHBV coated papers showed the lowest water vapor adsorption capacities, e.g., equilibrium moisture contents of less than 6 wt. % at RH=96% and 25^{o}C, as shown in Fig. 5.4. They also showed lower vapor adsorption in comparison to more hydrophobic commercial calendered (pigmented latex) coated papers. PHBV is more crystalline than PLA (Shogren, 1997), and for that reason it was expected to exhibit lower adsorption capacity than PLA coated paper. However, contrary to the expectation, this was not confirmed in this study. The method of preparation and the hydrophilic properties of hydoxyvalerate content in the PHBV might have caused slightly higher water vapor adsorption than in the PLA coated paper.

The zein grafted and commercial copy paper showed lower vapor adsorption capacities compared to unmodified papers because the zein and calcium carbonate fillers in the copy paper help in reducing equilibrium moisture content. The addition of sizing agents and fillers, are also expected to change the pore size distribution (Kinoshita et al., 1998). Moreover, fillers tend to decrease the overall moisture content, because of their lower hygroscopicity (Newman, 1995).

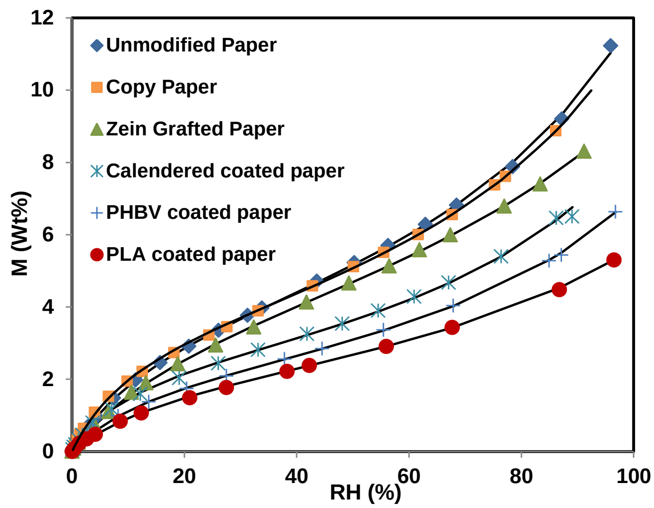

Figure 5.4. Experimental data and GAB-predicted adsorption isotherms at 25 °C (symbols are experimental data and solid lines are the model predictions).

Monolayer moisture content (M_h), and constants K and C are derived from GAB model for different paper samples and summarized in Table 5.3. The value of K is related to the energy of interaction of the water molecules in multilayers with the adsorbent surface. It is usually between the energy values of the molecules in the monolayer and liquid water energy of vaporization. When K value approaches one, the multilayers are considered to have the properties of liquid water, according to the GAB theory. The monolayer moisture contents for PHBV and PLA coated paper samples are lower compared to the control and commercial samples. Surprisingly, the monolayer moisture content of zein grafted paper is higher than the unmodified (control) sample, according to the values obtained from the GAB model. The M_h values obtained for the control samples are similar to mould fiber at 25 ^oC as reported by Sorensen and Hoffmann (2003) using the GAB model. From the GAB analyses, it seems that grafting zein on the paper has no influence in reducing the monolayer moisture content, and it is plausible that it does not block the primary surface groups but only fills the pores of the paper, thus only reducing the equilibrium moisture content at higher relative humidity affecting polylayer formation (Bedane et al., 2014). On the other hand, zein is more hydrophilic compared to PLA and PHBV, which may facilitate the adsorption of water vapor at lower humidity values. More details about water vapor adsorption on these papers are reported in our previous paper (Bedane et al., 2014). The monolayer moisture contents of the samples are also compared to their WVTR's (measured at ΔRH=50% (aver. RH=50±2.5%) and T=25 ^oC) in Table 5.4. As shown in Table 5.4, the low monolayer moisture content of the sample is generally related to low WVTR, except for zein grafted paper. Zein grafted paper showed high monolayer moisture content but still relatively low WVTR compared to unmodified and commercial copy paper samples, even though its WVTR is still much higher compared to the modified paper samples, e.g., PLA and PHBV coated samples. The low WVTR is primarily attributed to low solubility of water vapor, e.g., low monolayer content, which is directly related to permeability. In addition, diffusivities of water vapor in the coated samples were found to be about one order of magnitude smaller than in the unmodified and zein grafted papers (Bedane et al., 2012), thus further contributing to low permeability of the coated samples.

Table 5.4. GAB model's sorption parameters determined from water sorption isotherms, and related WVTRs of paper samples measured at ∆RH=50% and T=25 °C.

Paper samples	Monolayer moisture content (M_h) (%)	K	C	WVTR (g/m^2.day) [2]
Unmodified paper	4.12	0.674	9.62	514
Commercial copy paper	3.38	0.682	12.33	462
Zein grafted	4.32	0.582	8.12	224
Calendered coated pap. (Commercial)	2.70	0.694	13.49	187
PLA coated paper	2.29	0.619	9.26	95
PHBV coated paper	2.44	0.671	10.41	22

The change in water activities, $\ln(p/po)$, at different fixed loadings or equilibrium moisture contents (MC), versus $1/T$ for unmodified paper samples are shown in Fig. 5.5. The net isosteric heats of sorption, or the differential enthalpies, can be obtained from the slope of the lines using Eq. 5.5 (Clausius-Clapeyron equation). The net isosteric heats of sorption (q_{st}) increase with the moisture content until reaching the maximum (approximately corresponding to the monolayer moisture contents), after which they exhibit a decreasing trend, as shown in Fig. 5.6. This varied behavior is indicative of different intermolecular attraction forces existing between active adsorption sites and water vapor molecules. In the monolayer region, the water is tightly bound to the paper surface, corresponding to high energy of interactions. In this region (low moisture contents), the q_{st} values increase as the adsorption sites with the highest energies are fully occupied, reaching maxima upon completion of the monolayer formation. Consequently, the values of q_{st} start decreasing sharply by continuing adsorption, as second and subsequent layers of water are formed on the monolayer.

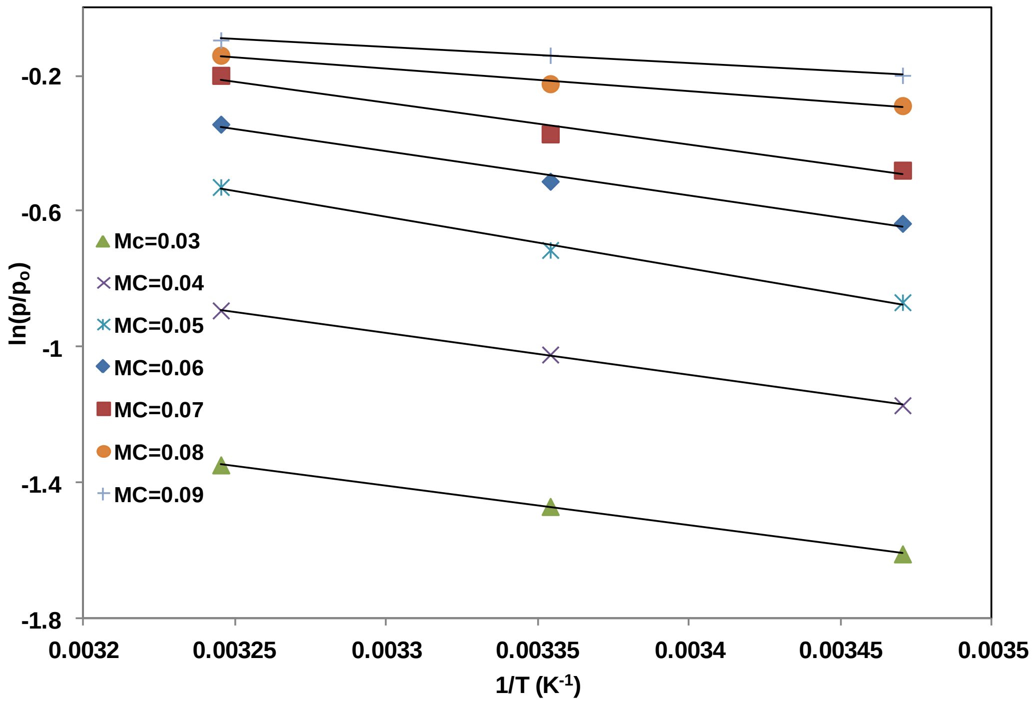

Figure 5.5. Temperature dependency of relative water vapor pressures of unmodified paper (60 gsm) at different equilibrium moisture contents.

The maximum net isosteric heats for unmodified paper (q_{st}=12.53 kJ/mol), zein grafted paper (15.25 kJ/mol), copy paper (17.4 kJ/mol) and calendered coated paper (14.71 kJ/mol) are obtained at the moisture contents of 5.0, 4.0, 3.0 and 2.9 %, respectively. The maximum net isosteric heats for PHBV and PLA coated paper are approximately 22.77 and 23.2 kJ/mol, respectively, at the moisture contents of about 2.0 %. This indicates that the strength of water vapor interactions with the primary binding sites is higher in the case of the PHBV and PLA coated papers but, at the same time, the amount (number) of active sites available for water vapor sorption is less compared to other paper samples, which is the indicative of the lower adsorption capacities.

The decreasing trends of isosteric heats with increased moisture contents on unmodified paper and zein grafted paper samples are less significant compared to other (modified) paper samples, due to the larger number of adsorption sites on the surface of unmodified and zein grafted paper samples, as can be revealed from Fig. 5.6. The results can also be explained by using GAB theory, e.g., the value of constant C indicates the strength of water bound to primary binding sites. The larger C values indicate the stronger water bounding in the monolayers, i.e., higher net isosteric heat of adsorption. For K values less than one (water molecules above the monolayer are structured in a multilayer), the water molecules are different from bulk water. On the other hand**,** the larger M_h value (the monolayer moisture content) indicates the larger availability of active sites for water sorption on the paper surface (Quirijns et al., 2005). According to the above discussion, C values shown in Table 3, should follow the same trend as the net isosteric heats calculated for different samples. However, our results show the largest C values for the commercial copy paper and calendered coated paper, which is not in line with the net isosteric heats that show relatively low values for these samples, in particular for the calendered coated paper. On the other hand, unmodified paper and zein grafted paper showed relatively lower values of C (i.e. low strength of water molecules that bound to the surface), which is in a better agreement with the lower values of net isosteric heats of adsorption. Further to that, PHBV coated paper showed relatively high C value corresponding to the higher net isosteric heat, as expected. The inconsistent agreements between the net isosteric heats and C values from the GAB model could be explained by uncertainties in determining net isosteric heats from only three different temperatures (points in Fig. 5.5) that were used for the q_{net} analysis, thus these results could only be considered as approximate at the best (Quirijns et al., 2005). Rhim et al. (2009) reported that the maximum net isosteric heats of adsorption for vegetable parchment (VP) paper, Kraft paper, and solid–bleached-sulfite (SBS) paperboard were 18.51, 27.39 and 26.80 kJ/mol, respectively, at lower moisture content. The maximum net isosteric heat of water vapor adsorption on cotton cellulose was found at about 19 kJ/mol, at low moisture content (Morrison et al., 1959).

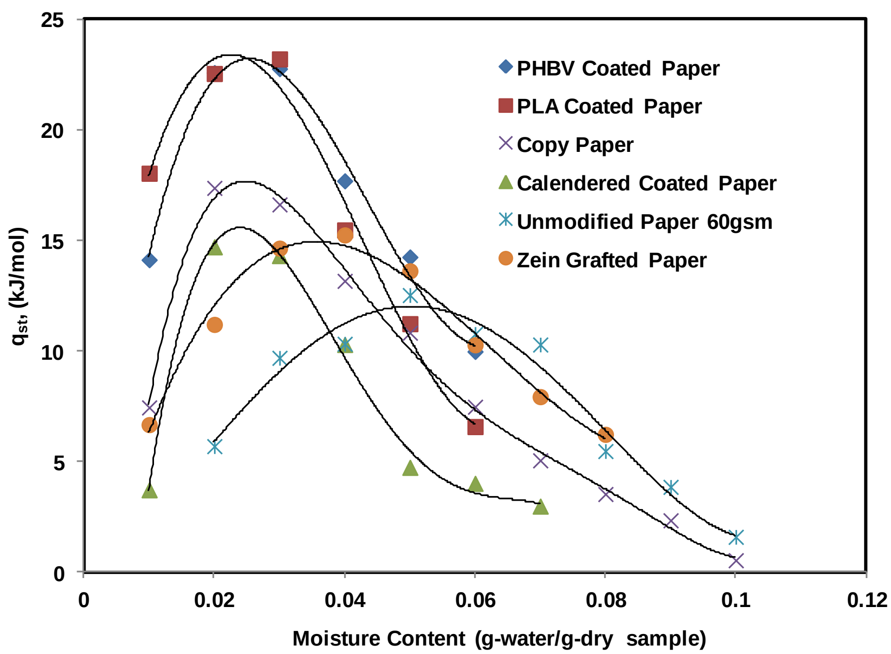

Figure 5.6. Effect of moisture content on the net isosteric heat of adsorption for different paper samples.

5.4.5. TGA-DSC Analysis

There have been a number of various studies concerning the states of water in cellulose fibers (Hatakeyama et al., 1998; Park et al., 2007). There are three types of waters that exist in cellulose (Nakamura et al., 1981; Hatakeyama et al., 2000): freezing unbound water (free water), freeze bound (slightly bound water) and nonfreezing water (tightly bound water). Freezing unbound and freeze bound water exhibit melting endothermic peaks (when the water is melted after freezing in cellulose fibers). These two types of water bindings do not create strong hydrogen bonds with the polymer matrix. Consequently, they show a greater degree of mobility. Bound (nonfreezing) water refers to the water molecules that are hydrogen-bonded to the polymer chain, and show no melting peak. They have the low mobility. Freeze bound water interacts with the polymer molecules and has a melting endotherm slightly below 0 ^{o}C (Hatakeyama et al., 1998). Freezing water content (unbound and loosely bound water) is calculated from the ratio of the endothermic peak areas, representing the heat of fusion**,** of the swollen cellulose and the pure water. Bound water is calculated as a difference between total water adsorbed in the material and freezing water.

Hatakeyama et al. (1988) showed a good agreement between bound water contents measured by DTA, DSC and TG techniques, when vaporization of water from hydrophilic polymers occurred. In this study, different forms of adsorbed water present on cellulose fiber-based materials were analyzed using TGA-DSC instrument. Three different regions were identified on the TGA-DSC curves (Fig. 5.7). These regions are defined by inflection points from the rate of mass loss and heat flow curves and this helps to get insight on the form of adsorbed water. The first region is assigned to the evaporation of free water from the crucible and water on the surface of the fiber; the onset point can be observed from heat flow curve or/and the change of slope of derivative weight loss curve (~up to 40 ^{o}C). The second region can be assigned to loosely bound water (the onset of heat flow was chosen as the boundary for free and bound water). The last, third, region is considered to be related to evaporation of tightly bound water, i.e., the onset of heat flow at the boundary of loosely and tightly bounded water, where rate of mass loss is less than 0.025 mg/min. The paper samples with higher moisture content showed a rapid loss of mass (dehydration), as shown on Fig. 5.8. Relatively large amount of moisture loss can also be observed for the unmodified paper compared to modified paper samples at a given relative humidity. PHBV and PLA coated paper showed lower percentage moisture loss. The evaporation of unbound water or loosely bound water was observed up to 60 ^{o}C, while for most of tightly bound water it was up to 90^{o}C with a small amount evaporating up to 150 ^{o}C (Fig. 5.7 and 5.8). Vyas et al. (2004) reported that evaporation of free water at the surface occurs at the temperatures up to 60 ^{o}C, and for tightly bound water at about 80 ^{o}C. Scheirs et al. (2001) also reported that the loss of adsorbed and chemically bound eliminated water from cellulose paper and kraft paper occurred at about 100 ^{o}C and 300 ^{o}C, respectively.

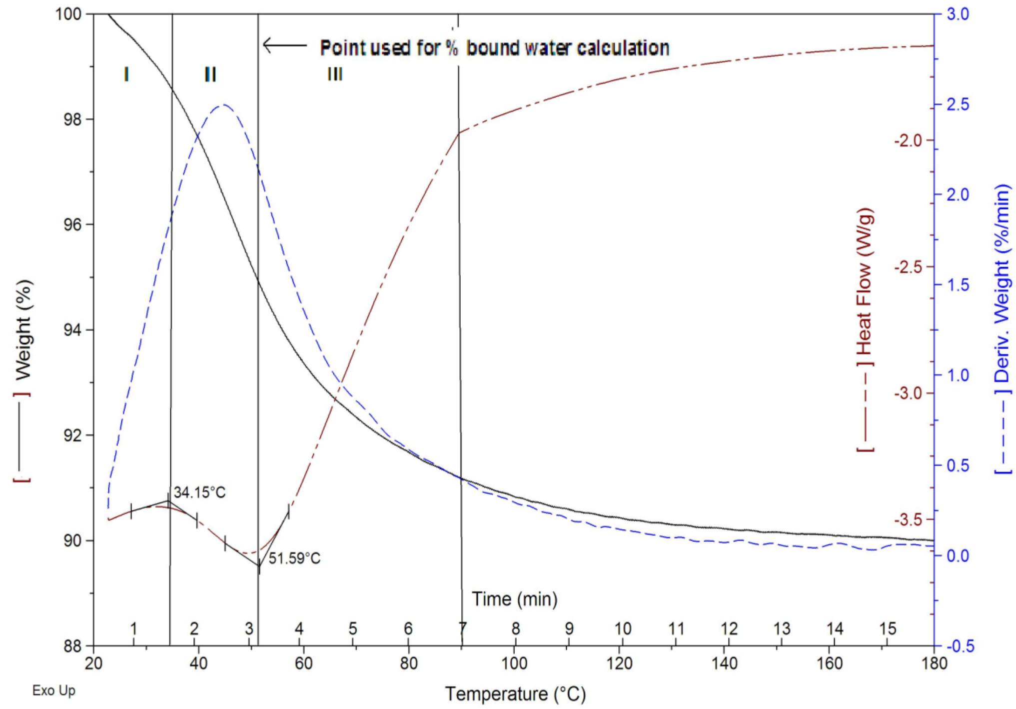

Figure 5.7. TGA-DSC analysis of free, loosely and tightly bound water on unmodified paper.

(Total weight loss (———), derivative weight loss (– – – – –), heat flow curve (——– – –))

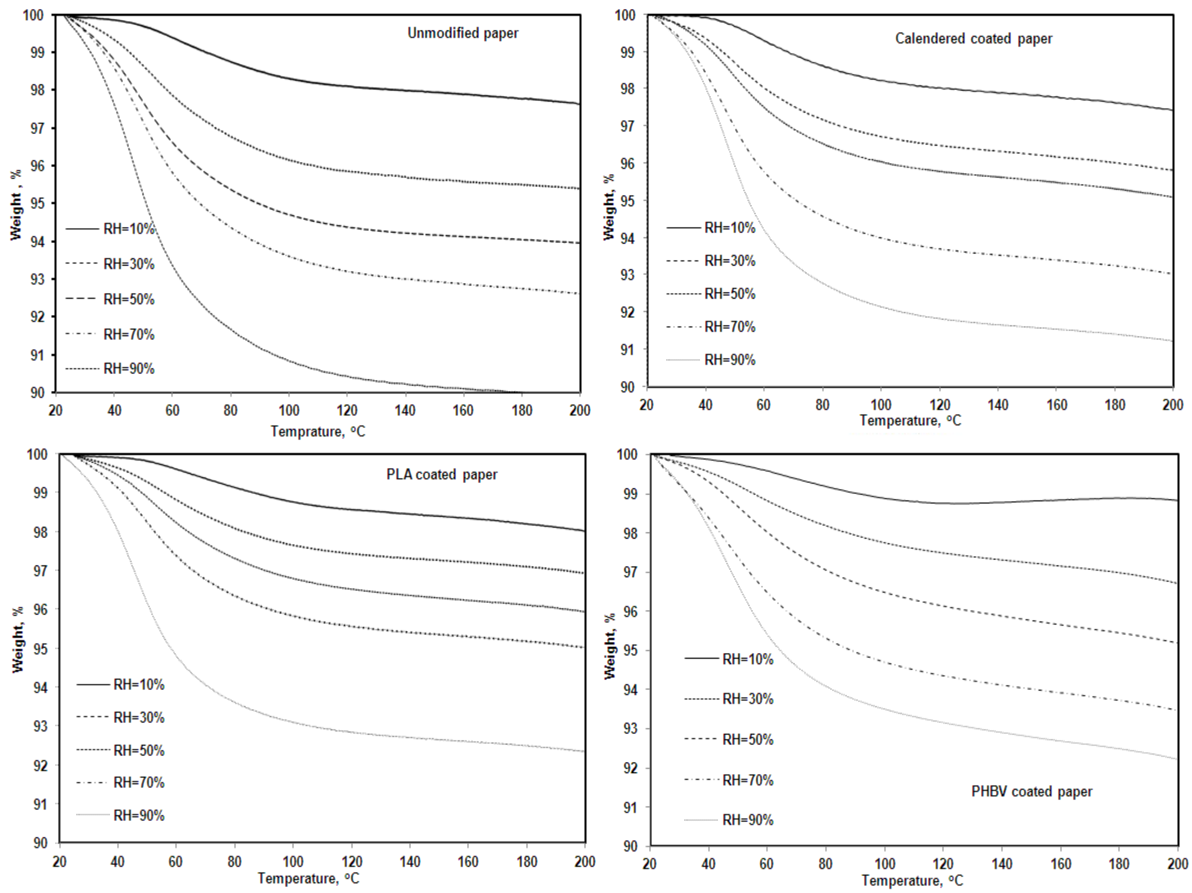

Figure 5.8. TGA curves representing moisture loss from unmodified and coated paper samples in equilibrium at different relative humidities.

Formations of adsorbed water on the different paper samples at 30 and 90% RH are shown in Table 5.5 (the rest is shown in Appendix-II).The percentages of tightly bound water on modified paper samples are lower compared to the control sample, and this is related to less hygroscopic properties of coated materials. Tightly bound water contents for unmodified paper, calendered coated paper, PHBV coated paper and PLA coated paper are found to be 4.6 %, 3.57 %, 2.93 % and 2.9 %, at 90% relative humidity, respectively. The tightly bound water's content is higher than the monolayer moisture content found from the model equations shown in Table 5.3, and the total moisture contents obtained are also higher for a given relative humidity from adsorption isotherms. This could be due to thermal dehydration of water from cellulose-fiber, in addition to physical desorption of water at higher temperatures (Scheirs et al., 2001).

Table 5.5. Moisture content of different water formation on paper samples at 25 ^oC for various relative humidities determined by TGA-DSC analysis.

Paper sample	Relative Humidity (RH), (%)	Free water, (%)	Loosely bound water, (%)	Tightly bound water, (%)	Total water content, (%)
Unmodified paper	30	0.677	1.471	2.470	4.618
	90	1.250	4.824	4.640	10.714
Calendered coated paper	30	0.373	1.787	1.610	3.770
	90	0.774	4.747	3.569	9.090
PLA coated paper	30	0.140	1.240	1.460	2.840
	90	0.730	2.310	2.760	5.800
PHBV coated paper	30	0.500	1.190	1.020	2.710
	90	1.380	3.500	2.930	7.810

Isosteric heats of desorption from calorimetric measurements

Cumulated average desorption/vaporization enthalpy (H_d) values were determined from the endothermic peaks obtained from the TGA- DSC measurements for unmodified, PHBV and PLA coated paper samples, as shown in Fig. 5.9. They were also calculated using Eq. 5.10. The parameters, c and b, were determined from fitting the experimental data (in Fig. 5.9) with Eq. 5.8 for unmodified, PHBV and PLA coated paper samples. The obtained values are shown in Table 5.6 together with comparisons between the calculated and experimental heats of desorption (H_d) at different relative humidities (moisture contents of the sample). Park et al. (2007) found constant parameters, c and b, in the range of 3-11 kJ/g and 330-382, respectively, for various cellulose fibers.

In general, heat required to remove the water from cellulose surface decreased as the moisture content increases, as shown in Fig. 5.9. The heat of desorption curves showed two different region; in the first region, at lower moisture contents, the heat of desorption significantly increased when the moisture is decreased. In this region, dehydration is mainly restricted due to the strong interactions between water molecules and cellulose surface groups, and consequently it is expected that the energy required to remove the water molecules is greater than for the unbound water. At the higher moisture content, the water molecules are loosely associated with the cellulose surface by forming multilayers. The energy required to remove water molecules attached to fiber surface is higher than the energy which holds water molecules in the liquid phase (Masuzawa and Sterling, 1968; Park et al., 2007). At the highest moisture contents, e.g., above 0.08 g/g, the heat of desorption tends to remain constant and in this region the isosteric heat of desorption is equal to the latent heat of evaporation of pure water (~2300 kJ/kg) (Sanchez et al., 1997).

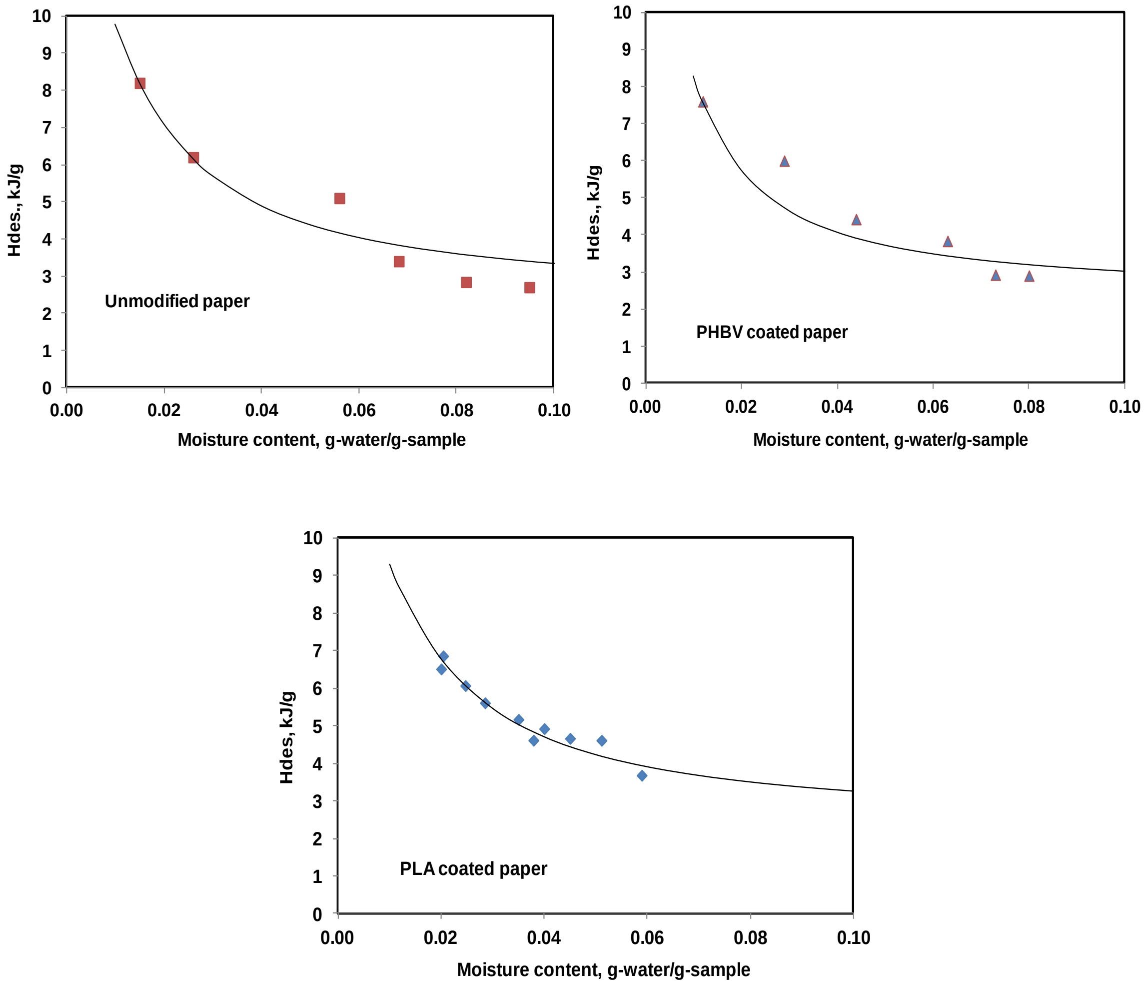

Figure 5.9. Cumulated average desorption/vaporization enthalpy (H_d) (fitting curve (———) based on Eq. 10).

Table 5.6. Constant parameters determined from Eq. 10 and comparison between experimental and calculated heat of desorption.

Relative Humidity (%)	Unmodified paper		PHBV coated paper		PLA coated paper	
	Constant parameters					
	C=13.1 kJ/g	b=126	C=13.4 kJ/g	b=190	C=12.36 kJ/g	b=127.40
	Heat of Desorption (H_d,kJ/g)					
	Exp.	Calc.	*Exp.	*Calc.	Exp.	Calc.
10	8.2	8.2	7.6	7.6	6.52	6.77
30	6.2	6.2	6.1	4.7	6.07	6.06
50	5.1	4.2	4.4	3.9	4.62	4.84
70	2.8	3.6	3.8	3.4	4.93	4.71
90	2.7	3.4	2.9	3.3	4.61	4.20

*Exp. =Experimental and Cal. =Calculated

5.4.4. FT-IR analysis

Fourier-Transform Infrared (FT-IR) spectroscopy can provide insights into the structure of water in paper sample films, as well as providing details about the water-paper sample film interactions and hydrogen bonding. The water vapor spectrum is measured in situ at different humidities by subtracting the spectrum of the dry paper sample from paper sample spectrum in equilibrium with water vapor. The basic features of the adsorbed water spectrum are very similar. Four different peaks (3610 cm^{-1}, 3510 cm^{-1}, 3360 cm^{-1}, 3260/3070 cm^{-1}) were observed in the OH stretching band. These peaks were deconvoluted using Gaussian function, which reflects different types of water molecules undergoing varying degrees of hydrogen bonding to the material, as shown in Table 5.7

and Fig. 5.10. The lowest frequency band is commonly attributed to the most strongly bound water molecules. The centers of the peaks are shifted to lower frequency compared to pure water as a result of interaction of water with the paper surface (Ide et al., 1999). At lower relative humidities, broad band peak was observed at lower frequencies (3070-3260 cm^{-1}) for unmodified paper, which indicates that water molecules are H-bound onto specific hydroxyl sites along the surface of the cellulose network. At the higher water activities, this broad band peak decreases in the size and the intensity at higher frequencies increase, which is characteristic of free or unassociated water (additional figures are available in the Appendix-II).

Table 5.7. Center of peaks for water molecules on unmodified paper and PLA coated paper from FT-IR measurements.

Peak	Center of peak (cm^{-1})		Molecular state/ strength of water bound to the polymer
	Unmodified paper	PLA coated paper	
1	3614	3615	Monomeric/ Free or unassociated water to the polymer
2	3505	3517	Dimeric/trimeric and or Weakly- bound water molecules to the polymer
3	3260	3360	Water clusters/ Medium strength hydrogen bounds to the polymer
4	3070	3100	Water clusters/ (Solid like clusters) and or hydrogen bonded onto specific polar sites along the polymer network

In unmodified paper sample, at lower relative humidities (low moisture contents) the hydrogen bond between water molecules and the polar surface of paper is relatively strong, and by further successively increasing the water vapor concentration, the strength of hydrogen bond with the surface decreases, as shown in Fig. 5.11a. The fraction of medium bound water molecules is relatively high at the lower relative humidity, and it decreases with increased moisture content of the sample. However, at the high water contents, e.g., above RH=60%, the medium bound water molecules start creating stronger bonds again due to formation of strong dimer/trimer assembles of water molecules (continuous phase cluster coalescence). Comparatively the PLA coated paper showed less strong interactions between water molecules and modified paper surface (Fig. 5.11b).The fraction of medium-bound water increases with increased relative humidities. At the higher relative humidities, the formation of weakly-bound water molecules (di/trimeric) decreases and it can be assumed that the water molecules are disposed to give stronger bonds by forming water molecule clusters (Laporta et al., 1999). In general, with increasing relative humidity (moisture content), cluster formation of water molecules with the pre-adsorbed water molecules increases, thus the number of bound water molecules eventually decreases. This indicates that the interaction between water molecules and the paper sample decreases as the relative humidity increases. FT-IR measurements confirmed formation of clusters at high humidity levels. The formation of clusters of water molecules also decreases the diffusivity of water vapor into the paper sample films at the higher relative humidities (Bedane, et al. 2012).

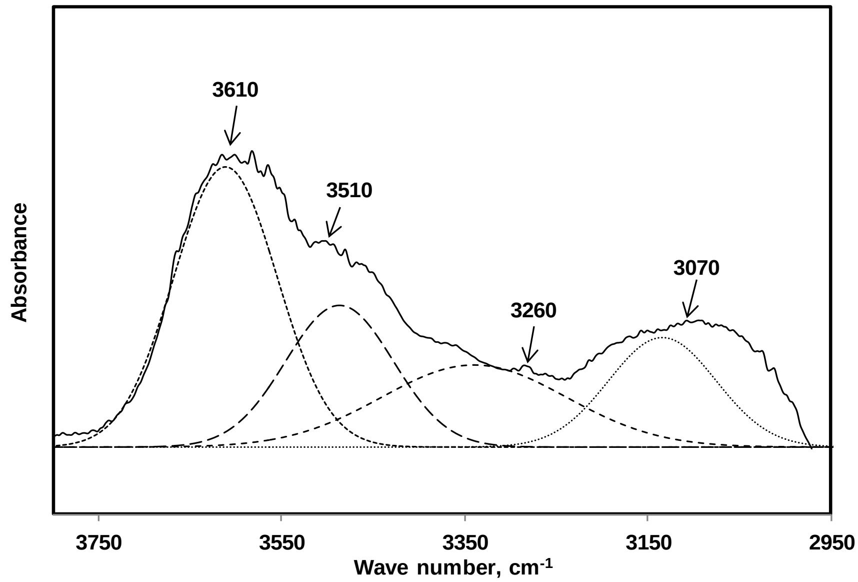

Figure 5.10. Example of deconvoluted spectrum of OH stretching band on unmodified paper equilibrated at RH=10%.

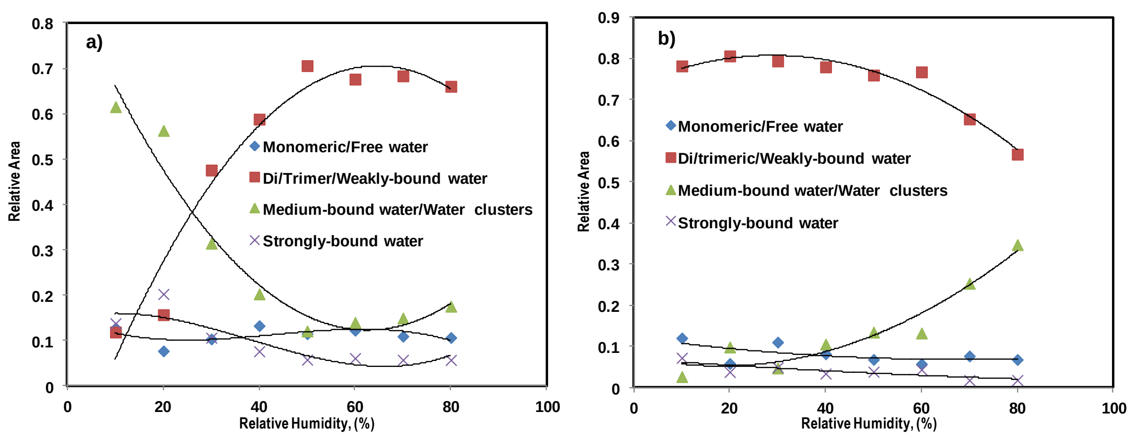

Figure 5.11. The relative peak area obtained from curve fitting as a function of the relative humidity for a) unmodified paper and b) PLA coated paper.

5.5. Conclusions

BET specific surface areas of different paper samples were measured from adsorption isotherm of N_2 at 77 K and water vapor adsorption isotherms at 25 ^oC. In general, low specific surface area and low pore volumes of investigated samples were obtained using the N_2 adsorption technique. Coating or grafting of biodegradable polymer on paper surface increases the specific surface area but decreases the mean pore diameter compared to the reference sample based on BET N_2 adsorption results. Pore size reduction of the modified paper samples, as well as a decrease of the hydrophilic properties, caused a reduction of water vapor transmission rates. Coated paper samples showed low water vapor adsorption and low specific surface areas based on the water vapor adsorption isotherms measured at 25 ^oC. The obtained monolayer moisture contents from GAB model for PLA and PHBV coated samples are the lowest in comparison to other investigated paper samples. The low monolayer moisture content of the sample is generally related to the low WVTR because of decreased water vapor transport by diffusion at the surface caused by interaction between the water vapor and the active sites on paper surface. The net isosteric heats of adsorption were determined from experimentally measured adsorption isotherms at 15, 25, and 35 ^oC. The net isosteric heats of adsorption for the paper samples decreased with an increase in the moisture content, approximately after reaching the maximum value corresponding to monolayer saturation content. Bound and unbound water formations, as well as the dehydration energies were determined for different paper samples using TGA-DSC analysis. Among other modified paper samples, PLA and PHBV coated paper samples showed lower percentage of bound water moisture content. The heat of desorption is higher at lower moisture contents, but decreases and remains constant at the higher moisture contents. This illustrates the strength of water-paper surface interaction; at lower relative humidities more energy is required to remove water molecules than at higher humidities. Moreover, FT-IR reveals the formation of water clusters at higher relative humidities, causing a decrease in the energy of interaction between water molecules and the paper sample surface. In general, both the surface pore size reduction and the less hygroscopic properties of the samples have contributed to the increase of water vapor barrier properties.

References

Al-Muhtaseb, A.H, McMinn, W.A.M, Magee, T.R.A. (2004). Water sorption isotherms of starch powders. Part 2: Thermodynamic Characteristics. J. Food Eng., 62,135-142.

Ashely, R.J. (1985). Permeability and plastic packaging. In polymer Permeability, Comyn J (Ed.). Elsevier Appl. Sci.: London, UK, 269-308.

Banquet, G. and Isoard, J.C. (1997). Synthetic latex binders for paper manufacture. Surface Appl. of Pap. Chem., 48-68.

Bismarck A., Aranberri-Askargorta, I., Springer J. (2002). Surface characterization of Flax, Hemp and Cellulose Fibers; Surface Properties and the Water Uptake Behavior. Polym. Compos. 23(5), 872-894.

Bedane, A.H, Qinglin H., Xiao, H. and Eić, M. (2012). Mass transfer of water vapor, carbon dioxide and oxygen on modified cellulose fiber-based materials. Nord Pulp Pap. Res. J., 27(2), 409-417.

Bedane, A.H, Xiao, H. and Eić, M. (2014). Water vapor adsorption equilibria and mass transport in unmodified and modified cellulose fiber-based materials, Adsorpt., 20, 863-874.

Borch, J., Lyne, M.B., Mark, R.E., Habeger, C.C. (2002): Handbook of physical testing of paper, Volume 2, Marcel Dekker, Inc., 2002, pp. 283-289.

Chinga, G. (2002). Structural studies of LWC paper coating layers using SEM and image analysis techniques, PhD thesis. Norwegian University of Science and Technology.

Daniel T. and Olle S. (2001). Diffusion of water absorbed in cellulose fibers studied with H-NMR, Langmuir 17, 2694-2702.

Davis, P.J. and Smith, D. M. (1989). Using NMR spectroscopy to analyze the pore structure of coatings. Tappi J. 72, 85-89.

Del Nobile, M.A., Baiano, A. Benedetto, A. and Massignan, L. (2006): Respiration Rate of Minimally Processed Lettuce as Affected by Packaging, J. Food Eng., 74(1), 60–69.

Dodson, C. T.J and Sampson, W.W. (1996). The effect of paper formation and grammage on its pore size distribution. J. Pulp Pap. Sci., 165-169.

Hatakeyama, H. and Hatakeyama, T., (1998). Interaction between water and hydrophilic polymers. Thermochimica Acta 308, 3-22.

Hatakeyama, T., Nakamura, K. and Hatakeyama, H. (1988). Determination of bound water content in polymers by DTA, DSC and TG. Thermochim. Acta. 123, 153-161.

Hatakeyama, T., Nakamura, K. and Hatakeyama, H. (2000). Vaporization of bound water associated with cellulose fibres. Thermochim. Acta 352-353, 233-239.

Hill, C.A.S., Andrew, N. Gary, N. (2009). The Water Vapor Sorption Behavior of Natural Fibers. J App. Polym. Sci., 112, 1524-1537.

Ide, M., Yoshikawa, D., Maeda, Y., and Kitano, H. (1999). State of Water inside and at the surface of Poly (ethylene glycol) Films Examined by FT-IR, Langmuir, 15,926-929.

International Union of Pure and Applied Chemistry (IUPAC) (1985). "Reporting physisorption data for gas/solid systems with special reference to the determination of surface area and porosity". Pure Appl. Chem., 57, 603-619.

Krassig, H.A. (1992). Cellulose: structure, accessibility and reactivity. Gordon and Breach Science Publishers, pp. 181.

Kinoshita, N, Noda, H., Toyotake, Y., Katsuzawa, H (1998). The effects of filler contents and beating on the porous structure of high-filler-containing papers. Sen'I Gakkaishi, 54(1), 46-53.

Koide, S. and Shi, J. (2007): Microbial and Quality Evaluation of Green Peppers Stored in Biodegradable Film Packaging, Food Control, 18(9), 1121–1125.

Laporta, M., Pegoraro, M., and Zanderighi, L. (1999). Perfluorosulfonated membrane (Nafion): FT-IR study of the state of water with increasing humidity. Phys. Chem. Chem. Phys, 1, 4619-4628.

Li, T. Q. (1991). Interaction between water and cellulose-Application of NMR techniques. Ph.D. Thesis, Royal Institute of Technology, Stockholm, Sweden, 1991.

Li, T-Q., Haggkvist, M., and Odberg, L. (1999). The porous structure of paper coatings studied by water diffusion measurements. Colloids Surf.; A: Physicochem. Eng. Asp. 159, 57-63.

Masuzawa, M. and Sterling, C. (1968). Gel-water relationship in hydrophilic polymers: the thermodynamics of sorption of water vapor. J. Appl. Polym. Sci., 12(9), 2023-2032.

Moreira, R., Chenlo, F., Torres, M.D. and Vallejo, N. (2008). Thermodynamic analysis of experimental sorption of loquat and quince fruit, J. Food Eng., 88, 514-521.

Morrison, J. L. and Dzieciuch, M. A. (1959). The thermodynamics properties of the system cellulose-water vapor, Canadian J. Chem., 37(9), 1379-1390.

Mulet, A., Garcia-Reverter, J., Sanjuan, R., Bon, J. (1999). Sorption isosteric heat determination by thermal analysis and sorption isotherms. J. Food Sci., 64(1), 64-68.

Nakamura, K., Hatakeyama, T., and Hatakeyama, H. (1981). Studies on bound water of cellulose by differential scanning Calorimetry, Text. Res. J., 51,607-615.

Newman, R.H. (1995). Adsorbed and absorbed moisture in bleached Kraft pulp. Industrial Research Ltd., Lower Hutt, New Zealand.

Olsson, AM. and Salmen, L. (2004). The association of water vapor to cellulose and hemicelluloses in paper examined by FTIR spectroscopy. Carbohydr. Res., 339,813-818.

Papadopoulos A. N, Hill , C. A. S, Gkaraveli. A. (2003). Determination of surface area and pore volume of holocellulose and chemically modified wood flour using the nitrogen adsorption technique, Holz als Roh- und Werkstoff, 61(6): p. 453-456

Park, S., Venditti, R. A, Jameel, H. and Pawlak, J.J. (2007). Hard-to-remove water in cellulose fibers characterized by thermal analysis: A model for the drying of wood-based fibers. Tappi J. 6(7).

Quirijns, E.J., Boxtel, A. JB., Loon, W. KP., and Straten, G. (2005). Sorption isotherms, GAB parameters and isosteric heat of sorption. J. Sci. Food Agri., 85, 1805-1814.

Resch, P., Bauer, W. and Hirn, U.(2010). Calendering effect on coating pore structure and ink setting behavior. Peer-Reviewed Tappi J., 27-35.

Rhim, J-W, Lee, J-H. and Hong, S-I. (2007): Increase in water resistance of paper board by coating with poly (lactide), Packag. Technol. Sci., 20(6), 393-402.

Rhim, J-W. and Lee, J.H. (2009). Thermodynamics Analysis of Water Vapor Sorption Isotherms and Mechanical Properties of Selected Paper-Based Food Packaging Materials, J. Food Sci., 74(9).

Riedel, L. (1977). Calorimetric measurement of heats of hydration of foods. Chem Mikrobiol Technol Lebensm, 5, 97-101.

Roben, E., Dabrowski, A. and Kutarov, V.V. (2004). Comments on surface structure analysis by water and nitrogen adsorption. J. Therm. Anal. Calorim. 76, 647–657.

Sanchez, E.S., SanJuan, N., Simal S., Rossello, C. (1997). Calorimetric techniques applied to the determination of isosteric heat of desorption for potato. J. Sci. Food Agric., 74(1), 57-63.

Scheirs, J., Camino, G., and Tumiatti, W. (2001). Overview of water evolution during the thermal degradation of cellulose. European Polym. J., 37,933-942.

Shogren, R. (1997). Water Vapor Permeability of Biodegradable Polymers. J. Environ. Polym. Degrad. 5(2), 91-95.

Sorensen, G. and Hoffmann, J. (2003). Moisture Sorption in Moulded Fibre Trays and Effect on Static Compression Strength. Packag. Technol. Sci., 16, 159-169.

Tolaba, M.P., Peltzer, M., and Pollio, M.L. (2003). Grain Sorption equilibria of quinoa grains. J. Food Eng., 61, 365-371.

Twede, D. and Selke, S.E.M. (2005). Cartons, Crates and Corrugated Board. Handbook of Paper and Wood packaging Technology, DEStech Publications, Inc., Lancaster, Penyslvania, U.S.A.

Vyas, S., Pradhan, S.D., Pavaskar, N.R., Lachke, A. (2004). Differential Thermal and Thermogravimetric Analyses of Bound Water Content in Cellulosic Substrates and Its Significance During Cellulose Hydrolysis by Alkaline Active Fungal Cellulases. Appl. Biochem. Biotechnol. 118, 2004.

Wang, N. and Brennan, J.G. (1991). Moisture Sorption isotherm characteristics of potatoes at four temperatures. J. Food Eng., 14, 269-282.

Yamada, K., Noguchi, A. and Takahashi, H. (1996). Effects of the solvents on properties of zein, Nippon Shokuhin Kagaku Kaishi, 43 (3), 306–312.

Chapter 6: Water vapor transport properties of regenerated cellulose and nanofibrillated cellulose films

Alemayehu H. Bedane[a], Mladen Eic[b], Madjid Farmahini-Farahani[a], and Huining Xiao[b]

University of New Brunswick

Journal of Membrane Science, 2015.

---

[a]Graduate Student, Department of Chemical Engineering, UNB

[b]Professor, Department of Chemical Engineering, UNB

Abstract

In this study, water vapor transport properties of nano-fibrillated cellulose (NFC) and regenerated cellulose films, derived from different sources, were investigated and compared with the transport properties of unmodified paper sample that was used as a reference sample. Gravimetric-IGA experimental system was used to measure the kinetics and water vapor permeabilities (WVPs) of the samples. Water vapor adsorption-desorption isotherms were measured for different cellulose films using Belsorp instrument. Monolayer moisture content was determined by fitting the adsorption isotherm with the Guggenheim-Anderson-De Boer equation (GAB model). The monolayer moisture contents of the regenerated cellulose and NFC films were found to be more than two times larger than the monolayer moisture content obtained for unmodified paper sample (made from bleached Kraft pulp ~ 4.12 wt. %), at saturation. This indicates a large number of hydrophilic sites available on the surface of regenerated cellulose and NFC films. The water transmission rates (WVTR's) of regenerated cellulose and NFC films were similar, but lower compared to the unmodified paper measured at a wide range of relative humidities. Furthermore, water vapor permeabilities (WVP's) of NFC and regenerated cellulose films were found to be concentration dependent exhibiting lower values up to RH=50%, but then showing a rapidly increasing trends above RH=50%. WVP's of the cellulose films revealed an Arrhenius type of dependency with temperature, indicating an activated process.

Water vapor diffusivities were also measured from the uptake rate measurements for a wide range of relative humidities. The diffusivities generally showed dependency on the moisture content of the sample. The effective diffusion coefficients (D_{eff}) of NFC and regenerated cellulose films are 1-2 orders of magnitude lower in comparison with the unmodified paper sample, depending on the moisture content. The mechanisms of water vapor transport through the cellulose films were also evaluated from the uptake rate experiments. The results showed that the external surface resistance was a more dominant mechanism to mass transfer in the NFC and regenerated cellulose films. On the other hand, water vapor uptakes on unmodified paper seem to be consistent with internal diffusion control mechanism, except at the high moisture contents. At the high relative humidity or moisture contents of the films, both the external surface resistance and diffusion control the transport in transparent cellulose films and paper samples.

Keywords: cellulose films, paper, relative humidity, kinetics, solubility, isotherms, water vapor transport rate (WVTR), water vapor permeability (WVP), diffusion, surface barrier.

6.1. Introduction

Cellulose materials have received much attention in the last decades as a potential replacement for synthetic polymers, because of their biodegradable character that can be conveniently used for different applications. Regenerated cellulose films, like cellophane, have not been commonly used for food packaging, due to their high water vapor permeability (low barrier properties) compared to their synthetic counterparts. On the other hand, transparent cellulose films exhibit good oxygen and CO2 barrier properties at dry conditions that are better than or comparable to dense polyethylene (HDPE) and low density polyethylene (LDPE) films (Syverud and Stenius, 2009; Yang et al., 2011; Spence et al., 2011; Lavoine et al., 2012, Meittinen et al., 2014). However, the gas barrier properties of the films decrease with increased moisture content in the film (Yang et al., 2012; Meittinen et al., 2014). Water has a high polarity and ability to form hydrogen bonds with the adsorbent (packaging) material and or between its molecules. The major limitations of the transparent cellulose films in the application for food packaging are their sensitivity to moisture and poor vapor barrier properties that result from the hydrophilic nature of their active surfaces. Water vapor and gas barrier properties of polymer material play a key role in maintaining food product quality. Moreover, these characteristics of the films could also affect the physical and mechanical properties of the material (Twede and Selke, 2005). Controlling water vapor and gas transmission rates is a critical factor in order to achieve the required quality, safety and also in extending shelf life for moisture sensitive foods and pharmaceuticals (Ashley, 1985; Koide et al., 2007; Del Nobile et al., 2006). High performance films with high flexibility, optical transparency, thermal stability, mechanical strength, biodegradability, and gas barrier properties are greatly in demand for several applications beyond packaging (Yang et al., 2011).

Regenerated cellulose films are made from purified wood or cotton pulp sheets. They are transparent, durable, flexible, non-water soluble and impermeable to air and grease. Other transparent cellulose films such as, microfibrillated cellulose film (MFC) and nanofibrillated cellulose (NFC) films have emerged as a potential packaging material due to their strong mechanical properties. NFC film is prepared by mechanical disintegration of wood pulp or fiber with high cellulose content into fibrils. The main difference from the regenerated cellulose films is that NFC or MFC films are comprised of one-dimensional nanofibers, whereas regenerated cellulose films are cast from fully dissolved cellulose (Stevanic et al., 2012). Literature values for microcrystalline cellulose density are in the range of 1400-1600 kg/m^3 (Sun, et al. 2005). The diameter for NFC/MFC films can be in the range from 5 to 100 nm (Hult et al., 2010; Cherian et al., 2008; Pääkkö et al., 2007; Garden et al., 2008).

Cellulose polymers have a high crystalline content, inaccessible to water molecules, but also containing a paracrystalline component to which water molecules can gain access, thus making them hydrophilic. The microfibril units have a high OH content accessible to water. The crystalline fraction can be measured by X-ray diffraction (XRD), NMR and Fourier transform IR-spectroscopy and is expressed in percentage, as the crystallinity index. The adsorbed water that is closely associated with OH groups in the cell walls is referred as monolayer water, in contrast to water vapor that is not intimately associated with OH groups, being referred as polylayer water (Hill et al., 2009).The crystallinity of microcrystalline cellulose (MCC) is higher than that of pre-treated cellulose in wood pulp, because of the partial removal of amorphous regions (Sun, 2008). The moisture content and water vapor transmission rate of those cellulose films depend on their percentage of crystallinity or composition, temperature and relative humidity of the environment. The study of the mass transport properties of water vapor in cellulose films is a far more difficult task than the study of other gas permeates due to their hydrophilic properties. Therefore, understanding the mode of moisture transport in cellulose films is critical for designing films with improved barrier properties for food and pharmaceutical packaging applications. This study will also give insight for further improvement of barrier properties of these cellulose films either by physical or chemical treatment on the cellulose films for end-use applications and also to optimize the performance of these hydrophilic films. The overall objectives of this study were (1) to investigate gas and water vapor permeability at variable relative humidity gradients, and (2) to determine the water vapor adsorption equilibria, kinetics and rate controlling mechanisms of different regenerated cellulose and NFC films, and to compare with kraft paper, which was used as a reference sample.

6.2. Materials and Experimental

6.2.1. Preparation of Samples

Nanofibrillated cellulose (NFC) and regenerated cellulose films as well as unmodified paper sample (unmodified Kraft pulp) were prepared for this study and their physical properties are listed in Table 1. Unmodified paper sample was made from pure cellulose at Limerick Pulp and Paper Centre, University of New Brunswick. Regenerated cellulose films were prepared according to procedures further explained in this section. The solvent mixture, LiOH/urea/H_2O with a weight ratio of 5:15:80 was precooled at -15 ^oC. The desired amount of microcrystalline cellulose (purchased from Alfa Aesar), bleached kraft pulp (kindly donated by Limerick Pulp & Paper, University of New Brunswick), and recycled cotton linter (purchased from Arnold Grummer, USA) were dispersed in the precooled solvent and the mixture was vigorously stirred for 5 minutes, after which it formed a transparent and viscous solution. The cellulose solution thus obtained was degassed by 8000 rpm centrifugation, then spread on a glass plate as a 0.6 mm thick layer, and finally immersed in acetone coagulation bath at 0 ^oC for 15 min for regeneration. The sheet hydrogel of regenerated celluloses was thoroughly washed with deionized water by soaking for 24 hr, fixing on a special polyethylene plate mold to prevent shrinkage, and dried with air at ambient temperature (Yang et al., 2011a; Yang et al., 2012). A nanofibrillilated cellulose (NFC) film was kindly provided from McGill University (Pulp and Paper Centre) and the film was prepared by TEMPO-oxidation (Isogai et al., 2011).

Table 6.1. Physical properties of different cellulose-based films.

Physical Properties	Cellulose film types				
	Unmodified paper (made from Kraft bleached pulp)	NFC	Avicel (MCC)	Cotton Linter	Cellulose film (made from Kraft bleached pulp)
Grammage (g/m^2)	60	51	88	84	78.5
Density (kg/m^3)	543	1456	1467	1403	1427
Thickness (µm)	110	35	60	60	55

6.2.2. Water vapor adsorption equilibria

Water vapor adsorption isotherms of the samples were measured by Belsorp-Max instrument (BEL JAPAN, INC., Osaka, Japan). The Belsorp-max is a volumetric gas adsorption /desorption measuring unit that can automatically measure adsorption isotherms in the range of p/po=10-8-0.997. The adsorption isotherms, of the samples used in this study, were measured at 5-35 ^oC temperature range, which is the temperature range of the Belsorp-Max instrument.

6.2.3. Water vapor transmission rates and uptake studies

Water vapor uptakes were measured by using gravimetric analyzer (IGA-001, supplied by Hiden Analytical, Warrington (UK)) combined with digital humidifier (HumiSys, supplied by InstruQuest Inc., Coconut Creek (USA)). For these measurements, the sample films were placed in the sample chamber and the film dried with pure nitrogen until constant weight was obtained, followed up by the chamber evacuation using a turbomolecular pump. The sample temperature was controlled by a thermo-regulated water bath.

The IGA permeation cell kit was used for direct measurements of water vapor transmission rates (WVTR's) in accordance to the method described by ASTM E 96/E96M-05 standard (2005). The cellulose film was sealed by compression in the cell and then the film was saturated at a preset RH using different salt solutions, e.g., LiCl (10.9 % RH), $MgCl_2$ (33 % RH), Mg $(NO_3)_2$ (52 % RH), NaCl (76 % RH), KNO_3 (92 % RH)) and pure de-ionized water (100 % RH), which were placed in the base of the sample holder. The outside environment was kept at 0 RH% by purging with pure dry gas (nitrogen). WVTR measurements were carried out at the relative humidity differences (ΔRH %) of 10, 33, 50, 90 & 100 % with accuracy of ±3 % ΔRH and at a temperature of 25±0.1^{o}C. The transfer rates (WVTR's) were calculated directly from the steady-state rate of weight change of the container, at a specified time interval, and the area of exposed film. Two to three replicates were made per each RH depending on the variation of the results and the average values were taken for analysis. Reproducibility of the results was within 5–10 % range.

6.3. Theory

6.3.1. Adsorption isotherm fitting

Guggenheim Anderson de Boer (GAB) Model has been commonly used for predicting moisture sorption isotherms of cellulosic products (Guggenheim, 1966). The GAB model is usually expressed in the form:

$$M = M_h \times \frac{C.K.a_W}{(1-K.a_W).(1-K.a_W+C.K.a_W)} \quad 6.1$$

Where *M* is the moisture content of the material in (%), M_h is the content of water sorbed in the first layer (monolayer moisture content), a_W is the water activity, and K and C are the Guggenheim constants corresponding to the heat of sorption of sorbed layer, i.e., C is a constant that relates to the strength of water molecule bindings to primary adsorption sites, and *K* is related to the heat of multilayer sorption.

6.3.2. Water vapor transmission rates (WVTR's)

At constant temperature and ΔRH (%), a steady state will be reached where WVTR can be calculated from the change in weight of the container, at a specified time interval, and the area of exposed film, as described by *Eq 6.2*:

$$WVTR = \frac{Weight\ Change}{Area \times time} \quad 6.2$$

WVTR refers to a specific sample configuration, e.g., thickness of the sample film. Water vapor permeability (WVP) can be calculated from WVTR as follows:

$$WVP = \frac{WVTR \times Z \times 100}{P^{sat} \times \Delta RH(\%)} \quad 6.3$$

where Z is film thickness, P^{sat} is water vapor saturation pressure at the experimental temperature, and ΔRH (%) is percentage relative humidity gradient.

6.3.3. Water vapor kinetics and mechanisms of water vapor transport

The Fickian diffusion model was used to determine moisture diffusion coefficient for different cellulose sample films. The mathematical model for transient fractional uptake, M(t)/M(∞), following Fickian diffusion for slab geometry is given by Eq. 6.4 (Crank, 1975):

$$\frac{M(t)}{M(\infty)} = 1 - \frac{8}{\pi^2}\sum_{n=0}^{\infty}\frac{1}{(2n+1)^2}\ exp\left(-\frac{\pi^2(2n+1)^2 D_{eff}}{4L^2}t\right) \qquad 6.4$$

where M (∞) is the asymptotic (equilibrium) uptake (% or mg), D_{eff} is effective diffusivity (m^2/s), L is a half thickness of the film (m) and t is an uptake time corresponding to M (t) (% or mg).

If the moisture uptake curves are fitted completely with the model Eq. 6.4, then the internal diffusion is considered to control the mass transfer resistance.

In the short time region (M(t)/M(∞) < 0.5) (Gu and Alexandridis, 2004; Balik, 1996), Eq. 6.4 can be replaced by:

$$\frac{M(t)}{M(\infty)} = \frac{2}{L}\quad\left[\frac{D\ t}{\pi}\right]^{1/2} \qquad 6.5$$

If the moisture uptake curves are fitted completely with the model Eq. 6.4, then the internal diffusion is considered to control the mass transfer resistance.

The corresponding equation for the rate controlled by surface resistance to mass transfer, for slab geometry, is given by Eq. 6.6 (Liu et al. 1996):

$$1 - \frac{M(t)}{M(\infty)} = e^{-k't/L} = e^{-kt} \quad 6.6$$

where $k^{'}$ is defined by the rate expression:

$$\frac{\partial \bar{M}}{\partial t} = \frac{k'}{2L}[M^* - M] \quad 6.7$$

In the short time region, M(t)/M(∞) < 0.5 (Gu and Alexandridis, 2004; Balik, 1996), Eq. 6.6 reduces to

$$\frac{M(t)}{M(\infty)} = \frac{k't}{2L} \quad 6.8$$

where $k' = k_c/K$, with k_c as the mass transfer coefficient and K is the equilibrium distribution constant.

For a case in which both surface and internal diffusional resistances are significant, the following equation (Eq. 6.9) describes the combined mass transfer mechanism (Hines and Maddox, 1985; Liu et al. 1996; Karger at al. 1992):

$$\frac{M(t)}{M(\infty)} = 1 - \sum_{n=1}^{\infty} \frac{2\alpha^2}{\beta_n^2[\alpha(\alpha+1)+\beta_n^2]}\ exp(-\beta_n^2\tau) \quad 6.9$$

where eigenvalues β_n are given by the following equation:

$$\beta_n\ tan\,\beta_n\ = Bi = \alpha = \frac{k_cL}{KD} \quad 6.10$$

and $\tau=Dt/L2$, $\alpha=Lkc/KD$ (K is the equilibrium distribution constant and k_c is convective mass transfer coefficient) and Bi (or α) is a Biot dimensionless number, which represents the ratio of the internal to external mass transfer resistance ((L/KD)/($1/kc$)), as described by Eq. 6.10. If $Bi>1$, then water vapor transport is controlled by internal diffusional resistance and if $Bi<1$, the mass transport is controlled by external surface resistance or relaxation rate of a polymer chains. Relaxation rate is related to the molecular motion in the polymer, which results in structural change of the film. If $Bi=1$, the water vapor uptake rate shows Non-Fickian diffusion or anomalous diffusion; both external surface resistance (and/or relaxation rates of polymer chain) and internal diffusional are comparable (Gu and Alexandridis, 2004; Weinmuller et al., 2005).

6.4. Results and Discussion

6.4.1. Water vapor adsorption equilibria

Water vapor adsorption isotherms of regenerated cellulose films (made from bleached Kraft pulp, cotton linter cellulose and microcrystalline cellulose), NFC films and unmodified paper (made from bleached Kraft pulp) at 25 ^{o}C are shown in Fig. 6.1. The isotherms generally exhibit extended linear trends without a clear indication of the monolayer to multilayer transition, which should be typical for the Type IV isotherms. However, the isotherms of the unmodified paper sample, and to some extent the microcrystalline cellulose film, are more of the typical type IV isotherms according to IUPAC classification. A hysteresis loop of type H3 was observed on all isotherms. Figure 6.2 shows the hysteresis loop of the regenerated cellulose and NFC films (isotherms for other samples are shown in Figure S1 in Appendix-III). The loops are elongated and are evident for the entire relative humidity range. Similar hysteresis loops were also observed for unmodified paper and coated paper samples (Bedane et al., 2014) and wood pulp derived cellulose powders (Nge et al., 2013). Cellulose chain swells during water vapor adsorption, thus significantly enlarging the surface area for water vapor molecules to attach to the adsorption sites. This provides conditions for the formation of hysteresis loop during desorption, since it requires a lower vapor pressure to desorb the same amount of water due to the strong bonding created in the adsorption stage of the process. Details of this are explained in our previous study (Bedane et al., 2014). At lower relative humidity range, e.g., RH= 0-30%, the isotherms, in particular for the paper samples, are almost linear, as discussed above, indicating relatively strong adsorption, but for the transparent cellulose films (regenerated cellulose and NFC films), this region extends up to RH=50%, as shown in Fig. 6.1. At intermediate relative humidity range (RH=30-75%), in the so-called multilayer sorption region, moisture content increases with an increase of partial pressure of water vapor. In this region the change in the slope of the curve is more noticeable, especially for the unmodified paper sample (at RH=30 %) and for the regenerated cellulose films (at about RH=50%). Therefore, this indicates that multilayer water vapor molecules formation is more pronounced for the paper samples, but less indicative in the NFC films and other samples shown in Fig. 6.1. At a very high relative humidity region (>RH=80%), the water vapor molecules condense in the capillary or in the pores of the film's surface. This is more significant in the paper samples than transparent cellulose films due to their higher porous content in structure. As the result of this, the adsorption isotherm curve of the paper sample showed more upward concave shape than other samples in this region.

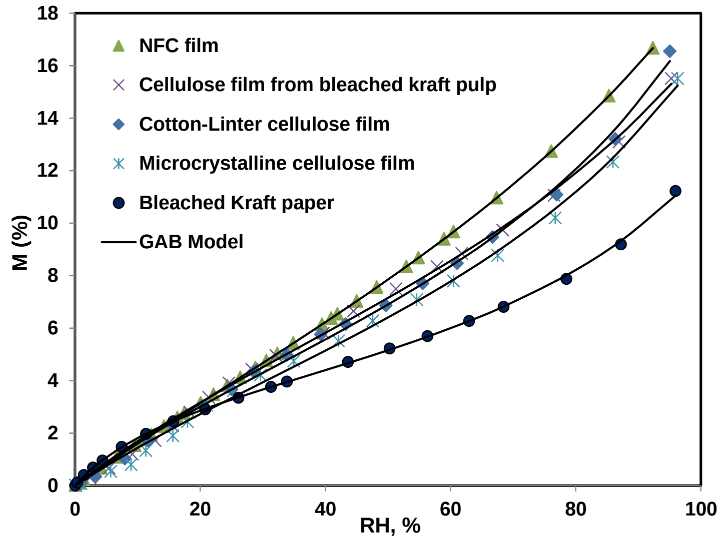

Figure 6.1. Experimental data and GAB-predicted adsorption isotherms at 25 ^oC.

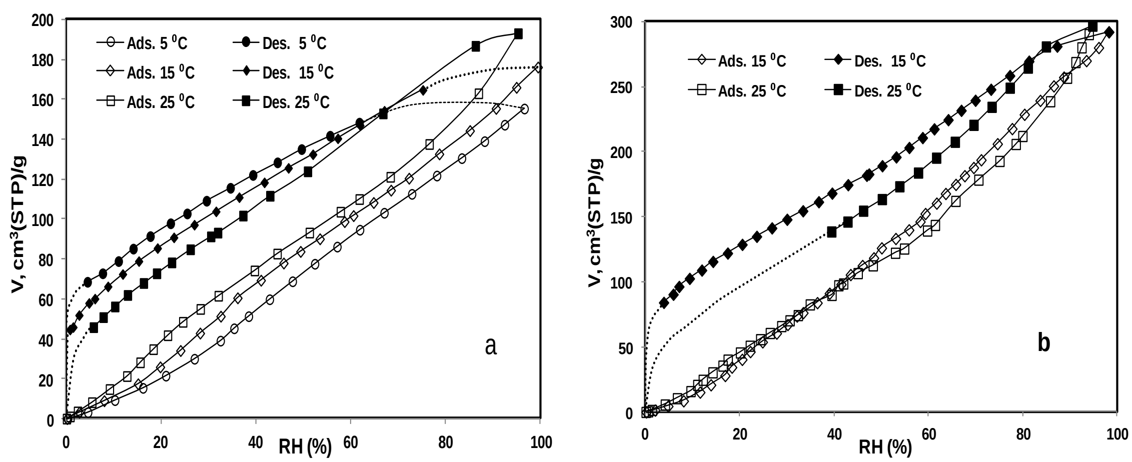

Figure 6.2. Water vapor adsorption-desorption isotherms of regenerated cellulose film made from Kraft pulp (a) and NFC film (b) at different temperatures.

At low moisture content (RH=0-20%), the water vapor adsorption on paper sample is higher than on the transparent films. This could be due to low crystallinity and high swelling effect of the paper sample compared to transparent cellulose films, i.e., the swelling of the film at very low concentration is negligible in the transparent films.

Microcrystalline film has a lower water vapor adsorption capacity than any of the other regenerated cellulose films, as shown at Fig. 6.1. This is expected since the microcrystalline films have higher crystallinity than the other investigated samples. The water vapor adsorption occurs on the surfaces but the molecules cannot penetrate further into the bulk solid structure in most crystalline solids due to close packing and high degree of order of the crystal lattice. Surprisingly, the adsorption capacities of these transparent cellulose films increase with the temperature increase up to 35 ^{o}C, especially at lower relative humidity ranges, as shown in Fig. 6.2 and Fig. 6.3. However, a change in this trend, e.g., decrease in adsorption capacities with increased temperature, is noticeable at about 35 ^{o}C. This characteristic could be due the change in the structure of the film. At low temperature the molecules in the polymer chain are more tightly bound to each other and the molecular motion is restricted by forming a glassy (stiff) type plastic. As a result there will be less exposed functional groups at the film surface and the adsorption of water vapor molecules will decline. However, at high temperatures, molecular motion occur in the polymer resulting in the soft (rubbery) type of plastic, as well as swelling of the polymer chain due to presence of moisture in the film, will create more available space for adsorption. As the amount of the adsorbed water increases, glass transition temperature (Tg) decreases and the glassy state approaches a "rubber or fluid" state. As a result, water mobility along the film increases significantly. This will be explained in more detail in the next section.

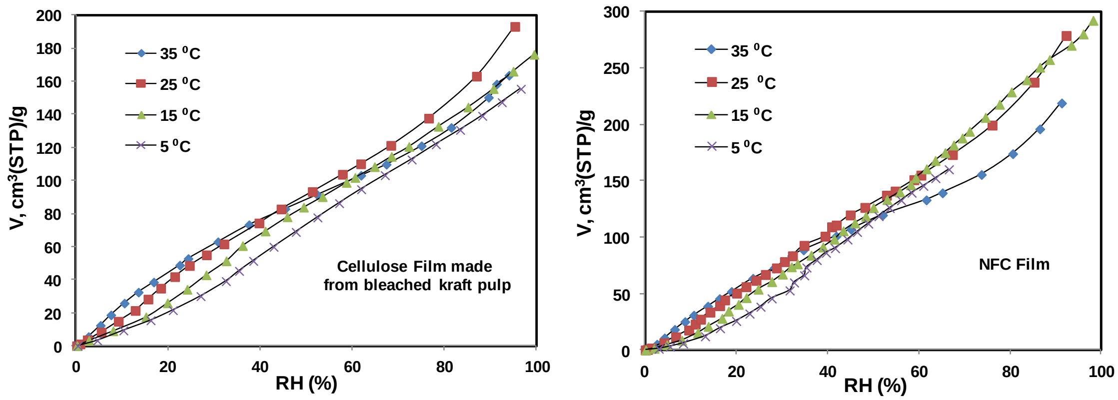

Figure 6.3. Water vapor adsorption isotherms of regenerated cellulose film and NFC film for four different temperatures.

Higher water adsorption was observed for the regenerated cellulose films and NFC films compared to the unmodified paper sample, even though they have greater crystalline properties than the paper samples. NFC films showed higher water vapor adsorption capacities for the entire relative pressure range, as shown in Fig. 6.3. This is due to the larger number of hydrophilic sites on the cellulose films compared to other investigated samples and relatively large surface to volume ratio of microfibrils due to their small sizes (Iijima and Takeo, 2000; Sun, 2007). Monolayer moisture contents, Mh and parameters K and C were extracted from the Guggenheim-Anderson-De Boer (the GAB) model for cellulose films and paper and are presented in Table 6.4. The GAB model fits satisfactory the experimental data, as shown in Fig. 6.1.The model was found adequate for fitting adsorption isotherms of cellulose films, as reported in other studies, e.g., Rhim et al. 2009, as well as on coated paper samples as was reported in our previous study (Bedane et al., 2014). Monolayer moisture contents of the transparent cellulose films thus determined are more than two times larger than the monolayer moisture content compared to our unmodified paper sample (made from bleached Kraft pulp ~ 4.12 wt.

%), as shown in Table 6.2. This is expected due to a large number of free hydroxyl groups present in the regenerative cellulose and NFC film surfaces compared to other fiber-based materials (e.g. paper). A significant portion of cellulose molecules is exposed on the surfaces of the transparent cellulose films due to the relatively small size of microfibrils, e.g., 5–10 nm (Iijima and Takeo, 2000; Sun, 2007).

Table 6.2. The GAB model parameters determined from water sorption isotherms.

Paper samples	Monomolecular (M_h) (%)	K	C
Unmodified paper	4.12	0.67	9.62
NFC	11.93	0.53	2.60
Cellulose Film from Bleached kraft pulp	7.96	0.56	4.95
Cotton Linter	7.19	0.65	3.83
Microcrystalline	7.16	0.62	3.47

The extracted GAB parameters *C* and *K* for the unmodified paper are 9.62 and 0.67, respectively. Similarly, Rhim et al. (2009) reported for unmodified paper, GAB constants C=9.85 and K=0.87, and Chatterjee (1997 & 2001) for bleached Kraft paperboard, C=56.0, K=0.75 and monolayer moisture content of 5.10%. The GAB parameter C is related to the magnitude of the enthalpy difference in the upper layers and in the monolayer, while the constant K is related to measurement of the difference of enthalpy in the sorbate's pure liquid state and in the upper layers (layers above the monolayer). The lower K value of the NFC film is consistent with the more structured configuration of water molecules adsorbed in multilayer, and also indicates that the adsorbed water is different from bulk water. When the K value is close to 1, the water molecules in the multilayers behave as pure liquid. The highest K and C values are obtained for the paper sample, as shown in Table 6.2.

6.4.2. Water vapor mass transport properties

6.4.2.1. Water Vapor Transmissions Rates (WVTR's) and Permeabilities (WVP's)

The steady-state water vapor transmission rates of different regenerated cellulose films at a temperature of 25 ^{o}C were determined at a constant total pressure of 100 kPa, according to Eq. 2, and shown in Table 6.3. Regenerated cellulose films exhibit better barrier properties than NFC film. This could be due to higher relative crystallinity of the regenerated cellulose films compared to NFC film. WVTR's of the investigated transparent cellulose films showed comparable results for all relative humidity gradients. The WVTR's of these films are low at relative humidity range below 60%. On the other hand, the WVTR's of transparent cellulose films showed lower values compared to the paper sample. In general, the lower WVTR's for transparent cellulose films are attributed to the higher crystallinity, thus creating a more tortuous path for the transport of water vapor molecules. However, the WVTR's of all samples increase with an increase of relative humidity gradients. Spence et al. (2011) found WVTR of microfibrillated cellulose film (MFC) film (grammage of 30 g/m^2) about 240 g/m^2.day at T=23 ^{o}C and ΔRH=50%.This result is greater than our measurement, and the reason could be due to the difference in the grammage or the thickness of the film. Yang et al. (2011) reported the WVTR of regenerated cellulose film close to 100 g/ m^2.day at 50 % and 23 ^{o}C.

Table 6.3. WVTR's of regenerative cellulose films at different relative humidity gradients (ΔRH) at T=25 ^{o}C and P=100kPa (normalized thickness Z=100 μm)

Relative humidity gradient (ΔRH, %)	WVTR (g/m^2 day)				
	Unmodified paper	NFC film	Cellulose film (made from bleached Kraft pulp)	Cotton linter film	Avicel (MCC) film
10	55	29	16	18	12
50	287	132	44	63	34
90	1500	652	598	450	584
100	2200	792	870	856	940

The water vapor permeability values (WVP's) of regenerated cellulose and NFC films were determined at different moisture contents of the samples (determined from the isotherm data based on the average relative humidity of the sample) and at a temperature of 25^{o}C, as shown in Fig. 6.4. The permeability was found to depend on the moisture content of the films. WVP's remained low at relative humidity below 25% (< 4.5 wt. %) and increased sharply above 25% (>5 wt. %). This could be attributed to the hydrophilic nature of these films, i.e. the solubility of water in the films increases considerably more compared to the decreased diffusivity at high moisture contents of the sample. As a result, increased or decreased permeability of a vapor through the films depends on both solubility and diffusivity of a vapor in the films according to the solubility-diffusion theory, which is explained in detail below. Water vapor permeabilities of regenerated and NFC film samples are much lower than for the unmodified paper sample and are dependent on the concentration, e.g., lower values at lower relative humidity gradients, but they show a rapidly increasing trend at higher relative humidity gradients. Minellie et al. (2010) reported water vapor permeabilities of microfibrillated cellulose film (MFC) between 1.8×10-13 -3.6 $\times 10^{-10}$ g/m.s.Pa for a wide range of relative humidities at 35 ^{o}C. Nobile et al. (2002) also reported that the water vapor permeability of cellophane increased with the water concentration in the film with the WVP's in the range of 2.22-7.12 $\times 10^{-11}$ g/m.s.Pa for different water vapor concentrations (RH's). Higher moisture contents of the film will generally result in losing of the closely packed structure due to swelling, which leads to an increase of free volume of the film structure, thus enhancing the vapor diffusivities and consequently reducing the barrier properties.

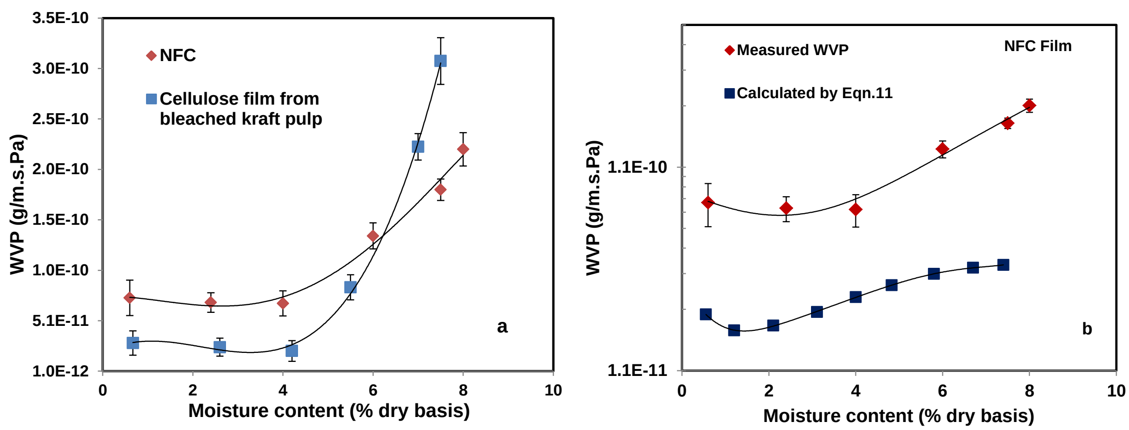

Figure 6.4. WVP of regenerated cellulose and NFC films (a) and comparison between measured water vapor permeability and calculated D×S of NFC film (b) at different moisture content and at 25^{o}C.

According to the solution-diffusion theory, the main water vapor transport mechanism through the polymer films, under water vapor concentration gradient, is due to adsorption by dissolution of vapor in the polymer material, followed by diffusion through the polymer matrix and desorption of water vapor at the lower concentration side of the film.

Thus, the permeability of water vapor can be explained by combining equilibrium and kinetics parameters as shown by Eq. 6.11.

$$WVP = K \times D_{eff} \qquad 6.11$$

where K is the equilibrium constant (e.g., Henry's constant), which can be calculated from adsorption isotherm data, and D_{eff} is the effective diffusivity of water vapor through polymer matrix. D_{eff} can be determined from experimental transient water vapor uptake rate measurements and the D_{eff} results are discussed and presented in section 6.2.3. As can be seen from Fig. 6.4b, there is a difference of about half an order of magnitude between the WVP's experimentally measured and calculated WVP's according to Eq. (6.11). Therefore Eq. (6.11) seems to be only useful for the qualitative analysis, e.g., by showing the same WVP's trends with RH, but cannot be used for the more quantitative analysis of permeability in hydrophilic films, because of strong interaction between water vapor and polymer matrix, which results in swelling of the cellulose chains (Debeaufort et al., 1994; Minelli et al., 2010; Shao and Huang, 2007). Swollen cellulose chains are more extended (further apart) resulting in less interactions between them, which leads to an increase in pore sizes or free volumes in the cellulose film matrix, thus increasing pore diffusion of water vapor. In addition, the variation of the film thickness due to swelling can influence on the certainty of the calculated effective diffusivity (D_{eff}) as the effective diffusivity was calculated based on the dry film thickness measurement (as shown in Table 6.1). The relation (Eq. 6.11) could be more successfully applied for non-swollen dense and non-porous membranes or films.

6.4.3. Activation energies

Water vapor permeabilities were evaluated at different temperatures, in the range of 15-40 ^{o}C, at a fixed relative humidity gradient of ΔRH=50% for regenerated cellulose and nano-fibrillated cellulose (NFC) films. The activation energy of permeation (E_{eff}) was determined from the Arrhenius plots shown in Fig. 6.5, according to the Arrhenius relation for WVP given by Eq. 6.12:

$$WVP = P_0 \, exp\left(\frac{-E_{eff}}{R\,T}\right) \qquad 6.12$$

where Po is a pre-exponential constant, R is the universal gas constant, T is absolute temperature and E_{eff} is the effective activation energy of permeation. The average E_{eff} of regenerated cellulose and nanofibrillated cellulose films were found to be 37.4 kJ/mol and 29 kJ/mol at the lower temperature range, and about -1.0 kJ/ mol and -19 kJ/mol at the higher temperature range, respectively. The E_{eff} of these films is higher at lower temperatures than E_{eff} of the unmodified paper film (23 kJ/mol), which was reported in our previous study (Bedane et al., 2012). This indicates that the permeability of the cellulose films decrease by increasing activation energy at the lower temperatures. The change in the slope of the activation energy for permeation is observed at the temperatures between 25-30 ^{o}C. This was also observed with other polymers, i.e. gliadin films, pollulan-starch blends, natural rubbers, and polyvinyl acetate (Balaguer et al., 2013; Biliaderis et al., 1999; Doty et al. 1946; Meares et al., 1954). In general, this could be ascribed to a change in the material structure due to thermal transitions such as crystallization or glass transition. We have measured the glass transition temperature for dried NFC and regenerated cellulose films using simultaneous DSC-TGA instrument.The glass transition temperature of NFC and regenerated cellulose film showed at 62 ^{o}C and 65 ^{o}C, respectively, by heating from room temperature to 120 ^{o}C (shown in Figure S2 in the Appendix-III). However, the glass temperature of the films can be shifted at room or even lower temperatures at high moisture contents of the films**,** which is indicative on Fig. 6.5. The moisture content of the cellulose films are between 6-8% at 25 ^{o}C. Szczesniak et al. (2008) reported the glass transition temperature of microcrystalline cellulose powder (66 % of crystallinity index) was between 22-25 ^{o}C and 48-50 ^{o}C for 7.0% and 5.3% moisture content of the powder, respectively. We could not determine the glass temperature of moist sample with our TGA-DSC instrument since the working condition of the instrument starts at a room temperature. The glass transition temperature of a polymer decreases with increased moisture content in a polymer due to the plasticizing effects of water, which produces a morphological change in the polymer (Oksanen et al., 1990). From water vapor adsorption isotherms (shown in Fig. 6.2), the upward inflection in the isotherms is noticeable at higher temperatures of 25 ^{o}C and 35 ^{o}C in the relative humidity range between 50-70%. This upward inflection is most likely related to the glassy to rubber transition due to water adsorption (Oksanen et al., 1990).

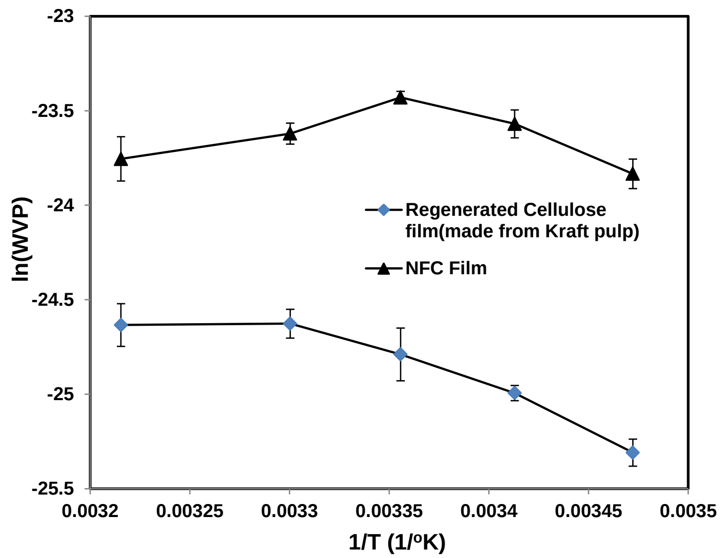

Figure 6.5. Effect of temperature on WVP of regenerated cellulose (made from bleached Kraft pulp) and NFC films.

Adsorption isotherm measurements showed that the water vapor adsorption on the films increases with temperature increase, as shown in Fig. 6.2, in particular, at low and intermediate water vapor activities or relative humidity ranges. At low temperatures, the material can become more compact or in a glassy state, thus rendering the films with better barrier properties or lower permeabilities. At the high relative humidities and temperatures, with more water adsorbed, the film's structure seems to change to a rubbery state, thus resulting in higher water vapor permeation. However, the decrease of permeability at the high temperatures (>20 ^{o}C) is due to a constant or slightly increased water vapor transfer rates despite increased temperature. Weinmuller et al. (2005) suggested a point where the formation of hysteresis during desorption measurement could be indicative of a change of state from rubber to glass in the polymer. In this study desorption hysteresis starts from the end point of adsorption isotherm. However, the hysteresis at a lower temperature, e.g., 5 °C, is wider than at 25 °C and 35 °C for cellulose films made from kraft pulp (i.e., broadness at 5 °C>25°C>35°C) and NFC films (i.e., broadness at 15 °C > 25 °C) as shown in Fig. 1. This is also indicative of the higher activation energies of permeation at lower temperatures due to glassy properties of the film. Moreover, adsorbed moisture has a plasticizing effect on the biopolymer network, which leads to changes from glassy to rubbery state of the material (Oksanen et al., 1990; Phan et al., 2005). At higher RH's film will swell and the swollen network of film, in addition to high temperature, will facilitate the diffusion of water molecules through the rubbery material. At low relative humidities and temperatures, the film structure can have a characteristic of strong hydrogen bonding between cellulose molecules keeping the film stiffer and more compacted in structure. Water vapor permeability is dependent on adsorption of water on the surface and diffusivity through film as described by Eq. 6.11. Therefore, the effective activation energy of permeation (E_{eff}) is the sum of the activation energy for diffusion (E_d) and the enthalpy of adsorption (ΔH) as shown by Eq. 6.13.

$$-E_{eff} = (-\Delta H) - E_d \qquad 6.13$$

The solubility of gas in a membrane, e.g., paper or cellulose membrane, is generally an exothermic process, so ($-\Delta H$) is normally a positive quantity, while (E_d) has always a positive value. Therefore, Eq. (6.13) can be rewritten as:

$$E_{eff} = |E_d| - |\Delta H| \qquad 6.14$$

Depending on the magnitude of the energy of adsorption ($|\Delta H|$) relative to the diffusional activation ($|E_d|$), one can therefore expect E_{eff} to have a positive or negative value, e.g., the permeability will either increase or decrease with temperature, respectively.

If $|\Delta H| > |E_d|$, then $E_{eff} < 0$ and if $|\Delta H| < |E_d|$, then $E_{eff} > 0$. Positive values of E_{eff} of the films were obtained at low temperatures, as discussed above, in relation to Fig. 6.5. This is a result of higher absolute values of activation energies (E_d) compared to heat of adsorption (ΔH), and is related to the lower adsorption and consequently lower heat effects at lower temperatures, as can be seen from isotherms in Fig. 6.2. In addition, it is also plausible to have activation energies for diffusion higher at lower temperatures due to hindering effect on water vapor motion in the films resulting from strong hydrogen bonding in the polymer or inter-fibre structure (Shogren, 1997; Balguer et al., 2013). Conversely, at higher temperatures, the higher water vapor adsorption produces higher heat of adsorption (ΔH) and consequently higher absolute values compared to (E_d) thus, according to Eq. (6.14), resulting in negative values for the effective activation energy (E_{eff}).

6.4.3. Water vapor diffusion and surface barrier kinetics

The effective diffusion coefficients were determined from uptake rate measurements on the plane sheet of cellulose film samples by fitting the data with combined internal diffusion and surface barrier model (Eq. 6.9). The combined model was found to provide the best fit for all experimental data involving water vapor transfer in the films, and from this model the most dominant water vapor transport mechanisms in the films will be discussed in section 4.2.4. In order to investigate the effect of moisture content, the uptake rates were measured by successively increasing the relative humidity, e.g., by increasing in increments of 10%. Fig. 6.6 shows typical water vapor uptake curves of cellulose films measured for incremental relative humidities and fitted by the combined model. The extracted diffusivity values are in the range of 2×10^{-14} - 10×10^{-14} m^2/s at different humidity conditions, as shown in Table 6.4. The water vapor diffusivity depends on the moisture content of the sample, as can be seen from Fig. 6.7 and Table 6.4. The maximum effective diffusivities were obtained between 50-70% RH. The overall trend was found to be similar with the results of our previous study on unmodified and coated paper samples (Bedane et al., 2012). The diffusivity in the transparent cellulose films (i.e., NFC, regenerated cellulose films) depends on moisture content for the entire relative humidity range, unlike the diffusivity in unmodified paper, which was found independent of moisture content at lower concentrations (< RH=30%), as shown in Figures 6.7a and 6.7b. This is indicative of different diffusion mechanisms of water vapor transport in the different materials, particularly at lower RH's. In the transparent cellulose films, it is possible that due to relatively strong adsorption, surface diffusion can play a more dominant role than in the case of unmodified paper. It is also expected that mass transfer resistance due to pore diffusion is more significant in case of transparent cellulose films as compared to unmodified paper due to the narrow pores (or micropores) in the films resulting in micropore diffusion as a predominant pore diffusion mechanism (Henriksson et al., 2008; Lavoine et al., 2012; Spence et al., 2011). The decrease in the diffusivity at high relative humidities in the film could be due to cluster formation in the film whereby sorbed water molecules associate or form clusters by hydrogen bonding, thus reducing molecular mobility, as explained in our previous study (Bedane et al., 2012). In general, the films showed lower diffusivity by up to two orders of magnitude compared to the unmodified paper samples and coated papers, but their adsorption capacity is higher than paper samples (Bedane et al., 2012). Minelli et al. (2010) reported moisture dependent water diffusivities for different MFC films in the range of 10^{-15} to 10^{-12} m^2/s at a temperature of 35 ^oC. Del Nobile et al. (2002) reported the water vapor diffusivity was in the range of $0.5\text{-}4.0\times10^{-13}$ m^2/s for different moisture concentrations. However, the curves used to fit their experimental data have a sigmoidal shape and did not show a decreasing trend at the very high moisture content. Other studies (Balaguer et al., 2013) showed similar profile on dependency of effective diffusion coefficients of water vapor as a function of relative humidity through gliadin film.

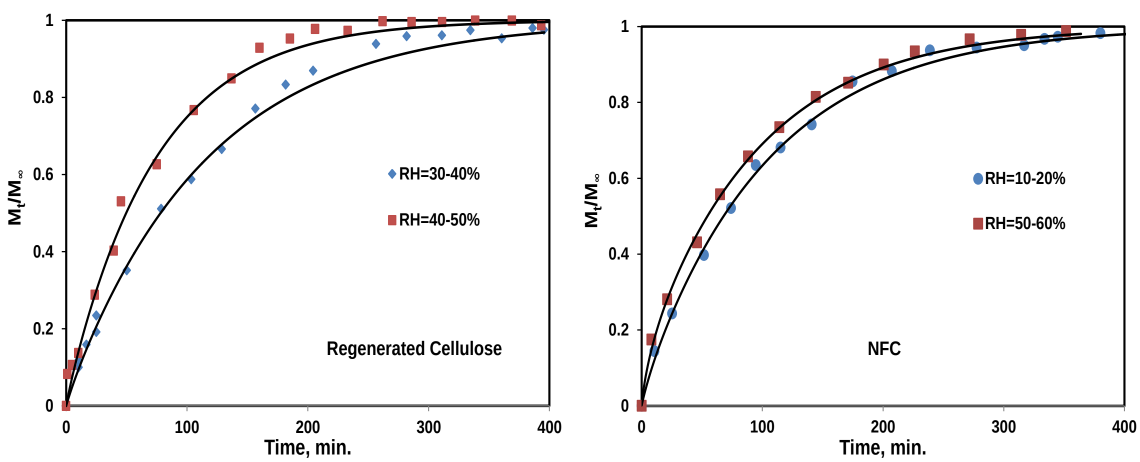

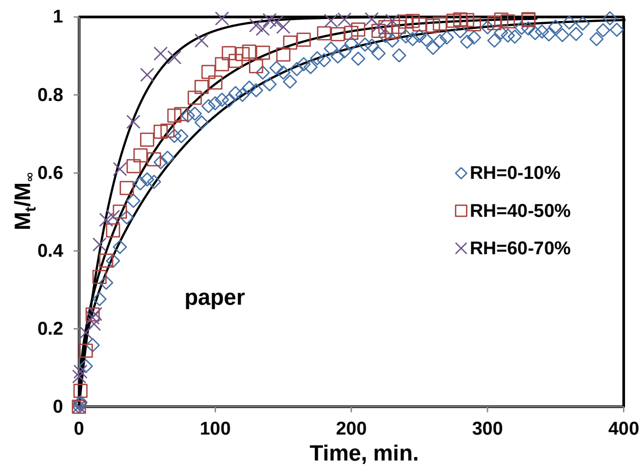

Figure 6.6. Water vapor uptakes of regenerated cellulose, NFC and paper samples fitted with Eq. 8 (combined model) at T=25 ^{o}C.

The Biot numbers were found to be less than one for the combined model (Eq. 6.8) that was used to fit the water vapor uptake rates of the transparent cellulose films shown in the Fig. 6.6 at the low and intermediate RH region. However, Biot numbers are close to one at the higher relative humidities indicating both internal diffusion and surface resistance are significant in this humidity range to moisture transfer in the films (Biot numbers are also given in Table S1 and water vapor uptake rates of regenerated cellulose film (at high RH) in Figure S1 of in in Appendix-III).

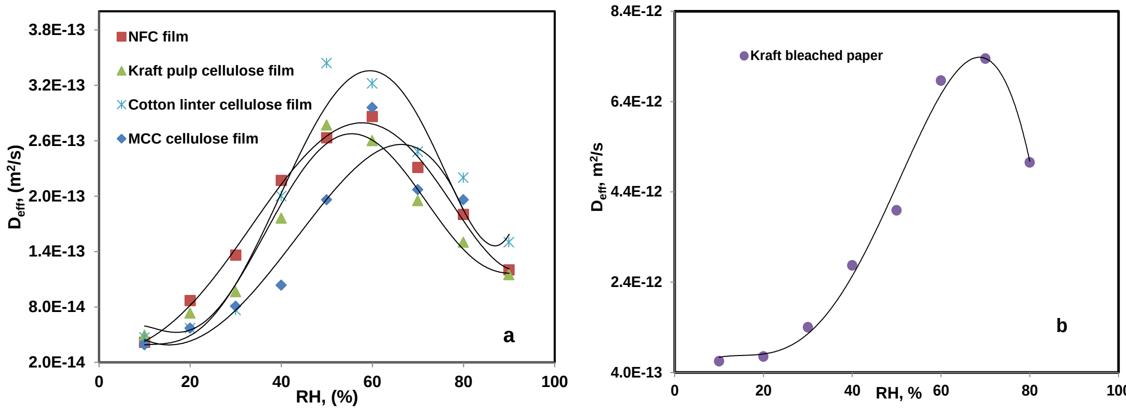

Figure 6.7. Dependence of effective diffusivity of regenerated cellulose and unmodified paper films on relative humidity at T=25°C.

Table 6.4. Effective water vapor (H_2O/N_2) diffusivities for cellulose films at different relative humidity values and T=25°C.

Relative Humidity (ΔRH, %)	$D\times10^{14}$ (m^2/s)				
	Unmodified paper	NFC	Cellulose film from kraft beached pulp	Cotton-Linter	Avicel (MCC)
0-10	42.0	4.16	5.01	4.69	3.90
10-20	65.0	8.68	7.33	5.71	5.70
20-30	68.0	13.6	9.65	7.66	8.88
30-40	120.0	21.7	17.6	20.0	10.4
40-50	349.0	26.3	27.7	34.4	19.6
50-60	687.0	28.6	26.0	32.2	29.6
60-70	705.0	23.1	19.5	24.8	20.7
70-80	510.0	18.0	15.0	22.8	19.6
80-90	280.0	12.0	12.5	15.0	-

6.4.4. Water vapor rate controlling mechanisms

The mechanism of water vapor transport through the cellulose films was evaluated by applying Eqs. 6.4-6.10. Diagrams in Figure 6.8 show the experimental uptake data fittings using the full time solutions of the internal diffusion model (Eq. 6.4) and surface barrier model (Eq. 6.6). In addition, Figures 6.9a and 6.9b,c depict short time solution fittings of internal diffusion model (Eq. 6.5) and surface resistance model (Eq. 6.8), respectively. As can be seen from these figures, water vapor uptake curves of unmodified paper samples at low to medium humidities, e.g., 3-10% to 50-60% (Figures 8a and 9a), show conformity with the diffusion model represented by Eqs. 6.4 and 6.5, and the poor agreement with the surface barrier model represented by Eq. 8, as shown in Figures S3 and S4 in in Appendix-III, indicating the dominance of diffusion resistance (i.e., diffusion in the inter-fiber space and intra-fiber diffusion). The Biot numbers calculated from Eq. (10) are in the range between 8-100,further supporting the dominance of diffusion resistance in the films (Bi numbers for different relative humidities are listed in Table S1 in Appendix-III). However, at the highest moisture content, e.g., relative humidity of 60-70% surface barrier model was shown to fit experimental uptake data satisfactory for unmodified paper (Fig. 6.8a). This change in mechanism could be attributed to the surface pores being filled with water thus providing additional resistance to mass transfer.

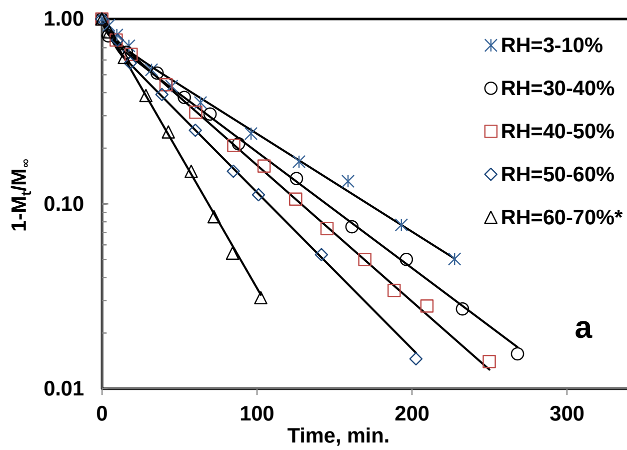

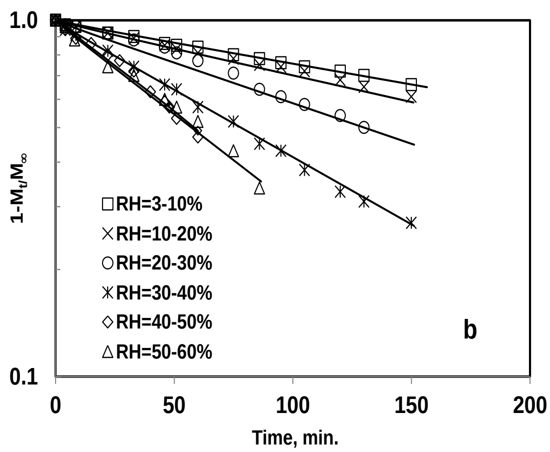

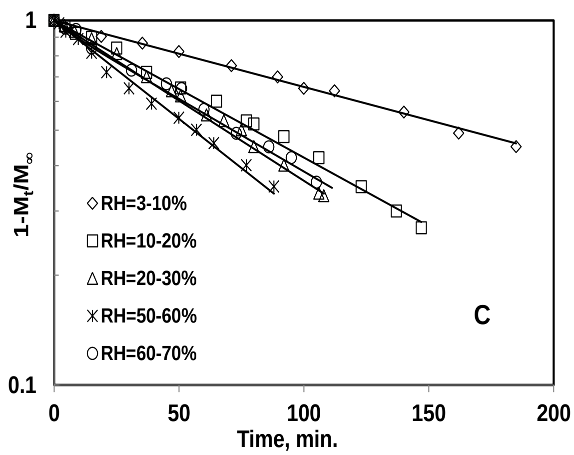

Figure 6.8. Model fittings of water vapor uptake curve measured at T=25 °C and different RH's of: (a) unmodified paper (using diffusion resistance model (Eq. 6.4) for all RH steps, except at RH=60-70%* where the surface resistance model (Eq. 6.6) was used; (b) regenerated cellulose film (Eq. 6.6) and (c) NFC film (Eq. 6.6).

[Symbols are used for the experimental data points and solid lines show the full time model solutions].

Water vapor uptake rate curves of NFC and regenerated cellulose films display better conformity with the surface resistance model, according to both short and full time solutions (Eq's 6.6 and 6.8), as shown in Figures 6.8b and c, and Figures 6.9b and c, respectively, for the relative humidities less than 60% (additional figures are available in in Appendix-III). The dominance of surface barriers in these films is due to physical obstruction of the pore mouths and higher percentage crystallinity or glassy structure compared to unmodified paper. However, at high moisture contents, e.g., RH>60% neither diffusion nor surface barrier model fits the NFC and regenerated cellulose films data satisfactorily, indicating a change in the mass transfer mechanism, i.e., diffusion and surface resistance are comparable (as indicated in Figure S5 in Appendix-III). This is plausible due to the change in the structure of the films caused by swelling of fibers with increased moisture content and/or pore blockages by the formation of multilayer consisting of water molecules, thus affecting the mass transfer process.

Similarly others studies reported/analyzed the rate controlling mechanisms of solvent or moisture in polymer materials based on the solvent diffusion rate and the polymer chain relaxation rate using the rate moisture uptake ratio (Alfrey et al., 1966; Balaguer et al., 2013). When the uptake rate is proportional to $t^{1/2}$ in the short time region, according to Fickian diffusion model, the rate of diffusion is much less than that of relaxation, and therefore, the diffusion process controls the sorption process. If the uptake rate is proportional to time (t) in the short time range, water vapor transfer in the film is controlled by the relaxation rate of polymer chains (surface barrier resistance), since the diffusion is very rapid in this case. If the uptake rate is proportional to the exponent of time between 0.5 and 1, then it is a non-Fickian diffusion or anomalous diffusion, e.g., both diffusion and relaxation rates will be dominant. At low relative humidity, the diffusion process controls the sorption process in the paper sample but the regenerated cellulose and NFC films showed consistency with surface barrier resistance. However, at high moisture contents, water vapor diffusion and relaxation rates occur simultaneously in all the film samples (indicated in Figure S3 in Appendix-III). Hence, both conditions (internal diffusion and surface barrier) control the water vapor transport comparably. Motion of substructure of the fiber or long chain molecules can occur at rubbery than glassy state. Non-Fickian character of a polymer at higher relative humidities can be due to relaxation which occurs slowly to accommodate the clustering process (Stannett et al., 1980).

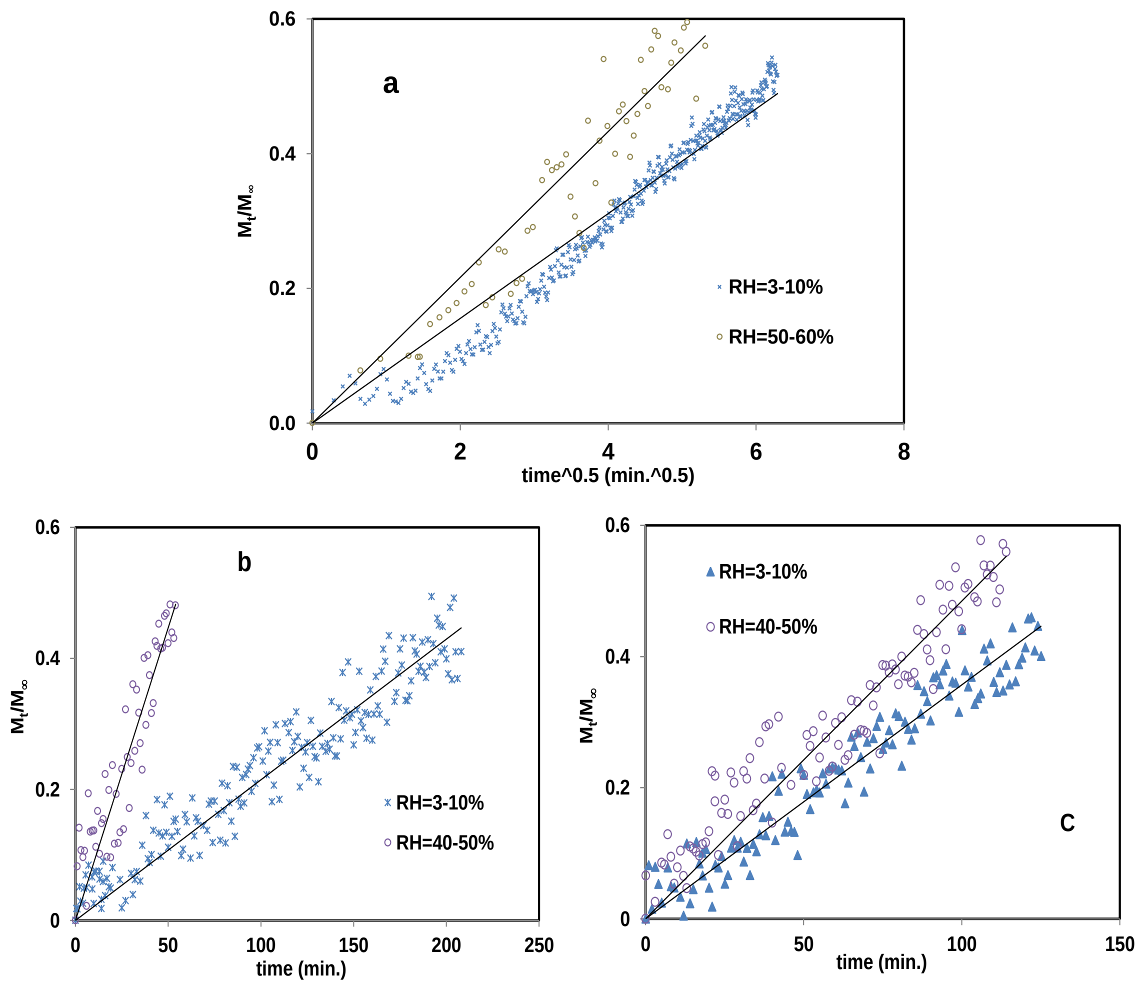

Figure 6.9. Model fittings of water vapor uptake data measured at T=25 °C of: (a) unmodified paper (using the diffusion resistance model (Eq. 6.5)); and (b) regenerated cellulose film and (c) NFC film (both (b) and (c) used the surface resistance model (Eq. 6.8)).

[Symbols are used for the experimental data points and solid lines show the short time model solutions].

6.5. Conclusions

Water vapor adsorption equilibria, transport and kinetic behaviors of regenerated cellulose, prepared from different cellulose sources and NFC films, were determined from water vapor adsorption isotherms and uptake measurements and compared with unmodified paper as a reference sample. The adsorption isotherms obtained experimentally at 25 ^oC were analyzed using GAB model to determine the monolayer moisture content of each sample. The monolayer moisture contents of NFC and regenerated cellulose films were more than double in comparison to unmodified paper, indicating more hydrophilic character of the transparent cellulose films. WVP's of those films were measured using different relative humidity gradients. At low moisture contents (relative humidities), the NFC and regenerated cellulose films showed low WVP's. However, at high contents (> 50% relative humidity), the WVP's increased rapidly compared to the paper sample. The effective water vapor diffusivities were also determined from uptake rate measurements. Water vapor diffusivities were found to depend on the moisture content of the films. The diffusivities increase with moisture content and the maximum values were obtained between 50-70% RH. The effective diffusion coefficients (D_{eff}) of NFC and regenerated cellulose films are 1-2 orders of magnitude lower in comparison to the paper film depending on the relative humidity. High activation energies of permeation were determined at low temperatures, but the activation energies were found to decrease at high temperature, which is attributed to the change in the structure of the polymer.

Surface resistance was found to be a more dominant mechanism for mass transfer in the NFC and regenerated cellulose films: the surface resistance (e.g., pore mouth obstruction or narrow pore size) hinders water vapor transport across the surface of the film at low and intermediate moisture contents. Water vapor uptake in unmodified paper seems consistent with internal diffusion control, except at high moisture contents. Both surface resistance and internal diffusion are significant at high moisture contents in all transparent cellulose films and the unmodified paper. In general, the availability of a large number of hydroxyl groups in these cellulose films causes high water vapor adsorption, thereby increasing water vapor permeability, i.e., poor barrier properties, in particular at high relative humidity conditions. This study recommends reducing the hydrophilic properties of the films either using coating or chemical treatment in order to obtain better barrier properties to water vapor.

References

Alfrey, T., Gurnee, E.F. , Lloyd, W.G. (1966). Diffusion in glassy polymers, J. Polym. Sci. Part C: Polym. Symposia 12, 249–261.

Ashely, R.J. (1985). Permeability and plastic packaging. In polymer Permeability, Comyn J (Ed.). Elsevier Appl. Sci.: London, UK, 269-308.

Balguer M.P., Cerisuelo, J.P, Gavara, R., Hernandez-Muñoz, P. (2013). Mass transport properties of gliadin films: Effect of cross-linking degree, relative humidity, and temperature. J. Memb. Sci. 428, 380-392.

Balik, C.M. (1996). On the extraction of diffusion coefficients from gravimetrical data for sorption of small molecules by polymer thin films. Macromol. 29, 3025-3029.

Bedane, A. H., Huang, Q., Xiao, H. and Eić, M. (2012). Mass transfer of water vapor, carbon dioxide and oxygen on modified cellulose fiber-based materials. J. Nord Pulp Pap. Res., 27(2), 409-417, 2012.

Bedane, A. H., Xiao, H. and Eić, M. (2014). Water vapor adsorption equilibria and mass transport in unmodified and modified cellulose fiber-based materials. J. Adsorpt. 20 (7), 863-874.

Biliaderis, C.G., Lazaridou, A., Arvanitoyannis, I. (1999). Glass transition and physical properties of polyol-plasticised pullulan–starch blends at low moisture, Carbohydr. Polym. 40 29–47.

Chatterjee, S.G., Ramarao, B.V., Tien, C. (1997). Water vapor sorption equilibria of a bleached-Kraft paperboard-a steady of the hysteresis region. J. Pulp Pap. Sci. 23(8), 366-373.

Chatterjee, S. G. (2001). Comparison of Domain and Similarity Models for Characterizing Moisture Sorption Equilibria of Paper. Ind. Eng. Chem. Res., 40(1), 188-194.

Cherian, B.M., Pothan, L.A., Nguyen-Chung, T., Mennig, G. Kottaisamy, M., Thomas, S. (2008). A novel method for the synthesis of cellulose nanofibril whiskers from banana fibers and characterization. J. Agric. Food Chem. 56, 5617-5627.

Crank, J. (1975). The Mathematics of Diffusion, Clarendon Press, Oxford, United Kingdom, P. 44.

Del Nobile, M.A., P Fava, P., Piergiovanni, L. (2002). Water transport properties of cellophane flexible films intended for food packaging application. J. Food Eng., 53, 295-300.

Del Nobile, M.A., Baiano, A. Benedetto, A. and Massignan, L. (2006). Respiration Rate of Minimally Processed Lettuce as Affected by Packaging. J. Food Eng., 74(1), 60–69.

Debeaufort, F., Voilley, A., Meares, P. (1994). Water vapor permeability and diffusivity through methylcellulose edible films. J. Membr. Sci. 91,125-133.

Doty, P.M., Aiken, W.H., Mark, H. (1946). Temperature dependence of water vapor permeability, Indus. Eng. Chem. 38, 788–791.

Gardner D.J., Oporto, G.S., Mills, R., Samir MASA (2008). Adhesive and surface issues in cellulose and nanocellulose. J. Adhes. Sci. Technol. 22, 545-567.

Guggenheim, E.A. (1966). Application of Statistical Mechanics, Clarendon Press, Oxford pp. 186.

Gu, Z. and Alexandridis, P. (2004). Sorption and Transport of Water Vapor in Amphiphilic Block Copolymer Films. J. Dispers. Sci. Tech. 25(5), 619-629.

Henriksson, M., Berglund, Isaksson, P., Lindstrom, T., Nishon, N. (2008). Cellulose nanopaper structures of high toughness. Biomacromol., 9(6), 299-333.

Hines, A.L. and Maddox, R. N. (1985). Mass Transfer Fundamentals and Applications. Englewood Cliffs, New Jersey.

Hill, C.A.S., Norton, A., Newman, G. (2009). The Water Vapor Sorption Behavior of Natural Fibers. J App. Polym. Sci., 112, 1524-1537.

Hult, E-L., Iotti, M. and Lenes, M. (2010). Efficient approach to high barrier packaging using microfibrillar cellulose and shellac. Cellulose 17, 575-586.

Iijima, H. and Takeo, K. (2000). Microcrystalline cellulose: an overview. G.O. Phillips, P.A. Williams (Eds.), Handbook of Hydrocolloids, Woodhead Publishing Ltd., Cambridge, UK (2000), pp. 331–346.

Isogai, A., Saito, T. and Fukuzumi, H. (2011). “TEMPO-Oxidized cellulose nanofibers”. Nanoscale 3, 71-85.

Karger, J. and Ruthven, D.M. (1992). Diffusion in Zeolites and other Microporous Solids, Ch.9, Wiley, New York.

Koide, S. and Shi, J. (2007). Microbial and Quality Evaluation of Green Peppers Stored in Biodegradable Film Packaging, Food Control. 18(9), 1121–1125.

Lavoine, N. Desloges, I., Dufresne, A., Bras, J. (2012). Microfibrillated cellulose-Its barrier properties and applications in cellulosic materials: A review. Carbohydr. Polym. 90, 735-764.

Liu, H. and Ruthven, D.M. (1996). Diffusion in Carbon Molecular Sieves. In Fundamentals of Adsorption, M.D. LeVan (ed.), Kluwer Academic Publishers, Boston, Massachusetts 356, pp. 529-536.

Meares, P. (1954). The diffusion of gases through polyvinyl acetate, J. Am. Chem. Soc. 76, 3415–3422.

Miettinen, A., Chinga-Carrasco, G. and Kataja, M. (2014). Three-Dimentional Microstructural Properties of Nanofibrillated Cellulose Films. Int. J. Mol.Sci. 15, 6423-6440.

Minelli, M., Baschetti, M.G., Doghieri, F., Ankerfors, M., Lindstrom, T., Siro, I., Plackett, D. (2010). Investigation of mass transport properties of microfibrillated cellulose (MFC) films. J Membr. Sci. 358, 67-75.

Nge, T.T., Lee, S-H., Endo, T. (2013). Preparation of nanoscale cellulose materials with different morphologies by mechanical treatments and their characterization. Cellulose 20, 1841-1852.

Oksanen, C.A. and Zografi, G. (1990). The relationship between the glass transition temperature and water vapor absortion by poly (vinylpyrrolidone). Phar. Res. 7 (6), 654-657.

Pääkkö, M., Ankerfors, M., Kosonen, H., Nykänen, A, Ahola, S., Osterberg M., Ruokolainen, J., Laine, J., Larsson, P.T., Ikkala, O., Lindström, T. (2007). Enzymatic hydrolysis combined with mechanical shearing and high-pressure homogenization for nanoscale cellulose fibrils and strong gels. Biomacromol. 8(6), 1934-1941.

Phan, T. D., Debeaufort, F., Luu, D., & Voilley, A. (2005). Functional properties of edible agar-based and starch-based films for food quality preservation. J. Agric. Food Chem., 53, 973–981.

Rhim, J.W. and Lee, J.H. (2009). Thermodynamics Analysis of Water Vapor Sorption Isotherms and Mechanical Properties of Selected Paper-Based Food Packaging Materials, J. Food Sci., 74(9).

Shao, P. and Huang, R.Y.M. (2007). Review: Polymeric Membrane Pervaporation. J Membr. Sci., 287, 162-179.

Shogren, R. (1997). Water vapor permeability of biodegradable polymers. J. Environ. Polym. Degrad., 5-2(1997), 91-95.

Spence, K.L, Venditti, R.A., Rojas, O.J., Pawlak, J.J., Hubbe, M.A. (2011).Water vapor barrier properties of coated and filled microfibrillated cellulose composites. BioResour. 6(4), 4370-4388.

Sun, C.C. (2005). True density of microcrystalline cellulose. J Pharm Sci. 94 (10), 2132-2134.

Sun, C.C. (2008). Mechanism of moisture induced variation in true density and compaction properties of microcrystalline cellulose. International J. Pharm. 346, 93-101.

Stannett, V., Haider, M., Koros, W.J., Hopfenberg, H.B. (1980). Sorption and transport of water vapor in glass poly (acrylonitrile). Polym. Eng. Sci., 20(4), 300-304.

Stevanic, J.S., Bergstrom, E.M., Gatenholm, P., Berglund, L., and Salmen, L. (2012). Arabinoxylan/nanofibrillated cellulose composite films. J. Mater. Sci., 27, 6724-6732.

Syverud, K. and Stenius, P. (2009). Strength and barrier properties of microfibrillated cellulose (MFC) films. Cellulose 16(1), 75-85.

Szczesniak, L., Rachocki,A. and Tritt-Goc, J. (2008). Glass transition temperature and thermal decomposition of cellulose powder. Cellulose 15, 445-451.

Twede, D. and Selke, S.E.M. (2005). Cartons, Crates and Corrugated Board. Handbook of Paper and Wood packaging Technology, DEStech Publications, Inc., Lancaster, Penyslvania, U.S.A.

Yang Q., Fukuzumi H., Saito T., Isogai A., Zhang L. (2011). Transparent cellulose films with high gas barrier properties fabricated from aqueous alkali/urea solutions. Biomacromol. 12, 2766–2771.

Yang, Q., Saito, T., Isogai, A. (2012). Facile fabrication of transparent cellulose films with high water repellency and gas barrier properties. Cellulose 19, 1913–1921.

Weinmuller, C., Langel, C. Fornasiero, F. Radke, C.J., and Prausnitz, J.M. (2005). Sorption kinetics and equilibrium uptake for water vapor in soft-contact-lens hydrogels. Wiley InterScience.

Chapter 7: Theoretical modeling of water vapor transport in cellulose-based materials

Alemayehu H. Bedane[a] , Mladen Eić[b] and Huining Xiao[b]

University of New Brunswick

[a]Graduate Student, Department of Chemical Engineering, UNB

[b]Professor, Department of Chemical Engineering, UNB

Abstract

The theory of mass transport in porous media is of fundamental importance for different applications such as food, paper, packaging, textile, wood, and building materials. In this study, theoretical water vapor transport has been developed for cellulose-based materials such as paper and regenerated cellulose film. Pore diffusivities were determined from the dynamic moisture breakthrough experiments comprising a stack of paper and regenerated cellulose films in a configuration similar to packed column. Other mass transfer parameters were determined from transient moisture uptake rate measurements. The model incorporates pore and surface diffusion into a variable effective diffusion coefficient. The mass transport, involving both pore and surface diffusions, is evaluated independently. The obtained theoretical water vapor transmission rates (WVTR's) were compared with experimentally determined WVTR's measured under steady state conditions. The theoretical model based on intrinsic diffusion stipulates higher WVTR values compared to the experimental results. However, the theoretical water vapor transfer rates agree well with the experimental results when external mass transfer resistance is incorporated in the model.

Keywords: water vapor transport, pore-surface diffusion, effective diffusivity, mass transfer kinetics, cellulose, paper, moisture content.

7.1. Introduction

With the increasing environmental concern regarding non-biodegradability and lack of sustainability of synthetic-based materials, the use of materials derived from plant–based fibers and chemical have been highly encouraged as potential replacements. Packaging materials are widely used to prevent foods and beverages, pharmaceuticals, cosmetics, and other consumer goods against physical, biochemical, and microbiological deterioration (Nair et al., 2014). However, cellulose-based packaging materials have limited application due to their poor barrier properties to water vapor compared to synthetic materials. The moisture content in a cellulose material has a significant influence on the material's physical properties, and this affects the practical and commercial importance. Hence, understanding moisture transport phenomena in cellulose films would be helpful for improving barrier properties of cellulose film for food and pharmaceutical packaging and also for membrane separation applications. Water vapor transfer rates in polymers are mainly affected by three factors: structure of the material itself, temperature and moisture content of the surroundings (Morillon et al., 2002; Pascat, 1986 Rogers, 1985). Many studies have indicated that moisture transport occurs in polymers by the permeation of small molecules via an activated diffusion process (Hedenqvist and Gedde, 1996; Crank and Park, 1968). In activated diffusion, the transport diffusion of small molecules includes adsorption of the penetrant onto the polymer at the high concentration side, diffusion of the penetrant through polymer matrix along the concentration gradient and desorption of the penetrant from the opposite side or low concentration side of the film. However, diffusion of water vapor through a porous hydrophilic medium, such as paper, is more complicated and does not fully comply with the diffusion-solution theory, as the transport of water vapor occurres by diffusion along solid surface.

A number of researchers have studied water vapor transport properties in porous media (e.g., paper) (Bandyopadhyay et al., 2002; Gupta and Chatterjee, 2003; Ramarao et al., 2003). However, this study aims to provide a simplified approach to analyze the water vapor transfer though paper and regenerated cellulose films. Del Nobile et al. (2002) reported a mathematical model to predict the water vapor permeability of the cellophane film from the sorption and diffusion processes. Regenerated cellulose film (i.e., cellophane paper) is widely used as wrapping paper due to its excellent gas barrier characteristics. Different mechanisms of water vapor transport through porous media were also reported (Nilsson et al., 1993). Paper is a one of the porous media, which exibits different mechanisms for water vapor transport. The transport mechanisms in the porous material can be: gas diffusion (e.g., molecular and/or Knudsen diffusion), surface diffusion of the adsorbed phase on the surface of the fiber, and capillary transport in condensed phase of the water in the pores. Surface diffusion is concentration dependent and is associated to activated process (Bandyopadhyay et al., 2002; Hedenqvist and Gedde, 1996; Nilsson et al., 1993). In most studies, the steady-state part of the weight loss curve is used to estimate the effective diffusivity, D_{eff}, in porous material (Hashimoto et al., 2003; Nilsson et al., 1993). In earlier studies, effective water vapor diffusivities in different cellulose fiber-based materials were determined from transient moisture uptake results for a wide range of relative humidities. Water vapor permeabilities and adsorption isotherms of different unmodified and modified paper samples were also determined and reported in many studies (Bedane et al., 2012; Bedane et al., 2014; Chatterjee et al., 1997). In this study, different mass transfer parameters were determined from experimental results to develop theoretical modeling of moisture transfer in cellulose-based films. Effective pore diffusion is determined from dynamic breakthrough experiments of a stack of paper and regenerated cellulose films in a configuration similar to a packed column. Based on the experimental parameters, theoretical water vapor transfer model is developed from parallel pore–surface diffusion analysis and compared to the experimentally measured steady-state water vapor transfer rates in paper and regenerated cellulose films.

7.2. Theory

The one–dimensional flux involving diffusion through an isotropic material can be described by the Fick's law:

$$N = D_{eff}\frac{dc}{dZ} \tag{7.1}$$

where N is flux (diffusion flow) through unit area of film, D_{eff} is effective diffusion coefficient, c is concentration of gas or vapor, and Z is distance in the direction of flux. For a steady state process at constant pressure difference across the film and assuming the ideal-gas law, the flux of component i as follows**:**

$$N_i = \frac{D_{eff}}{R\times T\times Z}(p_i - p_\infty) \tag{7.2}$$

where p_i is the partial pressure of species i on the the high pressure side of the membrane film, p_∞ is on the low pressure side of the membrane, R is the universal gas constant, and T is temperature. Diffusion of gas through a membrane pore can occur by bulk (molecular) diffusion, and/or by Knudsen diffusion when the pore diameter is very small compared to mean free path of a diffusing molecule (Hines and Maddox, 1985). Hence, the main mechanisms for water vapor transport through porous fiber-based material can be pore diffusion through the void space, i.e., Knudsen and molecular diffusion through intra-fiber and inter-fiber pore spaces, and surface diffusion along the fiber-void interfaces as shown in Fig. 7.1.

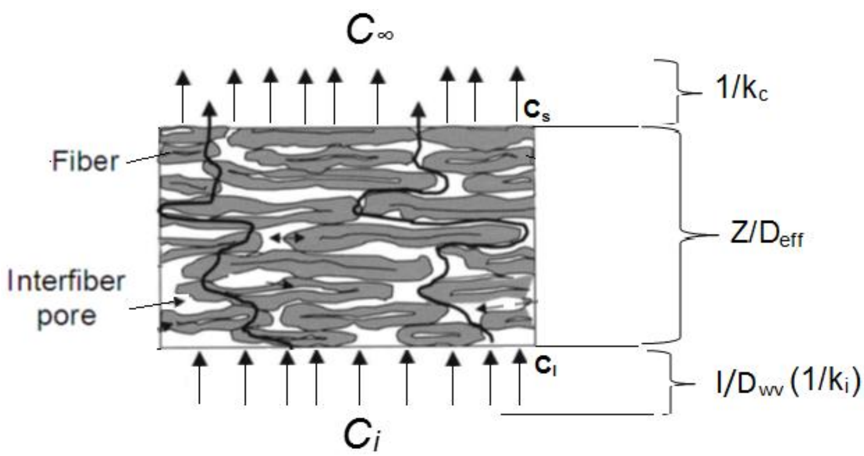

Figure 7.1. Mass transfer mechanism through paper sheet and the horizontal double head arrow indicates the diffusiom along the fiber-void interface.

Fig. 7.1, k_c and k_i are mass transfer coefficients at the top and bottom-side of the fiber surfaces, respectively, c_s is the concentration of vapor or gas at the top surface of the film, c_l is the concentration of vapor or gas at the bottom-side of the film surfaces, D_{wv} is the water vapor diffusivity in air, l is the stagnant air layer or the height above the water or saturated-salt solution to the sample film (e.g., in the cup method for WVTR measurement), Z is the thickness of the film, and D_{eff} is the effective water vapor diffusivity. The overall mass transfer resistance (K_o) of the film can be represented as the sum of both external resistances on both sides of the film and internal resistances, **as** given by Eq. 7.3:

$$\frac{1}{K_o} = \frac{1}{k_c} + \frac{Z}{D_{eff}} + \frac{1}{k_i} \quad 7.3$$

Assuming no change in the area of mass transfer across the thickness of the membrane, steady state flux of species *i*, through the three resistances is given by Eq. 7.4:

$$N_i = k_c(c_s - c_\infty) = \frac{D_{eff}}{Z}(c_s - c_l) = k_i(c_i - c_l) \quad 7.4$$

If these three equations are combined to eliminate the intermediate concentrations, C_s (the concentration of vapor or gas at the top surface of the film) and C_l (the concentration of vapor or gas at the bottom-side of the film surface), the following equation can be obtained:

$$N_i = \frac{c_i - c_\infty}{\frac{1}{k_c} + \frac{Z}{D_{eff}} + \frac{l}{k_i}} \quad 7.5$$

Transport of moisture in the cellulose sheet or film occurs through parallel pore and surface diffusion mechanism, i.e., by the diffusion of water vapor in the pores and in the fiber or cellulose surface. Mass flux for intrinsic diffusion, i.e., parallel pore and surface diffusion model, can also be determined using Eq. 7.6, and in this case the external resistance is disregarded:

$$N = -\varepsilon_p D_p \frac{\partial c}{\Delta z} - (1 - \varepsilon_p) D_q \frac{\partial q}{\Delta z} \qquad 7.6$$

where *Dp* and *Dq* are the pore and surface diffusion ceofficients, respectively, ε_p is the sample porosity, c is the concentration of vapor/gas in the pores and q is concentration of vapor /gas in the solid.

Determination of mass transfer coefficient

Mass transfer coefficient (k_i) on the high pressure side of the sample, can be determined by dividing the water vapor diffusivity in air (D_{wv}) at the experimental temperature (e.g., $D_{wv} \approx 2.5\times10^{-5} m^2/s$ at T=25 ^oC) with the height of the stagnant air from the water level of the container to the sample film (l), e.g., in the cup method for WVTR's measurement. The convective water vapor transfer coefficient (k_c) on the other (low pressure) side of the film can be calculated from effective water vapor diffusivities, which are determined from transient water vapor uptake rate measurement. The effective diffusion coefficients of water vapor were measured from transient moisture uptake rate of the sample at different relative humidities in our previous study (Bedane et al., 2012). Therefore, in this study convective mass transfer coefficients (k_c) are calculated from the effective diffusivities, determined from sample moisture uptake rate measurements. Effective diffusivities were determined by fitting the experimental moisture uptake rate measurement of the sample using Eq. 7.7. For a sample in which either or both surface and internal diffusion resistances are significant, Eq. 7.7 provides the best expression for gas/vapor uptake rate fitting to determine the effective diffusivity (Liu and Ruthven, 1996; Ruthven, 1984; Hines and Maddox, 1985):

$$\frac{M(t)}{M(\infty)} = 1 - \sum_{n=1}^{\infty} \frac{2\alpha^2}{\beta_n^2[\alpha(\alpha+1)+\beta_n^2]}\ exp(-\beta_n^2 T) \qquad 7.7$$

where eigenvalues β_n are given by the following equation:

$$\beta_n\ tan\,\beta_n\ = \alpha = \frac{k_c L}{KD} \qquad 7.8$$

and $T=Dt/L^2$, $\alpha=Lk_c/KD$, L is half thickness of the film, K is the equilibrium distribution constant, and k_c is convective mass transfer coefficient.

The effective diffusivity (D_{eff}) for the parallel pore and surface diffusion transfer mechanism can be expressed using Eq. 7.9 (Ruthven, 1984).

$$D_{eff}\ = \frac{1}{\tau}\left(\frac{\varepsilon_p D_p + (1-\varepsilon_p)\ KD_q}{\varepsilon_p + (1-\varepsilon_p)\ K}\right) \qquad 7.9$$

where τ is the tortuosity, ε_p is porosity of the solid material, D_p is pore diffusivity, and D_q is surface diffusion. Effective diffusivity can be determined from moisture or adsorbate uptake rate measurement over a small differential step. K is an equilibrium constant and it can also be applied outside the Henry's law region and replaced by the local slope of the isotherm (dq^*/dc). The effective diffusivity (D_{eff}) will show an increase with increasing water vapor concentration because the slope of the isotherm decreases with increasing moisture concentration.

Dynamic Breakthrough Modeling

The transport of water vapor through the stack of paper sheets in the column can be modeled in a similar way to the fixed bed flow system (Ruthven, 1984; Hines and Maddox, 1985), which is shown in Fig. 7.2 for the differential column section dZ.

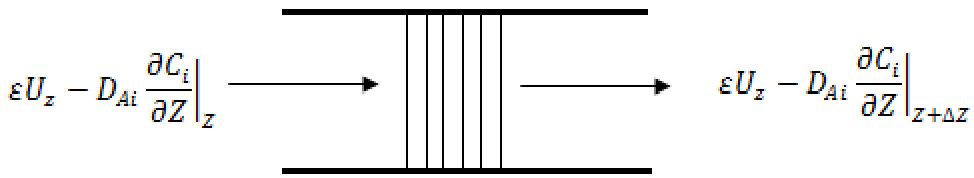

Figure 7.2. Cellulose-based films stacked in column

Component differential mass balance for the packed column becomes:

$$-D_{Ai}\frac{\partial^2 C}{\partial z^2} + u_z\frac{\partial C_i}{\partial z} + \frac{\partial C_i}{\partial t} + \left(\frac{1-\varepsilon}{\epsilon}\right)\frac{\partial \bar{q}_i}{\partial t} = 0 \tag{7.10}$$

where ε_b is void fraction in the bed, D_{Ai} is effective axial diffusional coeffiecient of i, m^2/s, C_i is concentration of i in the fluid phase, mol/m^3, q_i is concentration of i in the solid phase, mol/m^3, and u_z is interstitial velocity, m/s. The axial dispersion coefficient term can be neglected due to low concentration of the vapor in the fluid phase, and changes in fluid velocity across the mass transfer zone are therefore negligible.

Both pore diffusion and surface diffusion in the pores contribute to the flux of water vapor in the adsorbent or fiber material. The mass balance equation for the film involving parallel pore and surface diffusion mass transport can be written as:

$$\varepsilon_p\frac{\partial c_i}{\partial t} + (1-\varepsilon_p)\frac{\partial q_i}{\partial t} = \varepsilon_p D_p\frac{\partial}{\partial z}\left(\frac{\partial c_i}{\partial z}\right) + (1-\varepsilon_p)D_q\frac{\partial}{\partial z}\left(\frac{\partial q_i}{\partial z}\right) \tag{7.11}$$

Initial conditions

$$t = 0; \bar{C}_i(z,0) = C_{i0} \tag{7.12}$$

$$\bar{q}_i(z,0) = q_i^*(C_{i0}) \tag{7.13}$$

Boundary conditions

$$z = 0; t > 0;\ k_c\left(c_{i0} - c_i(0,t)\right) = \varepsilon_p D_p \left.\frac{\partial C_i(z,t)}{\partial z}\right|_{z=0} + \left(1 - \varepsilon_p\right) D_q \left.\frac{\partial q_i}{\partial z}\right|_{z=0} \tag{7.14}$$

$$z = L;\ t > 0;\ \left.\frac{\partial C_i(z,t)}{\partial z}\right|_{z=L} = 0 \tag{7.15}$$

The second term on the right side of Eq.'s 7.11 and 7.14 can be disregarded since the surface diffusion coefficient (D_q) is much lower than the pore diffusion coefficient (D_p) in which case the moisture transport occurs predominantly via pore diffusion (Gupta and Chatterjee, 2003). The change in moisture content of the sample and the fluid may be expressed in terms of the rate of adsorption $(\partial q_i/\partial t)$, and can be substituted in Eqs. 7.10 and 7.11. The uptake rate for this case can be given by Eq. 7.16 using the linear driving force (LDF) model:

$$\frac{\partial q_i}{\partial t} = k'(C_i - C_i^*) \tag{7.16}$$

where k' is the overall mass transfer rate constant (s^{-1}) ($k' = K_{eff}\ a$), a is the interfacial surface area of the sample (m^2/m^3) and K_{eff} or K_o is the effective mass transfer coefficient (m/s), C_i^* is fluid phase concentration of i in equilibrium with the solid, and C_i is the fluid concentration of i at time t. The equilibrium moisture uptake $(\bar{q}_i)$ can be determined using the GAB model from water vapor adsorption isotherm (Anderson, 1946).

$$\bar{q}_i = \frac{q_m\, C\, K\, (RT\bar{c}_i/p_{sat})}{[1-K(RT\bar{c}_i/p_{sat})][1-K(RT\bar{c}_i/p_{sat})+C\, K\, (RT\bar{c}_i/p_{sat})]} \qquad 7.17$$

where q_m is the monolayer moisture content of the solid (mol./m^3-drysolid), C and K are Guggenheim constants parametes, $\bar{c}_i$ is the vapor concentration that corresponds **to** C_i^* from Eq. (7.16). The water vapor concentration, C_i (mole/m^3) in the fluid phase can be calculated:

$$C_i = \frac{p_{sat}\times(RH(\%)/100)}{R\times T} \qquad 7.18$$

where p_{sat} is the saturation pressure of the water vapor at experimental temperature (T), R is the gas constant and RH is the relative humidity (*%*).

The above sets of partial differential equations (Eq. 7.10-7.18) were solved numerically by a reduction to a set of ordinary differential equations using the Crank-Nicholson finite difference techniques. These coupled equations are solved in the computer program using Matlab (v.8.3) software in order to obtain the best pore diffusivity (D_p) and mass transfer rate (k') values that fit the experimental breakthough moisture concentration for different inlet water vapor concentrations. Basically the curve fittings involve a two-parameter search for both D_p and k'. However, the approximate range of k' ($k'=K_{eff}\, a$) values is known since it is calculated from the overall mass transfer coefficient (K_o or K_{eff}) (Eq. 7.3) and the interfacial surface area (a) of the sample. Therefore, once the pore diffusion (D_p) is determined, the surface diffusion (D_q) of the samples can easily be calculated from the expression provided in Eq. 7.9 as the other parameters, i.e., D_{eff} and K are known from experimental measurement, and τ and ε_p can be obtained from published studies.

After mass transfer parameters are determined from the breakthrough and kinetics data, the mass or moisture flux (N) (mol/m^2.sec) through cellulose films can be easily obtained using Eq. 7.4 and 7.5 and then the water vapor transmission rate (WVTR) can easily be calculated in terms of g/(m^2.day) using Eq. 7.19:

$$WVTR = |N| \times 1.56 \times 10^6 (g/m^2.day) \qquad 7.19$$

7.3. Experimental

7.3.1. Sample preparation

Unmodified paper sample (70 g/m^2 and bulk density=539 kg/m^3) and regenerated cellulose film (79 g/m^2 and bulk density=1427 kg/m^3) were prepared for this study. The unmodified paper sample was made from pure cellulose (bleached kraft pulp) at Limerick Pulp and Paper Centre, University of New Brunswick. Regenerated cellulose films were prepared according to procedures further explained in this section. The solvent mixture, LiOH/urea/H_2O with a weight ratio of 5:15:80, was precooled at -15 ^oC. The desired amount of bleached Kraft pulp (kindly donated by Limerick Pulp & Paper, University of New Brunswick) was dispersed in the precooled solvent and the mixture was vigorously stirred for 5 min., after which it formed a transparent and viscous solution. The cellulose solution thus obtained was degassed by 8000 rpm centrifugation, then spread on a glass plate as a 0.6 mm thick layer, and finally immersed in an acetone coagulation bath at 0 ^oC for 15 min for regeneration. The sheet hydrogel of regenerated celluloses was thoroughly washed with deionized water by soaking for 24 hr, fixing on a special polyethylene plate mold to prevent shrinkage, and dried with air at ambient temperature (Yang et al. 2011a, Yang et al. 2012).

7.3.2. Water vapor transmission rates

The IGA permeation cell kit is used for direct measurement of water vapor transmission rate (WVTR) in accordance with the method described by ASTM E 96/E96M-05 standard (2005). The cellulose film is sealed by compression in the cell and the internal humidity is set by a different salt solution placed on the base of the cell. In these experiments, sample (cellulose film) was first saturated at different RH using a salt solution (LiCl (10.9 % RH), $MgCl_2$ (33 % RH), Mg $(NO_3)_2$ (52 % RH), NaCl (75 % RH), KNO_3 (92 % RH)) and pure de-ionized water (100 % RH) in the base of the sample holder. The outside environmental condition was kept at 0 RH% by purging with pure dry gas (nitrogen) at a flow rate of 20 ml/min.. The experimental set-up is shown in our previous study (Bedane et al., 2012). WVTR measurement was carried out at the relative humidity differences (ΔRH %) of 10, 33, 50, 75, 90 & 100 with accuracy of ±3 ΔRH and at a temperature of 25±0.1^{o}C. WVTR was calculated directly from the steady-state (linear) rate of weight change of the container, at a specified time interval, and the area of exposed film. Two to three replicates were made per each RH depending on the variation of the results and the average values were taken for analysis. Reproducibility of the results was within a 5–10 % range.

7.3.3. Dynamic breakthrough

A column with a diameter of 15 mm and a length 8.87 mm was used to pack the circular paper samples, while a column with a diameter of 10 mm and a length 0.44 mm was used to pack the regenerated cellulose film to measure the dynamic breakthrough concentration of water vapor as shown in Fig. 7.3. Based on availability of sample quantity, these specific column lengths were chosen for this study. The regenerated cellulose film is very thin (~60 μm) and 6-7 circular films were used to pack the column. Before the experiment, the samples in the column were dried by purging with dry nitrogen gas until the moisture was fully removed from the samples or until constant moisture content was attained. Then, different water vapor concentrations with nitrogen as the carrier gas , e.g., RH=10, 20, 30, 50, 60, 70 and 90% were introduced into the column at various inlet flow rates of 20, 30 and 60 ml/min., using a digital humidifier (HumiSys, supplied by InstruQuest Inc., Coconut Creek (USA)) at atmospheric pressure. The sample column temperature was kept constant at temperature of 25±1.5 ^{o}C inside the oven. The water vapor concentrations at the outlet of the column were measured using a Dycor-Dymaxion mass spectrometry (made by AMETEK, Process Instruments, Pittsburgh, PA, USA) and recorded automatically by a computer using the Dycor-System 2000 software. The measured breakthrough water vapor concentration curves were fitted using the theoretical breakthrough equations (Eqs. 7.10-7.17) in order to obtain the pore diffusion and the mass transfer coefficient for the samples at each inlet vapor concentration.

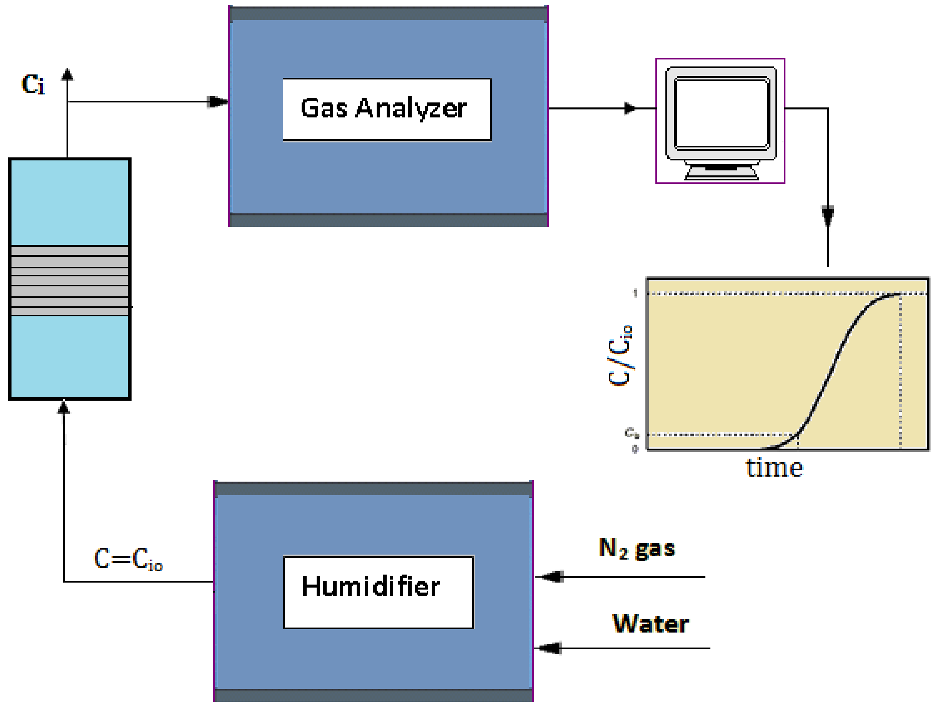

Figure 7.3. Experimental set-up for breakthrough dynamics studies.

7.4. Results and Discussion

7.4.1. Experimental Results

Convective mass transfer coefficient (k_c) $_{\text{was}}$ calculated from the effective diffusivity obtained from the transient uptake rate measurement using Eq. 7.7 and Eq. 7.8. The convective water vapor coefficients (k_c) were calculated at each relative humidity ranges, as shown in Table 7.1. The average water vapor convective coefficient on the paper sheet was about 3×10^{-3} m/s at T=25 ^{o}C. This value was close to the results for paper and paperboard materials reported by Foss et al., 2003 and Bandyopadhyay et al., 2002. *K* is the dimensionless equilibrium distribution constant determined from water vapor adsorption isotherm data (Bedane et al., 2014) and has an average value of about 3.5×10^{3} and 1x 10^{4} for paper and regenerated cellulose films, respectively.

Table 7.1. Convective water vapor transfer coefficients from the uptake rate measurement.

Relative Humidity (%)	Bleached Kraft paper			Regenerated cellulose film		
	α	D_{eff} (m^2/s)	k_c (m/s)	α	D_{eff} (m^2/s)	k_c (m/s)
10-20	100	0.65×10^{-12}	0.0040	0.9	0.73×10^{-13}	3.2×10^{-5}
20-30	80	0.78×10^{-12}	0.0038	0.6	0.97×10^{-13}	2.8×10^{-5}
30-40	10	1.65×10^{-12}	0.0020	0.9	1.76×10^{-13}	7.6×10^{-5}
40-50	10	3.49×10^{-12}	0.0022	0.5	2.77×10^{-13}	6.7×10^{-5}
50-60	8	6.87×10^{-12}	0.0034	1.0	2.60×10^{-13}	1.3×10^{-4}

The convective mass transfer coefficient of the regenerated cellulose film is lower than paper sample indicating high surface barrier of the regenerated cellulose film (as shown in Table 7.1). However, the mass transfer coefficient of the regenerated cellulose film increases with increased relative humidities. High moisture content of the film causes to disrupt the strong hydrogen bonding between cellulose chain molecules, and this result in swelling of cellulose and reduced the surface barrier of the film at high moisture content. The alpha (α) values and the convective mass transfer coefficients (k_c) of the paper sample decrease with increased relative humidity. This indicates diffusion resistance becomes dominant to mass transfer at low moisture contents but both surface barrier and diffusional resistance are comparable with increased relative humidities (or moisture content of the sample). The average water vapor transfer rates (WVTRs) were measured using the gravimetric method at steady state for different relative humidity gradients and the results are summarized in Table 7.2. An increase in relative humidty gradient showed an increase in water vapor. Regenerated cellulose film showed lower WVTR than paper due to higher mass transfer resistance and lower effective diffusivity.

Table 7.2. WVTR's measured at different relative humidities at 25 ^{o}C.

Relative humidity gradient (%)	WVTR for paper (120 μm thickness)	WVTR for cellulose film (65 μm)
10	106	8
33	435	25
50	686	41
75	1209	264
90	2033	897
100	2482	1450

7.4.2. Dynamic breakthrough model

The breakthrough experimental results that were determined from measurements at different relative humidities for a flow rate of 20, 30 and 60 ml/min. and T=25 ^{o}C are shown in Fig. 7.3. The experimental results were fitted using the dynamic breakthrough models (Eq.'s 7.10-7.18) to obtain the mass transfer coefficients and pore diffusion coefficients for paper and regenerated cellulose film samples. Those extracted parameters are listed in Table 7.3. The obtained pore diffusion coefficients are independent of moisture content except at very small relative humidity ranges (<10 RH %). At very low relative humidities, the pore diffusivity is relatively higher than at the high relative humidity ranges. This could be attributed to water vapor molecules that filled the pores and reduced the pore sizes when the moisture content of the film is increased. According to Liang et al. (1990), decreased porosity of the paper sheets increased the tortuosity of the pore spaces at high relative humidities and caused reduction of vapor phase diffusivity (see also Ramarao et al., 2003). However, the pore diffusivity seems independent at high moisture content of the paper as shown in Table 7.3. The obtained pore diffusion values are in close agreement with other authors studied for the paperboard materials (Bandyopadhyay et al., 2002; Nilsson et al., 1993). Nilsson et al. (1993) found the water vapor diffusivity in the pulp and different paper grades to be in the range from 2.1×10^{-8} m^2/s to 5.4×10^{-6} m^2/s. The pore diffusivity in the regenerated cellulose films is two orders of magnitude lower than the paper sheet due to small pore sizes. The pore diffusivity of the regenerated cellulose film was found to be 2.5×10^{-9} m^2/s. The average porosity for cellulose film is taken to be about 0.20 for this study based on related findings (Belbekhouchea et al., 2011; Bhatt, 2012; Henriksson et al., 2008; Spence et al., 2011; Ichwan and Son, 2011; Khare et al., 2007). The cellulose film is assumed to have small mesopore sizes structure (Tolle, 1971; Ichwan and Son, 2011). Therefore, in order to compare with the obtained pore diffusivity from moisture breakthrough experiment, the effective Knudsen diffusion was calculated in the Appendix-IV. Effective Knudsen diffusion is found to be 5.3×10^{-9} m^2/s and this value relatively close to experimentally obtained pore diffusivity.

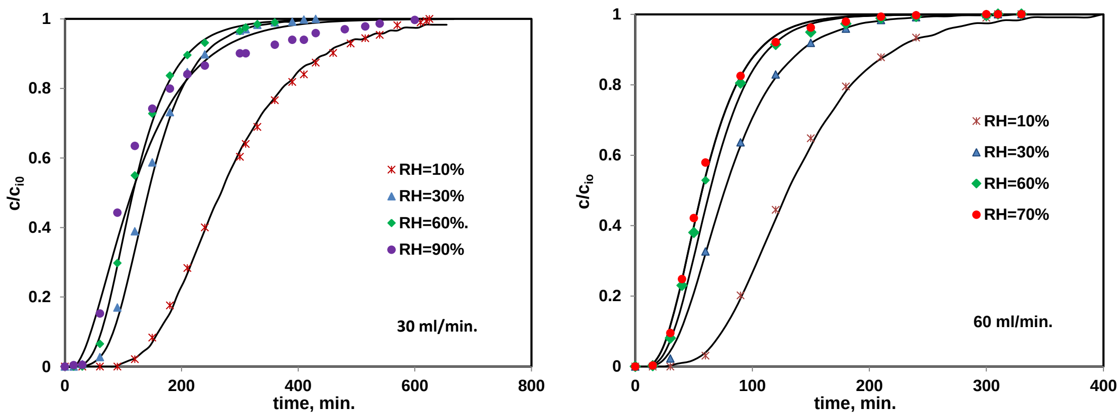

Figure 7.4. Breakthrough curves of water vapor in packed paper column for different flow rates of 30 ml/min. and 60 ml/min and T=25 ^{o}C.

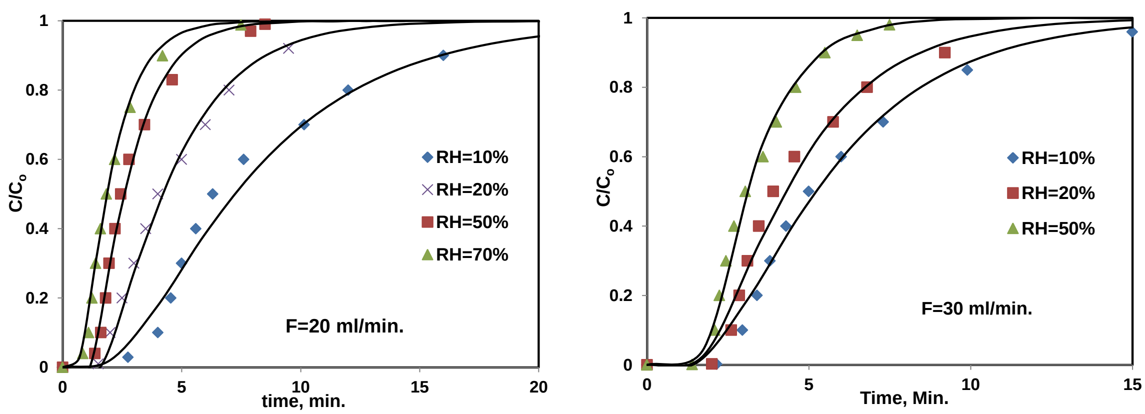

Figure 7.5. Breakthrough curves of water vapor in regenerated cellulose film column for different flow rates of 20 ml/min. and 30 ml/min and T=25 ^{o}C.

Table 7.3. Breakthrough curve fitting data at T=25 ^oC.

Flow rate (ml/min.)	Relative humidity (%)	Unmodified paper		regenerated cellulose	
		k' (=k_{eff}×a_i*) (s^{-1})	D_p (m^2s^{-1})	k' (=k_{eff}×a_i*) (s^{-1})	D_p (m^2s^{-1})
30	10	2.83	4.84×10^{-7}	0.5	5.70×10^{-9}
	20	-	-	0.5	4.00×10^{-9}
	30	1.21	2.54×10^{-7}	0.2	2.60×10^{-9}
	50	0.89	2.54×10^{-7}	0.5	2.30×10^{-9}
	60	0.84	2.54×10^{-7}	-	-
60 (for paper) 20 (for regen. cellulose film)	10	2.30	4.54×10^{-7}	0.5	5.80×10^{-9}
	30	0.86	3.54×10^{-7}	0.4	3.80×10^{-9}
	50	0.69	2.54×10^{-7}	0.5	2.50×10^{-9}
	60	0.64	2.54×10^{-7}	-	-
	70	0.58	2.54×10^{-7}	0.2	5.00×10^{-9}

a_i*=interfacial surface area of the material

Moisture dependent effective diffusivity of the paper sheet was determined from transient water vapor uptake rate in our previous study (Bedane et al., 2012). The effective diffusivities were independent of moisture content at low relative humidity ranges but they start to increase at relative humidity greater than 30% due to increased in the surface diffusion. Pore diffusivity and effective diffusivity are now known; therefore in order to determine the surface diffusivity from the relation given by Eq. 7.9, the tortuosity factor (τ) needs to be determined. The tortuosity is the path length that a gas or vapor molecule travels across a film thickness divided by the actual thickness of the film. The surface diffusivities for a variety of small molecules on glass and silica substrates have orders of magnitude in the range of 10^{-18}-10^{-16} m^2/s (Chen and Yang, 1993). Hence, the surface diffusivities on cellulose-based material would be expected to be higher than these values. The ratio of surface diffusion in the fiber to pore diffusion was also estimated to be about 0.01 (Defrenne et al., 2009; Spence et al., 2011) but this is not always true. Foss et al. (2003) reported diffusivity of a fiber surface to be around 3.8×10^{-14} m^2/s. Massoquete (2005) reported the tortuosity through experimental n-propanol diffusivity in lateral and transversal directions with bleached Kraft paperboard for different paper densities. The tortuosity determined for the transverse direction ranges were between 10 and 60 for 500-950 kg/m^3 paper density. Topgaard and Soderman (2001) reported the bulk tortuosity for cellulose fiber in the ranges between 10 and 150 for different moisture contents of the fiber. They suggested that the reason for the high tortuosity in the sample was constriction of the channels between and along the microfibrils. In order to find the approximate tortuosity factor at low moisture content of the sample and then compare with the findings of Topgaard and Soderman (2001), the surface diffusivity at the low relative humidity ranges can be neglected since surface diffusivities are not significant at low relative humidity ranges. Therefore, if we ignore the surface diffusivity at low moisture concentrations, tortuosity can easily be determined from the relation given by Eq. 7.9, using the obtained pore diffusivity (D_p) from moisture breakthrough experiment results that were fitted with dynamic breakthrough modelling and also the effective diffusivity (D_{eff}) obtained from uptake rate measurements.The tortuosity is found to be between 60-105 at low moisture concentrations of paper, and an average paper porosity of 0.35 that was used for the paper sample (Ahlen, 1970; Massoquete, 2005). This could demonstrate that these tortuosity results for the paper sample are reasonably close to the findings by Topgaard and Soderman (2001). Hence, the tortuosity factor used for the paper sample was 80 based on the average of the values reported by Topgaard and Soderman (2001). The tortuosity factor for regenerated cellulose films is taken to be around 25 to estimate the surface diffusivities in the film based on the tortuosity of diffusion of a small molecule in semicrystalline materials (Hedenqvist and Gedde, 1996). The moisture dependent surface diffusivity, D_q, therefore can be determined from the relation provided by Eq. 7.9 using the average tortuosity factor, the average pore diffusivity, and effective diffusivities determined from the moisture uptake rate at different relative humidities. The obtained moisture dependent surface diffusivities are described by the most common type of exponential relation and given by Eq. 7.20 for paper sample and by Eq. 7.21 for regenerated cellulose film. The exponential moisture dependent surface diffusivities of paper and regenerated cellulose films are shown in Fig. 7.6a and 7.6b, respectively. The obtained exponential moisture dependent surface diffusivity is in close agreement with the relation obtained by Lin et al. (1990) (see also Ramarao et al. 2003).

$$D_q = 1 \times 10^{-11} exp(0.062 \times RH(\%)) \qquad 7.20$$

The corresponding surface diffusion coefficient for regenerated cellulose film is given by Eq. 7.21.

$$D_q = 5 \times 10^{-13} exp(0.037 \times RH(\%)) \qquad 7.21$$

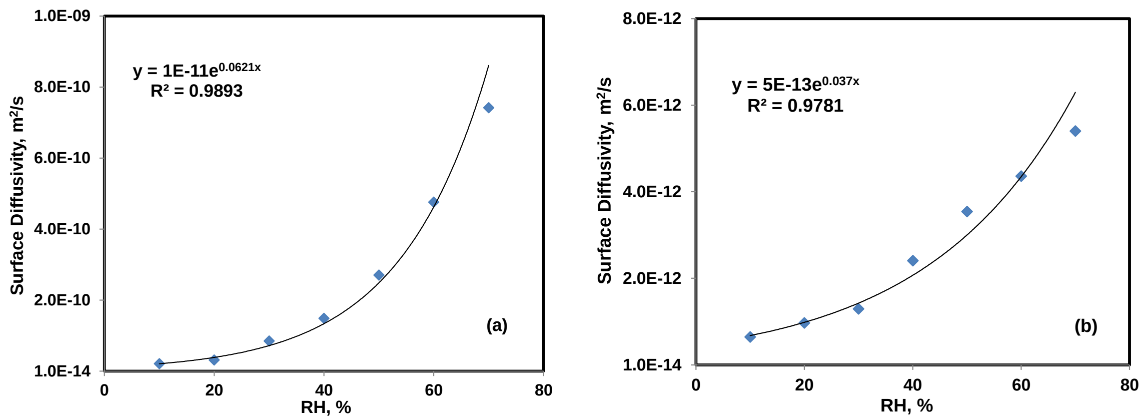

Figure 7.6. Moisture dependent surface diffusivity of paper (a) and regenerated cellulose film (b) [Symbols are used for calculated surface diffusivity and solid line shows the exponential fitting using Eq. 7.20 (a) and 7.21(b)].

The theoretical steady state water vapor transmission rates determined from the external resistance model and the intrinsic model are compared with the experimentally obtained WVTRs, as shown in Fig. 7.7. As seen in the figure, the external resistance model describes closely the water vapor transfer rates of the films compared to the intrinsic diffusion model. Intrinsic diffusional resistance in the film is not very significant in the films compared to external resistance. External surface resistance dominates the water vapor transfer at the interface of the film. In particular for the regenerated cellulose film, the external resistance due to narrow pore sizes plays a significant role in the water vapor barrier properties of the film. However, the external surface resistance is reduced slightly with increased moisture concentration. The reasons for the rapid increase of water vapor transmission rates in the cellulose films at high relative humidities are ascribed to increased surface diffusivity as well as reduced external surface resistance due to the relaxation of the cellulose chain. In general, incorporating the external resistance parameter in the model gives the best agreement with the experimental results.

Table 7.4. Model parameters used for the simulation

Parameters	Values (paper sample)	Values (regen. cellulose film)
$\boldsymbol{\varepsilon_b}$, Bed porosity,	0.43	0.35
$\boldsymbol{\varepsilon_p}$, Paper /cellulose film porosity,	0.35	0.20
$\boldsymbol{\rho_p}$, Paper/cellulose film density, (kg/m^3)	650	1450
D_p, Pore diffusivity, (m^2/s)	3×10^{-7}	3.96×10^{-9}
D_q, Surface diffusivity, (m^2/s)	$2\times10^{-11}\exp(0.06\times RH(\%))$	$5\times10^{-13}\exp(0.064\times RH(\%))$
k_c, External mass transfer coefficient, (m/s)	3×10^{-3}	4×10^{-5} for RH<50% 6×10^{-4} for RH>50%
k_i, mass transfer coefficient, (m/s)	6×10^{-3} -1×10^{-2}	6×10^{-3} -1×10^{-2}
Bed diameter (m)	0.008	0.010
Bed length (m)	0.015	0.00042
q_m, monolayer moisture content (mol./m^3-solid)	1478	6663
C, GAB constant parameter	10	4
K, GAB constant parameter	0.66	0.46

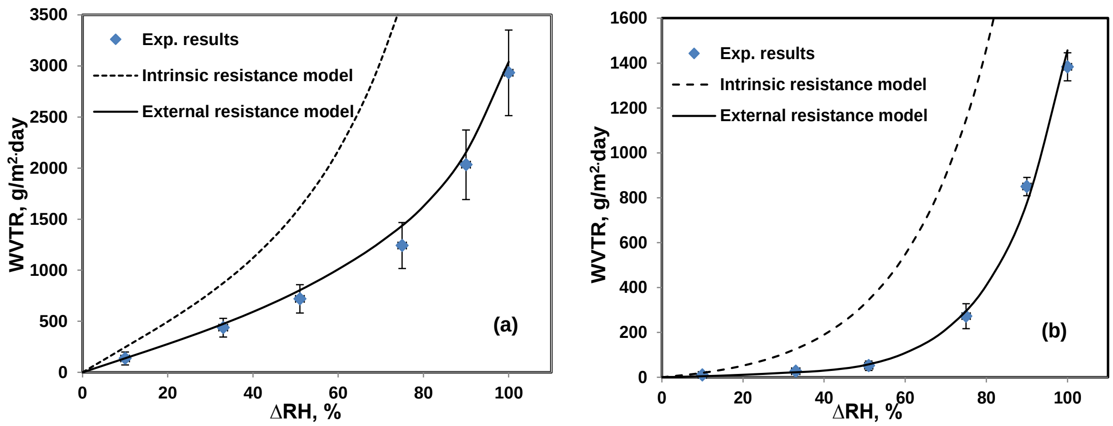

Figure 7.7. Comparison of WVTR's obtained from experimental results (shown using symbols) for paper (a) and regenerated cellulose film (b) and theoretical WVTR's (broken line, Eq. 7.6) and external resistance (solid line, Eq. 7.5).

The variation of the moisture flux in the films was analyzed using Eq. 7.22. The total moisture fluxes across the film thickness of the paper and regenerated cellulose films, which is kept on one side with RH=90% and the opposite side with RH=20%, are shown in Fig.'s 7.8 and 7.9. Initially, the total moisture flux is higher at the higher concentration side of the film, e.g., closer to entrance of the membrane, due to a high concentration gradient between the surface at the entrance and the ambient humidity. As can be seen from the figures, high moisture flux was observed for lower initial moisture content of the sample compared to the sample with higher initial moisture content. Eventually at the steady state, the moisture flux becomes equal for both samples with initial moisture content that is equilibrated with RH=0 and 50% due to a similar moisture gradient on both side of the samples.

$$N(t,z) = \varepsilon_p \left(D_p \frac{\partial c_i}{\partial z}\right) + \left(1-\varepsilon_p\right)\left(D_q \frac{\partial q_i}{\partial z}\right) \tag{7.22}$$

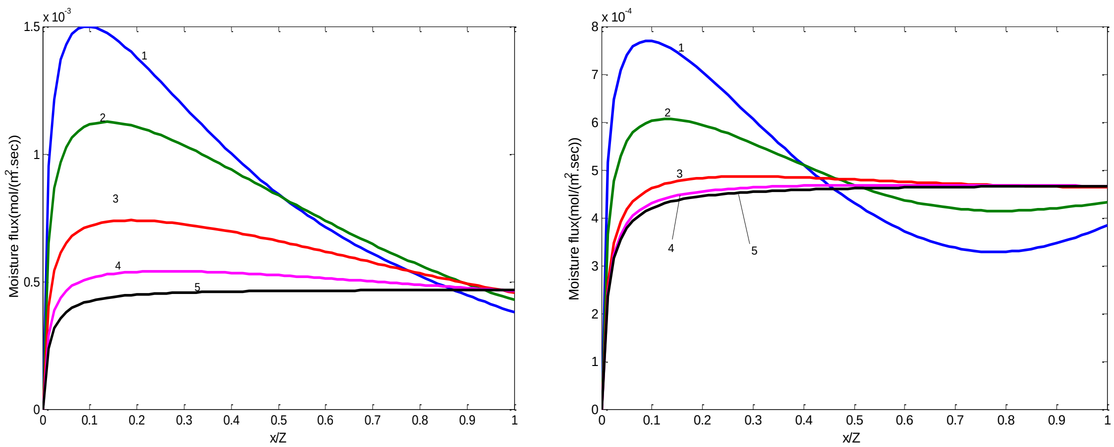

Figure 7.8. Moisture flux profile at different time for ((1)-5 min., (2)-10 min., (3)-24 min., (4)-48 min., (5)-500 min. (steady state)) for initial moisture content of paper sheet (Z=500μm) of RH=0 % & 50%.

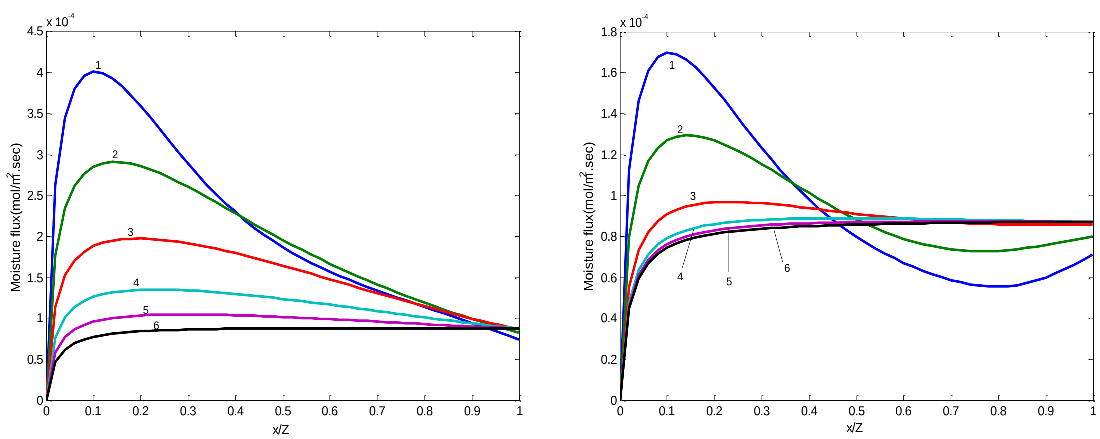

Figure 7.9. Moisture flux profile at different time for ((1)-27 min., (2)-67 min., (3)-167 min., (4)-333 min., (5)-533 min. & (6) 1000 min (steady state)) for initial moisture content of regen. cellulose film (Z=100μm) of RH=0 % & 50%.

Humidity profiles across the paper and regenerated cellulose films thickness, which is kept on one side with RH=90% and the opposite side with RH=20%, for different initial equilibrium moisture content of gas phase concentration (i.e., for RH=0 % and 50%) in the paper and regenerated cellulose film, are shown in Fig.'s 7.10 and 7.11, respectively. These figures reveal qualitative humidity profiles for the samples. As can be seen from the figures, initially the gas phase concentration profile for the samples equilibrated with RH=0% and 50% have different profiles before they reach steady conditions. At steady state, the relative humidity profiles for both samples have the same linear trend. Sample which is equilibrated with RH=50% reaches steady state conditions faster. Moreover, regenerated cellulose film takes longer to reach the steady state conditions than paper samples due to slow moisture diffusion in the film.

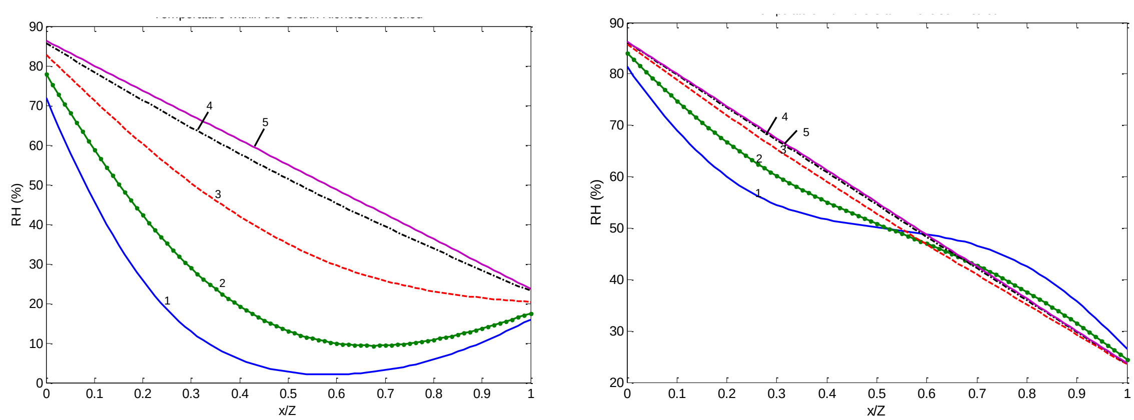

Figure 7.10. Relative humidity profile at different time ((1)-5 min., (2)-10 min., (3)-30 min., (4)-60 min., (5)-180 min. (steady state)) for initial moisture content of paper (thickness 500µm) (a) RH=0% and (b) RH=50%.

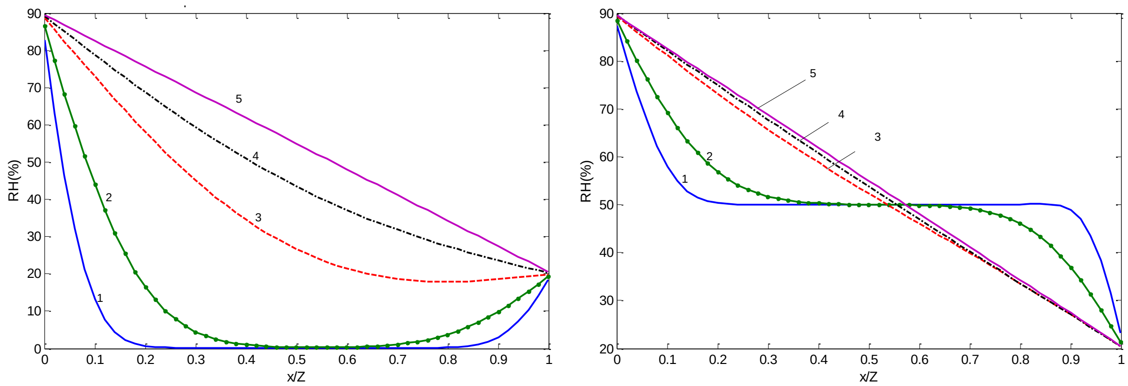

Figure 7.11. Relative humidity profile at different time ((1)-10 min., (2)-60 min.,(3)- 300 min., (4)-600 min., (5)-3000 min.(steady state)) for initial moisture content of regenerated cellulose film thickness of100μm, RH=0% and RH=50%.

The corresponding moisture content profiles of the samples are shown in Fig.'s 7.12 and 7.13. The profiles look similar to the humidity profiles shown in the Fig.'s 10 and 11, except that the time to reach steady state is longer due to the surface diffusion being slower than the gas phase diffusion. At steady state, the moisture profiles are not as linear as the relative humidity profiles in the paper sample. The linearity is more influenced by the *K* parameter in the GAB model of the equilibrium isotherm fitting. The higher *K* value leads to non-linearity, while the lower *K* value leads to linearity of the moisture profile at steady state. *K* has a value of 0.65 and 0.46 for the paper and regenerated cellulose film, respectively. The moisture profile of the paper sheet can also be affected by the value of the diffusivity of moisture through fiber matrix and intra-fiber mass transfer coefficients (Bandyopadhyay et al., 2002).

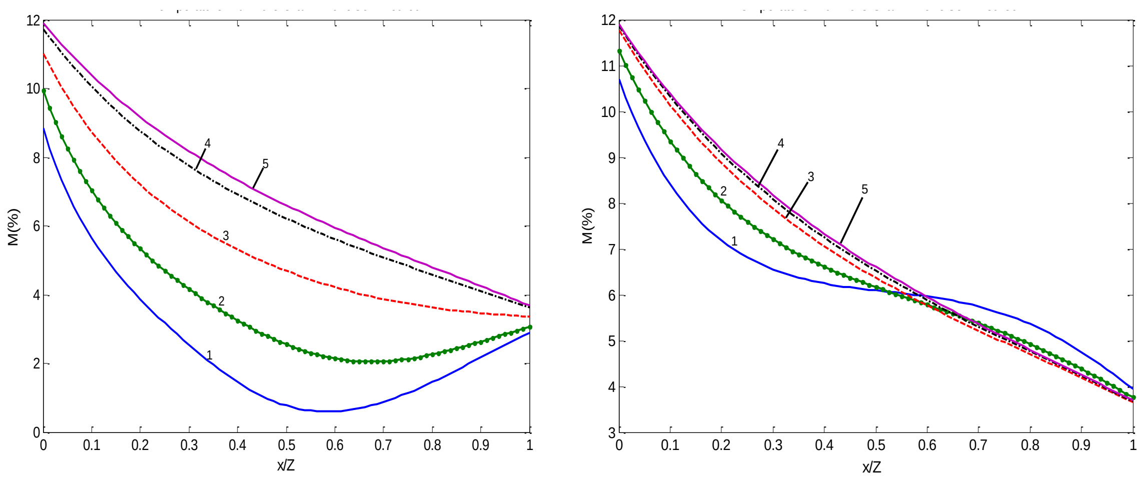

Figure 7.12. Moisture content profile at different time ((1)-5 min., (2)-10 min., (3)-30 min., (4)-60 min., (5)-180 min. (steady state)) for initial moisture content of paper sheet thickness of 500µm, RH=0% and RH=50%.

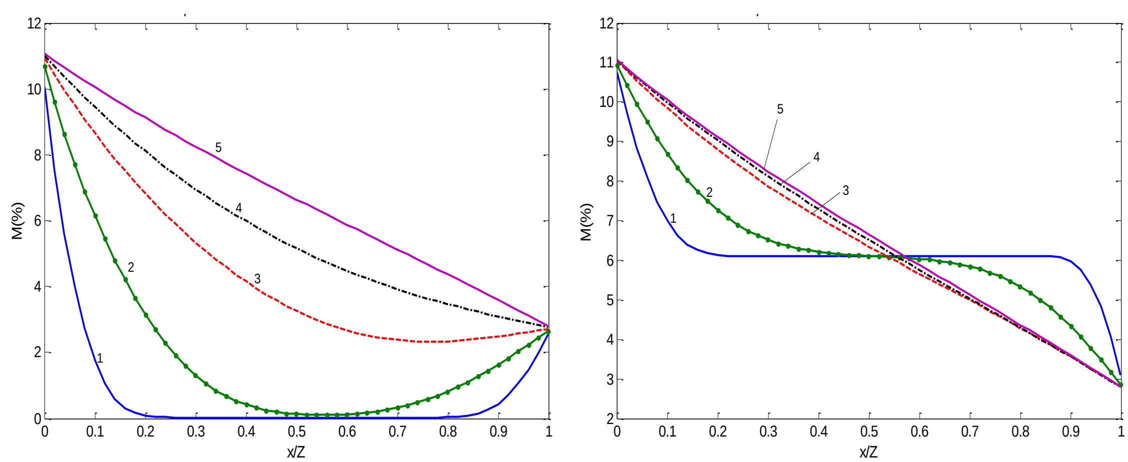

Figure 7.13. Moisture profile at different time ((1)-10 min., (2)-60 min.,(3)- 300 min., (4)-600 min., (5)-3000 min.(steady state)) for initial moisture content of regenerated cellulose film thickness of 100µm, RH=0% and RH=50%.

7.5. Conclusions

In this study, unsteady and steady state water vapor transfer rates in cellulose films were determined. The water vapor transmission rates (WVTRs) were measured experimentally at steady state conditions. Mass transfer parameters were extracted from experimental data in order to develop theoretical model of moisture transfer rates in the cellulose-based films. Pore diffusivities in the paper and regenerated cellulose films were determined from the experiment results of dynamic moisture breakthrough of a stack of paper films in a configuration similar to a packed column. Other mass transfer parameters, such as convective moisture transfers and effective diffusivities, were extracted from transient moisture uptake rate measurements. The pore diffusivities in the paper sheet are independent of moisture content of the sample, except at very low relative humidity (< RH=10%). The average obtained pore diffusivity in the paper sheet and regenerated cellulose film was found to be about 3.0×10^{-7} m/s and 3.96×10^{-9} m/s, respectively. The surface diffusion coefficients were determined by subtracting the obtained pore diffusivity from the effective diffusivities that were determined from the uptake rate measurements. Surface diffusion is more significant in regenerated cellulose film, whereas pore diffusion in the paper is more significant. The moisture flux increases rapidly at high moisture contents due to high surface moisture diffusion contribution parallel to pore diffusion in the films. Moisture flux is restricted highly by external mass transfer resistance in regenerated cellulose films, particularly at low moisture contents (<RH=50%), but as moisture increases in the film, the external mass transfer resistance no longer controls the moisture transfer into the film. The relaxation of the cellulose

chain is ascribed to high external mass transfer at high moisture contents of the film. The intrinsic diffusion model provides high WVTR results of the films compared to experimental results. However, the theoretical water vapor transmission rate (WVTRs) results (including the external resistances to water vapor transport) are in a close agreement with direct experimental measured WVTRs of paper and regenerated cellulose film. Finally, moisture transport dynamics can be successfully analyzed using parallel pore-surface diffusion model for the cellulose-based materials and the model can also be applied to other porous materials or polymers.

References

Ahlen, A.T. (1970). Diffusion of Sorbed Water Vapor through Paper and Cellulose Film, Tappi J. 53(7), 1320-1326.

Ahmet Kaya, Orhan Aydın, Ibrahim Dincer (2006). Numerical modeling of heat and mass transfer during forced convection drying of rectangular moist objects. Int. J. Heat and Mass Transf., 49 (17–18), pp. 3094–3103.

Anderson, R.B. (1946). Modifications of the Brunauer, Emmett and Teller equation. J. Am. Soc., 68, 681-691.

Bandyopadhyay, A., Ramarao, B.V., Ramaswamy, S. (2002). Transient moisture diffusion through paperboard materials. Colloids Surf., A: Physicochem. Eng. Asp. 206, 455-467.

Bedane, A. H., Huang, Q., Xiao, H. and Eić, M. (2012). Mass transfer of water vapor, carbon dioxide and oxygen on modified cellulose fiber-based materials. J. Nord Pulp Pap. Res., 27(2), 409-417, 2012.

Bedane, A. H., Xiao, H. and Eić, M (2014). Water vapor adsorption equilibria and mass transport in unmodified and modified cellulose fiber-based materials. J. Adsorpt. 20 (7), 863-874.

Belbekhouchea, S., Brasb, J., Siqueirab, G., Chappeya, C., Lebruna, L., Khelifib, B., Maraisa, S., Dufresneb, A. (2011). Carbohydr. Polym., 83(4), 1740-1748.

Bhatt, B. J. (2012). "Regenerated cellulose for controlled oral drug delivery." PhD (Doctor of Philosophy) thesis, University of Iowa, 2012. http://ir.uiowa.edu/etd/4577.

Chatterjee, S.G., Ramarao, B.V., Tien, C. (1997). Water-vapor sorption equilibria of a bleached-Kraft paperboard-a study of hysteresis region, J. Pulp Pap. Sci. 23(8), 366-373.

Chen, Y.D. and Yang, R.T. (1993). Surface diffusion of multilayered adsorbed species. AIChE. J. 39(4), 559-606.

Crank, J. and Park, G.S. (1968). Diffusion in Polymers, Academic Press, London, 1968.

Defrenne, Y., Zhdankin, V., Takagaki, S., Ramaswamy, S., Lavrykov, S., Ramarao, B. (2009). 'Multi-scale moisture transport in paper: Impact of pore and fiber tortuosity and anisotropy", Proc., Adv. Pulp Pap. Res., 455-473.

Del Nobile, M.A., Fava, P., Piergiovanni, L. (2002). Water transport properties of cellophane flexible films intended for food packaging applications. J. Food Eng., 53, 295-300.

Foss, W.R., Bronkhorst, C.A., Bennett, K.A. (2003). Simultaneous heat and mass transport in paper sheets during moisture sorption from humid air. Int. J. of Heat and Mass Transf. 46, 2875-2886.

Gupta, H. and Chatterjee S.G. (2003). Parallel Diffusion of Moisture in Paper. Part 1: Steady-State Conditions. Ind. Eng. Chem. Res., 42, 6582-6592.

Gupta, H. and Chatterjee S.G. (2003). Parallel Diffusion of Moisture in Papers. Part 2: Transient Conditions. Ind. Eng. Chem. Res., 42, 6593-6600.

Hashimoto, A., Stenstrom, S. and Kameoka, T. (2003). Simulation of Convective Drying of Wet Porous Materials. Dry. Technol., 21(8), 1411-1431.

Hedenqvist, M. and Gedde, U.W. (1996). Diffusion of small molecule penetrants in semicrystalline polymers. Prog. Polym. Sci., 21, 299-333.

Henriksson, M., Berglund, Isaksson, P., Lindstrom, T., Nishino, N.(2008). Cellulose nanopaper structures of high toughness. Biomacromol. 9(6), 1579-1585.

Hines, A.L. and Maddox, R. N. (1985). Mass Transfer Fundamentals and Applications. Prentice-Hall, Inc., Englewood Cliffs, New Jersey.

Karger, J. and Ruthven, D.M. (1992). Diffusion in Zeolites and other Microporous Solids, Ch.9, Wiley, New York.

Khare, V.P., Greenberg, A.R., Kelley, S.S., Pilath, H., Roh J.II, Tyber, J. (2007). Synthesis and Characterization of Dense and Porous Cellulose Films. J. Appl. Sci., 105, 1228-1236.

Liang, B., Fields, R.J., King, J.C. (1990). The mechanisms of transport of water and n-propanol through pulp and paper. Drying Tech., 8(4), 641-665.

Lin, S.H. (1990). Moisture absorption in cellulosic materials. Int. J. Engng. Sci., 28(11), 1151-1156.

Liu, H. and Ruthven, D.M (1996). Diffusion in Carbon Molecular Sieves. Fundamentals of Adsorption, 356, 529-536.

Massoquete A. (2005). Study of Anisotropic moisture diffusion in paper materials. PhD Thesis. State University of New York College of Environmental Science and Forestry Syracuse, New York.

Morillon, V., Debeaufort, F., Blond, B., Capelle, M., and Voilley, A. (2002). Factors Affecting the Moisture Permeability of Lipid-Based Edible Films: A Review. Critical Reviews in Food Science and Nutrition, 42(1), 67–89.

Nair, S. S., Zhu, J.Y., Deng, Y., Ragauskas, A.J. (2014). High performance green barriers based on nanocellulose. Sustainable Chemical Processes 2014, 2:23. doi:10.1186/s40508-014-0023-0.

Nilsson L., Wilhelmsson B., Stenstrom S. (1993). The Diffusion of Water Vapor through Pulp and Paper, Dry. Technol., 11, (6), 1205-1225.

Nilsson L., Wilhelmsson B., Stenstrom S. (1992). Effective Vapor Diffusivity in Paper, Dry. Techol. 92, 1115-1123.

Pascat, B. (1986). Study of some factors affecting permeability. In Mathlouthi, M., Ed., Food Packaging and Preservation. Theory and Practice, London, Elsevier Appl. Sci. Publishers, 1986, 7–24.

Radhakrishnan, H., Chatterjee, S.G., Ramarao, B.V. (2000). Steady-state moisture transport in a Bleached Kraft paperboard stack. J. Pulp Pap. Sci. 26(4), 140-144.

Ramarao, B.V., Massoquete, A. Lavrykov, S., Ramaswamy, S. (2003). Moisture Diffusion Inside Paper Materials in the Hygroscopic Range and Characteristics of Diffusivity Parameters. Dry. Technol. 21(10), 2007-2056.

Rogers, C.E. (1985). Permeation of gases and vapors in polymers. In: Comyn J., Ed., Polymer Permeability, New York, Elsevier Appl. Sci. Publishers, New York, 1985, 11–73.

Ruthven, D.M. (1984). Principle of Adsorption and Adsorption Processes. John Wiley & Sons, Inc.

Spence, K.L., Venditti, R.A., Rojas, O.J., Pawlak, J.J., Hubbe, M.A. (2011). Water vapor barrier properties of coated and filled microfibrillated cellulose composite films. Bioresour. 6(4), 4370-4388.

Tolle, W.E. (1971). Variables Affecting Film Permeability Requirements for Modified-Atmosphere. Agricultural Research Service, U.S. Dep. Agric., Tech. Bulletin No. 1422, pp. 59.

Topgaard, D. and Soderman, O. (2001). Diffusion of water absorbed in cellulose fibers studied with H-NMR. Langmuir, 17, 2694-2702.

Yang Q., Fukuzumi H., Saito T., Isogai A., Zhang L. (2011). Transparent cellulose films with high gas barrier properties fabricated from aqueous alkali/urea solutions. Biomacromol. 12, 2766–2771.

Yang, Q., Saito, T., Isogai, A. (2012). Facile fabrication of transparent cellulose films with high water repellency and gas barrier properties. Cellulose 19, 1913–1921.

Yiotis, A.G., Stubos, A.K., Boudouvis, A.G., Tsimpanogiannis, I.N., Yortsos, Y.C. (2005). Pore-Network Modeling of Isothermal Drying in Porous Media. Transp Porous Med., 58, 63–86.

Chapter 8: Conclusions and Recommendations

In this thesis, various modified, coated papers and transparent cellulose films (i.e., nanofibrillated cellulose (NFC) and regenerated cellulose film), were prepared and characterized with regard to mass transfer and equilibrium properties, in order to determine their potential as a packaging material. Water vapor mass transfer was studied using microbalance gravimetric technique (IGA-Hiden apparatus). This technique provided direct measurements of water vapor transmission rates (WVTRs) on paper or cellulose film samples at different relative humidity gradients and temperatures. These measurements were further used to determine water vapor permeabilities (WVP's) through different barrier media. Water vapor diffusivities of the samples were also measured from the uptake rate measurements using the Fickian diffusion model for slab geometry at a wide range of relative humidities. The water vapor permeabilities (WVP's) for the different paper samples were found to be relatively constant up to the modest relative humidity levels, but they showed an increasing trend at the higher relative humidity levels. This behavior is attributed to an increase of the surface diffusivities of the water vapor at the higher moisture contents. Nanofibrillated cellulose (NFC) films have good gas barrier properties at dry conditions but these barrier properties deteriorate with increased moisture content. Pigments, fillers and coatings clearly affect diffusion kinetics (diffusion and permeability), as well as equilibrium parameters. Coating on the cellulose material provides lower water vapor transmission rates, because it reduces the diffusion and the solubility of gas/vapor in the film. The availability of a large number of hydroxyl groups in the transparent cellulose films causes high water vapor adsorption, thereby increasing water vapor permeability (i.e., results in poor barrier properties), particularly at high relative humidity conditions. This study recommends reducing the hydrophilic properties of the films, e.g., regenerated cellulose and nanofibrillated cellulose films, using either coating or chemical treatment in order to obtain better barrier properties against water vapor. PLA shows a good barrier property against water vapor, but provides a poor barrier to oxygen. The NFC and regenerated cellulose films showed opposite behaviors in comparison to PLA coated papers. Therefore, coating of PLA on regenerated cellulose film or nanofibrillated cellulose films could provide the best barrier properties.

Oxygen transmission rates were measured for PLA and PHBV coated paper samples at dry and different relative humidity conditions. Oxygen permeabilities of PLA and PHBV coated paper samples were independent of relative humidity up to 50% RH but then starts to increases with increased RH. The increase in oxygen permeability is due to formation of moisture swelled fibers in the coated substrate, which creates free spacing for oxygen passage. PHBV coated paper showed lower oxygen permeability than PLA coated paper. However, PLA coated paper did not show significantly higher oxygen permeability compared to PHBV coated paper at high relative humidities.

The water vapor equilibrium adsorption properties of modified paper, NFC and regenerated cellulose films have been determined from their adsorption isotherms at three different temperatures (15, 25 and 35 ^{o}C). The monolayer moisture content of each sample was determined using BET, H-H and GAB models. The H-H and GAB model fit the experimental adsorption isotherms better than BET model. The monolayer moisture contents determined from H-H and GAB model are closer to each other than monloayer moisture determined from BET model. The monolayer moisture contents of zein grafted and commercial copy paper samples do not exhibit significant differences when compared to the reference paper sample. However, they show reduction in the multilayer moisture contents when compared to the unmodified paper. The monolayer moisture content of NFC and regenerated cellulose films were more than double in comparison to unmodified paper, indicating high hydrophilic character of the transparent cellulose films. Coated papers (e.g. using PLA and PHBV) have low monolayer moisture content and less hydrophilic properties, resulting in low WVTR's. Water vapor permeation through cellulose films showed an Arrhenius type of dependency on temperature, indicating an activated process. The average activation energies of water vapor permeation in regenerated cellulose and nanofibrillated films were 37.4 kJ/mol and 29 kJ/mol, at lower temperature ranges, respectively, whereas the activation energies of permeation decreases to -1.0 kJ/mol and -19 kJ/mol at higher temperature ranges, respectively. The changes in the slope of the activation energies of water vapor permeation were observed for the temperature range between 25-35 ^{o}C, indicating the change in the structure of the films that leads to high water vapor permeations.

According to the BET measurements, coating on the paper sample reduces the mean pore sizes but increases the specific surface area. Pore size reduction lowers the water vapor and gas diffusion in the paper as it influences the gas diffusion in the film. Modified paper samples showed low specific surface areas based on measured water vapor adsorption isotherms. The specific surface areas measured from water vapor adsorption isotherms are higher than from N_2 adsorption isotherms, because the fiber materials are more susceptible to a change in their structures when water is bound to the fiber –based surface. However, they provide a clue to identifying their hydrophilic character.

The strength of interaction between water vapor molecules and cellulose-fiber based materials, and also the formation of adsorbed water on the paper samples were investigated using TGA-DSC and FT-IR. Among the other modified paper samples, PLA and PHBV coated paper samples showed the lowest percentage of bound water moisture contents. The commercial coated (pigment-latex) paper provides relatively lower percentage of bound water than other samples, but a higher percentage than PLA and PHBV coated paper samples. The formation of water clusters at higher humidities, caused a decrease in the energy of interaction between water molecules and the paper sample surface. Results of this study confirmed that blocking of active surface sites by coating with PLA and PHBV is the most effective way to increase the water vapor barrier properties of modified papers, thus making them the appropriate candidates for green-based food packaging materials.

Surface resistance was found to be a more dominant mechanism for mass transfer in the NFC and regenerated cellulose films: the surface resistance (e.g., pore mouth obstruction or narrow pore size) hinders water vapor transport across the surface of the film at low and intermediate moisture contents. Water vapor uptake in unmodified paper seems consistent with internal diffusion control. However, both surface resistance and internal diffusion are significant at high moisture contents in all transparent cellulose films and the unmodified paper sample.

Furthermore, mass transfer parameters were extracted from experimental data in order to develop theoretical moisture transfer rates in the cellulose-based films. Mass transfer coefficients were determined from moisture uptake rate curves. The mass transfer coefficients were in the range 2×10^{-3}-6×10^{-3} m/s and 2×10^{-5}-6×10^{-4} m/s at various varies relative humidity ranges for paper and regenerated cellulose films, respectively. Pore diffusivities in the paper and regenerated cellulose films were determined from the experiment results of dynamic moisture breakthrough using a stack of paper films in a configuration similar to a packed column. The average pore diffusivity in the paper sheet and the regenerated cellulose film was found to be about 3.0×10^{-7} m^2/s and 3.96×10^{-9} m^2/s, respectively. The surface diffusion coefficients were determined by subtracting the obtained pore diffusivity from the effective diffusivities that were determined from the uptake rate measurements.The theoretical water vapor transmission rate (WVTR's) results (including the external resistances to water vapor transport) are in close agreement with direct experimental measured WVTR's of paper and regenerated cellulose films. Finally, moisture transport dynamics can be determined using parallel pore-surface diffusion model for the cellulose-based materials; this model can also be applied to other porous materials or polymers.

Recommendations for future research

In the current investigation, the barrier properties of different coated papers and cellulose films were elucidated with different parameters in an attempt to develop a better understanding of these materials for packaging applications. This study recommends that future work should focus on investigating the barrier properties of different compositions of nanocomposite films, e.g., on PLA and PHBV coated paper, and also coating of PLA on regenerated cellulose or nanofibrillated cellulose films, which could provide improved barrier properties. Fillers or nanofillers are relatively cheaper than biodegradable coating materials; therefore incorporating fillers into the biodegradable materials reduce the cost compared to coatings on cellulose fiber. It is hypothesized that applying a combination of filler and coatings would change the pore size and pore network structure, and thus would have a significant impact on improving the barrier properties. As mentioned above, the PLA film is a better barrier to water vapor than cellulose films; however, regenerated cellulose films show superior barrier properties to gases, e.g., oxygen and CO_2. Therefore, a combination of these films could generally provide the best barrier properties against gases and water vapors.

The effect of coated sample thicknesses and temperatures on mass transport properties and kinetics should also be investigated. This could also provide useful information to optimize the size of coating material required for specific applications and also for further improvement of the barrier properties. The activation energy of permeability (E_{eff}) was determined directly from the experimental measured water vapor permeability in the current study, but this should also be confirmed by independent measurement of heat of adsorption (ΔH) from water vapor adsorption isotherms and diffusional activation (E_d) to better understand the influence of these parameters on water vapor permeability of cellulose films. The pore diffusivity and surface diffusivity in the cellulose-films are determined at one temperature (25 ^{o}C) in the current investigation, and in future work investigating the effect of temperature on the pore diffusivity and surface diffusivity will develop understanding of the contribution of these different mechanisms to the water vapor transport through the cellulose-based material.

Appendix-I

1.1. Water Vapor Adsorption Equilibria

Water vapor adsorption isotherms of unmodified paper (control sample) and PLA coated paper samples at three different temperatures (15, 25 and 35 ^{o}C) are shown in Figure S1.

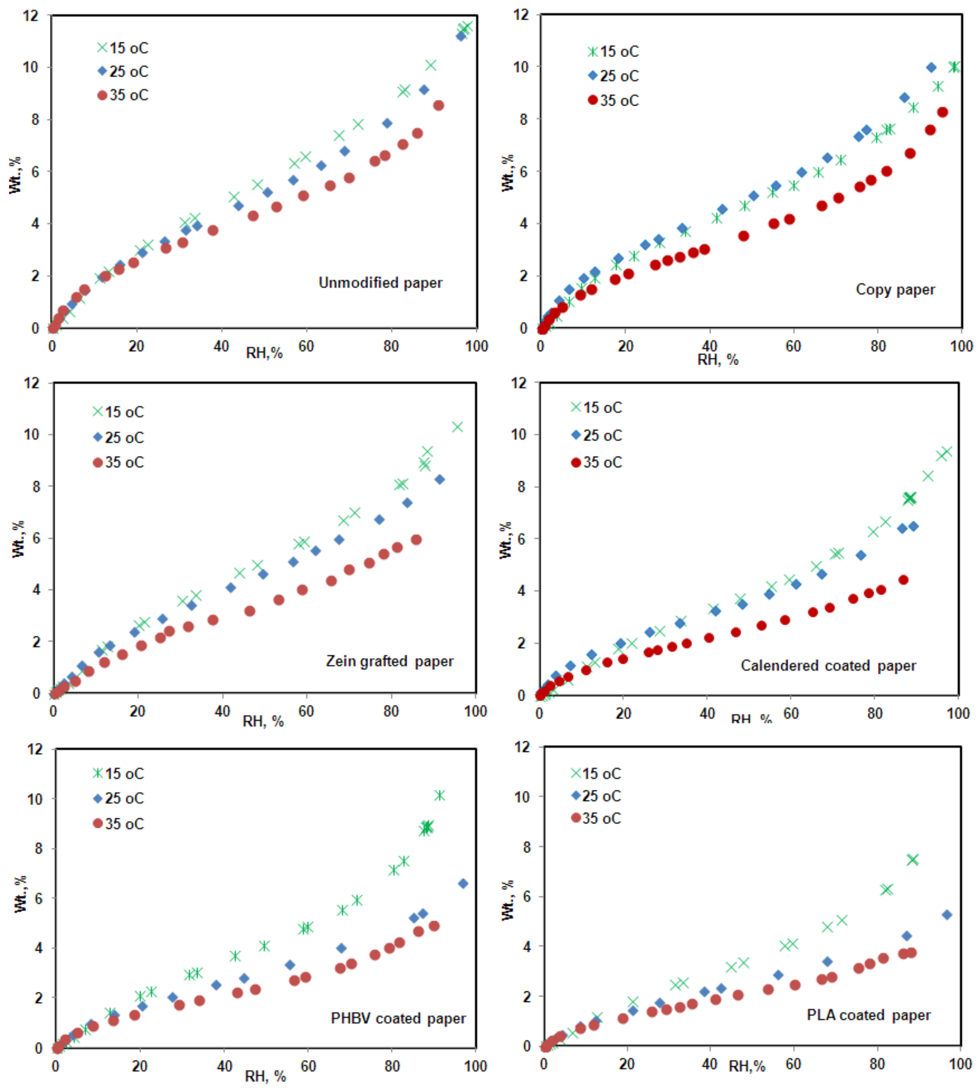

Figure S1. Adsorption isotherm of different paper samples at 15, 25 and 35 ^{o}C.

1.2. Hailwood-Horrobin (H-H) Data analysis

The fitting of H-H model to the experimental data for five samples is shown in the same figure. The extracted parameters of *A*, *B*, *C* , coefficients of determination (R^2), K_1, K_2 and *W* of different investigated paper samples are presented in Table S1. The high correlation coefficient (R^2) values in the table indicate good fit to the experimental results. The value of W for each coated paper is larger than for the unmodified paper. This reflects the decrease of moisture adsorption sites resulting in reduction in amount of adsorbed water.

Table S1. Fitted and calculated physical constants from the Hailwood-Horribon adsorption isotherms.

Paper Samples	*A*	*B*	*C*	K_1	K_2	*W*	R^2
Unmodified paper	3.75	0.190	0.0015	8.384	0.691	437	0.998
Copy paper	3.25	0.210	0.0016	10.56	0.683	462	0.999
Zein grafted paper	4.87	0.180	0.0012	7.194	0.585	421	0.999
Calendered coated pap.	5.52	0.320	0.0023	9.825	0.651	700	0.998
PLA coated paper	7.78	0.340	0.0024	8.10	0.620	787	0.974
PHBV coated paper	5.99	0.327	0.0024	9.32	0.670	730	0.953

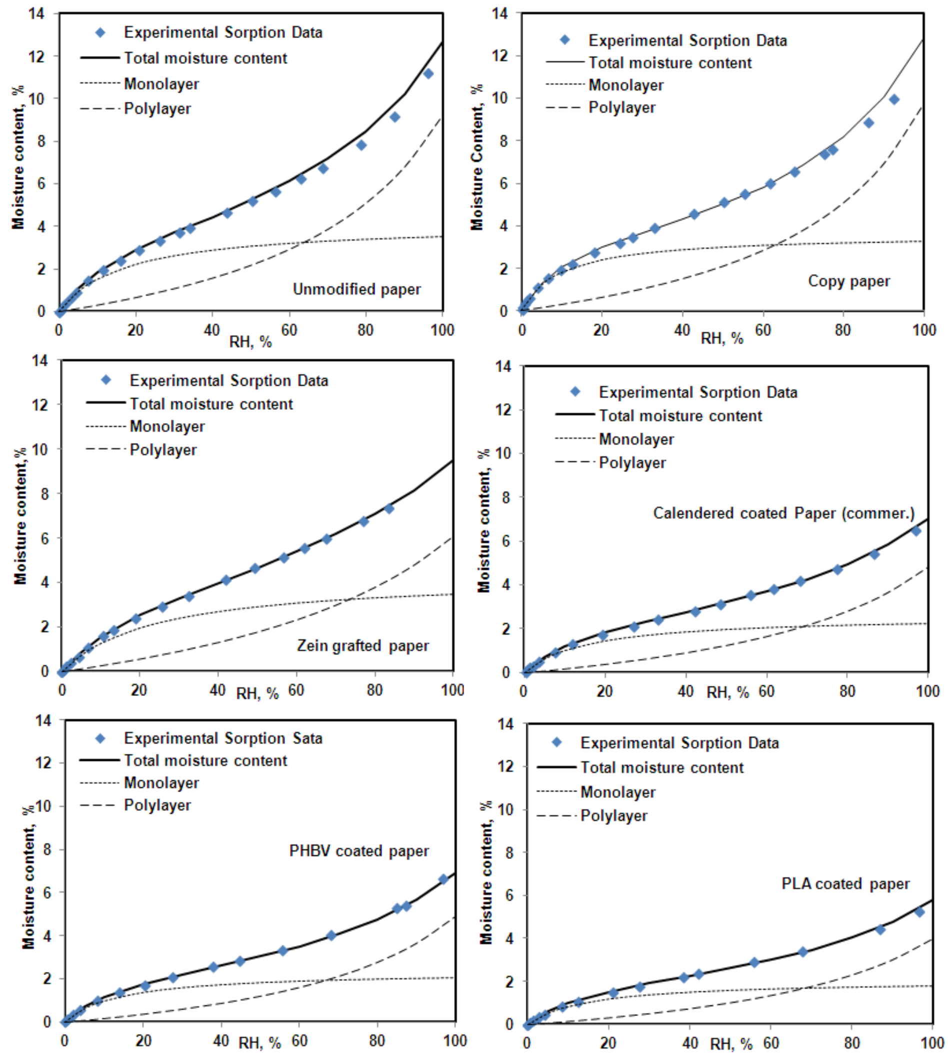

Figure S2. Water vapor adsorption experimental data showing agreement with H-H theory of multi-stage adsorption at T=25 ^{o}C.

1.3. Effect of temperature on moisture content of sample

Effects of temperature on monolayer and polylayer moisture content of paper samples (unmodified and PLA coated paper) are also shown in Figure S3. In general, the formations of monolayer and polylayer moisture contents decrease as the temperature increases, particularly with regard to the monolayer water content. According to Moreira (2008), this is due to reduction in the number of active sites available for water adsorption, because of the physical and chemical changes in the paper materials induced by temperature changes. Another possibility could be that an increase in temperature enhances activity of the water molecules, making them less stable and easier to break away from the binding sites of the material, thus decreasing the monolayer moisture content (Palipane and Driscoll 1992). Monolayer moisture content (M_h), and constants K and C are derived from GAB model for different paper samples and summarized in Table S2. The value of K is related to the energy of interaction of the molecules in multilayers with the adsorbent surface. It is usually between the energy values of the molecules in the monolayer and that of liquid water (energy of vaporization). When K value approaches one, the multilayers are considered to have the properties of liquid water according to the GAB model.

Table S2. Sorption parameters of GAB models determined from water sorption isotherms.

Paper samples	Monomolecular (M_h) (%)	K	C
Unmodified paper (Control)	4.12	0.674	9.62
Commercial copy paper	3.38	0.682	12.33
Zein grafted	4.32	0.582	8.12
Calendered coated pap. (Commercial)	2.70	0.694	13.49
PLA coated paper	2.29	0.619	9.26
PHBV coated paper	2.44	0.671	10.41

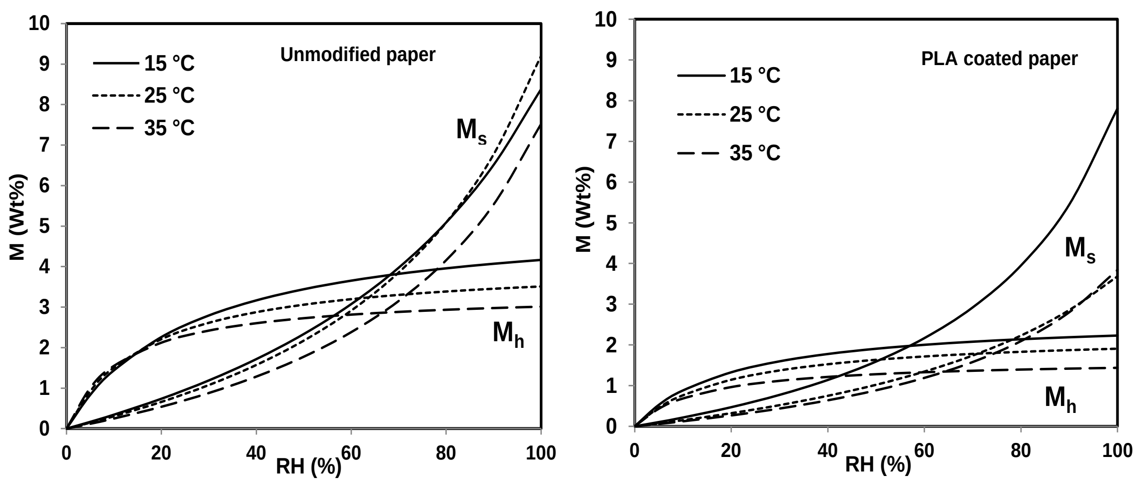

Figure S3. Effect of temperature on monolayer (M_h) and polylayer (M_s) moisture content of papers.

Appendix-II

2.1. HK-micropore size distribution

Figure S1 depicts the micropore size distribution analyses of the paper samples using the HK method (Horvath and Kawazoe, 1983). The micropores diameters of all samples are similar and these pores reflect the intrafiber pores present in the fiber wall and/or filler pigments.

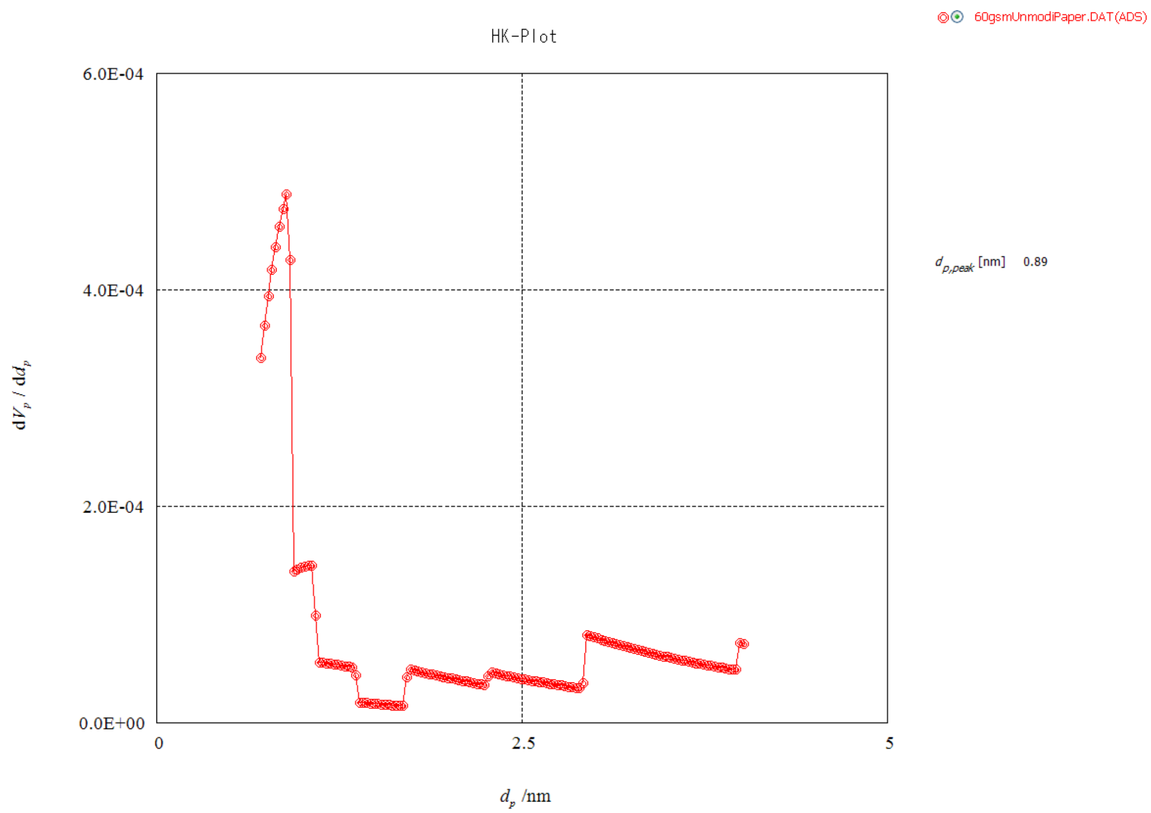

a. Unmodified paper sample

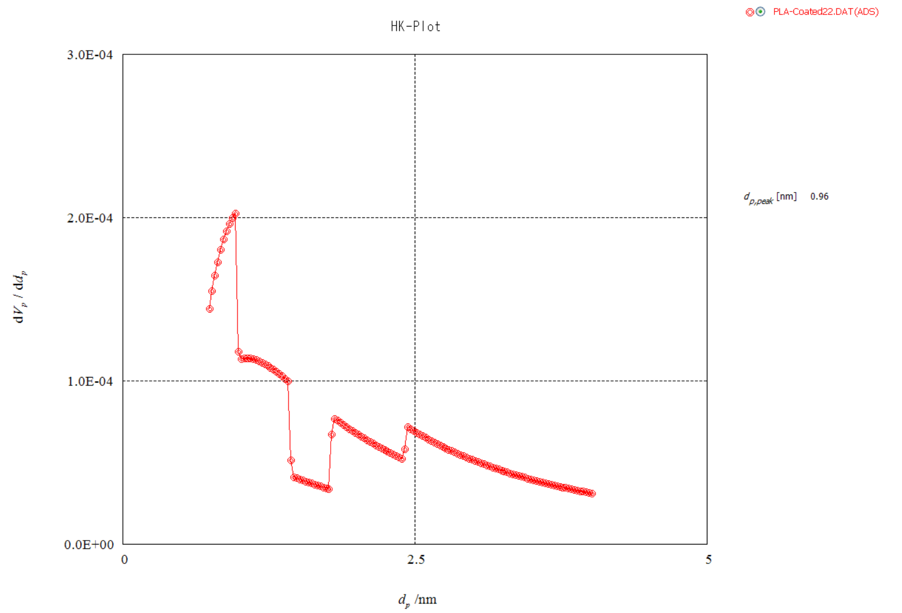

b. PLA coated paper

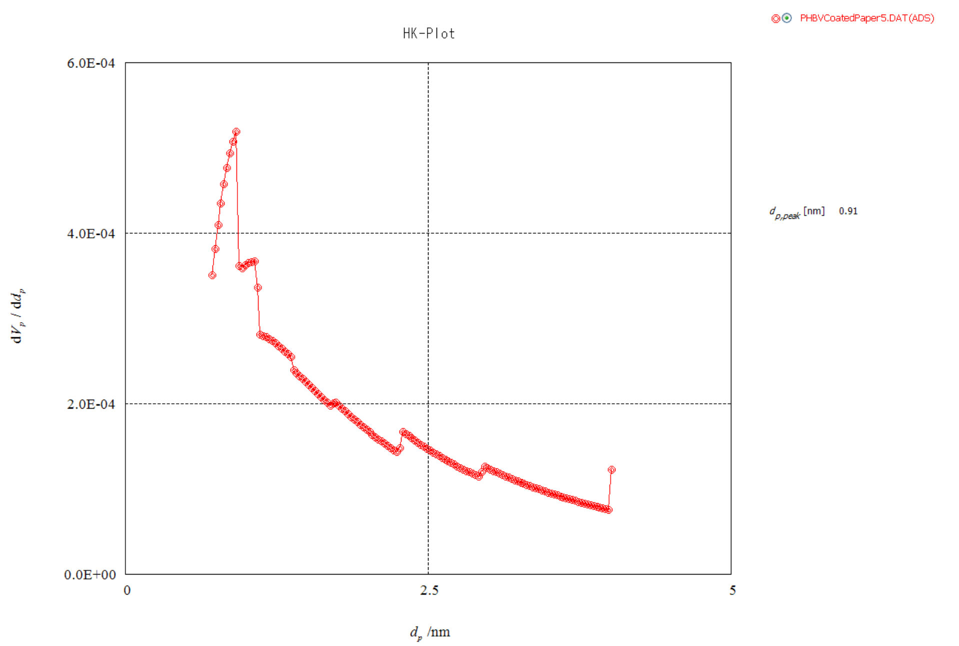

c. PHBV coated paper

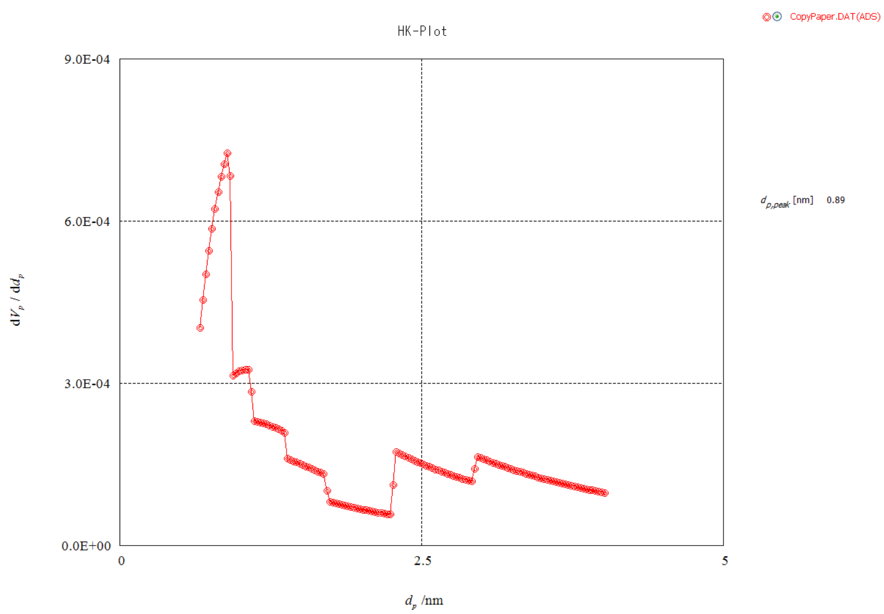

d. Copy paper

Figures S1. HK-Micropore size distribution of paper samples.

2.2. Mean pore diameter and pore volume of paper samples

Table 1S shows the mean pore diameter and total pore volume of different paper samples. Based on BET measurement, the coated paper samples showed higher specific surface areas than unmodified paper; however their mean pore diameters are smaller. All of the investigated paper samples exhibited very small micro- pore volumes.

Table S1. Mean pore diameter and total pore volume of paper samples.

Paper samples	Mean pore Diameter (nm)*	Total pore volume (mm^3/g)*
Unmodified paper (Control)	100.50	10.70
Commercial copy paper	44.80	9.90
Zein grafted	50.42	8.70
Calendered coated pap. (Commercial)	38.51	15.70
PLA coated paper	80.06	8.20
PHBV coated paper	50.79	9.80

*determined from N_2 adsorption isotherm measurements

2.3. Scanning electronic image of paper samples

Scanning electron microscope (SEM) image of different paper samples are illustrated in Figure S2. (Surface and cross section image of all coated papers sample are provided in the supplementary material). The micrograph of the unmodified paper clearly shows the fiber structure without any coating and fillers.

Surface Image **Cross section Image**

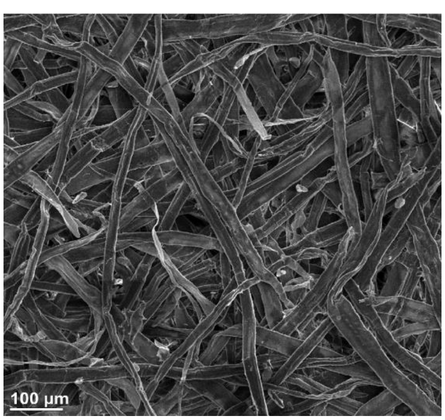

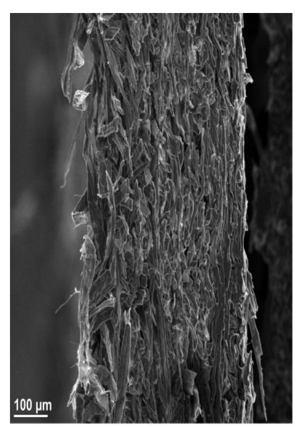

a.Unmodified paper (reference sample)

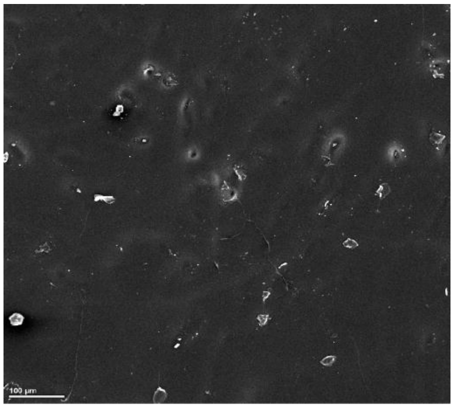

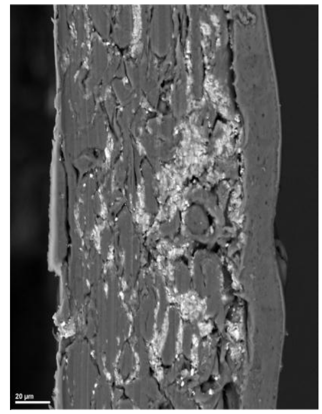

b. PLA coated paper **BSE(back scattered image scale=20 µm)**

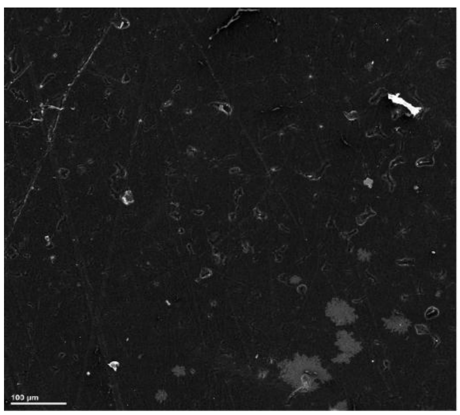

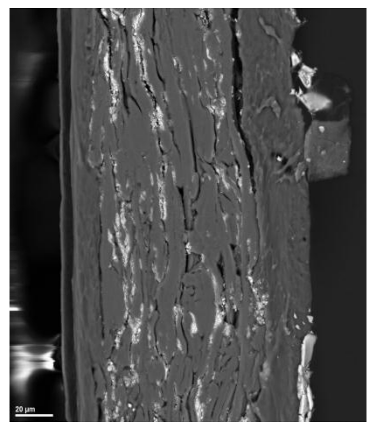

c. PHBV coated paper **BSE(back scattered image scale=20 µm)**

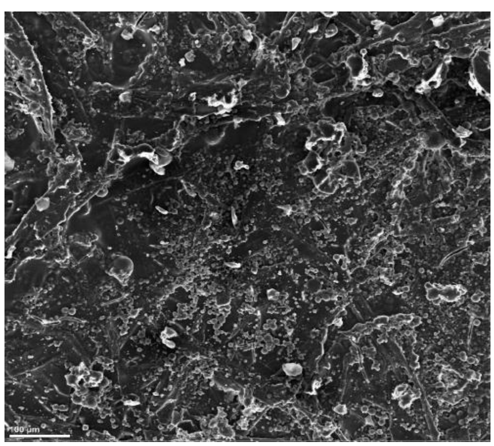

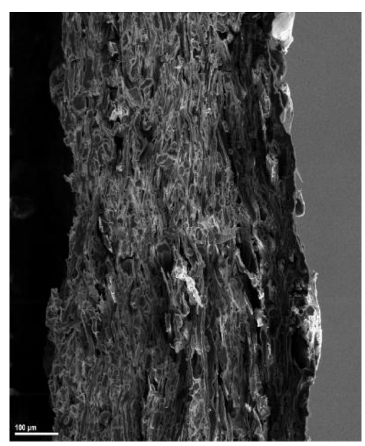

d. Zein grafted paper **(scale=100µm)**

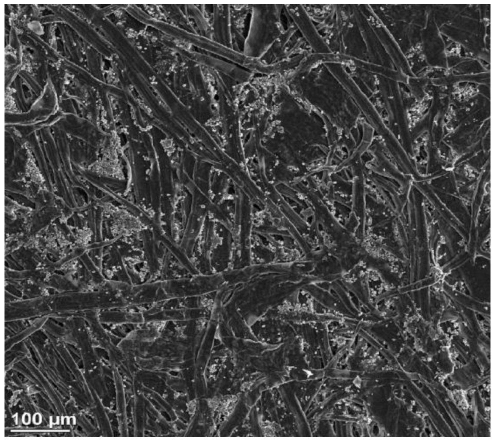

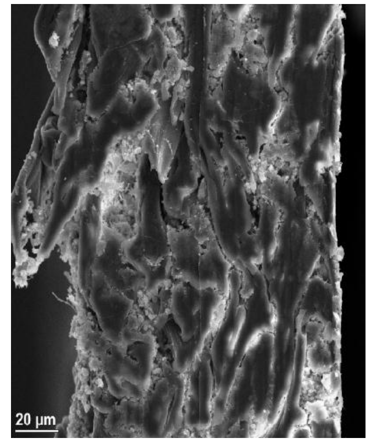

e.Copy paper **BSE(back scattered image)**

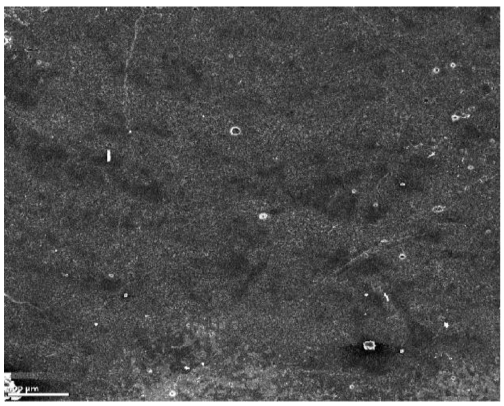

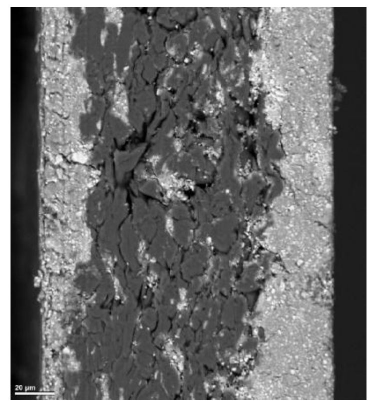

f. Calendered coated paper **BSE(back scattered image)**

Figure S2. SEM surface and cross section image of modified and unmodified paper samples.

2.4. TGA-DSC

In this study, different forms of adsorbed water present on cellulose fiber-based materials were analyzed using TGA-DSC instrument. Three different regions were identified on the TGA-DSC curves (Fig. 5.7 showed in the manuscript). These regions are defined by inflection points from the rate of mass loss and heat flow curves and this helps to get insight on the form of adsorbed water**.** The total amount and formations of adsorbed water on the different paper samples at 30, 50, 70 and 90% RH are shown in Table 2S.

Table S2. Moisture content of different water formation on paper samples at 25 ^oC for various relative humidity by TGA-DSC analysis.

Relative Humidity (RH), (%)	Paper samples	Free water, (%)	Loosely bound water, (%)	Tightly bound water, (%)	Total water content, (%)
30	Unmodified paper	0.677	1.471	2.470	4.618
	Calendered coated paper	0.373	1.787	1.610	3.770
	PLA coated paper	0.140	1.240	1.460	2.840
	PHBV coated paper	0.500	1.190	1.020	2.710
50	Unmodified paper	0.870	2.320	3.000	6.190
	Calendered coated paper	0.410	2.260	1.790	4.460
	PLA coated paper	0.570	1.830	1.420	3.820
	PHBV coated paper	1.170	1.410	1.560	4.180
70	Unmodified paper	1.200	2.657	3.800	7.657
	Calendered coated paper	0.620	3.252	2.694	6.656
	PLA coated paper	0.400	2.370	1.650	4.420
	PHBV coated paper	1.530	1.920	2.320	5.770
90	Unmodified paper	1.250	4.824	4.640	10.714
	Calendered coated paper	0.774	4.747	3.569	9.090
	PLA coated paper	0.730	2.310	2.760	5.800
	PHBV coated paper	1.950	2.150	2.930	7.810

2.5. FT-IR Spectra

The water vapor spectrum is measured in situ at different humidities by subtracting the spectrum of the dry paper sample from paper sample spectrum in equilibrium with water vapor as shown in Figure S3. The basic features of the adsorbed water spectrum are very similar. Four different peaks (3610 cm^{-1}, 3510 cm^{-1}, 3360 cm^{-1}, 3260/3070 cm^{-1}) were observed in the OH stretching band. The intensity of the spectra increases with increased relative humidity.

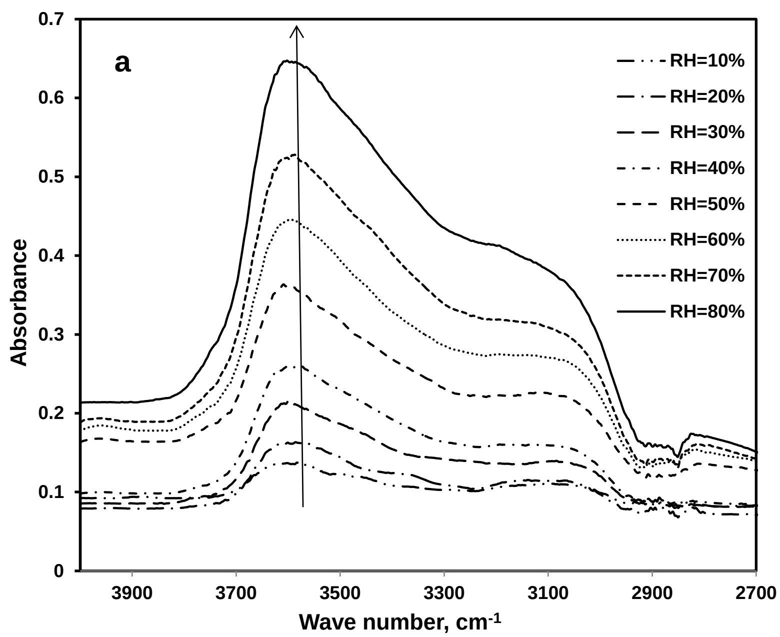

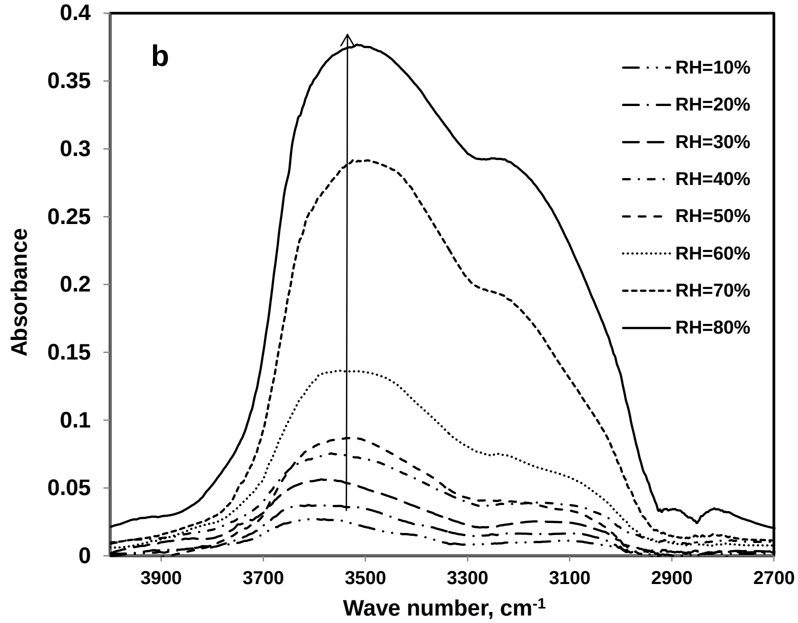

Figure S3. Water vapor sorption spectrum of a) unmodified paper, and b) PLA coated paper in equilibrium at different relative humidity.

Appendix-III

3.1. Adsorption-Desorption Isotherms:

Figure S1 shows the hysteresis loop of type H3 for the cotton linter cellulose and microcrystalline cellulose films.

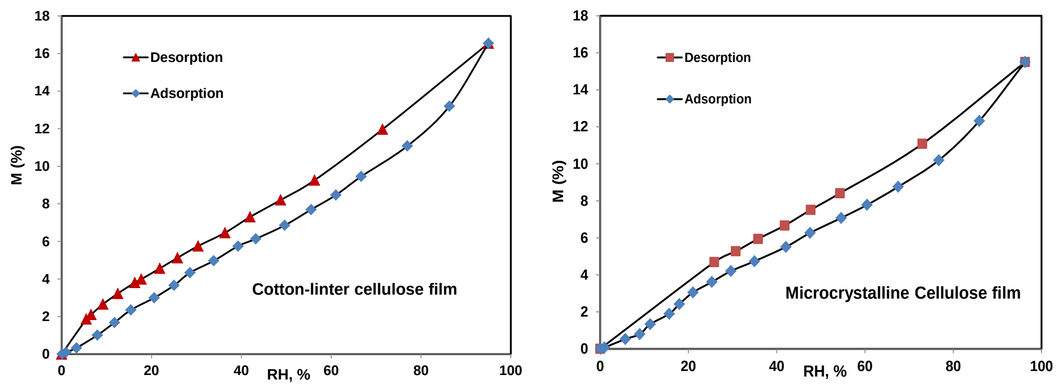

Figure S1. Water vapor adsorption-desorption isotherms of cotton-linter cellulose and microcrystalline films at 25 ^{o}C.

3.2. TGA-DSC

The cellulose films-based samples were analyzed by combined thermo gravimetric and differential scanning calorimeter instrument (TGA-DSC) to determine the glass transition temperature. The samples for these measurements were prepared by drying in an oven for two days at 100^{o}C. Then the sample placed immediately to the crucible and was heated at a heating rate of 10 ^{o}C/min and purged with 10 ml/min. N_2 gas. Weight loss and heat flow of the samples were recorded for the temperature range 20-300^{o}C. The heat flow curves for regenerated cellulose film (made from kraft pulp) and NFC film are shown in Figure S2. The DSC-TGA measurements showed the glass transition temperature of NFC and regenerated cellulose film at about 62 ^{o}C and 65 ^{o}C, respectively, by heating from room temperature to 100 ^{o}C (shown in Figure S2 in supplementary material). However, the glass temperature of the films can be shifted to atmospheric temperature or lower at high moisture contents of the film.

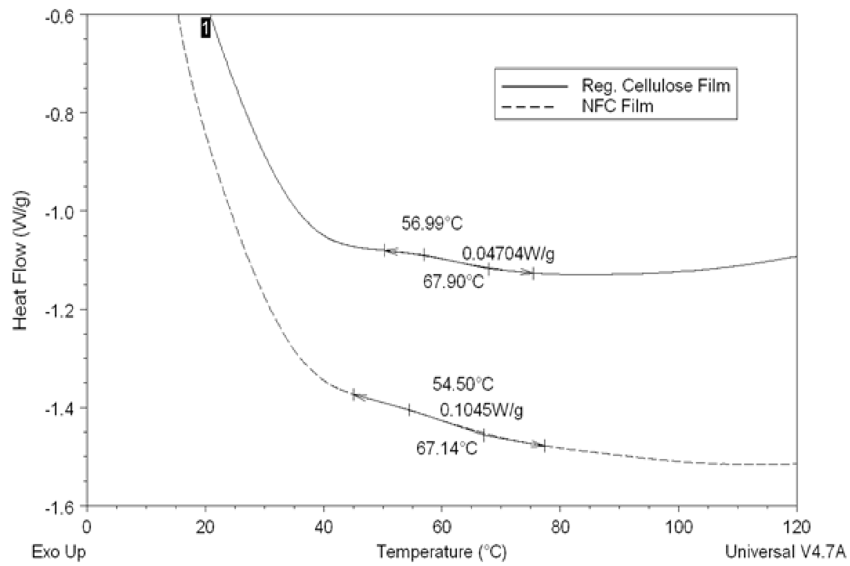

Figure S2. DSC measurement of dry regenerated cellulose and NFC films.

3.3. Percentage of Crystallinity

The percentage of crystallinity of cellulose films that were determined from XRD are listed in Table S1.

Table S1. Percentage of crystallinity determined from XRD

Type of Films	Percentage of Crystallinity (%)
Cotton Linter	39
Avicel (MCC)	51
Reg. alpha cellulose	46.5
Reg. cellulose film (made from bleached Kraft pulp)	38
NFC	20-75

3.4. Biot numbers used for fitting the water vapor uptake rate in the films

Biot dimensionless numbers that provide the best water vapor uptake fitting (for figure 6 in the manuscript) for cellulose-based samples in Eq. 8 at different relative humidities are listed in the Table S2.

Table S2. Biot numbers used to fit the water vapor uptake rate measurement of cellulose based-films at different relative humidities and T=25 ^{o}C.

Relative Humidity (%)	Biot number (Bi or α)		
	Paper sample	NFC film	Regenerated cellulose film
10-20	100	0.4	0.9
20-30	80	0.6	0.6
30-40	10	0.5	0.9
40-50	10	0.6	0.5
50-60	8	1.0	1.0
60-70	0.8	1.0	1.0
70-80	0.5	1.0	1.0

3.5. Rate controlling mechanism of water vapor transfer

The dominant rate controlling mechanism to water vapor transfer is internal diffusional resistance for unmodified paper in Figure S3 and external surface resistance and/or relaxation processes for regenerated cellulose and NFC films as shown in Figure S4. At high moisture content of the film, relaxation rate of the polymer chain is high and this result change in the structure of the film and internal diffusion also becomes significant. Hence, both conditions (internal diffusion and surface barrier) control the water vapor transport comparably. For example, the water vapor uptake rates for regenerated cellulose films are shown in the Figure S5. The coefficients of determination (R^2) for fitting the uptake rate curves in the film are the same for the surface barrier and internal diffusion model.

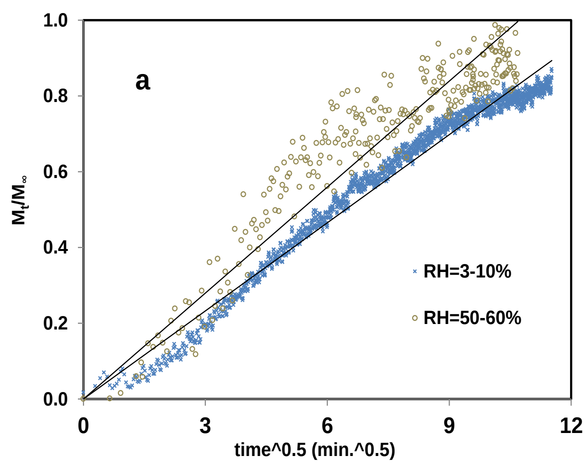

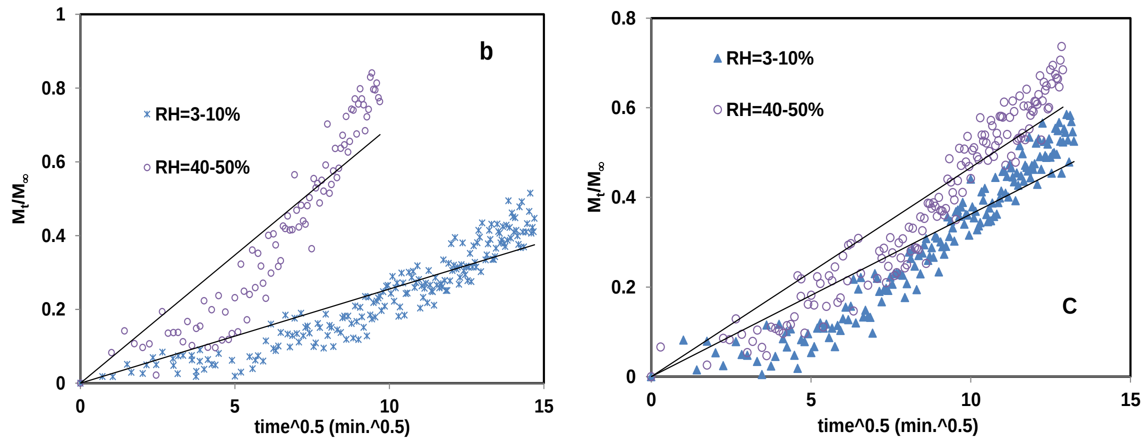

Figure S3. Model fitting of water vapor uptake fitting measured at T=25 ^{o}C of (a) unmodified paper showing better conformity with the diffusion resistance model than (b) regenerated cellulose film (b) and (c) NFC film [Symbols show experimental data and solid lines are short time solution according to the diffusional model (Eq. 5)].

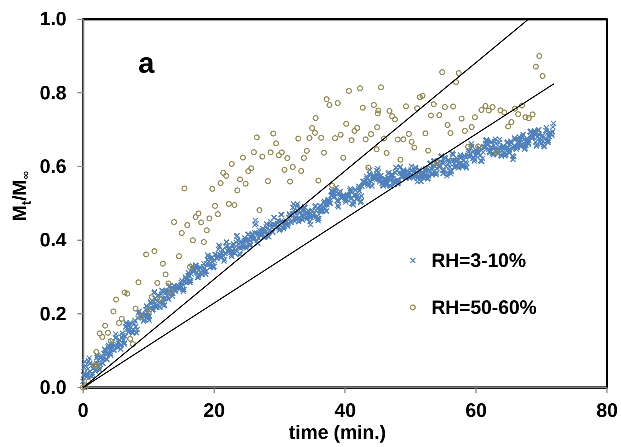

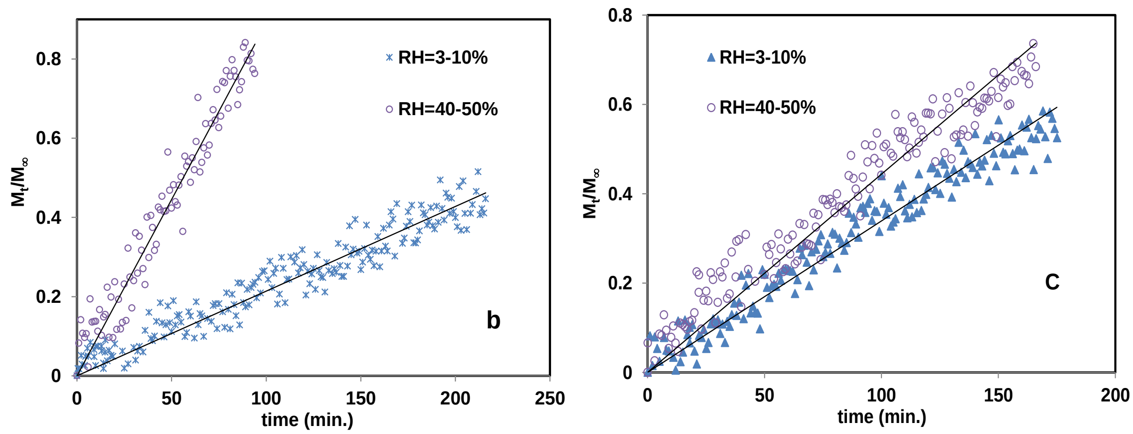

Figures S4. Model fitting of water vapor uptake fittings measured at T=25 °C of (b) regenerated cellulose film and (c) NFC film showing better conformity with the surface resistance model than unmodified paper (a) [Symbols are used for the experimental data and solid lines shows the short time surface resistance model (Eq. 8)].

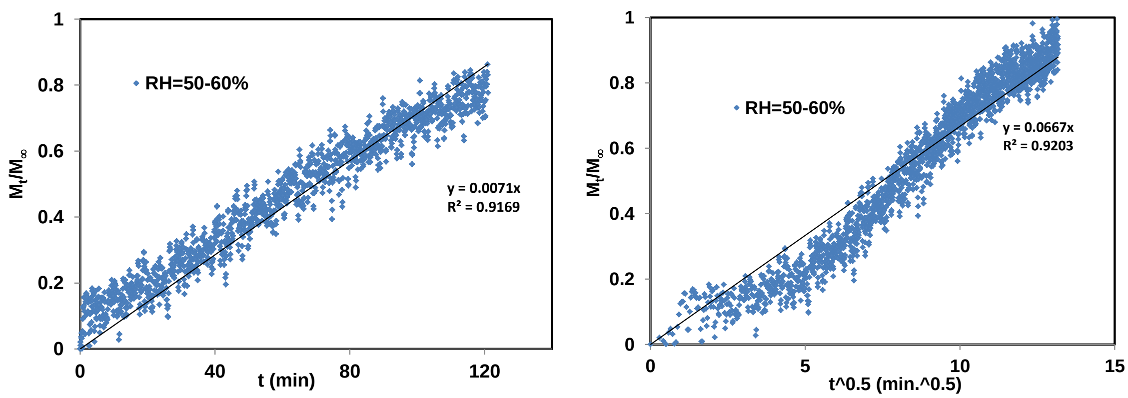

Figure S5. Water vapor uptake rate curves for regenerated cellulose film.

Appendix-IV

Calculated result for Knudsen diffusion coefficient

Knudsen diffusion is a means of molecular transport through pores which are small in comparison to the mean free path of the gas. For straight and round pores, the Knudsen diffusion coefficient can be predicted from the diameter of the pore by the expression (Hines and Maddox, 1985):

$$\frac{1}{D_{A,k}} = 97.0\, r \left(\frac{T}{M_A}\right)^{1/2} \qquad 1.1$$

where r is the pore radius, m, T is temperature, K, and $D_{A,K}$ is Knudsen diffusion coefficient, m^2/s, and M_A is molecular weight of component A.

In order to account for the tortuosity path of the molecule (τ) and the porosity of the material (ε), an effective Knudsen diffusivity ($D_{A, K, e}$) can be expressed as:

$$D_{A,K,e} = D_{A,k} \frac{\varepsilon}{\tau} \qquad 1.2$$

Regenerated cellulose film has small mean pore size and ranges between 0.5 to 2.0 nm (Tolle, 1971; Ichwan and Son, 2011). It is possibile that the regenerated cellulose film exhibits dominant Knudsen diffusion mechanism. Molecules collide more often with the pore walls than with other molecules in the Knudsen diffusion mechanism. Assuming straight and round pores in the cellulose film, the effective diffusivity can be calculated using Eq. 1.3.

$$D_{A,K,e} = 97.0\left(\frac{\varepsilon}{\tau}\right) r \left(\frac{T}{M_A}\right)^{1/2} \quad 1.3$$

The calculated $D_{A,K,e}$ is found to be around 5.3×10^{-9} m^2/s using the porosity value, ε=0.20, tortuosity, τ=15, molecular weight of water vapor molecule, M_A=18 g/mol, T=298 K, and pore radius, r ≈1.25 nm.

Reference

Tolle, W.E. (1971). Variables Affecting Film Permeability Requirements for Modified-Atmosphere. Agricultural Research Service, U.S Department of Agriculture, Technical Bulletin No. 1422, page 59.

Ichwan, M. and Son, T. W. (2011). Preparation and Characterization of Dense Cellulose Film for Membrane Application. J. Appl. Polym. Sci. 124(2), 1409-1418.

Appendix-V

Matlab coding for breakthrough modeling

```
% Moisture breakthrough medelling and WVTR

clc
    psat=0.0291;                % atm
    R=82.0567;                  % cm3 atm/(mol K)-1
    Tfeed =298.15;              % temperature, 25 oC;
    rhh(1)=0;                   % initialization, relative humidty
    WVTR(1)=0;                  % initialization, WVTR
    for rh1=9                   % loop to run for different RH
    rh=rh1/10;
    tw=0;
    RelHum(rh1)=rh1*10;
    y_feed =rh*(psat/(R*Tfeed*10^-6)); %mol/m^3
    diam=0.01578;          % Bed diameter, meter
    F =(1.0E-6)/2;         % gas/vapor flow rate, m^3/sec
    Area=(pi*diam^2)/4;    % surface area, m^2
    vb=1.7347E-6;          % bed volume,m^3
    kf=3.0*F/vb;       % 1/sec
    D0 =1.00E-011;     % surface diffusion constant parameter, m^2/s
    Dp =2.8*10^-7;    % pore diffusion, m^2/s
    qm =1478;            % #mol/m^3  1878.5
    Cgab = 10;           % GAB constant, Cgab = 75.417;
    Kgab = 0.65;         % GAB constant, Kgab = 0.749;
    ep=0.425;           % film porosity
    eb=0.43;            % bed porosity
lg=1;  % Dimensionless length of the column  0.00887
tt=1;  % Dimensionless time
L =0.00887;  % Bed length, meter
T =4.0*10^4; % Final time
% Parameters needed to solve the equation within the Crank-Nicholson
method
maxk=60;         % Number of time steps
dt = T/maxk;
n =400.;        % Number of space steps
```

```
dx = L/n;
c=kf*tt*dt*(1-eb)/eb;
a1= (-Dp*tt*dt/(2*lg^2*dx^2))+(F*tt*dt/(4*dx*lg*Area)); % Conductivity
% lg*(pi*diam^2/4)=vb o V=F/Area
a2=(-Dp*tt*dt/(2*lg^2*dx^2))-(F*tt*dt/(4*dx*lg*Area));
b1 = (Dp*tt*dt/(lg^2*dx^2))+1+0.5*c; % Parameter of the method
b2 = (Dp*tt*dt/(lg^2*dx^2))-1+0.5*c; % Parameter of the method
%%%%%% Pore Diffusion %%%%%%%%%%%%%%%%%%%%%%%%%%%%%%%%%%
kfp=0.0033;         % mass transfer coefficients
Dpp =2.5*10^-7;     % m^2/s
cond=Dpp/2;         % Conductivity
bp=cond*dt/(lg*lg*dx*dx); % Parameter of the method ((ep+(1-
ep)*ks)*dx*dx)
cp=Dpp*ep/(kfp*dx*lg);
% Initial moisture in the cellulose film:
for i = 1:n+1
x(i) =(i-1)*dx;
y(i,1)=0.0001;
yp(i,1)=0.0001;
end
%% moisture at the boundary (T=0)
for k=1:maxk+1
time(k) = (k-1)*dt;
end
cf=(F*lg*dx)/(0.35*Area*Dp);
%%%%%%%%%%%%%%Fluid phase mass balance %%%%%%%%%%%%%%%%%%%%%%%%%%%%%%%
% Defining the Matrices M_right and M_left in the method
aal(1:n-2)=a2;
bbl(1:n-1)=b1;
ccl(1:n-2)=a1;
MMl=diag(bbl,0)+diag(aal,-1)+diag(ccl,1);
aar(1:n-2)=-a2;
bbr(1:n-1)=-b2;
ccr(1:n-2)=-a1;
MMr=diag(bbr,0)+diag(aar,-1)+diag(ccr,1);
rr1(1,1)=-a2*y(1,1);
rr1(2:n-2,1)=0;
```

```
rr1(n-1,1)=-a1*y(1,1);
%%%%%%%%%%%%%%%%%%%%%%%%%% rr2
rr2(1,1)=a2*y(1,1);
rr2(2:n-2,1)=0;
rr2(n-1,1)=a1*y(1,1);
rr2;
qv0=0.0001*3640;
%%%%%%%%%%%%%%%pore diffusion%%%%%%%%%%%%%%%%%%%%%%%%%%%%%%
% Defining the Matrices M_right and M_left in the method
aalp(1:n-2)=-bp;
bblp(1:n-1)=2.+2.*bp+2*0.5*c;
cclp(1:n-2)=-bp;
MMlp=diag(bblp,0)+diag(aalp,-1)+diag(cclp,1);
aarp(1:n-2)=bp;
bbrp(1:n-1)=2.-2.*bp-2*0.5*c;
ccrp(1:n-2)=bp;
MMrp=diag(bbrp,0)+diag(aarp,-1)+diag(ccrp,1);
rr1p(1,1)=-bp*yp(1,1);
rr1p(2:n-2,1)=0;
rr1p(n-1,1)=-bp*yp(1,1);
%%%%%%%%%%%%%%%%%%%%%%%%%%%%%% rr2
rr2p(1,1)=bp*yp(1,1);
rr2p(2:n-2,1)=0;
rr2p(n-1,1)=bp*yp(1,1);
%%%%%%%%%%%%%%%%%%%%%%%%%%%%%%%%%%%%%%%%%%%%%%%%%%%%%%%%%%%%%%%%
r11(1:n-1,1)=0.0001;
r11p=r11;
% Implementation of the Crank-Nicholson method
for k=2:maxk+1 % Time Loop
yy=y(2:n,k-1);
FF=MMr*yy+(rr1-rr2)+c*r11;
y(2:n,k)=inv(MMl)*FF;
% moisture at the boundary (T=0)
y(1,k)=(y(2,k)+cf*y_feed)/(1+cf);
y(n+1,k)=y(n,k);
%%%%%%%%%%%%%%%%%%%%%%%%%%%%%% pore diffusion%%%%%%%%%%%%%%%%%%%%
yyp=yp(2:n,k-1);
```

```
yypp=MMrp*yyp+(rr1-rr2)+(2*c*(eb/(1-eb))*((1-ep)/ep)*r11);
yp(2:n,k)=inv(MMlp)*yypp;
%%%%%%%%%%%%%%%%%%%%%%%%%%%%%%%%%%%%%%%%%%%%%%%%%%%%%%%%%%%%%%%%%%%%
yp(1,k)=((cp*yp(2,k))-y(1,k))/(cp-1);
yp(n+1,k)=yp(n,k);
% Isotherm
qvv=0;
for m=1:n-1
 q(m,k)=(qm*Cgab*Kgab*y(m,k)*((R*Tfeed*10^-6)/psat))/(1-
Kgab*y(m,k)*((R*Tfeed*10^-6)/psat))/(1+(Cgab-
1)*Kgab*y(m,k)*((R*Tfeed*10^-6)/psat)); % # GAB isotherm model
  qv(m,k)=q(m,k)*1*dx+qvv;
    qvv=qv(m,k);
    qv0=abs(qv(m,k));
    qco=abs((qm*Cgab*Kgab*1*((R*Tfeed*10^-6)/psat))/(1-Kgab*y(9,k-
1)*((R*Tfeed*10^-6)/psat))/(1+(Cgab-1)*Kgab*y(9,k-1)*((R*Tfeed*10^-
6)/psat)));
    qf=(qm*Cgab*Kgab*y_feed*((R*Tfeed*10^-6)/psat))/(1-
Kgab*y_feed*((R*Tfeed*10^-6)/psat))/(1+(Cgab-
1)*Kgab*y_feed*((R*Tfeed*10^-6)/psat));
end
r11=(y(1:n-1,k-1)+y(1:n-1,k))/2;
r11p=(yp(1:n-1,k-1)+yp(1:n-1,k))/2;
%%%%%%%%%%%dq/dc=K%%%%%%%%%%%%%%%%%%%%%
aw=y_feed*((R*Tfeed*10^-6)/psat);
beta1=1/((1-Kgab*aw)*(1-Kgab*aw+Cgab*Kgab*aw));
beta2=aw/(((1-Kgab*aw)*(1-Kgab*aw+Cgab*Kgab*aw))^2);
beta3=(-Kgab*(1-Kgab*aw+Cgab*Kgab*aw)+(1-Kgab*aw)*(-Kgab+Cgab*Kgab));
beta(rh1)=(1550*Cgab*Kgab/1)*(beta1-beta2*beta3);
%%%%%%%%%%%%%%%%%%%%%%%%%%%%%%%%%%%%%%%%%%%%%%%%%%%%%%%%%%%%%%%%%%%
% RR values
rr1(1,1)=-a2*y(1,k-1);
rr1(2:n-2,1)=0;
rr1(n-1,1)=-a1*y(n,k-1);
%RR2
rr2(1,1)=a2*y(1,k);
rr2(2:n-2,1)=0;
```

```
rr2(n-1,1)=a1*y(n,k);
%%%%%%%%%%%%%%%%%%%Pore diffusion%%%%%%%%%%%%%%%%%%%%%%%%%%%%%
%%%%%%%%%%%%%%%%%%%parametrs%%%%%%%%%%%%%%%%%%%%%%%%%%%%%%%%%%%
% RR values
rr1p(1,1)=-bp*yp(1,k-1);
rr1p(2:n-2,1)=0;
rr1p(n-1,1)=-bp*yp(n,k-1);
%RR2
rr2p(1,1)=bp*yp(1,k);
rr2p(2:n-2,1)=0;
rr2p(n-1,1)=bp*yp(n,k);
%%%%%%%%%%%%%%%%%%%%%%%%%%%%%%%%%%%%%%%
end
Dq=D0*1*(2.72^(0.062*rh1*10/2.0));
ii=rh*10;
kfe=kf*vb/Area;
Dp11(ii,1)=((0.3*Dp*y_feed)/(1*1.0*10^-4))*1.5552*10^6;
Dss11(ii,1)=((0.7*Dq*10000*rh*3.2)/(1.0*10^-4))*1.5552*10^6;
%%%%%%%%%%%%%%%%%%%%%%%%%%%%%%%%%%%%%%%%%%%%%%%%%%%%%%%%%%%%%%%%%
Kext=1.8*10^-3;
%%%%%%%%%%%%%%%%%%%%%%%%%%%%%%%%%%%%%%%%%%%%%%%%%%%%%%%%%%%%%%%%%%%
WVTRkext(ii,1)=Kext*y_feed*1.5552*10^6;
Eq=beta(ii)/2;  %%%%%% Equilibrium constant
RRR(ii,1)=((1.3*10^-4/(0.3*Dp*1+0.70*Eq*Dq))+1/Kext);
WVTR1(ii,1)=(y_feed*1.5552*10^6)/((1.3*10^-
4/(0.3*Dp*1+0.70*Eq*Dq))+1/Kext+100);
WVTR2(ii,1)=(y_feed*1.5552*10^6)/((1.3*10^-4/(0.3*Dp*1+0.70*Eq*Dq)));
end
sol=ss/y_feed;   % Moisture breakthrough result
```

```
%%% Prediction of WVTR for paper sample
clear;
clc
    psat=0.0291;                %atm
    R=82.0567;                  %cm3 atm/(mol K)-1
    Tfeed =298.15;             % 25 oC;
    tr(1)=0;
    rhh(1)=0;
    WVTR(1)=0;
    D0 =1.00E-011       % Surface diffusion coefficient constant, #m^2/s
    Cgab =10;           % GAB constant
    Kgab =0.65;         % GAB constant
Dp = 3E-7;              % Average pore diffusion coefficient, #m^2/s
for RH1=1:10
rh=RH1/10;
tw=0;
RelHum(RH1)=RH1*10;
u_feed =rh*(psat/(R*Tfeed*10^-6));%%% RH at one side, %mol/m^3
u2_feed=0.02*(psat/(R*Tfeed*10^-6));   %%% RH in the other side,mol/m^3
%%%%%%%%%%%%%%%%%%%%%%%%%%%%%%%%%%%%%%%%%%%%%%%%%%%%%%%%%%%%%%%%%%%%%%
% Local Equilibrium constant calculation from GAB model derivative
aw=0.5*(u_feed*((R*Tfeed*10^-6)/psat));
beta1=1/((1-Kgab*aw)*(1-Kgab*aw+Cgab*Kgab*aw));
beta2=aw/(((1-Kgab*aw)*(1-Kgab*aw+Cgab*Kgab*aw))^2);
beta3=(-Kgab*(1-Kgab*aw+Cgab*Kgab*aw)+(1-Kgab*aw)*(-Kgab+Cgab*Kgab));
beta(RH1)=(1600*Cgab*Kgab/1)*(beta1-beta2*beta3);
rh=0.5;
ii=rh*10;
Eq(RH1)=beta(RH1)/1;           %% Local Equilibrium constant
Eqq(:,RH1)=Eq(RH1);
%%%%%%%%%%%%%%%%%%%%%%%%%%%%%%%%%%%%%%%%%%%%%%%%%%%%%%%%%%%%%%%%%%%%%%%%
Eq=beta(RH1)/1;
ii=RH1;
Dq=D0*1*(2.72^(0.064*RH1*10/1.9));
if ii<=7 %#ok<BDLGI>
Kext=3.4*10^-3;
else if ii<=8
```

```
    Kext=3.5*10^-3;
    else if ii<=9
      Kext=3.9*10^-3;
        else
            Kext=4.8*10^-3;
    end
    end
end
Epp=0.35;    %% porosity of paper sample
%%% external resistnace model
WVTR1(ii,1)=(u_feed*1.5552*10^6)/((125*10^-6/(Epp*Dp*1+(1-
Epp)*Eq*Dq))+1/Kext+1/Kext);
%%% Intrinsic resistnace model
WVTR2(ii,1)=(u_feed*1.5552*10^6)/((125*10^-6/(Epp*Dp*1+(1-
Epp)*Eq*Dq)));
end
RhExp=[0,10,33,50,76,90,100]; %%% x-axis delta RH
WVTRexp=[0,105,350,660,1450,2250,2850]; %%% y-axis WVTR
plot(RelHum,WVTR1,'-',RelHum,WVTR2,'*',RhExp,WVTRexp,'*-')
```

Curriculum Vitae

Candidate's full name: **Alemayehu Hailu Bedane**

Universities attended:

- University of New Brunswick, 2010-2015, PhD, Chemical Engineering.
- University of New Brunswick, 2009-2010, M.Sc., Forest Engineering.
- Otto-von-Guericke University of Magdeburg, 2007-2008, M.Sc, Quality, Safety and Environment (Thermal Process Engineering).
- Addis Ababa University, 1995-2000, B.Sc., Chemical Engineering.

Publications:

- **Alemayehu H. Bedane** and Mladen Eić. Thoeretical modelling of water vapor transport in cellulose-based film, 2015 (ready to submit).
- **Alemayehu H. Bedane**, Mladen Eić, Madjid Farmahini-Farahani, Huining Xiao. Mass transport properties of regenerated cellulose and nanofibrillated cellulose films. J. Membr. Sci. 2015 (Accepted).
- **Alemayehu H. Bedane**, Huining Xiao, Mladen Eić and Madjid Farmahini-Farahani. Structural and Thermodynamics Characterization of Modified Cellulose Fiber-Based Materials and Related Interactions with Water Vapor. Appl. Surf. Sci. J., 351, 725-737, 2015.
- **Alemayehu H. Bedane,** Huining Xiao and Mladen Eić. Water vapor adsorption isotherm equilibria on modified cellulose fiber-based materials. Adsorpt. J., 20, 863–874, 2014.
- **Alemayehu H. Bedane,** Qinglin Huang, Huining Xiao and Mladen Eić. Mass transfer of water vapor, carbon dioxide and oxygen on modified cellulose fiber-based materials. Nord. Pulp Pap. Res. J., 27(2), 409-417, 2012.
- T. Hoffman, **Alemayehu H. Bedane**, M.Peglow, E. Tsotsas, M.Jacob, Particle-Gas Mass Transfer in Spouted Bed Dryer with Controllable Air Inlet, Dry.Technol. J., 29(3), 257-265, 2011.
- **Alemayehu H. Bedane**, Muhammad T. Afzal, and Sokhansanj S. Simulation of temperature and moisture changes during storage of woody biomass owing to weather variability, Biomass and Bioenergy J., 35(7), 3147-3151, 2011.
- Donghua Jia, M. T. Afzal, Meng Gong**, Alemayehu H. Bedane**, Modeling of moisture diffusion and heat transfer during softening in wood densification, Int. Eng. J., 4(2), 2010.

- M. T. Afzal, **Alemayehu H. Bedane**, Shahab Sokhansanj, and Waseem Mahmood. Storage of comminuted and uncommunited woody biomass, and its effect on fuel quality, BioResour. 5(1), 55-69, 2010.

Selected Conference Presentations:

- **Alemayehu H. Bedane** and Mladen Eić, Water Vapor Transports Properties in Cellulose-based Materials, submited to 3rd Annual Fiber Conference 2015, École Polytechnique, Montreal, QC, May 11-13, Canada.
- **Alemayehu H. Bedane** and Mladen Eić. Water Vapor Transport Phenomena in Cellulose Fiber-based Materials, 2nd Annual Fiber Conference 2014, University of British Columbia, Vancouver, BC. May 12-16, Canada.
- **Alemayehu H. Bedane** and Mladen Eić**.** Water Vapor Permeability of Modified Cellulose Fiber-Based Materials. 63st Canadian Chemical Engineering Conference, CSChE 2013, Fredericton, Canada.
- **Alemayehu H. Bedane** and Mladen Eić**.** Gas Adsorption and Water Vapor Permeability of Modified Cellulose Fiber-based Materials, 1st Annual Fiber Conference 2013, Cornwall, ON, May 13-16, Canada.
- **Alemayehu H. Bedane**, Qinglin Huang and Mladen Eić, Gas Adsorption Equilibria and Water Vapor Transmission Rate of Modified Cellulose Fiber-Based Materials, 61st Canadian Chemical Engineering Conference, CSChE 2011, London-Ontario, Canada.
- **Alemayehu H. Bedane,** Qinglin Huang and Mladen Eić**,** Multicomponent Gas Adsorption Equilibrium on Zeolite 13X, 60th Canadian Chemical Engineering Conference, CSChE 2010, Saskatoon-Saskatchewan, Canada.
- **Alemayehu H. Bedane**, Storage of Comminuted and Uncommunited Forest Biomass, and its Effect on Fuel Quality, and Modeling of Natural Wind Drying, 2009, The Canadian Society for Bioengineering Annual General Meeting and Technical Conference, Prince-Edward-Island, Canada.